Anion and platinum group metal binding of bis(thioureido) ligands

Lenthall, Joseph T.

Anion and platinum group metal binding of bis(thioureido) ligands

A thesis submitted for the fulfilment of the requirements for the degree of

Doctor of Philosophy

In the faculty of Science of Durham University

by

Joseph T. Lenthall

Department of Chemistry

Durham University

South Road

Durham

2007

Abstract

A series of bis(thioureido) ligands have been synthesised, which show anion binding in acetone-d_6. Their structures have been determined by X-ray crystallography and some exhibit hydrogen bonding interactions with the π-electrons of the the thiocarbonyl bond. This hydrogen bonding interaction has been investigated for the general thiocarbonyl and carbonyl bond using the CSD, and a marked difference in the interaction of hydrogen bond donors with the π-electrons of carbonyl and thiocarbonyl bonds has been shown.

The bis(thioureido) ligands have been coordinated to platinum group metals and the differing binding modes of the ligands investigated. The reaction of ligands with 2 carbon atoms between thiourea groups with $[\{Ru(\eta^6\text{-}C_6H_4MeCH(Me)_2)Cl(\mu\text{-}Cl)\}_2]$, yields a mixture of products that may be consolidated into a single product with a water wash. The water instigates a deprotonation of an NH group that allows nitrogen coordination to ruthenium, yielding a S,S,N terdentate Ru(II) half-sandwich complex, with four- and seven-membered adjoining metallacycles. A chiral metal centre is formed and in the solid state, opposite enantiomers hydrogen-bond to each other through chloride counter-ions. Ruthenium complexes with an interaction from the pyridyl nitrogen in ligands containing pyridyl binding moieties have also been characterised. Bidentate S,S coordination is observed for the reaction of bisthiourea ligands with $[Pd(dppe)Cl_2]$, forming nine- and ten-membered metallacycles. A similar binding mode is observed in a Pt(II) analogue.

A polymer analogue of the bisthiourea ligands has been synthesised, and has been tested to extract metals from mixed metal solutions. Using well-defined metal salts in methanol, ruthenium(II) may be loaded onto the polymer from a single metal solution, acetontrile solvent inhibits the uptake of platinum group metals from mixed metal solutions, the polymer is selective for Cu(II) even when acetonitrile solvent is present and in the absence of Cu(II) or acetonitrile, can selectively extract Pt(II) over Ru(II), Fe(II), Cr(III) and Ni(II). The ruthenium loaded resin may be stripped of Ru(II) effectively using concentrated nitric acid solution in two hours. Testing the bisthiourea polymer in an acetic acid mixed metal solution demonstrated that the polymer was not suitable for platinum group metal extraction from the acetic acid medium, when compared to a commercially available resin.

To my parents, my sister and Ian.

"Chance favours the prepared mind" – Louis Pasteur

Acknowledgements

First and foremost I would like to thank Dr. Jon Steed for stimulating and challenging projects, and the knowledge that he has shared with me over the course of my studies. I would also like to thank Dr. Stephen Smith of B.P. Chemicals Ltd for useful discussions, support, chemicals and encouragement that he has provided.

In the group and department, I would like to thank Dr. Kirsty Anderson for all her help and crystal structure determination, especially with "crazy Cu(t-TUP)". A big thanks to Dr Richard Thompson, who has been most helpful with PIXE analysis. Thank you also to other crystallographers who have contributed to this work: Dr. Andres Goeta, Dr. Mike Probert and Gareth Lloyd. All the support staff have helped me hugely, in particular Alan Kenwright in NMR, as well as Jaroslava Dostal for elemental analyses and Mike Jones and Lara Turner for mass spectrometry. Thanks go to Doug Carswell for DSC, and Steve Lancaster of BP Chemicals Ltd for the ICP-MS results. I would also like to thank Professor Todd Marder for the generous use of his microwave reactor and GC-MS.

On a personal front, I would like to thank Shelley for putting up with all my crystal structure talk and diffusing work-related frustrations. Thanks also must go to Drs Dave Turner and Aled Jones for making me feel right back at home when I first started. A thank you to the rest of the Steed Group: Maria, Charlotte, Marc, Sara-Jane, Peter, Naseem, Gareth and Adam. Thanks also go to all the visitors and project students who have come through the group, especially to Lucas and Claire. I couldn't have lasted the three years without some respite from work, especially good conversation at tea, and for this I thank the following: Ricky, Big Dave, Smithy, Andy, Emma, Helen, Seb, Lucas, Dunwell, Nick, Skipsey, Jules, Pippa, Victoria, Carly and anyone I forgot.

Finally, I couldn't have done this without the support of my family, all of whom have encouraged me and supported me in different ways over the years.

Table of contents

List of Figures

List of Schemes

List of Tables

Abbreviatons

acac	acetylacetonate anion
br (NMR, IR)	broad
COD	cyclooctadiene (C_8H_{12})
Cp*	pentamethylcyclopentadiene (C_5Me_5)
CSD	Cambridge Structural Database
d (NMR)	doublet
dd (NMR)	doublet of doublets
ddd (NMR)	doublet of doublets of doublets
DMSO	dimethylsulphoxide
DNA	deoxyribose nucleic acid
DSC	differential scanning calorimetry
EDA	ethylenediamine
ee	enantiomeric excess
ESEM	environmental scanning electron microscopy
ESI-MS	electro-spray ionisation-mass spectrometry
GC-MS	gas chromatography mass spectrometry
hfac	1,1,1,5,5,5-hexafluoro-2,4-pentadionate anion
HIPE	high internal phase emulsion
Hz	Hertz
IC_{50}	inhibition concentration
K_{11}	1:1 host:guest binding constant
K_a	association constant
NMR	nuclear magnetic resonance
PET	photoinduced electron transfer
PGM	platinum group metal
PIXE	photon-induced X-ray emission
ppm	parts per million
ROMP	ring-opening metathesis polymerization
s (NMR)	singlet
t (NMR)	triplet
tu	thiourea ($H_2NC(=S)NH_2$)

Chapter 1: Introduction

1.1 Aims of the research

The aims of the research are based around thioureido and in particular bis(thioureido) ligands, and their interactions with themselves, anions and platinum group metals (PGMs). Therefore, a range of thioureido ligands will be synthesised and characterised fully. The general form of the ligands is shown in figure 1.1 and consists of a spacer group between the two thioureido functionalities that may be varied to alter the proximity of the two groups or incorporate another potential coordinating moiety. Each thioureido functionality is terminated by an R group that may be altered to change the solubility and crystallinity of the ligands and their metal complexes. Their anion binding ability will also be investigated using ^{1}H NMR spectroscopic titrations.

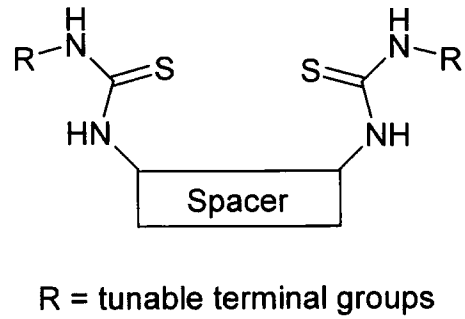

Figure 1.1: general form of bis(thioureido) ligands.

Coordination of the ligands to form discrete coordination complexes will be undertaken in order to investigate how bipodal thioureido ligands interact with platinum group metals. In particular, the coordination to ruthenium(II) to form half-sandwich complexes will be investigated. Bipodal ligands potentially exhibit a number of binding modes. X-ray crystallography will be employed where possible to confirm the coordination mode.

It is aimed to develop solid-supported polymer analogues of the bis(thioureido) ligands that may selectively extract platinum group metals over first row transition metals. Extraction experiments using solutions of both well defined metal salts and less well defined catalytic and corrosion metal product streams will be undertaken. The metal uptake and thus selectivity for PGMs of these solid-supported

bis(thioureido) ligands will be analysed by percentage metal content and IR spectroscopy. Comparison of the metal interaction with the small molecule analogues and the polymer-bound ligands will be made using IR spectroscopy.

This introduction, therefore, will summarise the background and recent developments in the areas of metal-thiourea coordination chemistry, ruthenium(II) half-sandwich complexes and methods for the recovery of PGMs.

1.2 Metal-thiourea chemistry

1.2.1 Early coordination compounds

Coordination of thiourea and its derivatives to metals through the soft[1] sulphur donor atom has been known for many years, and the ligand forms strong complexes with Cu(I), Ag(I), Au(I) and Hg(II).[2-6] It is also well documented that thiourea reduces Cu(II) to Cu(I), Au(III) to Au(I), and Te(IV) to Te(II). While there is some evidence from infrared spectroscopy that some derivatives may bind through the nitrogen atom, many X-ray crystal structure examples show interaction through the sulphur atom and its lone pairs, and early examples include complexes of Zn(II),[7] Pb(II),[8] Cd(II),[9,10] Pd(II),[11,12] Cu(I),[13,14] Co(II)[15-17] and Ni(II).[18-20]

After the first coordination compounds of thiourea, there was little work on metal-thiourea chemistry until the early 1990s, when the ligand's application in catalysis, and novel N,S metallacycle binding modes were explored. The chemistry of these two different applications will be discussed in the following sections.

1.2.2 Catalysis

Metal–thiourea complexes have most effectively been used in catalysis, in particular in the form of palladium catalysts.

1.2.2.1 Homogeneous Catalysis

The oxidative carbonylation of terminal alkynes by palladium-iodide thiourea catalysts has been known for some time.[21-23] The reaction may occur in the absence of oxidants and with catalytic quantities of the palladium complex, if the oxidation is

coupled with a reductive carbonylation of some of the terminal alkyne species, Scheme 1.1.

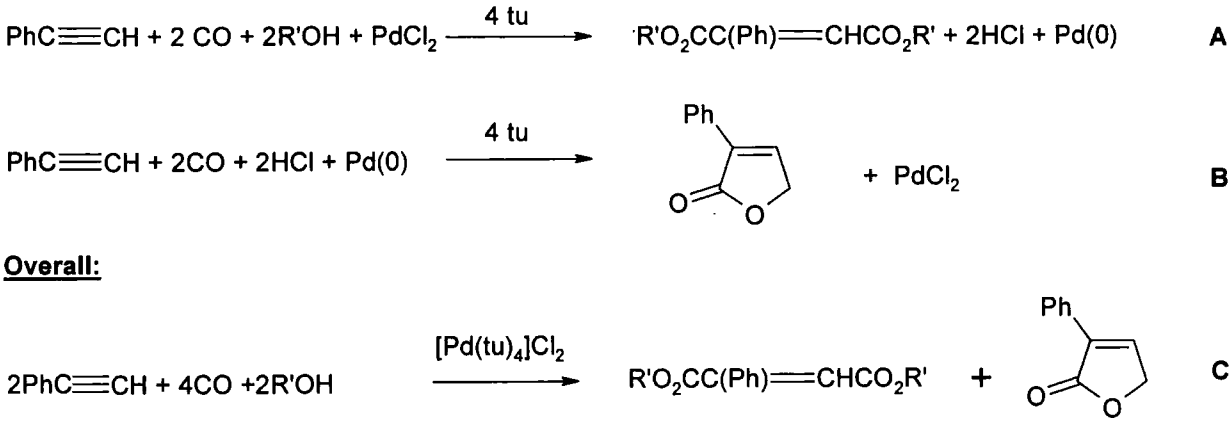

Scheme 1.1: The oxidative carbonylation of terminal alkynes (A), coupled with reductive carbonylation of the same terminal alkyne species (B) to give overall carbonylation (C) of terminal alkynes with catalytic quantities of Pd(II)-thiourea complex.[21]

While it is probable that only two thiourea (tu) molecules are coordinated to the active palladium species in the catalytic cycle, the best conversions were found by varying the Pd:tu ratio. For most substrates the best yields improve by changing the PdI_2:tu ratio from 1:4 to 1:3 and further improvement is observed by altering the ratio to 1:3.5. Efforts to isolate $[Pd(tu)_3I]I$ resulted in the formation of a mixture of $[Pd(tu)_4]I_2$ and $[Pd(tu)_2I_2]$, despite the solution species appearing catalytically different from a sum of the last two.

More recently, catalysis of the bis(methoxycarbonylation) of terminal olefins has been developed using a palladium tetramethylthiourea chloride catalyst.[24] This catalyst gave the desired bis(methylester) product, but in yields of less than 30 %. So further N,N'-substituted thiourea ligands (**1.1-1.10**) were synthesised and tested as palladium ligand catalysts, fig. 1.2. A decrease in yield is observed when the ligand used is less bulky at the nitrogen atom, as observed by changing from ligand **1.5** to ligand **1.7**, and an increase in yield is observed for a more rigid nitrogen backbone (ligand **1.9**). Therefore, by incorporating the thiourea group into a cyclic arrangement and functionalizing the nitrogen atoms with bulky groups, ligand **1.10** produces the greatest yields for a range of terminal olefins in the range of 75 – 90 %. These bulky heterocyclic thiourea ligands have been further used in palladium cross-coupling reactions with arenediazonium salts (ArN_2BF_4).[25,26]

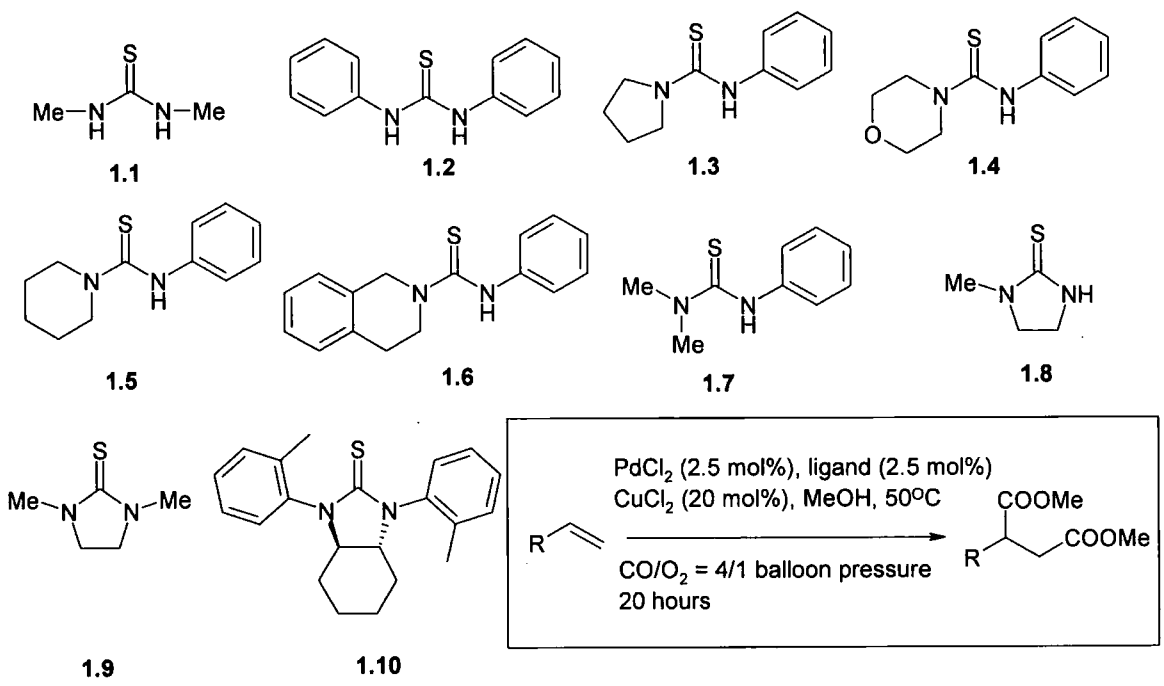

Figure 1.2: Structures of thiourea ligands 1.1-1.10 and general reaction scheme for the bis(methoxycarbonylation of terminal olefins.[24]

Using $Pd(OAc)_2$ and ligand **1.10** in 1 mol% quantities in MeOH at room temperature yields of up to 98 % are achieved with a variety of arenediazionium salts. Furthermore, bulky bisthiourea ligands have also been utilized for Pd-catalysed Heck and Suzuki reactions.[27]

1.2.2.2 Heterogeneous Catalysis

The area of heterogeneous catalysis is also of interest as it allows the facile extraction of the catalytic species from the product solution. The incorporation of thiourea functional groups into silica xerogels and anchoring of catalytically active metals to these groups has produced some active hybrid catalysts. Rh(I) anchored to N-benzoyl-N'-propylthiourea derived silica xerogel is an active, insoluble and recoverable catalyst for the hydroformylation of styrene.[28] Rh(I) *p*-phenylene bisthiourea has also been used to model the binding of these xerogels to Rh(I),[29] and chelating phosphino-thourea Rh(I) and Pd(II) complexes for the hydroformylation and hydrogenation of alkenes, respectively.[30]

Commercially available resins functionalised with a thiourea group, such as Deloxan® THP II*, have been used to bind palladium and provide a solid platform for the Suzuki cross-coupling of a variety of aryl halides and arylboronic acids.[31] Isolated yields for most of the couplings attempted range from 70 – 99 %, and the catalyst can be recycled. However, the activity deteriorates after 2-3 cycles.

1.2.3 Deprotonation of thiourea ligands to yield four-membered N,S metallacycles

Interest in the coordination of thiourea ligands was revived when methods for deprotonating one or both of the NH protons followed by coordination to platinum(II) were developed independently by Okeya and Henderson in 1992.[32,33] Henderson utilised silver(I) oxide to double deprotonate the thiourea and form a dianionic ligand, which coordinates to platinum(II) to form a four-membered metallacycle. Okeya formed similar four-membered platinum(II) metallacycles by displacing coordinated β-diketonates, which in turn deprotonate the coordinating thiourea ligands, scheme 1.2.[32]

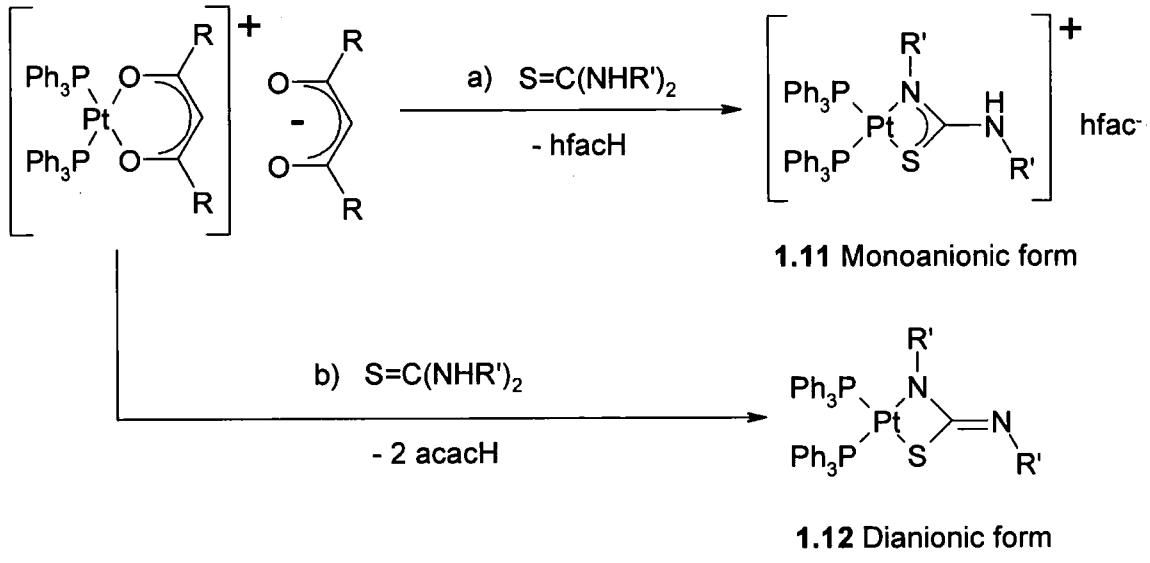

Scheme 1.2: Displacement of β-diketonates to form a) monoanionic thiourea-platinum complexes when R = CF_3 and b) dianionic thiourea- platinum complexes when R = CH_3. R' = Et, H.[32]

* Available from Degussa A.-G. at the time publication of ref. 31

The extent of deprotonation depends on the β-diketonate that is displaced, whereby single deprotonation occurs with the 1,1,1,5,5,5-hexafluoro-2,4-pentadionate anion (hfac; route a, scheme 1.2) to form the monoanionic thioureato coordinating species, **1.11**, and double deprotonation occurs through displacement of the acetylacetonate anion (acac; route b), to from the dianionic thioureato complex, **1.12**, scheme 1.2. The two structures can be differentiated by the loss of ν(NH) bands in the IR spectrum in the region of 3100 – 3500 cm^{-1} from the monoanionic to the dianionic form. The structure of **1.12** was also characterised by X-ray crystallography. Similar deprotonation is observed when $Cr(CO)_6$ is reacted with N,N'-diphenylthiourea, which initially yields the known $Cr(CO)_5(S{=}C(NHPh)_2)$ complex, however upon heating, the complex decarbonylates and reacts further with N,N'-diphenylthiourea to yield tris(thioureato)chromium(III).[34] The complex has three N,S chelating ligands arranged facially around the chromium as observed by X-ray crystallography. Henderson and co-workers extended this work to incorporate chiral, fluorescent and chromophoric groups into the thioureato ligands coordinated to Pt(II).[35]

Another mode of coordination for the dianionic thiourea is observed by X-ray crystallography with rhodium(III) and ruthenium(II), when chloride bridged dimeric species of the metals are reacted with monoanionic thiourea salts and excess triethylamine in hot methanol.[36]

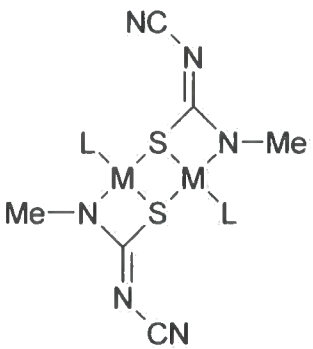

1.13, M = Rh(III), L = Cp*
1.14, M = Ru(II), L = *p*-cymene

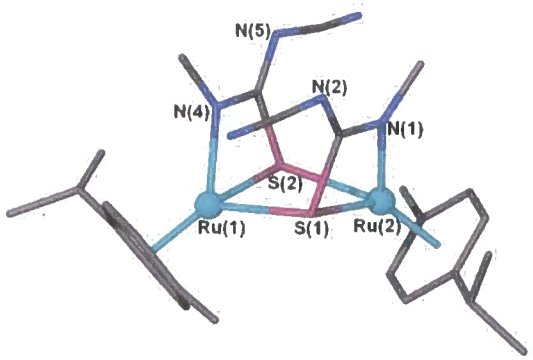

Figure 1.3: Molecular structure for Ru and Rh dimeric thioureido complexes, and molecular structure for $[Ru(\eta^6\text{-}C_6H_4MeCH(Me)_2)(SC(=NCN)NMe)]_2$ determined by X-ray crystallography. H atoms omitted for clarity.[36]

The X-ray crystal structure was obtained for the $[(\eta^6\text{-}C_6H_4MeCH(Me)_2)Ru(SC(=NCN)NMe)]_2$, and shows a dimeric ruthenium complex with chelating N,S ruthenium(II) four-membered metallacycles with bridging sulphur coordination, figure 1.3. This coordination brings in a further four-membered S-Ru-S-Ru metallacycle with Ru...Ru distance in the region 3.65 Å. In the same study, mononuclear Rh(I) complexes with chelating thiourea have also been synthesised with N,S binding motifs similar to those with platinum. Mononuclear ruthenium, osmium and iridium diphenylthioureido complexes involving N,S chelation were obtained from refluxing thiourea with metal hydride starting materials in benzene.[37] An analogous chelating binding mode was also found for the coordination of selenourea to Pt(II) diphosphines,[38] but in contrast the silver(I) oxide-mediated double deprotonation and dianionic coordination of urea derived ligands to Pt(II) is through both nitrogen atoms.[39]

Similar deprotonation of thioureas to form N,S four-membered metallacycles has also been observed in cadmium,[40] zinc,[41] gold(III),[42] and gold(I).[43] An N,S thiourea chelating ligand is also observed for complexes with rhenium(V) of a thiol-amide-thiourea ligand,[44] and it is observed in both coordinating thioureas for the related dithiourea ligand.[45] For the dithiourea complex, methanolic acetate solution deprotonates three of the four NH protons leading to coordination of one monoanionic and one dianionic thiourea-derived moiety within the same molecule, fig. 1.4.

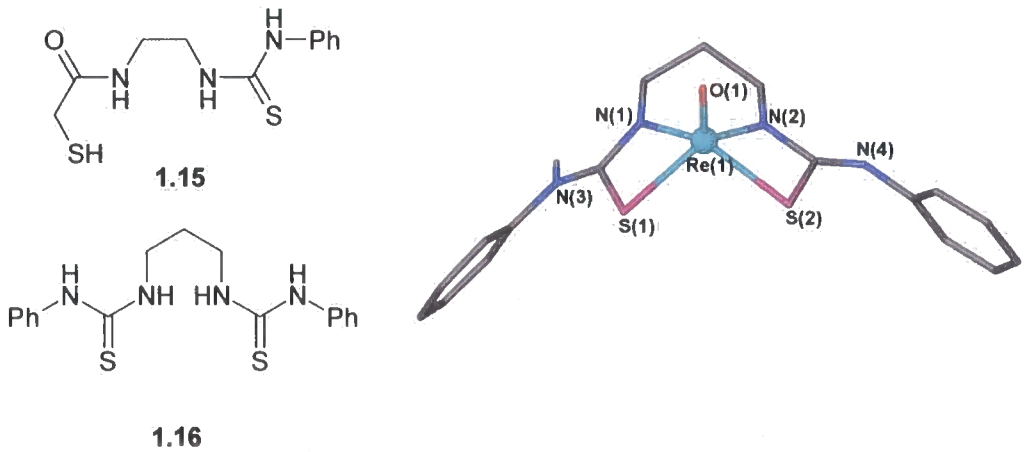

Figure 1.4: Thiol-amide-thioureido and bis(thioureido) ligands, and the molecular structure of the rhenium(V) oxide bis(thioureido) complex, as determined by X-ray crystallography. H atoms omitted for clarity. [44,45]

There has been a lot of interest in ruthenium half-sandwich complexes in the last 25 years, however relatively little work on ruthenium thiourea complexes. The chemistry of ruthenium half-sandwich complexes, and more recent advances in this area are detailed in the proceeding section.

1.3 Ruthenium half-sandwich π-arene complexes

1.3.1 Preparation and early coordination of arene ruthenium compounds

The first η^6 arene ruthenium(II) complexes were formed by the displacement of chloride anions from $RuCl_3$ in the presence of arenes with Lewis acids under reducing conditions.[46-48] One of the most commonly used starting materials for accessing Ru(II) half-sandwich π-arene complexes is from the dehydrogenation of cyclohexadienes, reducing $RuCl_3.xH_2O$ in ethanol.[49] This yields ruthenium(II) arene compounds that are chloride bridged structures in the solid state, but the bridging chlorides may be easily cleaved in weakly coordinating solvents to yield a half-sandwich compound with a free coordination site. These compounds have been reacted with a range of monodentate tertiary phosphines, tertiary arsines and pyridine ligands, by Bennett, and Zelonka and Baird in 1972 to form monomeric compounds of formula $[RuCl_2(arene)L]$, scheme 1.3.[50-53]

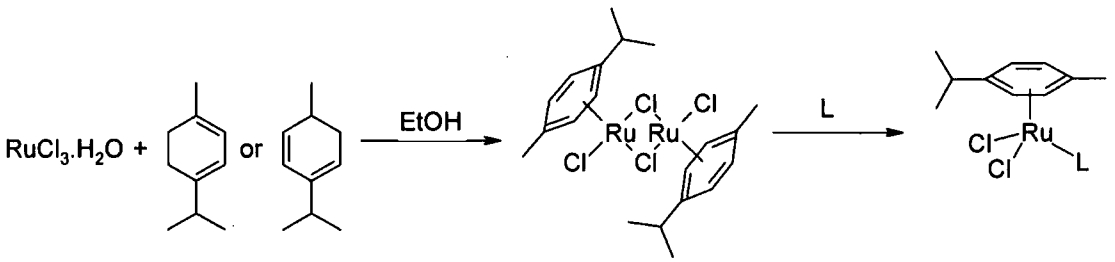

Scheme 1.3: Synthesis of dimeric[{Ru(η^6-$C_6H_4MeCH(Me)_2$)Cl(μ-Cl)}$_2$] chloride bridged complex, and reaction with monodentate two-electron ligands to form monomeric [Ru(η^6-$C_6H_4MeCH(Me)_2$)Cl_2L] complex. [50-53]

Around the same time, similar rhodium and iridium Cp*-derived complexes were being developed by Maitlis and coworkers.[54-57] Access to all three labile coordination sites was achieved by reacting with silver(I) salts with non-coordinating

counter-ions, AgX, (X = PF_6, BF_4, *etc*) in order to extract the chloride ions as AgCl, and leave a solvated half sandwich complex. This method was repeated with the [{Ru(arene)Cl(μ-Cl)}$_2$] compound to produce a series of monomeric compounds with weakly coordinated solvent ligands – [Ru(arene)S_3](X^-)$_2$. These complexes allow all three coordination sites to be accessed by displacement of the solvent molecules. This method was used by Bennett and co-workers in the formation of mixed bis-arene ruthenium complexes.[58]

Further coordination followed these initial experiments with coordination from: sulphur donors,[59] nitrogen donors,[60] with reducing agents to form hydride complexes, RuHCl(C_6Me_6)(PPh_3)[61] and with amino acid anions to form chiral η^6-C_6H_6 ruthenium complexes.[62]

1.3.2 Recent ruthenium(II) half-sandwich complexes and applications

1.3.2.1 New coordination modes and chirality

Since these first coordination experiments to form Ru(arene) half-sandwich coordination compounds, there has been much interest in them for a variety of uses.[63] By the nature of the metal half-sandwich complex, chirality at the metal centre may result by coordinating three different ligands to the metal in addition to the aryl ring. The work on organometallic half-sandwich complexes with defined chirality about the metal has been recently reviewed,[64] and so this account will not go into detail on this subject. However, an interesting and unusual example from the literature shows the synthesis of a phosphino-amino-chloro mononuclear ruthenium aryl complex, whereby the phosphorus group is tethered to the aryl ring.[65] Enantiopure ((*R*)-3-phenylbutyl)phosphine is reacted with [{Ru(η^6-C_6H_5COOMe)Cl(μ-Cl)}$_2$] dimer to coordinate *via* the P atom, and tethered to the η^6-aryl ring through a methyl ester group on the aryl ring with elimination of methylbenzoate, scheme 1.4.

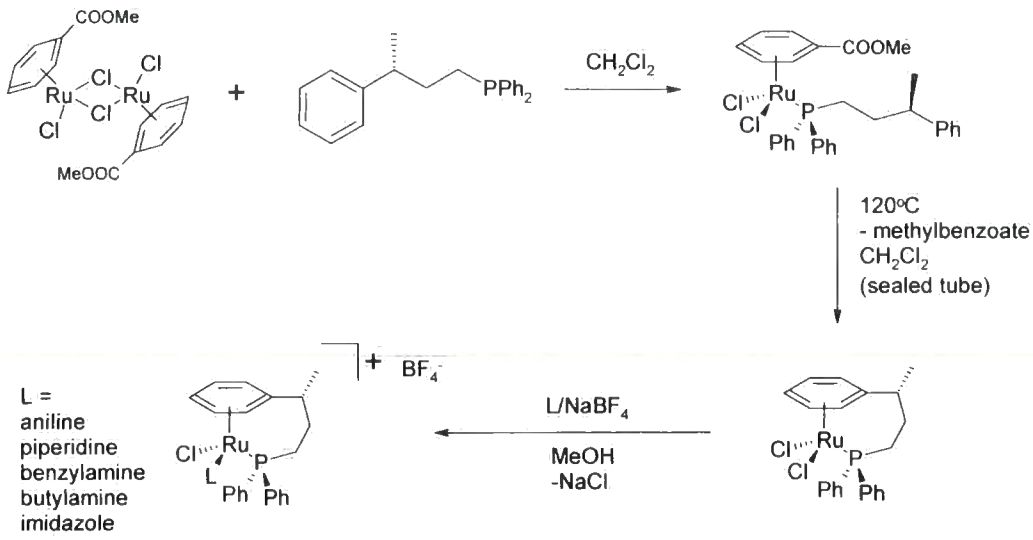

Scheme 1.4: reaction scheme for the tethered phosphino-amino-chloride ruthenium half-sandwich complex.[65]

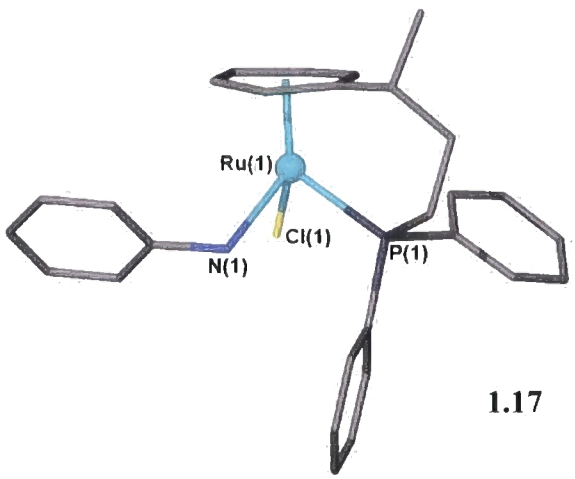

Figure 1.5: the molecular structure of the tethered phosphino-amino-chloride ruthenium half-sandwich complex aniline analogue, 1.17, as determined by X-ray crystallography.[65]

This process yields the monomeric dichlororuthenium species, and coordination of a variety of amines in the presence of $NaBF_4$ leads to diastereomeric [RuCl(amine)-((*R*)-η^1-$PPh_2(CH_2)_2CH(CH_3)$-η^6-C_6H_5)]BF_4, an example of which can be seen in the molecular structure of the aniline adduct, **1.17**, fig. 1.5. The molar ratios for the production of **1.17** show a good diastereoselectivity, with a molar ratio of 95:5 in favour of the $S_{Ru}R_C$ diastereoisomer shown in the X-ray crystallographically determined molecular structure, fig. 1.5.

Another example of stereoselective binding to Ru half-sandwich complexes is observed by the coordination of a chiral P,O ligand, (*4S*)-2-[(S_P)-2-(diphenylphosphanyl)ferrocenyl]-4-(methylethyl)oxazoline (FcPN).[66] NOESY NMR spectroscopy experiments suggest that the solution state configuration of the [Ru(η^6-$C_6H_4MeCH(Me)_2$)(FcPN)].PF_6 complex is only R_{Ru}, and this stereochemistry is confirmed in the solid state.

In contrast, the coordination of pyridylpyrazole ligands, 2-[3-(4-chlorophenyl)pyrazol-1-ylmethyl]pyridine, **1.18**, 3-(2-pyridyl)pyrazole, **1.19**, 1-benzyl-[3-(2'-pyridyl)]pyrazole, **1.20**, and a pyridylimidazole ligand, 2-(1-imidazol-2-yl)pyridine, **1.21**, to [{Ru(η^6-C_6H_6)Cl(μ-Cl)}$_2$] yields complexes of formula [Ru(η^6-C_6H_6)(κ-*N*,*N*-**L**)Cl](PF_6), where **L** = **1.18** – **1.21**, as a racemic mixture.[67]

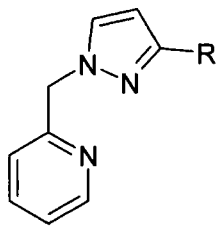

R = -C_6H_5-*p*-Cl

1.18

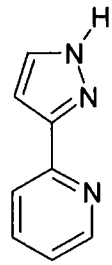

1.19

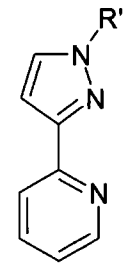

R' = -CH_2-C_6H_5

1.20

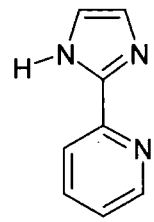

1.21

This is confirmed by the solid-state structures of the complexes, in which both enantiomers are present. The two pyridylpyrazole complexes of ligands **1.18** and **1.20** are not protonated at any of the nitrogen atoms, and thus do not hydrogen-bond in the crystal structure. However, the two other complexes [Ru(η^6-C_6H_6)(κ-*N*,*N*-**1.19**)Cl](PF_6) and [Ru(η^6-C_6H_6)(κ-*N*,*N*-**1.21**)Cl](PF_6) which have NH groups capable of hydrogen bonding, hydrogen bond to the coordinated chloride atom of their opposite enantiomers, fig 1.6.

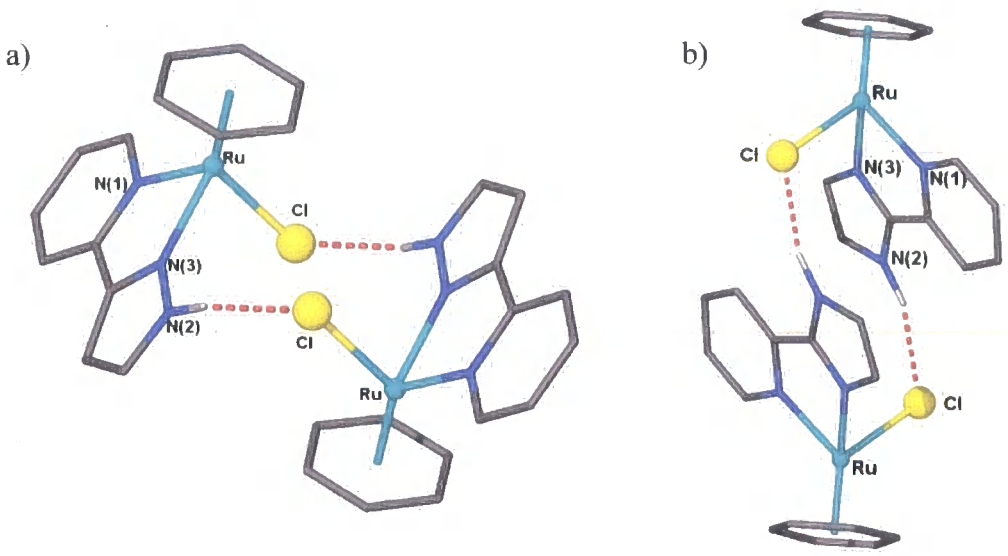

Figure 1.6: X-ray crystal structures of a) [Ru(η^6-C_6H_6)(κ-*N*,*N*-1.19)Cl](PF_6) and b) [Ru(η^6-C_6H_6)(κ-*N*,*N*-1.21)Cl](PF_6) showing pairing of opposite enantiomers. PF_6^- counter-ions and H atoms excluded for clarity.[67]

An unusual example of an intramolecular rearrangement of a ligand as part of a ruthenium(II) half-sandwich complex has recently been reported.[68] Reaction of a helical tetradentate N-donor, **1.22** with [{Ru(η^6-C_6H_6)Cl(μ-Cl)}$_2$], leads to the isolation of a product in which the ligand on the ruthenium has cyclised, **1.24**.

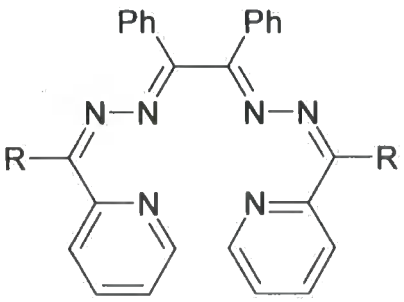

1.22 R = H
1.23 R = Me

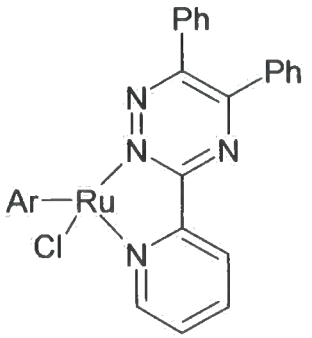

1.24

Ar = C_6H_6

This process however, does not occur when the ligand R group is methyl, **1.23**, and so the ability to lose this proton must be key to the cyclisation mechanism. A proposed mechanism for the cyclisation is given in scheme 1.5.

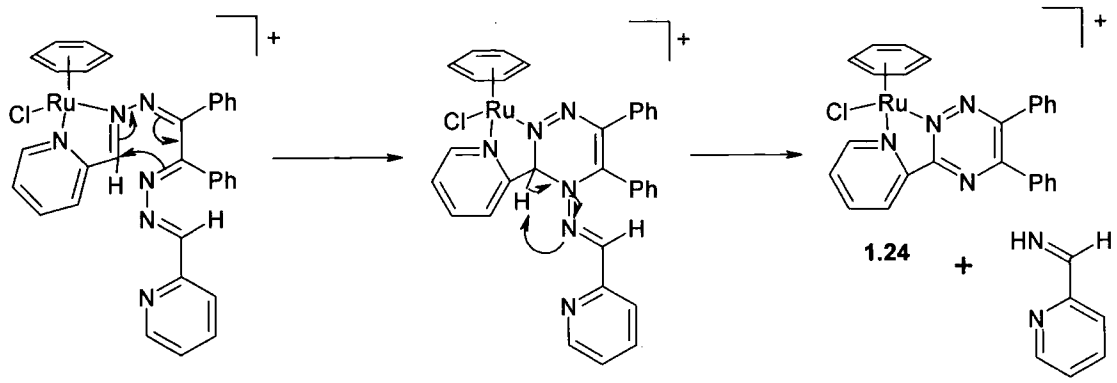

Scheme 1.5; proposed mechanism for the cyclisation reaction of the complex formed by the reaction of 1.22 with [{Ru(η^6-C_6H_6)Cl(μ-Cl)}$_2$] to form the new ruthenium(II) half-sandwich complex, 1.24.[68]

1.3.2.2 Catalysis with Ru half-sandwich complexes

Chiral ruthenium(II) half-sandwich complexes have been used effectively in catalysis, and in particular in transfer hydrogenation. In a recent example, the hemilability of *P,N,O*-iminophosphorane-phosphine ligands coordinated to Ru(II) and Ru(IV) species was exploited for the transfer hydrogenation catalysis of cyclohexanone.[69] Selective κ^1-*P*-, κ^2-*P,O*- and κ^3-*P,N,O*-coordination modes were found, however catalytic yield and turnover frequencies (TOFs) both decreased with increasing ligand coordination. Higher yields and TOFs were found for [Ru(η^3:η^3-$C_{10}H_{16}$)L] complexes.

After the success of Noyori's catalyst,[70-73] several chiral Ru half-sandwich complexes have been developed to catalyse the hydrogenation of acetophenone to the diastereomeric 1-phenylethanol under basic conditions.

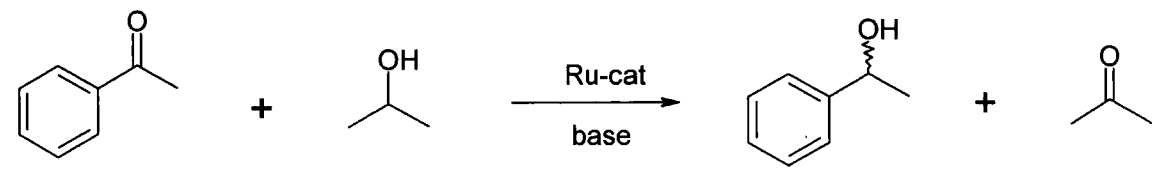

Scheme 1.6: Transfer hydrogenation of acetophenone catalysed by Ru half-sandwich complexes.[74-76]

Complexes formed by the reaction of $[\{Ru(\eta^6\text{-}C_6H_4MeCH(Me)_2)Cl(\mu\text{-}Cl)\}_2]$ with amino amide,[74] enantiopure 2-aminocyclohexanol derivative,[75] and diphosphinite[76] ligands, fig 1.7, have been used to catalyse the transfer hydrogenation of acetophenone, scheme 1.6.

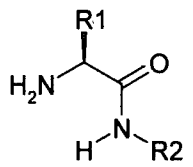

1.25

R1 = Me, iPr, Bz, sec-Bu

R2 = alkyl, Ar

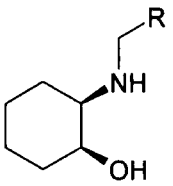

1.26

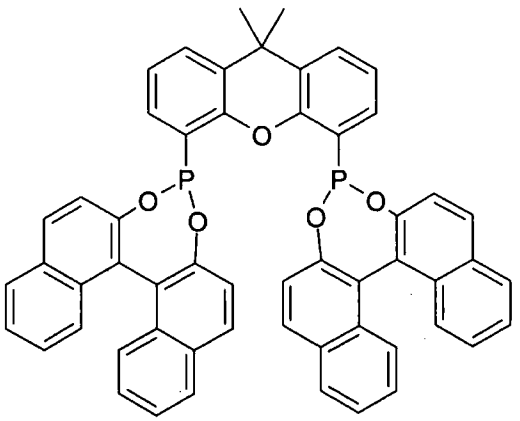

1.27

Figure 1.7: Ligands that coordinate Ru half-sandwich complexes for the catalysis of the transfer hydrogenation of acetophenone.

While studies involving the amino amide ligands, **1.25**, around the active Ru centre[74] show relatively good conversion yields of up to 98 % after a reaction time of just 15 minutes, the diastereoselectivity of the catalyst is poor with enantiomeric excess (ee) values no higher than 30 % typically. The study did allow for catalytic intermediates to be ascertained by means of electro-spray ionization mass spectrometry (ESI-MS), and confirmed a similar proton transfer mechanism as Noyori's catalyst. The aminocyclohexanol derived catalysts, **1.26**,[75] generally give good yields within 3 hours at room temperature, but still struggle to obtain enantiopure products with ee values in the region of 50 %.

Some increase in enantioselectivity is observed when the substituents were placed trans to one another on the cyclohexyl ring and in particular the isopropyl-amine derivative produces 94 % conversion with an ee of 92 % in favour of the S-enantiomer product. The diphosphinite[76] ligand, **1.27**, has to date proved the most successful, and under idealized conditions hydrogenates acetophenone to 99 % conversion with ee of 99 %. These results were obtained over a relatively long period of 22 hours in comparison to the more efficient amino amide catalyst.

Orthometallation of amines with late transition metal complexes has been demonstrated with Pt(II), Rh(II)[77] and Ir(II), and cyclometallation with Ru(II).[78] This methodology has been used to produce well-defined amino cyclometallated ruthenium catalysts for the transfer hydrogenation of acetophenone, fig 1.8.[79]

a)

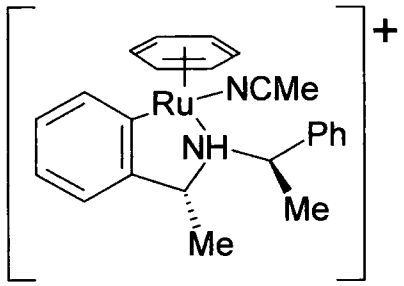

1.28

b)

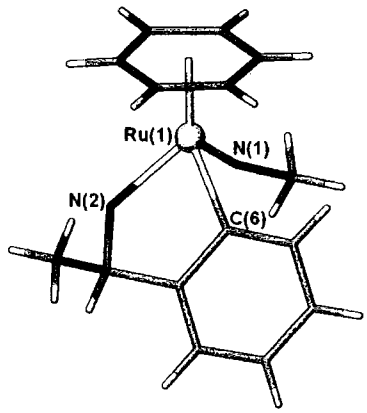

Figure 1.8: a) orthometallated Ru amine complex, and b) molecular structure of the ethylamine analogue.[79]

The catalyst, **1.28**, displays good efficiency with the best performing system obtaining 95 % conversion in 2 hours, but some enantioselectivity is lost, reaching an ee of 85 %.

Ruthenium(II) arene β-diketimite complexes have recently been prepared, and by extraction of chloride ion, a $[Ru(\eta^6\text{-}C_6H_6)(\beta\text{-diketimite})]^+$ complex with one vacant site has been formed, scheme 1.7.[80] This permits the unusual binding of ethylene, acetylene and dihydrogen as shown in scheme 1.7. Each structure was confirmed by X-ray crystallography, and is representive of species present during the catalytic hydrogenation of styrene. Other examples of hydrogenation catalysis include using the Noyari catalyst to hydrogenate a cyclic ketone in halohydrins up to ee of 99 %,[81] using a ruthenium half-sandwich coordinated with two 1,3,5-triaza-7-phosphaadamantane (PTA) ligands for the selective hydrogenation of the double bond in benzylidene acetone,[82] Cp*Ru(P,N) catalysts for the isomerisation of allylic alcohols[83] and the use of a Ru half-sandwich complex coordinated to an ethylenediamine derivative as an artificial metalloenzyme for transfer hydrogenation reactions.[84]

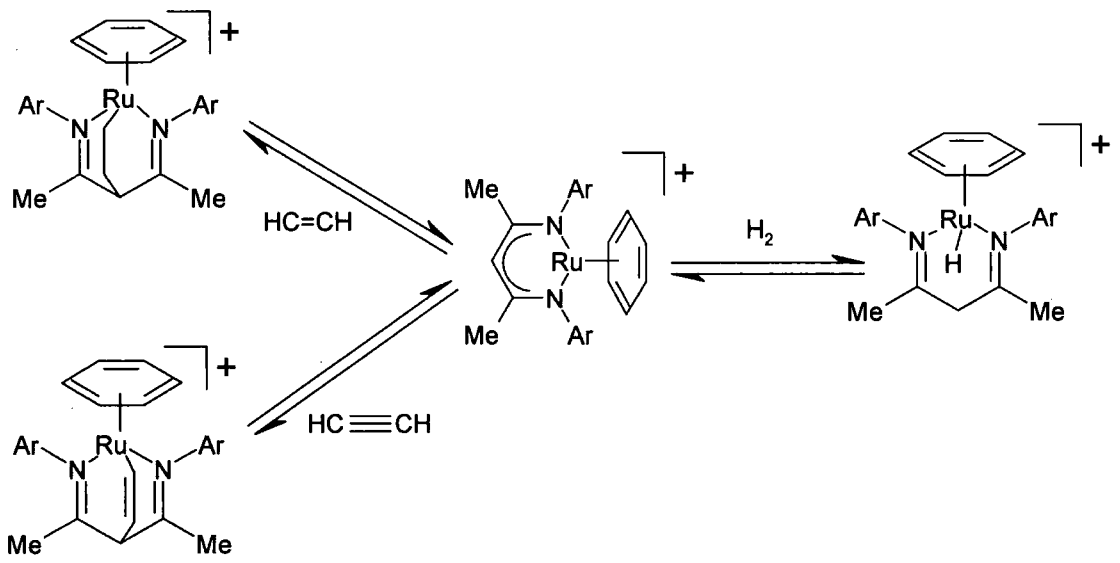

Scheme 1.7: Reaction scheme of [Ru(benzene)(β -diketimite)]$^+$ complex with dihydrogen, ethylene and acetylene.[80]

It should also be noted that ruthenium half sandwich complexes may be used in ring opening methathesis polymerisations (ROMPs),[85] as well as ring closing metathesis catalysts.[86] A systematic study of the catalysis of the polymerisation of styrene by [Ru(arene)(phosphine)] complexes has shown that steric bulk of both phosphine ligands and arene ligands is the greatest influence on the TOF and efficiency of the catalyst.

1.3.2.3 Biological Applications

Ruthenium half-sandwich complexes have also proved important in biological and medicinal applications. Their role as pharmaceuticals has been reviewed recently.[87] Studies of the binding ability of ruthenium complexes to biologically important molecules such as nucleic acids, nucleosides and DNA have attracted interest as they have been shown to be cytotoxic towards ovarian cancer cells.[88] The interaction of Ru half-sandwich complexes of type $[Ru(arene)(en)Cl]^+$ where en = ethylenediamine, arene = biphenyl (Bip), tetrahydoranthracene (THA), dihydroanthracene (DHA), *p*-cymene (η^6-$C_6H_4MeCH(Me)_2$) or benzene (Ben) towards DNA has been studied. The results suggest that there is strong preferential binding to the guanine residue in the DNA double helix, which acts to disrupt and inhibit the DNA replication process.[89] To further understand the interaction with

DNA, the binding of these anti-tumour complexes to nucleic acids was studied. The complexes show great selectivity towards guanosine over other nucleic acids, binding to the ruthenium through one of the cyclic nitrogen atoms, N7, of cyclic guanosine monophosphate (cGMP), fig. 1.9a.[90]

a)

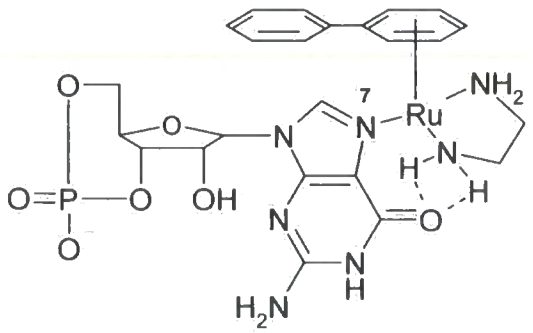

1.29

b)

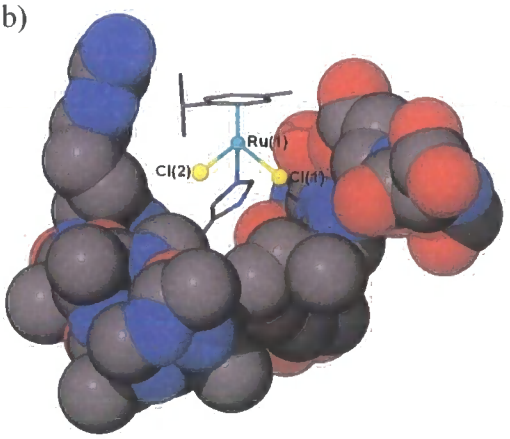

Figure 1.9: a) coordination of cGMP to $[Ru(arene)(en)]^{2+}$ with favourable H-bond interactions between the coordinated ethylenediamine NH protons and the exocyclic nucleic acid oxygen,[90] and b) fragment of X-ray crystal structure of $[Ru(\eta^6\text{-}C_6H_4MeCH(Me)_2)(lysozyme)Cl_2]$ showing coordination of the protein histidine residue to the Ru within a protein fold.[91]

The selectivity arises from complementary and favourable hydrogen bonding between the ethylenediamine NH protons and the exocyclic oxygen atom in guanosine. It was also found that increasing the size of the coordinated arene ligand, enhanced the binding of nucleic acids to ruthenium complexes.[90]

Ruthenium half-sandwich complexes can similarly bind to proteins and enzymes, and of note is the recent publication of the 1.6 Å X-ray crystal structure of $[(\eta^6\text{-}C_6H_4MeCH(Me)_2)Ru(lysozyme)Cl_2]$, the first Ru(II) half-sandwich arene protein complex to be added to the protein data bank (PDB).[91] The ruthenium is bound to the nitrogen atom of the imidazole ring of the only histidine residue of the protein, as seen in figure 1.9b.

1.3.2.4 Supramolecular Applications

The supramolecular "self-assembly" of metal half-sandwich complexes into squares and boxes has been reported recently.[92,93] However, the use of ruthenium(II) half-sandwich structures to form supramolecular structures is rare.

Amino-substituted 3-hydroxy-2-pyridone ligands, **1.30-1.33**, have been reacted with Rh, Ir and Ru arene half-sandwich complexes to form monomeric complexes in aqueous solutions.[94] However, upon addition of base, the complexes form trimeric self-assembly complexes, **1.34-1.37**, scheme 1.8. The trimeric structures show host properties towards Li^+ ions incorporating one cation into the cavity of the structure. The association constant for the cation binding is determined by ^1H NMR spectroscopy, and the highest binding constant is found for **1.36**, the ruthenium complex with **1.32** of K_a = 5.8 x 10^4 M^{-1} using 2 equivalents of CsOH as base in aqueous solution. There is also a 10,000:1 selectivity for Li^+ over the larger Na^+ due to the small cavity size created by the trimeric structure, as observed by X-ray crystallography. Interestingly, the solid state structures of the monomeric complexes, which are chiral at the metal centre, hydrogen bond with their opposite enantiomers. This occurs in all three structures, which possess hydrogen bonding groups.

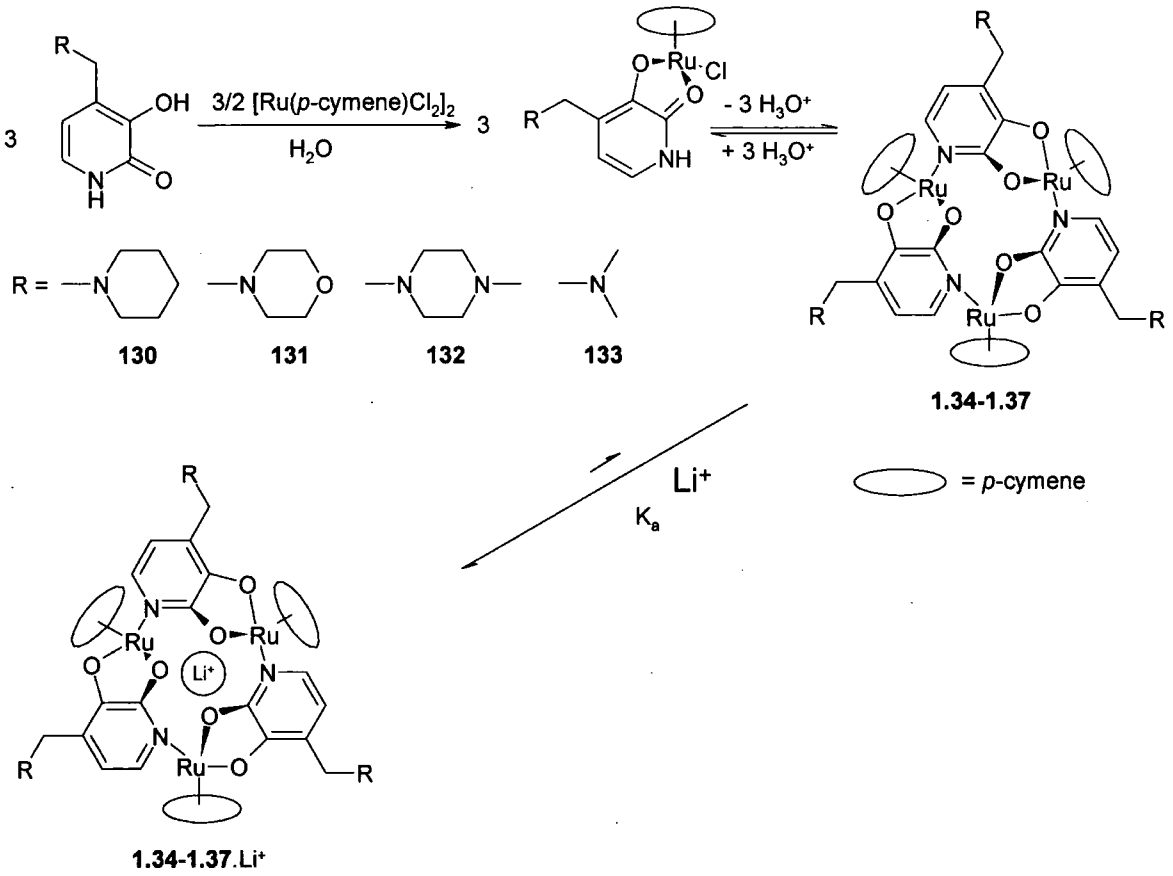

Scheme 1.8: formation of trimeric ruthenium half-sandwich macrocycles, which can selectively bind lithium ions.[94]

One study incorporates a common crystal engineering motif, a carboxylic acid,[95-97] into simple phosphorus-donor ligand designs.[98] Reaction of the phosphine ligands with the chloride bridged $[\{Ru(\eta^6\text{-}C_6H_4MeCH(Me)_2)Cl(\mu\text{-}Cl)\}_2]$ starting material affords the expected half-sandwich complexes $[(\eta^6\text{-}p\text{-cymene})Ru(L)Cl_2]$ where L = $Ph_2PCH_2NHC_6H_4(2\text{-}CO_2H)$ (**1.38a**), $Ph_2PCH_2NHC_6H_4(3\text{-}CO_2H)$ (**1.38b**), $Ph_2PCH_2NHC_6H_3(3\text{-}CO_2H)(6\text{-}OCH_3)$ (**1.38c**), $Ph_2PCH_2NHC_6H_4(4\text{-}CO_2H)$ (**1.38d**), $Ph_2PCH_2NHC_6H_3(2\text{-}CO_2H)(4\text{-}OH)$ (**1.38e**), $Ph_2PCH_2NHC_6H_3(3\text{-}OH)(4\text{-}CO_2H)$ (**1.38f**), $Ph_2PCH_2NHC_6H_3(2\text{-}CO_2H)(5\text{-}CO_2H)$ (**1.38g**) and Ph_2PCH_2OH (**1.38h**).

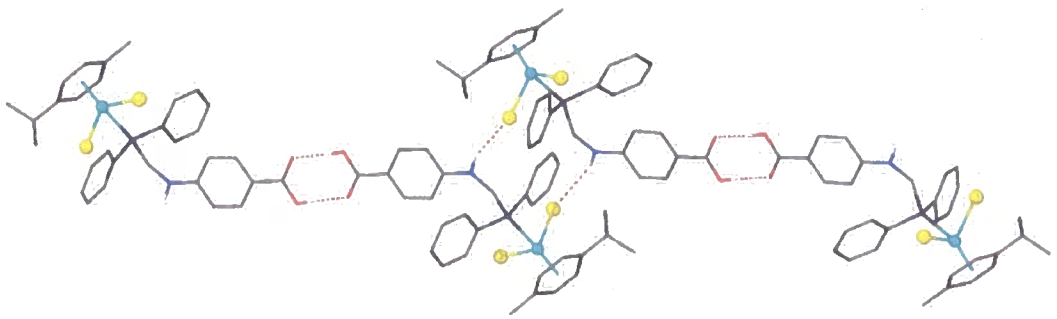

Figure 1.10: X-ray crystal structure of $[Ru(\eta^6\text{-}p\text{-cymene})(1.38d)Cl_2]$ showing carboxylic acid head-to-tail hydrogen bonding between ligands and intermolecular NH···Cl hydrogen bonding. Only O-H and N-H hydrogen atoms have been shown for clarity.[98]

The expected hydrogen bonding dimer formation of the carboxylic acid groups is found for all except one carboxylic acid species, but the position and nature of the other substituents of the aryl ring affects the 3-D assembly beyond this motif. So for the simplest ligand system (**1.38a**) just the head to tail dimer is observed. The intramolecular hydrogen bonding between the amino NH and the carbonyl oxygen atom prevents any further intermolecular interactions. However, by moving the carboxylic acid away from the amino group it allows the NH to interact with solvent (**1.38b**) and chloride ligands coordinated to other ruthenium complexes (**1.38d**, **1.38f**), fig 1.10. Further functionality on the aryl ring such as hydroxyl groups (**1.38e**, **1.38f**) and another carboxylic acid group (**1.38g**) produces further intermolecular interactions between these groups and the chloride ligands of other complexes.

Ruthenium half-sandwich complexes have also been utilized as anion receptors.[99] 2,2'-Biimidazole (biim) possesses two NH proton donors that are known to act as receptors to anions, in a similar way to ureas and thioureas, for example.[100-

[106] However, it is generally insoluble due to strong self-association, which makes it unsuitable for anion recognition. While functionalizing biim with organic substituents will alter its solubility and produce interesting solid-state structures[107] and render it able to interact with anions in solution,[108] there are several advantages to coordinating biim to a metal centre for the application of anion sensing. First, coordination locks the ligand into a *syn* conformation so that the NH binding functionalities are preorganised in solution. Second, the coordination will suppress self-association, and thus reduce competition for the anion. Furthermore, the polarization of the NH bonds will be enhanced to form better hydrogen bond acceptors, and finally the presence of the cationic metal centre will add columbic attraction, figure 1.11a.

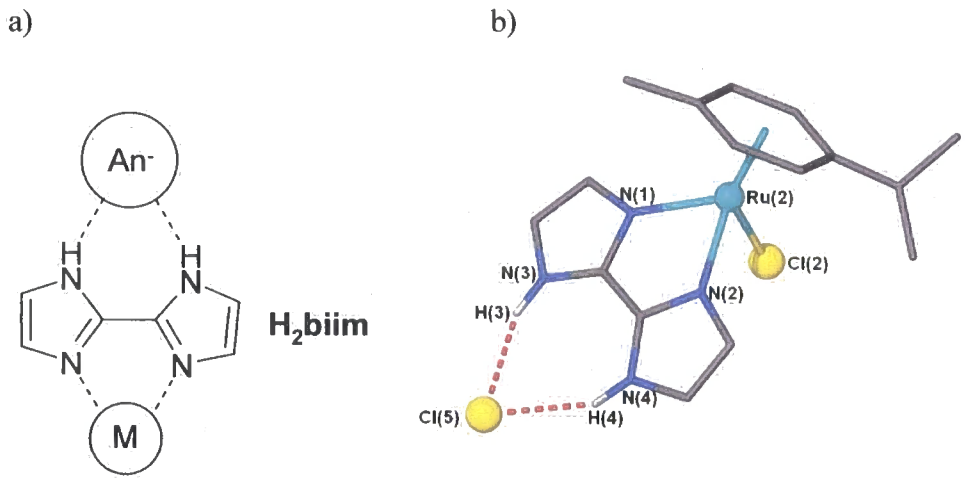

Figure 1.11: a) schematic structure of 2,2'-biimidazole showing how coordination to a metal may lock conformation and enhance anion binding, and b) X-ray crystal structure of $[RuCl(cym)(H_2biim)]^+Cl^-$ showing the chloride anion binding.[99]

Therefore Morales and co-workers[99] have recently used the easily prepared and readily soluble Ru(II) half-sandwich complex $[RuCl(\eta^6\text{-}C_6H_4MeCH(Me)_2)(H_2biim)]^+$ (**1.39**) cation as an anion receptor with success. ^1H NMR spectroscopic titrations of the complex with monoanions in CD_3CN and DMSO-d_6 have shown that the complex binds anions in a 1:1 fashion with the strongest binding occurring with HSO_4^- with an association constant of K = 5920 M^{-1} in CD_3CN. The NH signals in CD_3CN broadened in the presence of less than equimolar quantities of chloride anions, indicating a very strong association. Therefore the titrations were repeated in DMSO-d_6 and binding was observed for chloride anions with an association constant of K_a = 970 M^{-1}. The anion binding adducts of chloride and nitrate anions were characterised

by X-ray crystallography, showing the binding of both of the NH groups to each anion, and the crystal structure of the chloride adduct is shown in Figure 1.11b. The anion binding ability of these Ru complexes appears to be enhanced over the organic analogues of Causey and Allen,[108] as the organic binding studies were performed in the less polar and thus less competitive solvent of dichloromethane, compared to the Ru complex studies in DMSO. This metal-enhancement of anion receptors has been observed before in the study of metal enhanced anion binding by ureas and thioureas.[109] Anion binding complexes that have a Ag(I) ion bound within a NS_2O_2 crown ether with a urea or thiourea lariat arm sulphur bound to the silver atom display enhanced anion binding over the neutral organic analogue.

1.4 Solid-support metal scavengers

There have been many functional groups incorporated into porous polymers for the use as selective coordinating ion exchange resins.[110] An importance use of metal scavenging resins is the treatment of water for the removal harmful metal ions, such as Cu, Ni, Co, Cd.[111,112] The removal of Hg(II) is of particular importance, and a few recent examples selectively bind Hg over other metals. By grafting poly(acrylamide) side chains onto solid polymer particles, rapid removal of mercury from aqueous solutions can be effected.[113] The mercury is predominantly bound by diamido-mercury linkages, which cross-link the side chains. The uptake of mercury is large and fast with an overall adsorption of 3.6 mmol g^{-1} at a rate of 1.1 x 10^{-3} s^{-1}. The mercury-amide cross-links may be broken with hot acetic acid, with removal of all of the mercury as mercury acetate. The mercury sorption was found to be highly selective over other metal cations such as Fe(III), Cd(II), Zn(II) and Pb(II). A related carbazide (NH-NH-C(=O)-NH) functionality immobilized on a sol-gel also effectively and selectively removes mercury from aqueous solutions.[114]

The work of Driessen and co-workers[115-122] on multidentate amine resins for the recovery of metals is among the most detailed. Benzimidazole ligands incorporated into resins and immobilized on silica are effective at ligating copper(II) in aqueous solutions in competition with other metal cations such as Ni(II), Co(II), Cd(II) and Zn(II).[115-117] Silica-based chelating N,S donor ion-exchangers, **1.40, 1.41**, were developed for the recovery of rhodium-containing catalysts.[119] The ion-

exchangers displayed a selectivity for Rh(III) over Cu(II) in the form of $RhCl_3.3H_2O$, but the Rh(I) complex, $RhCl(PPh_3)_3$ was adsorbed less effectively due to the steric bulk of the triphenylphosphine ligands. Decomplexation of the polymers was found to be difficult due to the strong Rh-S association, but a reasonable amount of Rh(III) could be stripped using thiourea.

To avoid the difficult decomplexation issues, polyamine resins, **1.42, 1.43a-h**, have been developed for the extraction of Rh-containing catalysts.[118,120-122]

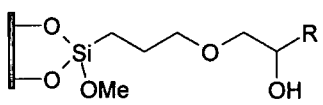

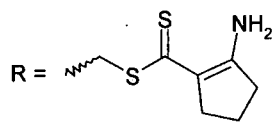

1.40

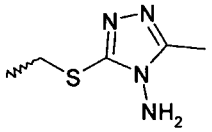

1.41

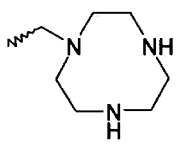

1.42

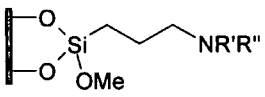

1.43a = R' = R" = H
1.43b = R' = R" = Me
1.43c = R' = H, R" = $(CH_2)_2NH_2$
1.43d = R' = H, R" = $(CH_2)_3NH_2$
1.43e = R' = H, R" = $(CH_2)_2N(Me)_2$
1.43f = R' = Me, R" = $(CH_2)_2N(Me)_2$
1.43g = R' = Et, R" = $(CH_2)_2N(Et)_2$
1.43h = R' = H, R" = $(CH_2)_2N(CH_2)_2NH_2$

Most adsorption of Rh^{3+} by these amine based scavengers was found in ethanolic solutions with the moderately bulky **1.43f**, but recovery was only slightly lower from aqueous solution, and in 1 M HCl solutions, the adsorption was significantly lowered, as amine protonation disfavours cation binding. Based on these considerations, up to 90 % decomplexation of Rh from the solid-support was achieved with 2 M HNO_3.

The removal of catalysts and corrosion metals from industrial process streams is a purification and cost-recovery problem. There have been several patents published recently that use differing methods to solve the problem: one method is to mix the product stream containing the catalyst in solution with another solvent, such as alcohol or water, in order to precipitate the catalyst.[123-125] This method has several problems though, as further purification of the product stream to remove additional solvent may be required, and purification of the precipitate may be required as it may contain corrosion metal impurities. Another patent describes a method for recovering catalyst from a slurry of residual hydrocarbons by vapourising the hydrocarbons.[126] These methods may require a great deal of adaptation of processing equipment and may slow the processing down, and thus become uneconomical.

A simpler and more effective way to recover the catalyst would be to use a solid-supported metal scavenger that may be introduced to one section of the process stream, and removed by filtration. Ion-exchange resins have recently been used for the purpose of removing corrosion metal such as Fe, Cr, and Ni,[127] and Ir and Ru catalysts[128] from an acetic acid product stream of the Cativa™ process. The catalysts are removed by a thiourea based resin Lewatit™ TP214.

Recently, a dithiocarbamate derived lipophilic cellulose has been designed for the extraction of platinum group metal (PGM) and Cu ions.[129] The natural product derivative is selective for Cu(II) ions over Ni(II) and Zn(II) cations, especially at pH values above 4. It is less selective between the PGMs, however. While good adsorption of Pt(IV), Rh(III) and Pd(II) is achieved successfully in single metal ion solutions, both Pd(II) and Rh(III) is adsorbed from a solution containing both cations, with a slight preference for Pd(II).

It has been shown that although metal-thiourea chemistry has been known for a long time, binding modes other than through the sulphur atom alone have not been fully explored. In particular, there has been little development in the area of bisthiourea coordination. While ruthenium(II) half-sandwich complexes have been well studied and their chemistry established, the complexes are extremely versatile and may be applied to many areas. Subsequently, there has been much interest in ruthenium half-sandwich complexes in terms of novel binding modes, chirality, catalysis, biological and supramolecular applications. Extensive use of platinum group metals in catalysis has led to a need to recover and reuse costly catalytic metals. A variety of functional groups have been incorporated into solid-supports for the efficient and selective recovery of a variety of metals.

Aims

Given the success of thiourea functionalised Lewatit TP214 in the extraction of platinum group metals from a mixed metal acetic acid solution from the Cativa™ process, this research hopes to build on this success by incorporating bisthiourea functionalities into a resin. This resin will be tested for its efficiency and selectivity of

platinum group metal uptake. To better understand the interactions of the bis(thioureido) resin with platinum group metals, small molecule bisthiourea analogues will be developed and reacted with platinum group metals. The synthesis, anion binding of the bisthiourea ligands and solid state hydrogen bonding interactions will be discussed, before discussing the coordination to PGMs, and metal salt extraction experiments with the polymer analogues.

1.5 References

(1) Pearson, R. G. *Chemical Hardness: Applications from Molecules to Solids*; Wiley-VCH, Weinheim, **1997**.

(2) Livingstone, S. E. *Q. Rev. Chem. Soc.* **1965**, *19*, 386.

(3) Lane, T. J.; C., C. S.; Yamaguchi, A.; Quagliano, J. V.; Ryan, J. A.; Mizushima, S. *J. Am. Chem. Soc.* **1959**, *81*, 3824.

(4) Schafer, M.; Curran, C. *Inorg. Chem.* **1966**, *5*, 265.

(5) Gosavi, R. K.; Agarwala, U.; Rao, C. N. R. *J. Am. Chem. Soc.* **1967**, *89*, 235.

(6) Gosavi, R. K.; Rao, C. N. R. *J. Inorg. Nucl. Chem.* **1967**, *29*, 1937.

(7) Kunchur, N. R.; Truter, M. R. *J. Chem. Soc.* **1958**, 2551.

(8) Nardelli, M.; Fava, G. *Acta Crystallogr.* **1959**, *12*, 727.

(9) Cavalca, L.; Nardelli, M.; Fava, G. *Acta Crystallogr.* **1960**, *13*, 125.

(10) Nardelli, M.; Gasparri, G. F.; Boldrini, P. *Acta Crystallogr.* **1965**, *18*, 618.

(11) Ooi, S.; Kawase, T.; Nakatsu, K.; Kuroya, H. *Bull. Chem. Soc. Jpn.* **1960**, *33*, 861.

(12) Berta, D. A.; Spofford, W. A.; Boldrini, P.; Amma, E. L. *Inorg. Chem.* **1970**, *9*, 136.

(13) Okaya, Y.; Knobler, C. B. *Acta Crystallogr.* **1964**, *17*, 928.

(14) Vranka, R. G.; Amma, E. L. *J. Am. Chem. Soc.* **1966**, *88*, 4270.

(15) O'Connor, J. E.; Amma, E. L. *Chem. Commun.* **1968**, 892.

(16) Hall, D. D.; Horrocks, W. D. *Inorg. Chem.* **1969**, *8*, 1809.

(17) O'Connor, J. E.; Amma, E. L. *Inorg. Chem.* **1969**, *8*, 2367.

(18) Luth, H.; Truter, M. R. *J. Chem. Soc. A.* **1968**, 1879.

(19) Weininge, M. S.; O' Connor, J. E.; Amma, E. L. *Inorg. Chem.* **1969**, *8*, 424.

(20) Adams, D. M.; Smardzew, R. R. *J. Chem. Soc. A.* **1971**, 10.

(21) Gabriele, B.; Salerno, G.; Costa, M.; Chiusoli, G. P. *J. Organomet. Chem.* **1995**, *503*, 21.

(22) Bonardi, A.; Costa, M.; Gabriele, B.; Salerno, G.; Chiusoli, G. P. *J. Chem. Soc., Chem. Commun.* **1994**, 2429.

(23) Costa, M.; De Souza Santos, L.; Chiusoli, G. P.; Gabriele, B.; Salerno, G. *J. Mol. Cat.* **1993**, *78*, 151.

(24) Dai, M. J.; Wang, C. H.; Dong, G.; Xiang, J.; Luo, T.; Liang, B.; Chen, J.; Yang, Z. *Eur. J. Org. Chem.* **2003**, *2003*, 4346.

(25) Dai, M. J.; Liang, B.; Wang, C. H.; Chen, J. H.; Yang, Z. *Org. Lett.* **2004**, *6*, 221.

(26) Dai, M. J.; Liang, B.; Wang, C.; You, Z.; Xiang, J.; Dong, G.; Chen, J.; Yang, Z. *Adv. Synth. Cat.* **2004**, *346*, 1669.

(27) Chen, W.; Li, R.; Han, B.; Li, B. J.; Chen, Y. C.; Wu, Y.; Ding, L. S.; Yang, D. *Eur. J. Org. Chem.* **2006**, 1177.

(28) Cauzzi, D.; Lanfranchi, M.; Marzolini, G.; Predieri, G.; Tiripicchio, A.; Costa, M.; Zanoni, R. *J. Organomet. Chem.* **1995**, *488*, 115.

(29) Cauzzi, D.; Costa, M.; Gonsalvi, L.; Pellinghelli, M. A.; Predieri, G.; Tiripicchio, A.; Zanoni, R. *J. Organomet. Chem.* **1997**, *541*, 377.

(30) Cauzzi, D.; Costa, M.; Cucci, N.; Graiff, C.; Grandi, F.; Predieri, G.; Tiripicchio, A.; Zanoni, R. *J. Organomet. Chem.* **2000**, *593-594*, 431.

(31) Zhang, T. Y.; Allen, M. J. *Tetrahedron Lett.* **1999**, *40*, 5813.

(32) Okeya, S.; Fujiwara, Y.; Kawashima, S.; Hayashi, Y.; Isobe, K.; Nakamura, Y.; Shimomura, H.; Kushi, Y. *Chem. Lett.* **1992**, 1823.

(33) Henderson, W.; Kemmitt, R. D. W.; Mason, S.; Moore, M. R.; Fawcett, J.; Russell, D. R. *J. Chem. Soc., Dalton Trans.* **1992**, 59.

(34) Bodensieck, U.; Carraux, Y.; Stoeckli-Evans, H.; Suss-Fink, G. *Inorg. Chim. Acta* **1992**, *195*, 135.

(35) Henderson, W.; Nicholson, B. K.; Rickard, C. E. F. *Inorg. Chim. Acta* **2001**, *320*, 101.

(36) Henderson, W.; Nicholson, B. K.; Dinger, M. B.; Bennett, R. L. *Inorg. Chim. Acta* **2002**, *338*, 210.

(37) Robinson, S. D.; Sahajpal, A.; Steed, J. W. *Inorg. Chim. Acta* **2000**, *306*, 205.

(38) Henderson, W.; Nicholson, B. K.; Dinger, M. B. *Inorg. Chim. Acta* **2003**, *355*, 428.

(39) Dinger, M. B.; Henderson, W.; Nicholson, B. K.; Wilkins, A. L. *J. Organomet. Chem.* **1996**, *526*, 303.

(40) Shen, X.; Shi, X.; Kang, B.; Liu, Y.; Tong, Y.; Jiang, H.; Chen, K. *Polyhedron* **1998**, *17*, 4049.

(41) Marek, J.; Kopel, P.; Travnicek, Z. *Acta Crystallogr. Sect. C.* **2003**, *59*, M558.

(42) Henderson, W.; Rickard, C. E. F. *Inorg. Chim. Acta* **2003**, *343*, 74.

(43) Henderson, W.; Nicholson, B. K.; Tiekink, E. R. T. *Inorg. Chim. Acta* **2006**, *359*, 204.

(44) Lipowska, M.; Hansen, L.; Taylor, A.; Marzilli, L. G. *Inorg. Chem.* **1996**, *35*, 4484.

(45) Lipowska, M.; Hayes, B. L.; Hansen, L.; Taylor, A.; Marzilli, L. G. *Inorg. Chem.* **1996**, *35*, 4227.

(46) Fischer, E. O.; Bottcher, R. *Z. Anorg. Chem.* **1957**, *291*, 305.

(47) Fischer, E. O.; Fritz, H. P. *Angew. Chem. Int. Ed.* **1961**, *73*, 353.

(48) Fischer, E. O.; Elschenb.C *Chem. Berichte* **1970**, *103*, 162.

(49) Winkhaus, G.; Singer, H. *J. Organomet. Chem.* **1967**, *7*, 487.

(50) Zelonka, R. A.; Baird, M. C. *J. Organomet. Chem.* **1972**, *35*, C43.

(51) Bennett, M. A.; Smith, A. K. *J. Chem. Soc., Dalton Trans.* **1974**, 233.

(52) Zelonka, R. A.; Baird, M. C. *J. Organomet. Chem.* **1972**, *44*, 383.

(53) Zelonka, R. A.; Baird, M. C. *Can. J. Chem.* **1972**, *50*, 3063.

(54) J. Thompson, S.; White, C.; M. Maitlis, P. *J. Organomet. Chem.* **1977**, *136*, 87.

(55) Thompson, S. J.; White, C.; Maitlis, P. M. *J. Organomet. Chem.* **1977**, *136*, 87.

(56) White, C.; Thompson, S. J.; Maitlis, P. M. *J. Chem. Soc., Dalton Trans.* **1977**, 1654.

(57) White, C.; Thompson, S. J.; Maitlis, P. M. *J. Organomet. Chem.* **1977**, *134*, 319.

(58) Bennett, M. A.; Matheson, T. W. *J. Organomet. Chem.* **1979**, *175*, 87.

(59) Robertson, D. R.; Stephenson, T. A. *J. Organomet. Chem.* **1976**, *107*, C46.

(60) Crabtree, R. H.; J. Pearman, A. *J. Organomet. Chem.* **1977**, *141*, 325.

(61) Bennett, M. A.; Huang, T. N.; Smith, A. K.; Turney, T. W. *J. Chem. Soc., Chem. Commun.* **1978**, 582.

(62) Dersnah, D. F.; Baird, M. C. *J. Organomet. Chem.* **1977**, *127*, C55.

(63) Bennett, M. A. *Coord. Chem. Rev.* **1997**, *166*, 225.

(64) Ganter, C. *Chem. Soc. Rev.* **2003**, *32*, 130.

(65) Pinto, P.; Marconi, G.; Heinemann, F. W.; Zenneck, U. *Organometallics* **2004**, *23*, 374.

(66) García-Fernández, A.; Gimeno, J.; Lastra, E.; Madrigal, C.; Graiff, C.; Tiripicchio, A. *Eur. J. Inorg. Chem.* **2007**, *2007*, 732.

(67) Mishra, H.; Mukherjee, R. *J. Organomet. Chem.* **2006**, *691*, 3545.

(68) Tocher, D. A.; Drew, M. G. B.; Nag, S.; Pal, P. K.; Datta, D. *Chem. Eur. J.* **2007**, *13*, 2230.

(69) Cadierno, V.; Crochet, P.; Diez, J.; Garcia-Alvarez, J.; Garcia-Garrido, S. E.; Gimeno, J.; Garcia-Granda, S.; Rodriguez, M. A. *Inorg. Chem.* **2003**, *42*, 3293.

(70) Ohkuma, T.; Ooka, H.; Hashiguchi, S.; Ikariya, T.; Noyori, R. *J. Am. Chem. Soc.* **1995**, *117*, 2675.

(71) Ohkuma, T.; Ishii, D.; Takeno, H.; Noyori, R. *J. Am. Chem. Soc.* **2000**, *122*, 6510.

(72) Ohkuma, T.; Koizumi, M.; Muniz, K.; Hilt, G.; Kabuto, C.; Noyori, R. *J. Am. Chem. Soc.* **2002**, *124*, 6508.

(73) Noyori, R. *Angew. Chem. Int. Ed.* **2002**, *41*, 2008.

(74) Pelagatti, P.; Carcelli, M.; Calbiani, F.; Cassi, C.; Elviri, L.; Pelizzi, C.; Rizzotti, U.; Rogolino, D. *Organometallics* **2005**, *24*, 5836.

(75) Schiffers, I.; Rantanen, T.; Schmidt, F.; Bergmans, W.; Zani, L.; Bolm, C. *J. Org. Chem.* **2006**, *71*, 2320.

(76) Reetz, M. T.; Li, X. *J. Am. Chem. Soc.* **2006**, *128*, 1044.

(77) Gaw, K. G.; Slawin, A. M. Z.; Smith, M. B. *Organometallics* **1999**, *18*, 3255.

(78) Davies, D. L.; Al-Duaij, O.; Fawcett, J.; Giardiello, M.; Hilton, S. T.; Russell, D. R. *Dalton Trans.* **2003**, 4132.

(79) Sortais, J.-B.; Ritleng, V.; Voelklin, A.; Holuigue, A.; Smail, H.; Barloy, L.; Sirlin, C.; Verzijl, G. K. M.; Boogers, J. A. F.; deVries, A. H. M.; deVries, J. G.; Pfeffer, M. *Org. Lett.* **2005**, *7*, 1247.

(80) Phillips, A. D.; Laurenczy, G.; Scopelliti, R.; Dyson, P. J. *Organometallics* **2007**, *26*, 1120.

(81) Ros, A.; Magriz, A.; Dietrich, H.; Fernandez, R.; Alvarez, E.; Lassaletta, J. M. *Org. Lett.* **2006**, *8*, 127.

(82) Mebi, C. A.; Frost, B. J. *Organometallics* **2005**, *24*, 2339.

(83) Ito, M.; Kitahara, S.; Ikariya, T. *J. Am. Chem. Soc.* **2005**, *127*, 6172.

(84) Letondor, C.; Pordea, A.; Humbert, N.; Ivanova, A.; Mazurek, S.; Novic, M.; Ward, T. R. *J. Am. Chem. Soc.* **2006**, *128*, 8320.

(85) Jan, D.; Delaude, L.; Simal, F.; Demonceau, A.; Noels, A. F. *J. Organomet. Chem.* **2000**, *606*, 55.

(86) Furstner, A.; Picquet, M.; Bruneau, C.; Dixneuf, P. H. *Chem. Commun.* **1998**, 1315.

(87) Clarke, M. J. *Coord. Chem. Rev.* **2002**, *232*, 69.

(88) Morris, R. E.; Aird, R. E.; del Socorro Murdoch, P.; Chen, H.; Cummings, J.; Hughes, N. D.; Parsons, S.; Parkin, A.; Boyd, G.; Jodrell, D. I.; Sadler, P. J. *J. Med. Chem.* **2001**, *44*, 3616.

(89) Novakova, O.; Chen, H.; Vrana, O.; Rodger, A.; Sadler, P. J.; Brabec, V. *Biochemistry* **2003**, *42*, 11544.

(90) Chen, H.; Parkinson, J. A.; Morris, R. E.; Sadler, P. J. *J. Am. Chem. Soc.* **2003**, *125*, 173.

(91) McNae, I. W.; Fishburne, K.; Habtemariam, A.; Hunter, T. M.; Melchart, M.; Wang, F. Y.; Walkinshaw, M. D.; Sadler, P. J. *Chem. Commun.* **2004**, 1786.

(92) Yamamotoa, Y.; Suzuki, H.; Tajima, N.; Tatsumi, K. *Chem. Eur. J.* **2002**, *8*, 372.

(93) Klausmeyer, K. K.; Rauchfuss, T. B.; Wilson, S. R. *Angew. Chem. Int. Ed.* **1998**, *37*, 1694.

(94) Grote, Z.; Scopelliti, R.; Severin, K. *J. Am. Chem. Soc.* **2004**, *126*, 16959.

(95) Emsley, J. *Chem. Soc. Rev.* **1980**, *9*, 91.

(96) Vishweshwar, P.; Beauchamp, D. A.; Zaworotko, M. J. *Cryst. Growth Des.* **2006**, *6*, 2429.

(97) Wenger, M.; Bernstein, J. *Angew. Chem. Int. Ed.* **2006**, *45*, 7966.

(98) Dann, S. E.; Durran, S. E.; Elsegood, M. R. J.; Smith, M. B.; Staniland, P. M.; Talib, S.; Dale, S. H. *J. Organomet. Chem.* **2006**, *691*, 4829.

(99) Ion, L.; Morales, D.; Perez, J.; Riera, L.; Riera, V.; Kowenicki, R. A.; McPartlin, M. *Chem. Commun.* **2006**, 91.

(100) Nishizawa, S.; Buhlmann, P.; Iwao, M.; Umezawa, Y. *Tetrahedron Lett.* **1995**, *36*, 6483.

(101) Santacroce, P. V.; Davis, J. T.; Light, M. E.; Gale, P. A.; Iglesias-Sanchez, J. C.; Prados, P.; Quesada, R. *J. Am. Chem. Soc.* **2007**, *129*, 1886.

(102) Gunnlaugsson, T.; Glynn, M.; Tocci (nee Hussey), G. M.; Kruger, P. E.; Pfeffer, F. M. *Coord. Chem. Rev.* **2006**, *250*, 3094.

(103) Filby, M. H.; Steed, J. W. *Coord. Chem. Rev.* **2006**, *250*, 3200.

(104) Turner, D. R.; Paterson, M. J.; Steed, J. W. *J. Org. Chem* **2006**, *71*, 1598.

(105) Filby, M. H.; Humphries, T. D.; Turner, D. R.; Kataky, R.; Kruusma, J.; Steed, J. W. *Chem. Commun.* **2006**, 156.

(106) Turner, D. R.; Smith, B.; Spencer, E. C.; Goeta, A. E.; Evans, I. R.; Tocher, D. A.; Howard, J. A. K.; Steed, J. W. *New J. Chem.* **2005**, *29*, 90.

(107) Allen, W. E.; Fowler, C. J.; Lynch, V. M.; Sessler, J. L. *Chem. Eur. J.* **2001**, *7*, 721.

(108) Causey, C. P.; Allen, W. E. *J. Org. Chem.* **2002**, *67*, 5963.

(109) Amendola, V.; Esteban-Gomez, D.; Fabbrizzi, L.; Licchelli, M.; Monzani, E.; Sancenon, F. *Inorg. Chem.* **2005**, *44*, 8690.

(110) Sahni, S. K.; Reedijk, J. *Coord. Chem. Rev.* **1984**, *59*, 1.

(111) Gorshkov, V.; Muraviev, D.; Warshawsky, A. *Solvent Extraction and Ion Exchange* **1998**, *16*, 1.

(112) Korngold, E.; Belayev, N.; Aronov, L.; Titelman, S. *Desalination* **2001**, *133*, 83.

(113) Bulbul Sonmez, H.; Senkal, B. F.; Bicak, N. *J. Polymer Sci. A* **2002**, *40*, 3068.

(114) Khan, A.; Mahmood, F.; Khokhar, M. Y.; Ahmed, S. *React. Funct. Polym.* **2006**, *66*, 1014.

(115) Sahni, S. K.; Driessen, W. L.; Reedijk, J. *Inorg. Chim. Acta* **1988**, *154*, 141.

(116) van Berkel, P. M.; Dijkstra, D. J.; Driessen, W. L.; Reedijk, J.; Sherrington, D. C. *React. Funct. Polym.* **1995**, *28*, 39.

(117) Hoorn, H. J.; deJoode, P.; Dijkstra, D. J.; Driessen, W. L.; Kooijman, H.; Veldman, N.; Spek, A. L.; Reedijk, J. *J. Mat. Chem.* **1997**, *7*, 1747.

(118) Kramer, J.; Garcia, A. R.; Driessen, W. L.; Reedijk, J. *Chem. Commun.* **2001**, 2420.

(119) Kramer, J.; Scholten, A.; Driessen, W. L.; Reedijk, J. *Inorg. Chim. Acta* **2001**, *315*, 183.

(120) Kramer, J.; Scholten, A.; Driessen, W. L.; Reedijk, J. *Eur. J. Inorg. Chem.* **2002**, 1488.

(121) Kramer, J.; Erkelens, J. A.; Garcia, A. R. A.; Driessen, W. L.; Reedijk, J. *New J. Chem.* **2002**, *26*, 822.

(122) Kramer, J.; Driessen, W. L.; Koch, K. R.; Reedijk, J. *Hydrometallurgy* **2002**, *64*, 59.

(123) Kondo, S.; Kawanaka, T.; T., M. *JP20020306161 20021021* 2004

(124) Makhanya, L. T.; Crause, C.; Phaho, D. S.; Grove, J. J. C. *WO2004IB00080 20040115* 2004

(125) Nitsuseki, H. H.; Inoue, T. T. *JP2006151890* 2006

(126) Spena, M. D.; Jack, D. S.; Fraenkel, D. *10/994,506* 2005

(127) Poole, A. D.; Smith, S. J. *GB 2004-10289* 2004

(128) Poole, A. D.; Smith, S. J. *GB 2004 - 11185* 2004

(129) Dhakal, R. P.; Inoue, K.; Ohto, K.; Baba, Y. *Chem. Lett.* **2006**, *35*, 1064.

Chapter 2: Bis(thiourea) ligand synthesis

2.1 Introduction

2.1.1 Thiourea synthesis

The synthesis of thiocarbimide functional groups from isothiocyanates was first utilised by Dyson and co-workers in the early 20th Century. By reacting an amine with thiophosgene, isothiocyanates may be generated,[1] which readily react with amines.[2-4] Transfer of an amino proton to the isothiocyanato group allows a reaction whereby no by-products are formed, and thus purification is simple. Isothiocyanato groups positioned on adjacent carbon atoms such as ortho-phenylene diisothiocyanate first produced by Billeter in 1887,[1] may form cyclised products with amines rather than bisthioureas.[5-7]

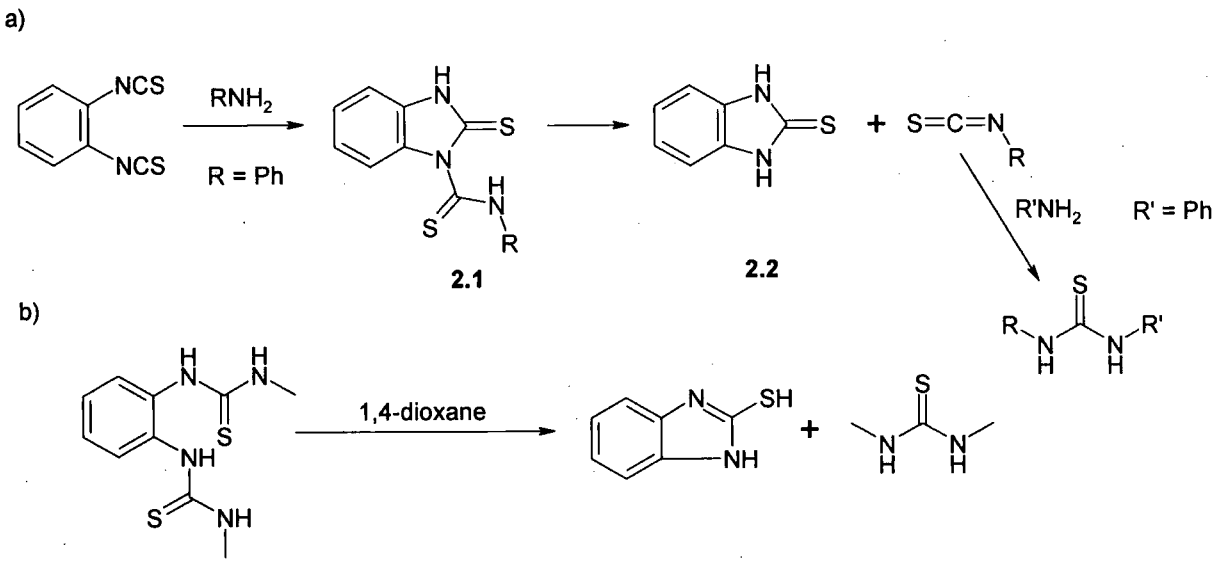

Scheme 2.1: a) reaction of o-phenyldiisothiocyanate with primary amines to form benzimidazoline-2-thione, and b) a similar cyclisation reaction observed from a bisthiourea.[7,8]

Nucleophilic attack by the unreacted isothiocyanate on the thiourea group generated initially gives the dithiocarbamide product (**2.1**), which then decomposes to benzimidazoline-2-thione (**2.2**), and an isothiocyanate, scheme 2.1. This isothiocyanate reacts with another amine molecule to yield the symmetrical thiourea derivative rather than the bisthiourea. Benzimidazoline-2-thione (**2.2**) may also be

generated from the cyclisation of bisthioureas.[8] In this reaction, the nitrogen lone pair of the thiourea group is nucleophilic enough to attack the thiocarbonyl carbon and instigate the cyclisation process. The similarity of the end products in both reactions should be noted.

2.1.2 Thiourea as anion sensors

The reaction of isothiocyanates with amines has been widely used to generate thioureas. These thiourea derived compounds have been used for metal coordination as discussed in Chapter 1.2, but more recently they have been used as anion sensors. A range of these compounds will be discussed in the following section.

One of the first anion binding thiourea compounds was formed by reaction of 1,4-bis(aminomethyl)benzene with butyl-isothiocyanate to form the *para* arranged bisthiourea, **2.3**.[9] This molecule shows an affinity for the glutarate dianion and a 15-fold increase in stability of the host-guest bimolecular complex over the analogous urea complex as observed by ^{1}H NMR spectroscopy in DMSO-d_6. From ^{1}H NMR spectroscopic titrations, the K_a is calculated to be 1.0 x 10^4 M^{-1}, which is relatively strong for a neutral host in a highly polar competitive solvent.

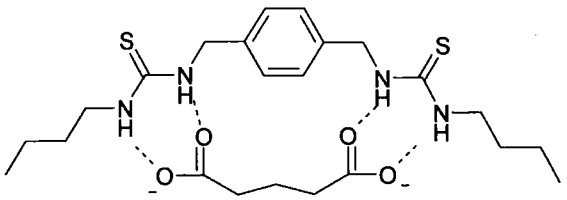

2.3.dicarboxylate

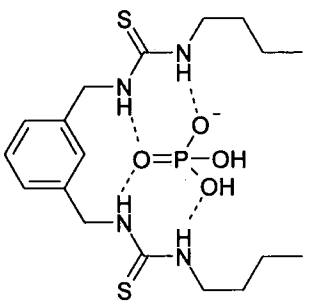

2.4.$H_2PO_4^-$

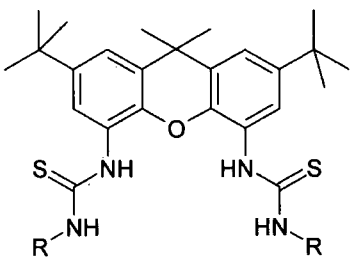

2.5 R = Bu
2.6 R = Ph

Figure 2.1: Bis(thioureido) ligands designed for anion binding.[9-11]

A related host derived from 1,3-bis(aminomethyl)benzene and butyl-isothiocyanate was synthesised by Umezawa and co-workers, **2.4**, and the anion-binding ability investigated.[10] This host shows a large affinity for dihydrogenphosphate and acetate anions with 1 host to 1 guest binding constants, K_{11}, of 820 and 470 M^{-1} respectively in DMSO-d_6. Again, as urea is less acidic than thiourea, the urea analogue host did not effectively bind these anions in DMSO-d_6, with K_{11} of 110 and 43 M^{-1} for dihydrogenphosphate and acetate anions respectively. Further bisthiourea anion binding hosts, **2.5-2.6**, were developed by Umezawa in 1997 based around a xanthene spacer group, to yield a more preorganised binding site.[11] This host shows a large enhancement in binding, with K_{11} in DMSO-d_6 of 1.95 x 10^5 and 3.8 x 10^4 M^{-1} binding of $H_2PO_4^-$ for the phenyl (**2.5**) and butyl (**2.6**) derivatives, respectively. This motif was subsequently incorporated into monolayers to mimic ion-channel sensing of hydrophilic anions,[12] and as a phase transfer agent from water to nitrobenzene for hydrophilic anions such as Cl^-, AcO^-, $H_2PO_4^-$, HPO_4^{2-}, and SO_4^{2-}.[13]

The binding of anions is most usefully exploited by including a sensing module into the functionality of the thiourea so that a change in conformation or electronic properties may trigger a detectable response on binding of anions. Such sensing thiourea compounds will be discussed in this section.

2.1.2.1 Monothioureas

A fluorescent sensor based on a pyrene electron acceptor linked to a thiourea donor, and a colorimetric sensor based on *p*-nitrophenylthiourea were synthesised by Teramae in 1998.[14,15] For the fluorescent sensor, **2.7**, addition of acetate anions, the fluorescence is quenched in acetonitrile solutions, and an association constant of K_{11} = 5.7 x 10^3 M^{-1} is calculated by the change in fluorescence at 398 nm. This is rationalized by the complexed acetate lowering the thiourea oxidation potential so that the complex may quench the excited pyrene more effectively. Other monovalent anions are also bound, but less strongly, and quenching is only observed in less polar, less competitive solvent of acetone. In acetone solutions the K_{11} binding constants are calculated from the Benesi-Hildebrand plot of the change in fluorescence intensity at 398 nm to be 7.0 x 10^3, 5.2 x 10^3, and 1.0 x 10^3 M^{-1} for AcO^-, $H_2PO_4^-$, and Cl^- respectively. The *p*-nitrophenyl thiourea host, **2.8**, displays a colour change from colourless to yellow upon addition of acetate anions, with absorbance decreasing at

λ_{max} at 340 nm while increasing at 365 nm. The binding constant for this ligand was found to be greater than for the pyrene ligand with a K_{11} of around 5 x 10^5 M^{-1} in acetonitrile.

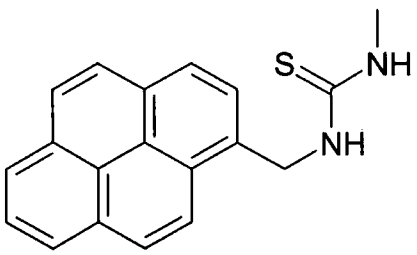

2.7

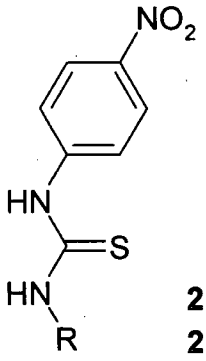

2.8 R = CH_3
2.9 R = p-nitrophenyl

The bis(*p*-nitrophenyl)thiourea host, **2.9**, was shown to selectively bind acetate anions over $H_2PO_4^-$ and Cl^- anions in a 99:1 MeCN/H_2O solution.[16] At a ligand concentration of 20 μM, the ligand absorbance λ_{max} of 343 nm decreases in favour of a ligand-acetate complex absorption at 392 nm, while no such change is observed for $H_2PO_4^-$ or Cl^- anions. In MeCN the binding constant K_{11} is found to be 1.7 x 10^6 M^{-1} which shows the increased hydrogen bonding ability of adding an extra *p*-nitrophenyl group to ligand **2.8**. This ionophoric ligand was also used by Teramae as a phase transfer agent to transport the hydrophilic chloride anion from water to nitrobenzene.[17]

Gunnlaugsson and coworkers developed similar chemosensors for anions with anthracene based fluorescent sensors.[18,19] The anthracene acts as a photoinduced electron transfer (PET) sensor, and for these hosts it was found that fluorescence emission is quenched selectively for AcO^-, $H_2PO_4^-$ and F^- anions, but not for Cl^- or Br^- in DMSO solution. The binding constants for **2.10** were calculated from both ^1H NMR spectroscopic titrations and fluorescence quenching titrations as 2.2 x 10^3, 350, and 110 M^{-1} for AcO^-, $H_2PO_4^-$ and F^-, respectively.

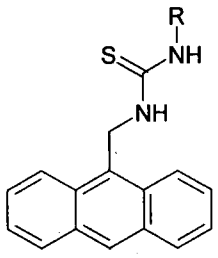

2.10 R = 4-(C_6H_4)-CF_3
2.11 R = C_6H_5
2.12 R = CH_3

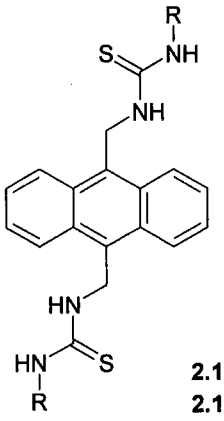

2.13 R = 4-(C_6H_4)-CF_3
2.14 R = C_6H_5

These binding constants are significantly lower than those observed by Teramae, but in such a polar competitive solvent such as DMSO, greatly reduced binding constants are to be expected. More recently, the binding of bisthiourea ligands based on anthracene, **2.13** and **2.14**, and their anion binding ability has been reported.[20] The ligands were titrated against simple monodentate anions and again fluorescence was quenched by AcO^-, $H_2PO_4^-$ and F^- anions with 1:2 host to anion binding. The luminescent quenching with F^- anion suggested 1:1 binding, but this is attributed to complete quenching by one equivalent followed by an unobserved binding of a second anion. For bidentate anions a 1:1 binding was observed with guests possessing greater separation between anions, such as pyrophosphate and malonate, but a 1:2 binding for glutarate. For the strongest binding host, **2.13**, the K_{11} binding constants in DMSO were 1.35 x 10^4, 5.5 x 10^3, 2.5 x 10^3, and 200 M^{-1} for fluoride, glutarate, pyrophosphate, and malonate, respectively.

Other examples of thiourea sensors synthesised recently include hosts with the thiourea group linked to fluorescent sensor moieties by a rigid hydrazine (HN-NH) spacer for the selectivity for and sensitivity towards acetate anions,[21-24] hosts based on coumarin sensors that act as both fluorescent and colorimetric sensors,[25] and compounds that utilise cooperativity between the thiourea group and an amine group adjacent to a naphthalimide sensor.[26,27]

2.1.2.2 Bisthioureas

Sensors using bisthiourea groups have been developed based on azophenol, **2.15**.[28] Absorbance at λ_{max} at 376 nm decreases upon addition of $H_2PO_4^-$ anions while

a new λ_{max} increases at 529 nm in $CHCl_3$. For a host concentration of 1.5 x 10^{-5} M, addition of 3 equivalents of $H_2PO_4^-$ or AcO^- produces a visible colorimetric response from the pale yellow of the host to a deep red complexed species. However binding constants for this species are relatively low: 2.6 x 10^4 and 1.9 x 10^4 M^{-1} for $H_2PO_4^-$ and AcO^- respectively based on UV-Vis titrations in $CHCl_3$. A similar anion sensor, **2.16**, displays some selectivity for tetrahedral oxoanions with a hypsochromic shift from 678 to 632 nm upon addition of $H_2PO_4^-$ anions.[29]

A fluoride chemosensor based on a biaryl fluorophore, **2.17**, that displays a 2.4-fold increase in fluorescence upon addition of up to 2.5 equivalents of F^-.[30] Further addition of F^- leads to a decrease in fluorescence. It is proposed that the initial increase in fluorescence is caused by cooperative binding of both arms to a fluoride anion, but addition of further anions induces a conformational change so that each thiourea functional groups bind separate fluoride anions independently. A limited response was observed with other anions.

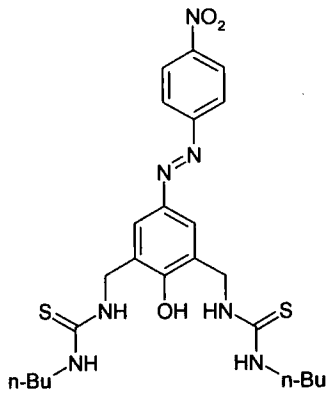

2.15

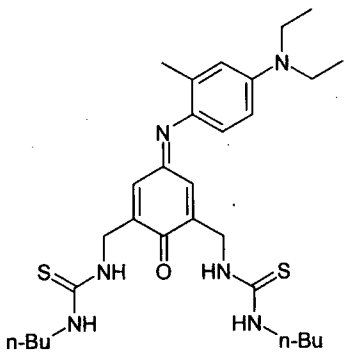

2.16

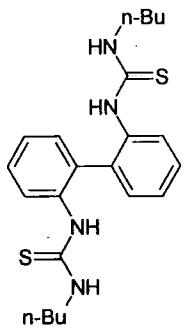

2.17

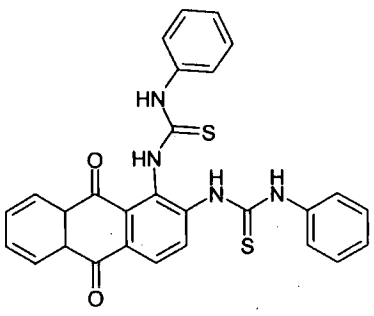

2.18

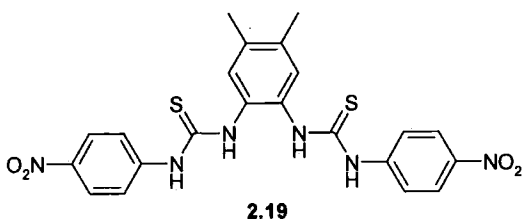

2.19

More recently, sensors with a smaller anion binding cleft compared to the *meta* and *para* hosts of Hamilton and Umezawa have been developed by synthesising

the thiourea groups positioned *ortho* to one another on an aryl ring.[31,32] The anthraquinone derivative, **2.18**, shows a large bathochromic shift from 459 to 562 nm upon addition of phosphate anions, and a binding constant of 1 x 10^6 M^{-1} in acetonitrile/DMSO 9:1 v/v. The host also binds acetate, benzoate, and hydroxyl ions with association constants in the order of magnitude of 1 – 5 x 10^5 M^{-1}. In contrast the phenylene-derived colorimetric *p*-nitrophenyl sensor, **2.19**, demonstrates strong binding towards F^- in DMSO. Addition of F^- anions leads to an increased absorption at 498 nm and a visible response with a yellow solution emerging from a colourless ligand solution in a 1:1 ligand to anion ratio at a concentration of 2.5 x 10^{-5} M. A response is also observed with AcO^- anions, but is not observed for Cl^- or Br^- up to 200 equivalents, however the response is likely to be caused by a deprotonated species A similar *p*-nitrophenyl anthraquinone based receptor with bisthiourea arranged *para* to one another displays a colorimetric response to the addition of isomeric dicarboxylates.[33] A change from blue to green or dark-green is observed upon addition of maleate and phthalate, but not for fumarate, isophthalate, or terephthalate anions. This sensitive naked eye detection is observed at a concentration of parts per million.

2.1.2.3 Poly- and Cyclic thioureas

Macrocyclic hosts can bind anions more strongly then their acyclic counterparts due to the rigid pre-organisation of the host to suit the guest. Several cyclic thiourea hosts have thus been synthesised.

Cyclophane based hosts were synthesised by Tobe and coworkers to form bisaryl macrocycles containing two thiourea binding moieties, for example **2.20**.[34] These macrocycles were titrated with anions in DMSO-d_6 and from the ^{1}H NMR spectroscopic measurements, all display selective binding towards dihydrogenphosphate. The binding constants obtained are greater in value than their acyclic analogues. In particular, the host with a third lariat thiourea moiety, **2.21**, displays the largest binding, which was too large to be accurately determined.

Larger cyclophane-type macrocycles containing three thiourea binding moieties were synthesised by Hong in 2000.[35] These macrocycles also showed an affinity for dihydrogenphosphate over acetate, but binding constants are relatively low for host **2.22** (800 and 320 M^{-1} respectively) in DMSO, suggesting that the

conformationally more flexible larger ring held no advantage over the acyclic thioureas. The addition of ethyl groups into host **2.23** increases the anion binding by reducing flexibility, and in contrast the host displays stronger binding towards acetate anions than dihydrogenphosphate anions with binding constants in DMSO-d_6 of 5300 M^{-1} and 1600 M^{-1}, respectively.

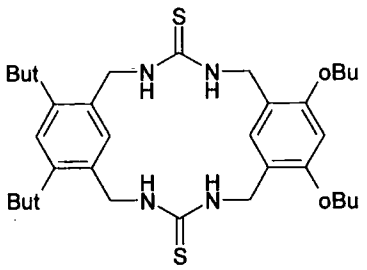

2.20

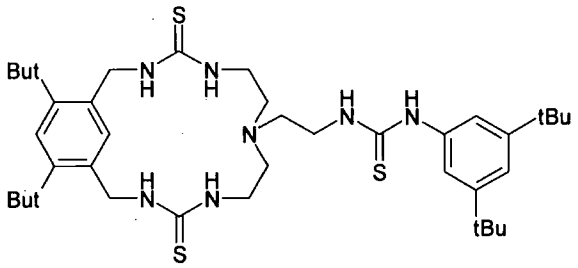

2.21

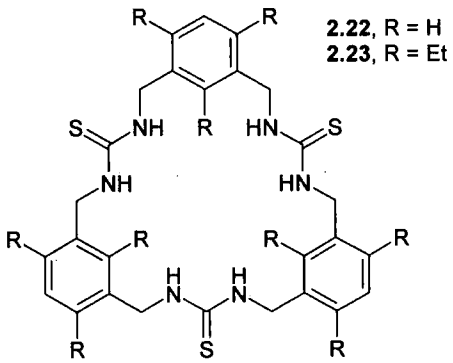

2.22, R = H
2.23, R = Et

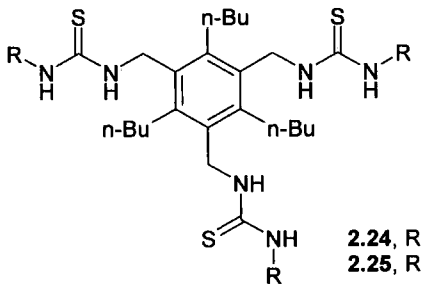

2.24, R = pyren-1-yl
2.25, R = 9-anthrylmethyl

The tripodal thiourea hosts, **2.24** and **2.25**, also show a strong binding for dihydrogenphosphate and acetate anions, with binding constants calculated in acetonitrile from UV-Vis titrations for the pyrene-derived host and fluorescence titrations for anthracene-derived host.[36] K_{11} for the host **2.24** were 3.7 x 10^5 and 1.9 x 10^5 M^{-1} for $H_2PO_4^-$ and AcO^- respectively, while lower values were obtained for host **2.25**: 1.9 x 10^4 and 1.4 x 10^4 M^{-1} for $H_2PO_4^-$ and AcO^-, respectively.

2.2 Aims of research

The synthesis of the thiourea functional group is facile through the reaction of amines with isothiocyanates. The aim of the research presented in this chapter is to synthesise a range of versatile bisthiourea ligands that may bind anions and chelate to transition metals, especially platinum group metals.

2.3 Results and discussion

2.3.1 Synthesis of methyl derivatives

The bisthiourea ligands, 1-methyl-3-[2-(3-methyl-thioureido)-ethyl]-thiourea (MMTET, $\mathbf{L^1}$), 1-methyl-3-[2-(3-methyl-thioureido)-phenylene]-thiourea (MMTPhT, $\mathbf{L^2}$) and 1-methyl-3-[6-(3-methyl-thioureido)-pyridin-2-yl]-thiourea (MMTPyT, $\mathbf{L^3}$) were easily synthesised by reacting methyl isothiocyanate with ethylenediamine, 1,2-phenylenediamine, and 2,6-diaminopyridine respectively. The low yield for pyridyl ligand, $\mathbf{L^3}$, may be attributed to the reduced nucleophilicity of the pyridyl diamine. The ligands were isolated in a pure form as a precipitate after concentration of the original reaction solutions. In all reactions an excess (~10 %) of methyl isothiocyanate was used, and this excess is washed away from the product with diethyl ether. The monothiourea, 1-pyridin-2-yl-3-p-tolyl-thiourea (t-TUP, $\mathbf{L^4}$), was also synthesised from the reaction of 2-aminopyridine with *p*-tolyl isothiocyanate in good yield.

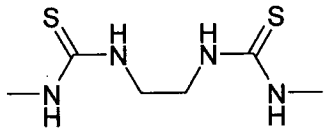

$\mathbf{L^1}$ (95 %)
(MMTET)

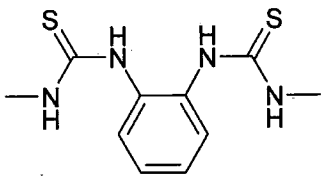

$\mathbf{L^2}$ (65 %)
(MMTPhT)

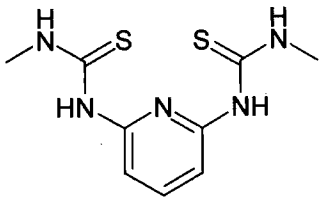

$\mathbf{L^3}$ (40 %)
(MMTPyT)

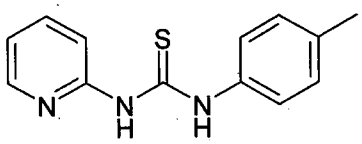

$\mathbf{L^4}$ (65 %)
(t-TUP)

Crystals suitable for X-ray structural analysis were grown MeOH/H_2O solution for $\mathbf{L^1}$, and from hot EtOH for $\mathbf{L^2}$ and $\mathbf{L^3}$. The structures will be discussed further in Chapter 3. Characterisation data for all new compounds is given in the experimental section (section 2.5).

2.3.2 Derivatives with bulky substituents

In order to increase the solubility and crystallinity of coordination complexes with bis(thioureido) ligands, reactions of 1,2-phenylenediamine with bulkier isothiocyanates, such as *i*Pr-NCS and *t*Bu-NCS, were undertaken.

2.3.2.1 Thermal and microwave reactions

Refluxing the reagents *t*Bu-NCS and 1,2-phenylenediamine in CH_2Cl_2 and $CHCl_3$ as with ligand synthesis of $\mathbb{L}^{1\text{-}3}$, resulted in no reaction. This may be attributed to the increased electron donating nature of the tBu and iPr groups, thus disfavouring the nucleophilic attack on the adjacent isothiocyanate group. Following a literature procedure for the synthesis of 1-tert-butyl-3-[2-(3-tert-butyl-thioureido)-phenylene]-thiourea,[37] where the reagents are refluxed in CCl_4 for 2 hours, also did not produce the desired bipodal ligand. After 2 hours, very little 1,2-phenylenediamine had been consumed (as observed by ^{1}H NMR spectroscopy), and so the mixture was left to reflux overnight. The prolonged heating precipitated a white crystalline solid that could be identified as the cyclised product, benzimidazoline-2-thione, **2.2**. Repeating the reaction in toluene had the same effect, and so alternative synthetic methods were sought.

Microwave synthesis allows accelerated rates of reaction to occur through a focused beam of microwaves, and a system where the temperature, pressure and time of reaction can be finely tuned,[38,39] and is used synthetically in organic,[40,41] organometallic[42,43] and coordination chemistry.[44] Microwave reaction of *t*Bu-NCS with 1,2-phenylenediamine in MeOH at 100 Watts for 1 hour displayed a mixture of products by GC-MS, fig. 2.7. The products are (retention times in parentheses): unreacted 1,2-phenylenediamine (A – 3.25 mins); a product of 1,2-phenylenediamine with one amine functionalised with a thiourea group and the other amine unfunctionalised (C – 8.25 mins); and the two products of the cyclisation, benzimidazoline-2-thione (D – 10-12 mins) and N-N-di-*t*Bu-thiourea (B - 5.5 mins).

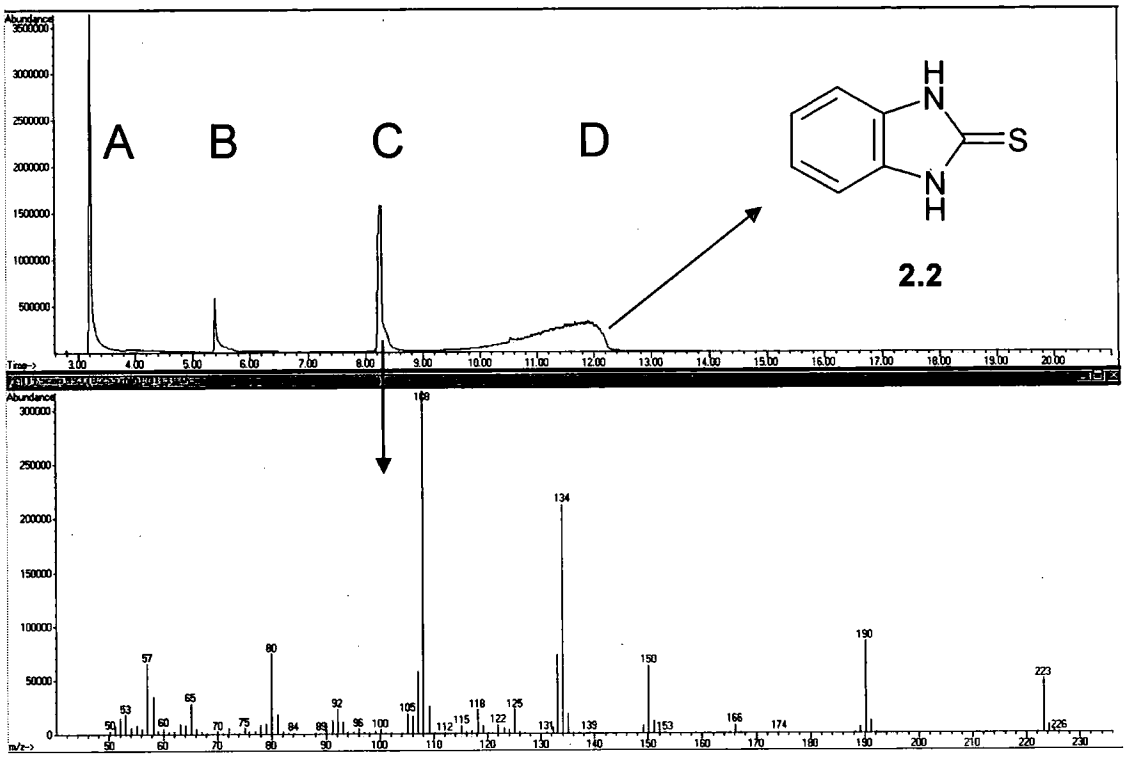

Figure 2.2: GC-MS chromatograph for the reaction of 1,2-phenylenediamine with tBu-NCS in MeOH at 80 °C at 100 W for 1 hour. The mass spectrum of the compound at a retention time of 8.25 minutes is shown with a product peak of m/z = 223, assigned to the singly functionalised 1-(2-amino-phenylene)-3-tert-butyl-thiourea (APBT).

Control of time, temperature and solvent has led to the isolation of some 1-(2-amino-phenyl)-3-tert-butyl-thiourea (APBT, $\mathbf{L^6}$), **C**, before cyclisation reduces the yield. There are two possible routes to cyclised product: 1) formation of the desired bisthiourea, followed by cyclisation as observed by Ambati,[8] or 2) formation of single functionalised compound, followed by intramolecular nucleophilic attack by the free amine, as observed by Griffiths.[7] As no disubstitued ligand is observed in the GC-MS trace, it is more likely that the reaction proceeds by the second route.

Most of the microwave reactions were contaminated with varying degrees of starting material, 1,2-phenylenediamine, so thermal reaction of the reactants to synthesise the single functionalised ligands was attempted concurrently. The isolation of both 1-(2-amino-phenyl)-3-isopropyl-thiourea (APIT, $\mathbf{L^5}$), 1-(2-amino-phenyl)-3-tert-butyl-thiourea (APBT, $\mathbf{L^6}$) can be achieved by thermal reaction: for $\mathbf{L^5}$, 24 hour reflux in CH_2Cl_2 yielded the ligand in high yield; $\mathbf{L^6}$ is formed by refluxing in MeOH for 2 hours. This yields the product in 70 % yield, by GC-MS, and it is possible to recrystallise the product from hot toluene in 50 % yield. Refluxing for longer than 2 hours decreases the yield of $\mathbf{L^6}$ by the formation of the cyclised product. From the

recrystallisation from toluene solution, crystals of L^6 suitable for X-ray analysis were grown, and the structure will be discussed in Chapter 3.

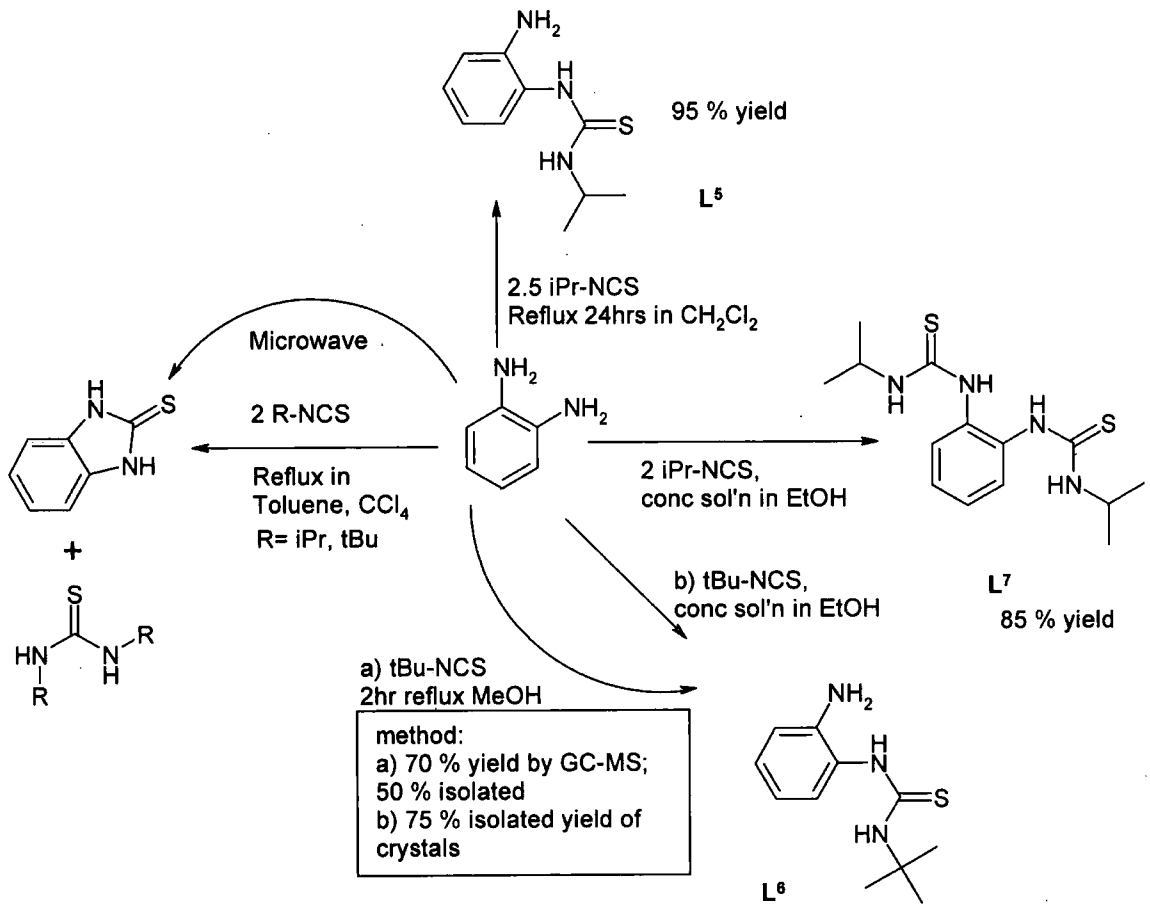

Scheme 2.2: summary of the thermal and microwave reactions of 1,2-phenylenediamine with isopropyl- and tert-butyl-isothiocyanate.

2.3.2.3 Concentrated ethanol solution method

To disfavour the internal cyclisation and to favour the reaction of the singly functionalised ligands with a further equivalent of isothiocyanate, reaction of 1,2-phenylenediamine and the isothiocyanates in high concentrations was attempted. Initially 1,2-phenylenediamine and isopropyl isothiocyanate were added together without solvent, and sonicated together for 5 minutes. There appeared to be no reaction, and so the minimum amount of hot ethanol was added to the mixture to dissolve the phenylenediamine. The mixture was sonicated for a further 5 minutes, and left overnight. From this concentrated solution, crystals of 1-isopropyl-3-[2-(3-

isopropyl-thioureido)-phenylene]-thiourea (IITPhT, $\mathbf{L^7}$) emerge. If left for a further 2 days, the solution yields further product. This method increases in yield as the reaction is scaled up, where minimal amounts of solvent may be added more stringently. This indicates that the use of concentrated solutions to favour the intermolecular reaction of the intramolecular cyclisation is a key factor in the synthesis.

Using this technique with *t*BuNCS yielded overnight large crystals of the previously obtained singly functionalised compound (APBT, $\mathbf{L^6}$). It is not clear whether the bulky nature of the *t*Butyl groups is sufficient to prevent further reaction to form the bifunctional thiourea, whether the additional electron-donating nature of the tBu group disfavours further reaction, or whether the formation of hydrogen bonds and crystal formation isolates the singly functionalised molecule before it can react further. It is likely that it is a combination of all these factors. The reactions of isopropyl isothicyanate and *tert*-butyl isothiocyanate with 1,2-phenylenediamine are summarised in Scheme 2.2.

2.3.3 Anion binding with IITPHT, $\mathbf{L^7}$

2.3.3.1 ^{1}H NMR spectroscopy titrations

The anion binding ability of bisthiourea ligands is known, so the isopropyl terminated orthophenylene bisthiourea ligand, IITPhT ($\mathbf{L^7}$), was titrated against various anions in acetone-d_6 and the shift in ^{1}H NMR spectroscopic chemical shift was monitored. The titrations were initially performed in CD_3CN, but it was found that the ligand was insufficiently soluble in this medium. The acetone-d_6 solution of ligand was titrated against acetone-d_6 solutions of F^-, Cl^-, Br^-, I^-, NO_3^-, AcO^-, and ReO_4^- as tetrabutylammonium (TBA) salts, and ^{1}H NMR spectra taken after each addition of anion solution. For all anions, except ReO_4^-, a significant downfield shift in the thiourea NH protons was observed. For the stronger binding anions, a small change in the chemical shift of the aromatic CH protons was also observed. As the two resonances of the NH protons from each arm remained equivalent throughout the addition of anions, there is a strong indication that anion binding occurs symmetrically by both arms.

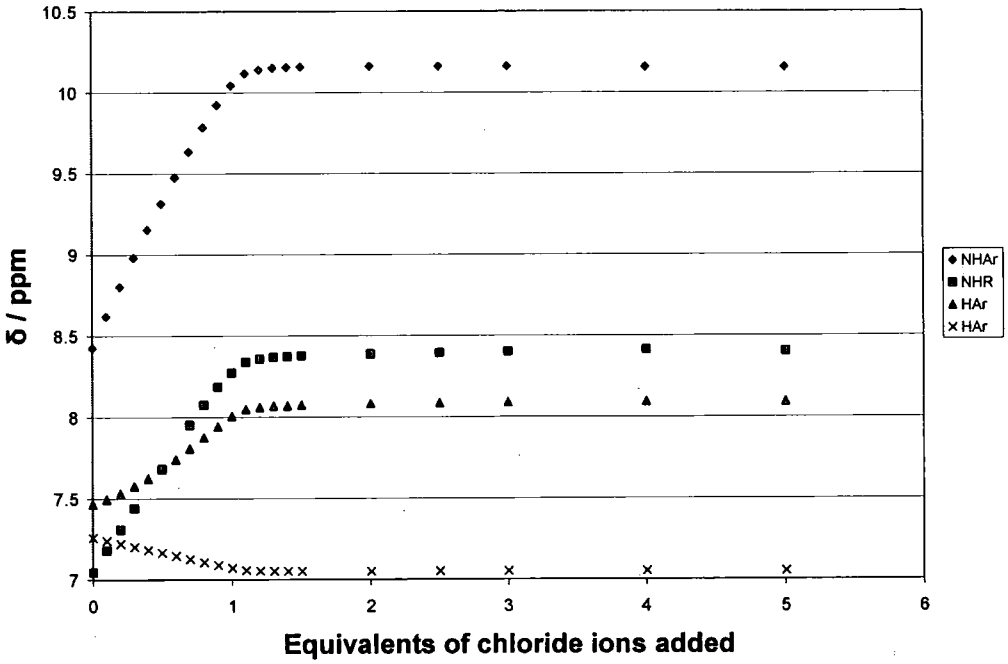

Figure 2.3: Change in chemical shift of protons in IITPhT host against equivalents of TBA chloride added.

A plot of the chemical shift of the thiourea NH protons and the aromatic protons against equivalents of Cl^- added is given in Figure 2.3. The chemical shifts of both the thiourea NH protons increase linearly up to the addition 1 equivalent of anion, and quickly level off to form a plateau. This is indicative of strong 1:1 guest to host binding complex. Both NH resonances from each arms of the host remain equivalent, thus indicating a symmetrical binding of the anion within the binding cleft, or anion exchange between the arms is faster than the NMR spectroscopy timescale. A slight sigmoidal curve is observed in the aryl protons on the carbon adjacent to the functionalised ring carbon, which is indicative of a conformational change. The resonance of the NH groups adjacent to the aryl ring show the greatest change in chemical shift, and the chemical shift of this resonance may be compared for all the titrated anions, fig 2.4.

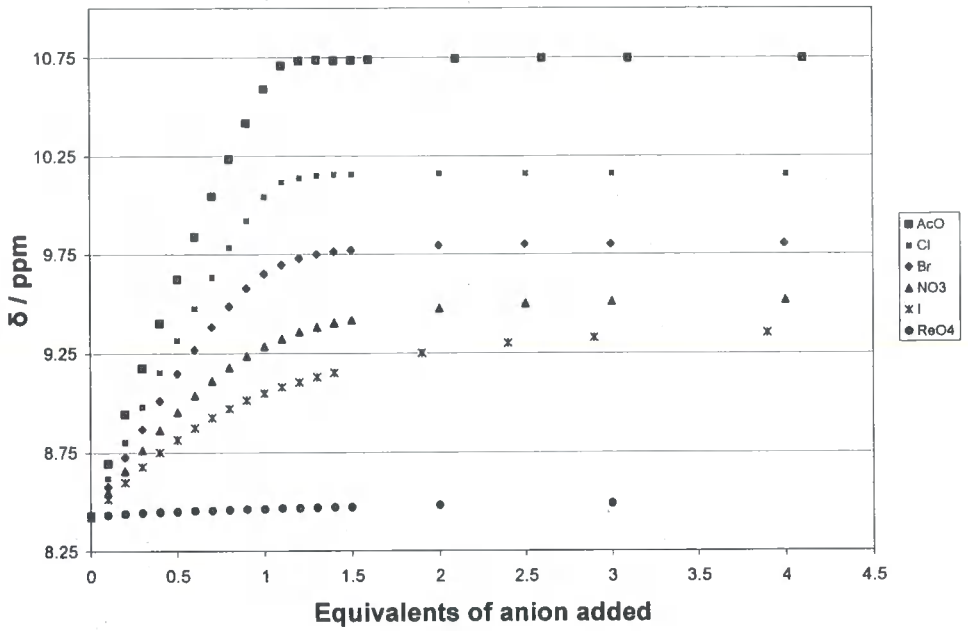

Figure 2.4 The change in chemical shift for the NH adjacent to the aryl ring resonances with added equivalents of a range of anions.

It should also be noted that gradual deprotonation of the thiourea NH protons occurred upon addition of Cl^- and AcO^- anions, as indicated by the reduced integration of the NH signals with reference to the aryl resonances. This is to be expected in the case of the acetate anions due to the high basicity of these anions but is more unusual for chloride anions. In figure 2.4, it may be seen that AcO^- yields the greatest change in chemical shift, however, this is to be expected as it is more basic than the other anions. Initial titrations with fluoride anions gave a large initial increase in the NH shift of almost 1 ppm upon addition of 0.2 equivalents of TBA fluoride. However, upon addition the NH proton resonances became very broad and disappeared after the addition of 0.3 anion equivalents indicating some deprotonation of the ligand. Given only 0.3 equivalents of the fluoride anions were added, the disappearance of the NH proton resonances is caused by deprotonation of a small proportion of the ligand (i.e. 0.3 equivalents or fewer), and fast proton exchange between protonated and deprotonated molecules. This fast exchange leads to a greatly broadened signal. Deprotonation of the acidic thiourea protons with strong bases is known,[45] and expected for anions such as fluoride and acetate. However, it is more unusual to see the deprotonation of thioureas with chloride anions. A colour change from the colourless host solution to a pale orange/brown was observed upon large

addition of F-, Cl- and AcO- anions, presumably due to deprotonation of the host. No colour change in the colourless host solutions was observed upon addition of other anions.

To compare the binding of this host with others for anions, the binding constants must be calculated, and anion preference and selectivities may be found.

2.3.3.2 Binding constant calculations

The binding constants associated with the anion ligand complex may be calculated by fitting the titration curves using the fitting program, HypNMR.[46,47] The program uses the chemical shifts obtained in NMR titrations to calculate equilibrium constants. In the case of anion binding this relates to the equilibrium between host, guest and host-guest complex.

$$\text{Host} + \text{Guest} \overset{K}{\rightleftharpoons} \text{Host-guest complex}$$

$$K = \frac{[\text{Complex}]}{[\text{Host}][\text{Guest}]}$$

The model assumes that the equilibrium is attained rapidly on an NMR timescale, so that the observed chemical shift is a mole fraction weighted average chemical shift for all the species present with the observed nucleus is present. In other words, for the anion binding observed in this study, the obseverd chemical shifts are a mole fraction weighted average of the free ligand and the anion-complexed ligand. Users must guestimate an initial binding constant and the program applies a Gauss-Newton-Marquardt method in the refinement to fit the binding constant accurately.[47]

The program was used to fit a 1:1 binding constant to four proton resonances that exhibited a significant change in their chemical shift, both NH proton and both CH aryl proton resonances. The results for all titrated anions are shown in Table 2.1.

Anion (as TBA salt)	Binding constant (M^{-1})
Fluoride	**Deprotonation**
Chloride	2260 ± 50
Acetate	2210 ± 50
Bromide	1020 ± 10
Nitrate	200 ± 2
Iodide	70 ± 1
Perrhenate	<10

Table 2.1: Binding constants for IITPhT (L^7) with various anions in acetone-d_6 from ^{1}H NMR titrations.

It can be seen that this ligand is selective for acetate and chloride anions, with moderate binding constants of around 2250 M^{-1}. As the titrations were performed in acetone which is less polar and therefore less competitive than other solvents such as acetonitrile, water and DMSO, the anions are less well bound than many other neutral thiourea anion receptors, and the binding constants found in this study are lower than related molecules, **2.18** and **2.19**.[31,32] However, the binding constants for **2.18** and **2.19** were found from UV-Vis spectrophotometric titrations, and it is possible that their associated high binding constants may be attributable to deprotonation of the ligand, rather than neutral host and anion association.

It was noted that one of the aryl proton resonances changes in a sigmoidal manner upon addition of chloride anions. Within the HypNMR program, it was possible to manually fit the chloride curves to a model with not only a 1:1 host to guest ratio, but also with a further 2:1 host to guest ratio. It is possible to envisage two hosts aggregating about a single anion when anion concentration is low, followed by the formation of monomeric species upon further addition of anions. So a Job plot of the ligand with chloride anion addition was constructed based on the thiourea NH proton resonance. The plot investigates the true molar ratio of host to guest based upon the change of the host chemical shift ($\Delta\delta$) as a function of host:guest molar ratio (x). The Job plot for the titration with chloride anions can be seen in figure 2.5. The maximum of the Job plot lies at a host mole fraction of 0.5, therefore giving a true 1:1 host to guest ratio. It is more likely therefore that the sigmoidal curve is associated with the deprotonation of the host. Further evidence of this is given by the fluoride titration: complete deprotonation of the thiourea NH protons occurs after only 0.3

equivalents of fluoride addition, however the aryl protons may still be monitored upon addition of further equivalents of fluoride anion. It is evident that with the addition of fluoride anions, the aryl proton in question shifts in a sigmoidal curve more dramatically than in the case of chloride addition.

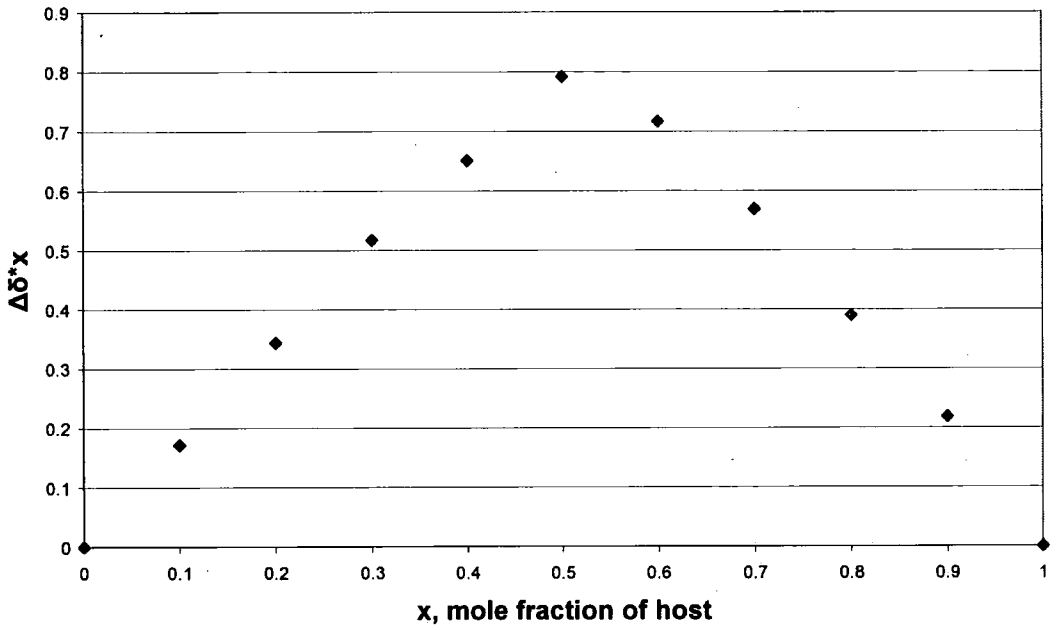

Figure 2.5: Job plot of the change in chemical shift multiplied by host mole fraction (Δδ*x) against host mole fraction, x.

2.3.3.3 Solid-state investigation of ligand-anion interaction

Crystallisations of the host IITPhT, **L**[7], with TBA salts of AcO^-, F^-, Cl^-, Br^-, I^-, NO_3^- and $H_2PO_4^-$ were set-up in 1:1 and 1:2 host to guest ratios in two different solvent systems, methanol and acetone. From slow evaporation of these solutions, crystals suitable for X-ray analysis were obtained from a 1:1 host to TBABr methanol solution. The structure was solved in space group $P2_1/m$ with an R-factor of R = 7.0 %. The ligand, bromide anion and the TBA counter-ion all lie along a mirror plane, which confirms the symmetrical binding of the ligand with the anion as observed in the ^1H NMR spectra. There is disorder in the TBA terminal methyl groups.

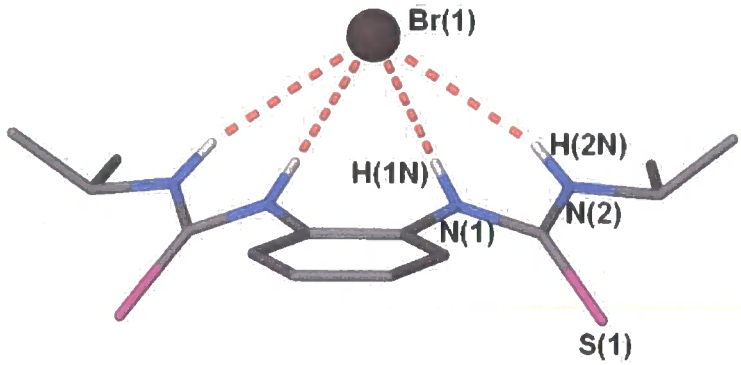

Figure 2.6: structure of host IITPhT binding a bromide anion symmetrically in the solid-state. H-bond distances are: H(1N)-Br 2.52(4) Å, H(2N)-Br 2.86(4) Å.

The hydrogen bond distances 2.52(4) and 2.86(4) Å for H(1N)-Br and H(2N)-Br respectively. The closer association of the bromide ion to the NH adjacent to the aryl ring is also reflected in the greater downfield shift of this proton in the ^{1}H NMR spectroscopic titrations. These compare well with the bond distances from thiourea to bromide found, with H-Br distances of 2.509, 2.528, 2.603 and 2.723 Å in the crystal structure of two thiourea molecules hydrogen bonding to the bromide anion as a TBA salt.[48] To date there have been no solid-state structures of bipodal or cyclic thiourea anion hosts binding to an anion deposited in the CSD, and thus this is the first of its kind to be reported.

From the same host:guest ratio and methanol series, crystals of suitable size for X-ray diffraction were obtained, however these were all found to contain the ligand only.

2.4 Conclusions

Thiourea hosts and ligands may be easily synthesised by the reaction of an amine with an isothiocyanate. Isothiocyanates with bulky, electron donating substituents tend to form benzimidazoline-2-thione with 1,2-phenylenediamine, but this may be controlled, and new thioureidoamine ($\mathbf{L}^{5,6}$) and diisopropylthiourea ($\mathbf{L}^{7}$) ligands may be isolated. $\mathbf{L}^{7}$ shows moderate anion binding ability, with symmetrical binding of the two podal arms, as evidenced by ^{1}H NMR spectroscopic titrations and a solid-state structure, characterised by X-ray crystallography.

2.5 Experimental

2.5.1 General Methods

All reactions were performed using reagents and solvents obtained from commercially available sources as received, and experiments were performed and worked up in air.

^{1}H and $\{^{1}H\}$-^{13}C spectroscopy was performed on Varian Unity 300 MHz, Varian Mercury 400 MHz, Bruker Avance 400 MHz and Varian Inova 500 MHz NMR spectrometers at frequencies specified in the experimental data. Chemical shifts (δ) are reported in parts per million (ppm) relative to a tetramethylsilane internal reference. Coupling constants (J) are reported in Hertz (Hz), and multiplicities are reported as singlet (s), doublet (d), doublet of doublets (dd), multiplets (m) or broad (br). Mass spectra were performed on a Micromass LCT or a Thermo LTQ FT spectrometer in ES+ mode. Micro-analysis for C, H and N atomic percentages were recorded on an Exeter Analytical Inc. CE 440 – Elemental analyzer. IR spectra were run on a Perkin-Elmer 100 FT-IR spectrometer as KBr discs. Peaks are reported in wavenumbers (cm^{-1}) and are described as broad (br), weak (w), medium (m) or strong (s). GC-MS were run on an Agilent Technologies 3973 mass spectrometer. Microwave reactions were performed in 10 ml sealed, thick-walled microwave vials on an Emrys Optimizer microwave reactor.

2.5.2 Bisthiourea ligands

2.5.2.1 1-Methyl-3-[2-(3-methyl-thioureido)-ethyl]-thiourea (MMTET)

Ethylenediamine (0.6 g, 10.3 mmol) and methylisothiocyanate (1.6 g, 21.9 mmol) were dissolved in 30 ml of dichloromethane, and the solution was refluxed for 1.5 hours. After this time the white precipitate was removed by filtration. Yield = 1.9 g, 9.2 mmol, 89 %.

^{1}H NMR (CD_3CN + DMSO-d_6, 400 MHz) δ (ppm): 2.88 (6H, br, CH_3), 3.58 (4H, br, CH_2), 7.10 (2H, br, $NH(CH_2)$), 7.23 (2H, br, $NH(CH_3)$).

$\{^{1}H\}$-^{13}C NMR (DMSO-d_6, 101 MHz) δ (ppm): 31.15, 43.49, 182.68.

EI-MS: 206 $[M]^+$

Analysis: calc'd for $C_6H_{14}N_4S_2$: C 34.93, H 6.84, N 27.15 %; found: C 34.74, H 6.96, N 27.18 %.

IR (ν, cm^{-1}): 3267 (br, N-H), 3209 (br, N-H), 1557 (s, NH), 1224 (m, C=S), 1063 (m, C=S).

2.5.2.2 1-Methyl-3-[2-(3-methyl-thioureido)-phenylene]-thiourea (MMTPhT)

1,2-Phenylenediamine (0.88 g, 8.2 mmol) was dissolved in 50 ml of methanol and added slowly (c. 1hr) to a stirring solution of methylisothiocyanate (1.28 g, 17.6 mmol) in 30 ml of methanol. The mixture was refluxed for 2 hours. Removal of the solvent *in vacuo* and washing the resulting solid with anhydrous diethyl ether (2 x 10 ml) and methanol (4 x 5 ml) yielded a white solid. Yield = 1.35 g, 5.3 mmol, 65%.

^{1}H NMR (DMSO-d_6, 300 MHz) δ (ppm): 2.89 (6H, br, CH_3), 7.20 (2H, br, CH_{Arom}), 7.41 (2H, br, CH_{Arom}), 7.73 (2H, br, NH), 9.03 (2H, br, NH).

{^{1}H}-^{13}C NMR (DMSO-d_6, 101 MHz) δ (ppm): 31.81, 126.62, 128.18, 134.23, 182.21.

ESI-MS: 255.1, 100 % rel. abundance for $[M + H]^+$.

Analysis: calc'd for $C_{10}H_{14}N_4S_2$: C 47.22, H 5.55, N 22.03 %; found: C 47.04, H 5.64, N 21.66 %.

IR (ν, cm^{-1}): 3275 (br, N-H), 3224 (br, N-H), 1613 (s, NH), 1262 (s, C=S), 1055 (s, C=S).

2.5.2.3 1-Methyl-3-[6-(3-methyl-thioureido)-pyridin-2-yl]-thiourea (MMTPyT)

2,6-Diaminopyridine (1.0 g, 9.2 mmol) and methylisothiocyanate (1.5 g, 20.5 mmol) were dissolved in 20 ml of methanol. The mixture was refluxed for 4 hrs, cooled and the grey precipitate filtered. Yield = 0.97 g, 3.8 mmol, 42 %.

^{1}H NMR (DMSO-d_6, 400 MHz, *J*/Hz) δ (ppm) 3.03 (6H, d, ^3J = 4.4, CH_3), 6.90 (2H, d, ^3J = 8.4, H_{Ar}), 7.66 (1H, t, ^3J = 8.4, H_{Ar}), 9.75 (2H, br, $NH_{(Me)}$), 10.36 (2H, br, $NH_{(Ar)}$).

{^{1}H}-^{13}C NMR (DMSO-d_6, 101 MHz) δ (ppm): 32.04, 106.60, 140.72, 150.92, 180.33.

Analysis: calc'd for $C_9H_{13}N_5S_2$: C 42.33, H 5.13, N 27.42 %; found: C 42.29, H 5.13, N 27.43 %.

ESI-MS (MeCN): 256.0, 100 % rel. abundance for $[M + H]^+$.

IR (**v**, cm^{-1}): 3238 (s, N-H), 1633 (m, N-H), 1618 (s), 1225 (s, C=S), 1156 (s, C=S), 1066 (s, C=S).

2.5.2.4 1-Isopropyl-3-[2-(3-isopropyl-thioureido)-phenylene]-thiourea (IITPhT)

1,2-Phenylenediamine (0.7 g, 6.5 mmol) and isopropyl isothiocyanate (1.5 g, 14.8 mmol) were sonicated together for 5 minutes in 2 ml of hot EtOH. Crystals suitable for X-ray crystallography came out of solution over the course of 2 days. More product may be isolated from the mother liquor over a period of a few days. Yield = 1.9 g, 6.1 mmol, 95%.

^1H NMR (acetone-d_6, 400 MHz, *J*/Hz): 1.21 (12H, d, ^3J = 6.4 Hz, C-$(CH_3)_2$), 4.50 (2H, br, CH-$(Me)_2$), 7.05 (2H, br, NH), 7.24 (2H, m, CH_{Ar}), 7.45 (2H, br, CH_{Ar}), 8.43 (2H, br, NH).

{^1H}-^{13}C NMR (DMSO-d_6, 101 MHz) δ (ppm): 22.31, 46.41, 126.52, 128.24, 134.36, 180.06.

ESI-MS: 311.1, 100 % rel. abundance for $[M + H]^+$.

Analysis: calc'd for $C_{14}H_{22}N_4S_2$: C 54.16, H 7.14, N 18.04 %; found: C 54.15 H 7.23 N 18.02 %.

IR (**v**, cm^{-1}): 3315 (br, N-H), 3256 (br, N-H), 1598 (s, NH), 1264 (s, C=S), 1126 (s, C=S).

2.5.3 Monothioureas

2.5.3.1 1-(2-Amino-phenylene)-3-tert-butyl-thiourea (APBT)

1,2-Phenylenediamine (0.6 g, 5.5 mmol) and *tert*-butyl isothiocyanate (1.3 g, 11.3 mmol) were dissolved in 30 ml of methanol and refluxed for 2 hours. The solvent was removed *in vacuo* and the white precipitate washed with hexane. The product could

be isolated by recrystallising the crude product in toluene. Yield = 0.6 g, 2.7 mmol, 49 %.

^{1}H NMR ($CDCl_3$, 400 MHz, *J*/Hz): 1.43 (9H, s, C-$(CH_3)_3$), 4.00 (2H, br, NH_2), 5.78 (1H, br, NH), 6.71 (1H, dd, ^3J = 8.0, CH_{Ar}), 6.77 (1H, d, ^3J = 8.0, CH_{Ar}), 7.00 (1H, d, ^3J = 8.0, CH_{Ar}), 7.10 (1H, dd, ^3J = 8.0, CH_{Ar}), 7.66 (1H, br, NH).

{^{1}H}-^{13}C NMR ($CDCl_3$, 101 MHz): 28.66, 53.68, 116.46, 118.82, 121.10, 128.19, 129.32, 143.25, 179.46.

ESI-MS: 224.1, 100 % rel. abundance for $[M + H]^+$.

Analysis: calc'd for $C_{11}H_{17}N_3S$: C 59.19, H 7.67, N 18.81 %; found: C 59.12, H 7.72, N 18.81 %.

Alternative synthesis:

1,2-Phenylenediamine (0.3 g, 2.7 mmol) and *tert*-butyl isothiocyanate (0.65 g, 5.6 mmol) was dissolved in 2 ml of hot EtOH and left at room temperature for 3 days. Large crystals of 1-(2-amino-phenylene)-3-tert-butyl-thiourea were isolated from the mother liquor. Yield = 0.45 g, 2.0 mmol, 75 %.

2.5.3.2 1-(2-Amino-phenylene)-3-isopropyl-thiourea (APIT)

1,2-Phenylenediamine (0.7g, 6.5 mmol) and isopropyl isothiocyanate (1.5 g, 14.8 mmol) were dissolved in 25 ml of dichloromethane and refluxed for 24hrs. After this time, all solvent was removed *in vacuo* and the crude product washed with diethyl ether to remove excess isothiocyanate, to yield a white powder. Yield = 1.3 g, 6.2 mmol, 96 %.

^{1}H NMR (CD_3CN, 400 MHz, *J*/Hz) δ (ppm): 1.12 (6H, d, ^3J = 6.8, CH_3), 4.22 (2H, s, NH_2), 4.45 (1H, br, CH), 6.02 (1H, br, NH), 6.68 (1H, ddd, ^3J = 7.6, ^3J = 7.6, ^4J = 1.2, CH_{Ar}), 6.80 (1H, dd, ^3J = 8.0, ^4J = 1.2, CH_{Ar}), 6.98 (1H, dd, ^3J = 7.6, ^4J = 1.2, CH_{Ar}), 7.10 (1H, ddd, ^3J = 7.6, ^3J = 7.6, ^4J = 1.2, CH_{Ar}), 7.50 (1H, br, NH).

{^{1}H}-^{13}C NMR (DMSO-d_6, 101 MHz) δ (ppm): 22.52, 46.20, 116.37, 116.93, 124.08, 127.48, 128.29, 144.45, 180.25.

ESI-MS: 210.2, 100 % rel. abundance for $[M + H]^+$.

Analysis: calc'd for $C_{10}H_{15}N_3S$: C 57.38, H 7.22, N 20.08 %; found: C 58.02, H 7.36, N 20.28 %.

2.5.3.3 1-Pyridin-2-yl-3-p-tolyl-thiourea (t-TUP)

p-Tolyl isothiocyanate (0.96 g, 6.4 mmol) and 2-aminopyridine (0.62 g, 6.3 mmol) were dissolved in 25 ml of dried dichloromethane, and refluxed for 24 hours. The colourless solution was reduced in volume to *c.* 3 ml and a white crystalline precipitate formed. Yield = 0.98 g, 4.0 mmol, 62 %.

^{1}H NMR ($CDCl_3$, 400 MHz, *J*/Hz) δ (ppm): 2.30 (3H, s, CH_3), 6.79 (1H, d, ^3J = 7.2, CH_{Ar} pyr), 6.92 (1H, d, ^3J = 7.2, CH_{Ar} pyr), 7.15 (2H, d, ^3J = 7.6, CH_{Ar} tolyl), 7.45 (2H, d, ^3J = 7.6, CH_{Ar} tolyl), 7.59 (1H, m, CH_{Ar} pyr), 8.15 (1H, m, CH_{Ar} pyr), 8.84 (1H, s, NH), 13.46 (1H, s, NH).

{^{1}H}-^{13}C NMR ($CDCl_3$, 101 MHz) δ (ppm): 21.1, 112.3, 118.2, 125.0, 129.4, 136.1, 136.2, 139.0, 145.8, 153.2, 179.0.

ESI-MS: 244.0, 100% rel. abundance for $[M+H]^+$.

Analysis: calc'd for $C_{13}H_{13}N_3S$: C 64.17, H 5.38, N 17.27 %; found: C 63.98, H 5.36, 17.27 %.

IR (ν, cm^{-1}): 3223 (br, N-H), 3170(br, N-H), 1605 (s, NH), 1266 (s, C=S), 1183 (s, C=S), 1145 (s, C=S).

2.5.4 ^{1}H NMR spectroscopic titration experiments

^{1}H NMR spectroscopic titration experiments were carried out on a Varian Inova 500 MHz NMR spectrometer. All chemical shifts are reported in ppm relative to tetramethylsilane as an internal reference. A solution of the host species, IITPhT, of a known concentration, typically 0.06 M, was made up in a NMR tube using 0.5 ml of deuterated acetone. Solutions of the anions, as TBA salts, were made up in deuterated acetone in volumetric flasks (2 ml) at a concentration five times greater than the host. Guest solution was titrated into the host solution at initial volumes of 10 μl (0.1 equivalents with respect to the host) and, after rigorous shaking to homogenise the solution, spectra recorded after each addition. Larger aliquots were added when little change was observed in the spectra. Results were analysed using the curve-fitting program HypNMR, simultaneously fitting as many resonances that could be accurately monitored during the experiment.

2.5.5 Crystal structure data

2.5.5.1 General

The diffraction experiment, using graphite-monochromated MoKα radiation (λ = 0.71073 Å), was carried out on SMART 1K (X-rays from a 60 W microfocus Bede Microsource® with glass polycapillary optics), covering a full sphere of the reciprocal space by three or four runs of narrow-frame (0.3°) ωscans. The crystals were cooled using Cryostream (Oxford Cryosystems) open-flow N_2 cryostats. The structures were solved by direct methods and refined by full-matrix least-squares on F2 for all the data using SHELXTL software.[49,50]

2.5.5.2 IITPhT +TBABr

Crystals suitable for X-ray diffraction were grown by slow evaporation of a methanol solution (5 ml) containing 40 mg of IITPhT and 44 mg TBABr.

Crystal data: $C_{30}H_{58}BrN_5S_2$, M = 632.84, colourless block, 0.40 × 0.20 × 0.10 mm^3, monoclinic, space group $P2_1/m$ (No. 11), a = 8.922(2), b = 14.512(3), c = 13.570(3) Å, β = 99.736(5)°, V = 1731.7(7) $Å^3$, Z = 2, D_c = 1.214 g/cm^3, F_{000} = 680, SMART 1K, MoKα radiation, λ = 0.71073 Å, T = 273(2)K, $2\theta_{max}$ = 59.2°, 17021 reflections collected, 4955 unique (R_{int} = 0.1156). Final *GooF* = 1.024, *R1* = 0.0703, *wR2* = 0.1134, R indices based on 2748 reflections with I >2σ(I) (refinement on F^2), 219 parameters, 0 restraints. Lp and absorption corrections applied, μ = 1.333 mm^{-1}.

2.6 References

(1) Billeter, O. *Berichte* **1887**, *20*, 288.

(2) Dyson, G. M.; George, H. J.; Hunter, R. F. *J. Chem. Soc.* **1924**, 1702.

(3) Dyson, G. M.; George, H. J.; Hunter, R. F. *J. Chem. Soc.* **1926**, 3041.

(4) Dyson, G. M.; George, H. J.; Hunter, R. F. *J. Chem. Soc.* **1926**, 436.

(5) Faull, A. W.; Griffiths, D.; Hull, R.; Seden, T. P. *J. Chem. Soc. Perkin 1* **1980**, 2587.

(6) Griffiths, D.; Hull, R.; Seden, T. P. *J. Chem. Soc. Perkin 1* **1980**, 2608.

(7) Griffiths, D.; Hull, R.; Seden, T. P. *J. Chem. Soc. Perkin 1* **1980**, 1240.

(8) Ambati, N. B.; Babu, V.; Anand, V.; Hanumanthu, P. *Synth. Comm.* **1999**, *29*, 289.

(9) Fan, E.; Van Arman, S. A.; Kincaid, S.; Hamilton, A. D. *J. Am. Chem. Soc.* **1993**, *115*, 369.

(10) Nishizawa, S.; Buhlmann, P.; Iwao, M.; Umezawa, Y. *Tetrahedron Lett.* **1995**, *36*, 6483.

(11) Buhlmann, P.; Nishizawa, S.; Xiao, K. P.; Umezawa, Y. *Tetrahedron* **1997**, *53*, 1647.

(12) Xiao, K. P.; Buhlmann, P.; Umezawa, Y. *Anal. Chem.* **1999**, *71*, 1183.

(13) Nishizawa, S.; Yokobori, T.; Shioya, T.; Teramae, N. *Chem. Lett.* **2001**, 1058.

(14) Nishizawa, S.; Kaneda, H.; Uchida, T.; Teramae, N. *J. Chem. Soc., Perkin Trans. 2* **1998**, 2325.

(15) Nishizawa, S.; Kato, R.; Hayashita, T.; Teramae, N. *Anal. Sci.* **1998**, *14*, 595.

(16) Kato, R.; Nishizawa, S.; Hayashita, T.; Teramae, N. *Tetrahedron Lett.* **2001**, *42*, 5053.

(17) Nishizawa, S.; Yokobori, T.; Kato, R.; Shioya, T.; Teramae, N. *Bull. Chem. Soc. Jpn.* **2001**, *74*, 2343.

(18) Gunnlaugsson, T.; Davis, A. P.; Glynn, M. *Chem. Commun.* **2001**, 2556.

(19) Gunnlaugsson, T.; Davis, A. P.; Hussey, G. M.; Tierney, J.; Glynn, M. *Org. Biomol. Chem.* **2004**, *2*, 1856.

(20) Gunnlaugsson, T.; Davis, A. P.; O'Brien, J. E.; Glynn, M. *Org. Biomol. Chem.* **2005**, *3*, 48.

(21) Wu, F.-Y.; Li, Z.; Wen, Z.-C.; Zhou, N.; Zhao, Y.-F.; Jiang, Y.-B. *Org. Lett.* **2002**, *4*, 3203.

(22) Nie, L.; Li, Z.; Han, J.; Zhang, X.; Yang, R.; Liu, W. X.; Wu, F. Y.; Xie, J. W.; Zhao, Y. F.; Jiang, Y. B. *J. Org. Chem.* **2004**, *69*, 6449.

(23) Wen, Z.-C.; Jiang, Y.-B. *Tetrahedron* **2004**, *60*, 11109.

(24) Liu, B.; Tian, H. *Chem. Lett.* **2005**, *34*, 686.

(25) Ghosh, K.; Adhikari, S. *Tetrahedron Lett.* **2006**, *47*, 8165.

(26) Pfeffer, F. M.; Buschgens, A. M.; Barnett, N. W.; Gunnlaugsson, T.; Kruger, P. E. *Tetrahedron Lett.* **2005**, *46*, 6579.

(27) Pfeffer, F. M.; Seter, M.; Lewcenko, N.; Barnett, N. W. *Tetrahedron Lett.* **2006**, *47*, 5241.

(28) Lee, D. H.; Lee, K. H.; Hong, J. I. *Org. Lett.* **2001**, *3*, 5.

(29) Lee, D. H.; Lee, H. Y.; Hong, J. I. *Tetrahedron Lett.* **2002**, *43*, 7273.

(30) Lee, D. H.; Im, J. H.; Lee, J. H.; Hong, J. I. *Tetrahedron Lett.* **2002**, *43*, 9637.

(31) Jose, D. A.; Kumar, D. K.; Ganguly, B.; Das, A. *Tetrahedron Lett.* **2005**, *46*, 5343.

(32) Kim, Y.-J.; Kwak, H.; Lee, S. J.; Lee, J. S.; Kwon, H. J.; Nam, S. H.; Lee, K.; Kim, C. *Tetrahedron* **2006**, *62*, 9635.

(33) Yen, Y. P.; Ho, K. W. *Tetrahedron Lett.* **2006**, *47*, 7357.

(34) Sasaki, S. I.; Mizuno, M.; Naemura, K.; Tobe, Y. *J. Org. Chem.* **2000**, *65*, 275.

(35) Lee, K. H.; Hong, J.-I. *Tetrahedron Lett.* **2000**, *41*, 6083.

(36) Sasaki, S.; Citterio, D.; Ozawa, S.; Suzuki, K. *J. Chem. Soc., Perkin Trans. 2* **2001**, 2309.

(37) Deohate, P. P.; Berad, B. N. *Oriental J. Chem.* **2004**, *20*, 139.

(38) Baghurst, D. R.; Mingos, D. M. P. *J. Chem. Soc., Dalton Trans.* **1992**, 1151.

(39) Baghurst, D. R.; Mingos, D. M. P. *J. Chem. Soc., Chem. Commun.* **1992**, 674.

(40) Gedye, R.; Smith, F.; Westaway, K.; Ali, H.; Baldisera, L.; Laberge, L.; Rousell, J. *Tetrahedron Lett.* **1986**, *27*, 279.

(41) Giguere, R. J.; Bray, T. L.; Duncan, S. M.; Majetich, G. *Tetrahedron Lett.* **1986**, *27*, 4945.

(42) Ali, M.; Bond, S. P.; Mbogo, S. A.; McWhinnie, W. R.; Watts, P. M. *J. Organomet. Chem.* **1989**, *371*, 11.

(43) Baghurst, D. R.; Michael, D.; Mingos, P.; Watson, M. J. *J. Organomet. Chem.* **1989**, *368*, C43.

(44) Baghurst, D. R.; Cooper, S. R.; Greene, D. L.; Mingos, D. M. P.; Reynolds, S. M. *Polyhedron* **1990**, *9*, 893.

(45) Gomez, D. E.; Fabbrizzi, L.; Licchelli, M.; Monzani, E. *Org. Biomol. Chem.* **2005**, *3*, 1495.

(46) Frassineti, C.; Ghelli, S.; Gans, P.; Sabatini, A.; Moruzzi, M. S.; Vacca, A. *Anal. Biochem.* **1995**, *231*, 374.

(47) Frassineti, C.; Alderighi, L.; Gans, P.; Sabatini, A.; Vacca, A.; Ghelli, S. *Anal. Bioanal. Chem* **2003**, *376*, 1041.

(48) Babb, J. E. V.; Burke, N. J.; Burrows, A. D.; Mahon, M. F.; Slade, D. M. K. *CrystEngComm* **2003**, *5*, 226.

(49) *SHELXS*, Sheldrick, G. M. University of Göttingen, 1997.

(50) *SHELXL*, Sheldrick, G. M. University of Göttingen, 1997.

Chapter 3: Hydrogen bonding interactions with thiocarbonyl π-electrons

3.1 Introduction

The use of π-electron density in molecular recognition is of great interest, in particular interactions with carbonyl bonds, arenes and CH/π association.[1-3] One of the earliest examples of the interaction between hydrogen bonds and the π-electrons of carbonyls occurs in the crystal structure of urea.[4-7] It was observed that the oxygen atom is involved in four hydrogen bonds; two through the nonbonding lone pairs on the oxygen atom, and two through the π-electrons of the carbonyl double bond. The π-bonded hydrogen bond donors are situated out of the O=C-N plane and the angle to the carbonyl C=O bond of 106 ° is more acute than "conventional" hydrogen bonding to the oxygen lone pairs. The analogous structure of thiourea displays several polymorphs,[8,9] however four hydrogen bonds are consistently observed in each structure; two bonded to the lone pairs and two others situated out of the S=C-N plane. The angle between the thiocarbonyl bond and the two out of plane hydrogen atoms is close to 90 ° in all polymorph structures.

Urea derivatives display different hydrogen bonding patterns to thiourea derivatives due to differing preferences in the conformation of the hydrogen atoms relative to one another; the *syn*- and *anti*-conformations are shown in figure 3.1.[10] While the *syn*-conformation is most common in urea derivatives, the *anti*-conformation is most common in thiourea derivatives. The hydrogen bonding motifs that arise from these preferences are chains formed by the tape motif of the *syn*-conformation, and centrosymmetric dimers formed the *anti*-conformation.

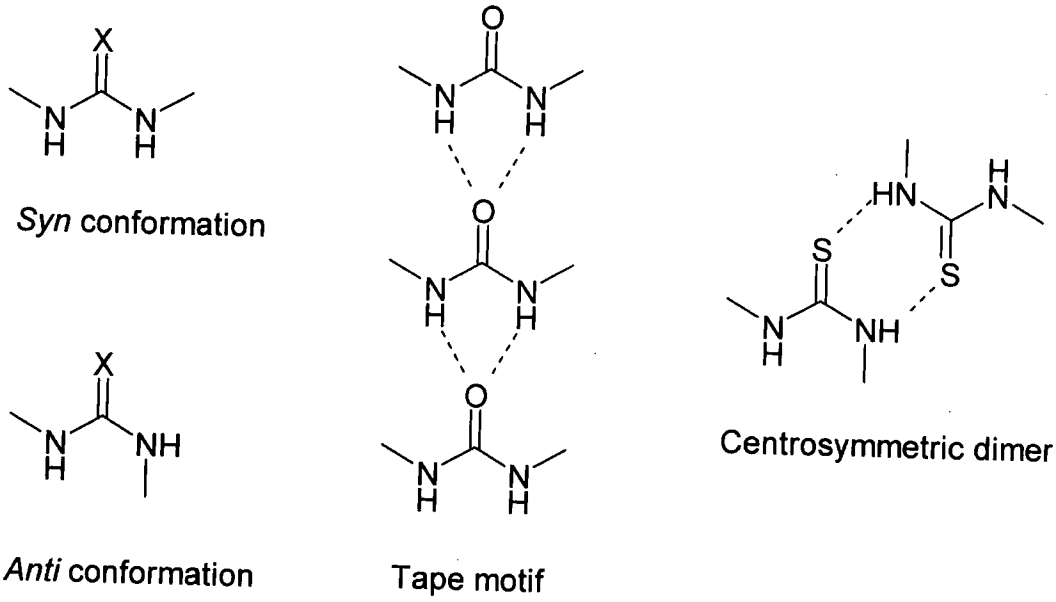

Figure 3.1: *Syn* and *anti* conformations that urea and thiourea derivatives may adopt in the solid-state. The *syn*-tape hydrogen bonding motif is common for urea derivatives, whereas the *anti*-centrosymmetric dimer formation is common for thiourea derivatives.[10]

The difference between hydrogen bonding to carbonyl and thiocarbonyl bonds has been sparsely discussed. An important study into the differences of hydrogen bonding to carbonyl and thiocarbonyl fragments utilized the Cambridge structural database (CSD) to compare the metrics of crystal structures from the literature.[11] It is shown that hydrogen bonds to C=S bonds are weaker than to C=O bonds, and that C=S fragments are more likely to accept more than one hydrogen bond donor. Interestingly, in the orientation distribution of H-bond donors it is observed that the distribution out of the plane of the lone pairs is more diffuse for thiocarbonyls, extending from the ideal 0 ° to a plane···H angle of 70 °, whereas the carbonyl bond tends to exist within the range of 0 to 20 °. Within the lone pair plane, the hydrogen bonding is more directional than carbonyl bonds.

Some recent work has been carried out on the electron density of the lone pairs on the sulphur atom in a thioureido group.[12] Bogdanović and co-workers have identified that the sulphur atom in the crystal structure of salicylaldehyde thiosemicarbazone has three different hydrogen bonds to it, fig. 3.2. One hydrogen bond is from a NH of a thioureido group of another molecule of salicylaldehyde thiosemicarbazone in a centrosymmetric dimer fashion (H(2N)···S(1)), while there is hydrogen bonding from a NH from another molecule (H(3A)···S(1)). Both of these interactions are in the thioureido plane. There is also a weak C-H donation from a

third molecule, which is out of the lone pair plane. This is a relatively long hydrogen bond with H(7)···S(1) distance of 3.008(8) Å and a C(7)-H(7)···S(1) angle of 124.64(7) °. The final NH, H(3B), hydrogen bonds to O(1).

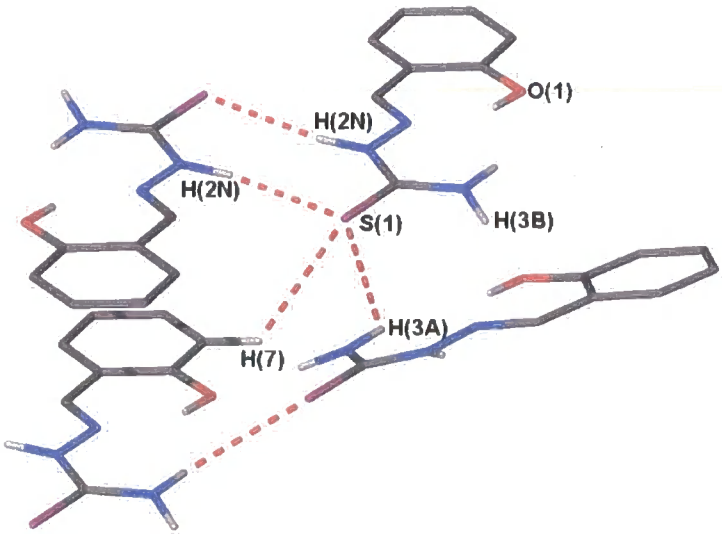

Figure 3.2: X-ray crystal structure of salicylaldehyde thiosemicarbazone displaying hydrogen bonding.[12]

A survey of the CSD found that 495 out of a total of 835 N-H hydrogen bond interactions to the thioureido crystal structures exist as centrosymmetric dimers, and these dimers were compared to the more general hydrogen bonding interaction to thioureido functional groups, D-H···S=C (D = C, O, N), where 3630 interactions are found at the time of publication. For the dimer, the average C=S···H bond angle is in the region of 110 to 115 °, whereas a wider distribution is observed for the general case, with an average in the region of 80 – 100 °. A lack of directionality in C=S···H bonding is attributed to the torus of the lone pair electrons around the sulphur atom being equally polarisable in or out of the plane.

3.2 Aims

From the crystal structures of several of the ligands synthesised in Chapter 2, it is apparent that an interaction with the sulphur atom orthogonal to the thiourea plane is present in some cases. The aim of the research is to quantify that interaction, and

compare it to the general hydrogen bonding interaction with carbonyl and thiocarbonyl groups.

3.3 Results and Discussion

To the best of our knowledge the interaction of hydrogen bond donors and the π-electrons of thiocarbonyls has not previously been identified or discussed. Here the synthesis and structure of several of the bisthiourea ligands and an analysis of the CSD covering incidence and metrics of the thiocarbonyl-π hydrogen bond interaction is presented.

3.3.1 Ligand crystal structures

1-(2-Amino-phenylene)-3-tert-butyl-thiourea (APBT) was synthesised as part of work undertaken in Chapter 2, and its structure determined by X-ray crystallography by Dr. Mike Probert (figure 3.3).

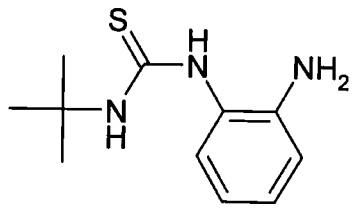

APBT

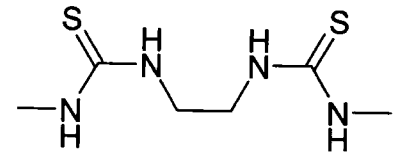

MMTET

The molecular bond lengths and angles are within expected ranges. Dimer formation through hydrogen bonded thiourea groups is common for thioureas[8,10] and is observed in this case for S(1) and H(2A), figure 3.3. The short H···S contact of 2.530 Å, the obtuse C=S···H angle of 107.3 °, and the low torsional angle between N(2)-C=S(1)···H(2A) of 11.1° with the thiocarbonyl bond is typical of conventional hydrogen bonding with the nonbonding lone pair. However, in the structure it can also be seen that one of the hydrogen atoms on the primary amine, H(1B), is directed towards the thiocarbonyl bond. In contrast to conventional hydrogen bonds, an acute angle of the hydrogen donor with the thiocarbonyl bond of 83.6 ° is observed. This brings the hydrogen almost as close to the centre of the double bond as it is to the

sulphur atom, with distances of 2.83 and 2.80 Å, respectively. Furthermore, the torsional angle between the hydrogen, the thiocarbonyl bond and the adjacent nitrogen atom (N-C=S···H) is 100.1 °; well out of the conventional lone pair hydrogen bonding plane. The interaction is weaker than that of S(1) and H(2A), with H(1B)···S(1) distance of 2.79(2) Å.

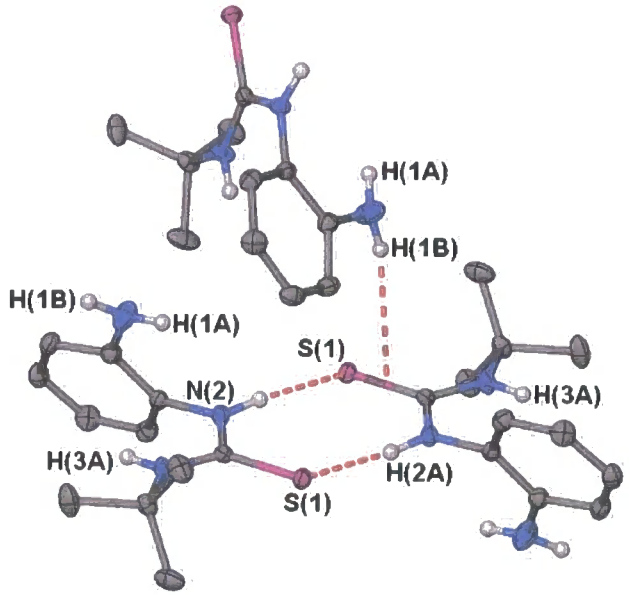

Figure 3.3: crystal structure of APBT showing one molecule hydrogen bond pairing with another in the 'centrosymmetric dimer' fashion, while a second molecule hydrogen bonds through N··H *into the π-electron density of the thiocarbonyl bond.*

These parameters give a strong indication of interaction between the hydrogen and the π-electron density of the double bond, and thus evidence that π-electrons of thiocarbonyl bonds act as hydrogen-bond acceptors, fig 3.4. Interestingly, there appears to be no interaction with other molecules from the remaining two hydrogen bond donor NH groups. The hydrogen from the other thioureido nitrogen N(3) appears to be hindered by the tertiary butyl group and aryl ring within the same molecule to it. There may be a weak N-H···π aromatic interaction. The other free hydrogen is also turned towards the aryl ring of another molecule, presumably from the interaction of the other hydrogen on the amine with the thiourea sulphur atom.

Therefore the lack of hydrogen bonding in these two NH groups is most likely attributable to surrounding steric bulk and dominance of the other hydrogen-bonding interactions.

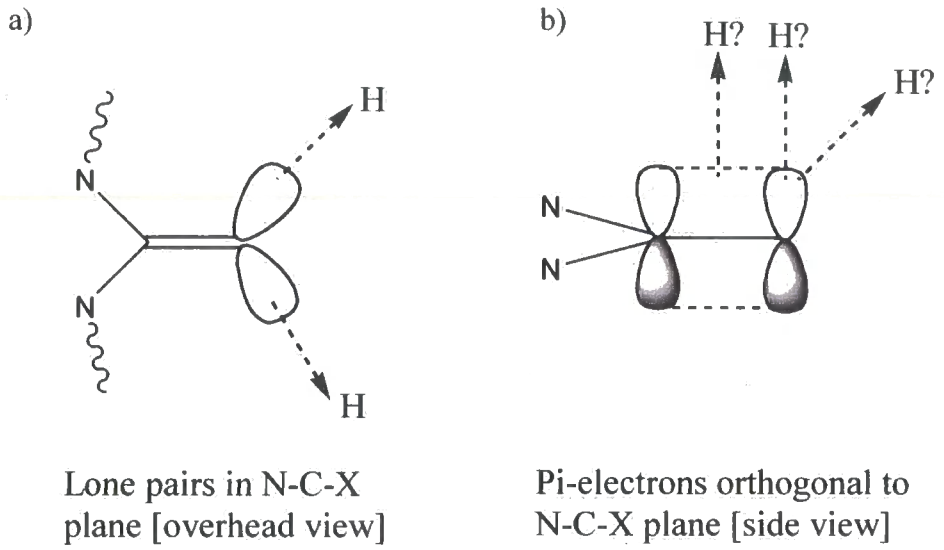

Figure 3.4: Schematic diagrams of hydrogen bonding to (thio)carbonyl a) lone pairs and b) π-electrons.

The structure of 1-methyl-3-[2-(3-methyl-thioureido)-ethyl]-thiourea (MMTET) was also determined by X-ray crystallography by Dr. Kirsty Anderson, and it exhibits very similar hydrogen bonding interactions to APBT, fig 3.5.

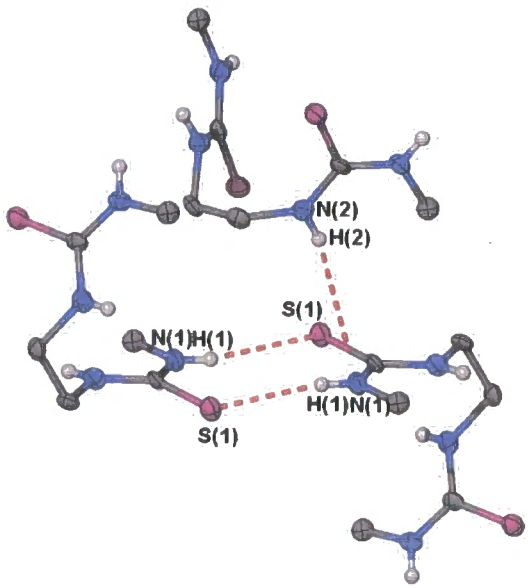

Figure 3.5: crystal structure of MMTET showing similar H-bond interactions to APBT.

A centrosymmetric dimer is present, as well as an interaction into the π-electrons of the thiocarbonyl bond. Again, the two different types of interaction display markedly different metrics, in particular the C=S···H angle is 110.2 ° for the centrosymmetric dimer pattern, whereas a C=S···H angle of 82.8 ° is found for the hydrogen-bond donor that is out of the thioureido plane, Table 3.1.

APBT	Hydrogen atom	
	H(2A)-S(1)	H(1B)-S1
S···H (Å)	2.5300	2.79(2)
C=S···H (°)	107.3	83.6
N-C=S···H (°)	11.2	100.1
S···N (Å)	3.3551(11)	3.6130(15)
C=S···N (°)	111.5	88.4
N-C=S···N (°)	173.7	95.8
MMTET	Hydrogen atom	
	H(1)-S1	H(2)-S1
S···H (Å)	2.55(6)	2.68(8)
C=S···H (°)	110.2	82.8
N-C=S···H (°)	11.8	71.5
S···N (Å)	3.348(6)	3.514(6)
C=S···N (°)	112.6	87.0
N-C=S···N (°)	10.2	109.9

Table 3.1: H-bond metrics for the structures of APBT and MMTET.

Further ligand crystal structures were obtained that show interesting hydrogen bonding.

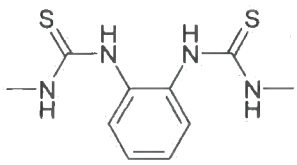

MMTPhT, L^2

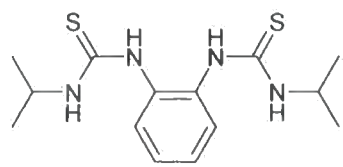

IITPhT, L^7

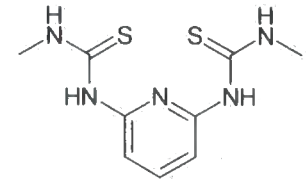

MMTPyT, L^3

The crystal structure of 1-methyl-3-[2-(3-methyl-thioureido)-phenyl]-thiourea (MMTPhT) was determined, and one thiourea group is arranged in the *anti* conformation, and thus arranged for the centrosymmetric dimerisation, while the other is arranged in the *syn* conformation. However in contrast to the structures of APBT and MMTET, MMTPhT does not exhibit the centrosymmetric dimerisation typical of thioureas. Each molecule (**A**), in fact, forms hydrogen bond dimers with three other MMTPhT molecules (**B-D**), fig 3.5.

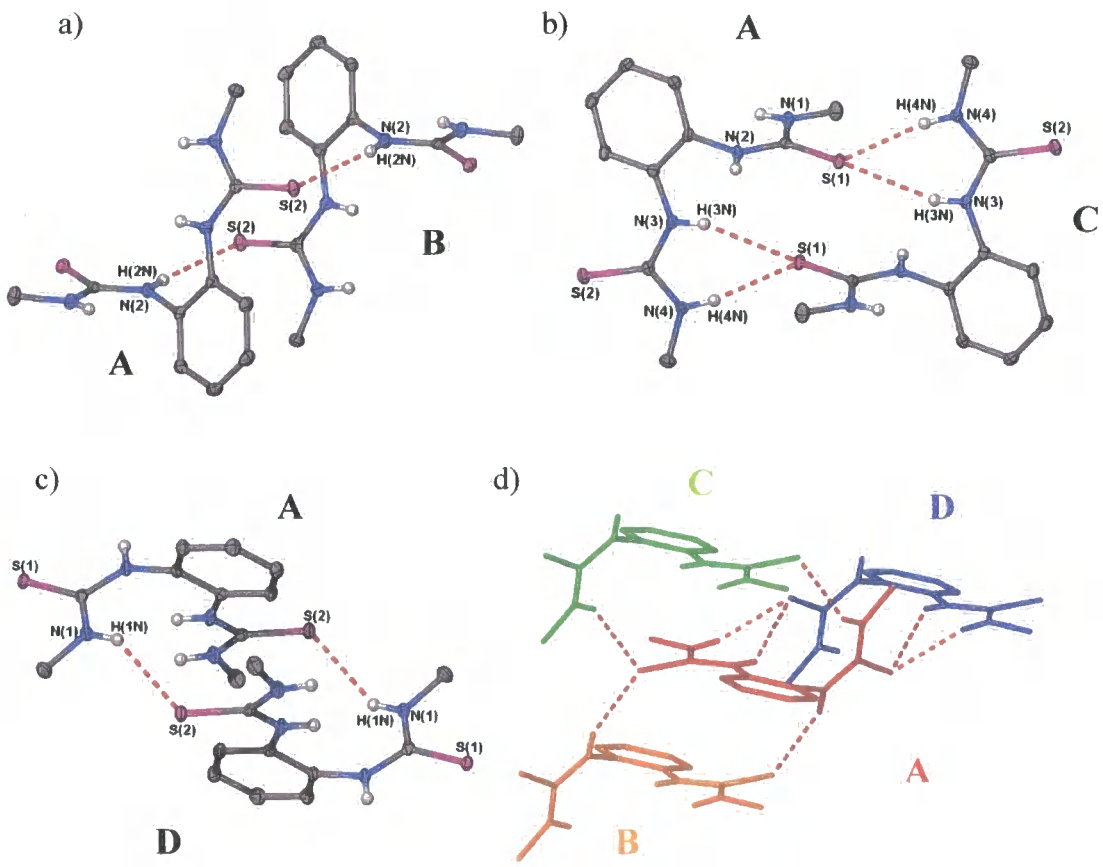

Figure 3.6: X-ray crystal structure of MMTPhT showing hydrogen bond dimerisation with three other MMTPhT molecules (a-c), and d) the eight hydrogen bonding interactions to a single MMTPhT molecule (red) from the three hydrogen bond dimers (green, blue and orange).

The structure of 1-isopropyl-3-[2-(3-isopropyl-thioureido)-phenyl]-thiourea (IITPhT) was also obtained, and does exhibit the centrosymmetric dimer, H(2N)···S(1), fig. 3.7. The other hydrogen of the thiourea group in the *anti* confirmation, H(1N), exhibits an intramolecular hydrogen-bond to the sulphur of the thiourea group in the *syn* conformation, S(2). The hydrogen atoms of this *syn* thiourea group bond to a sulphur atom of an adjacent molecule, and while one, H(4N), is reasonably in the plane of the thiourea group with a torsional angle of 24 °, the other, H(3N), is more out of the plane with a torsional angle of 55 °, Table 3.1. There is a significant difference in the C=S···H angle observed for these two hydrogen bonds as well: the C=S···H(3N) angle is 120 °, whereas for the H atom that is out of the plane the C=S···H(4N) angle is 88 °.

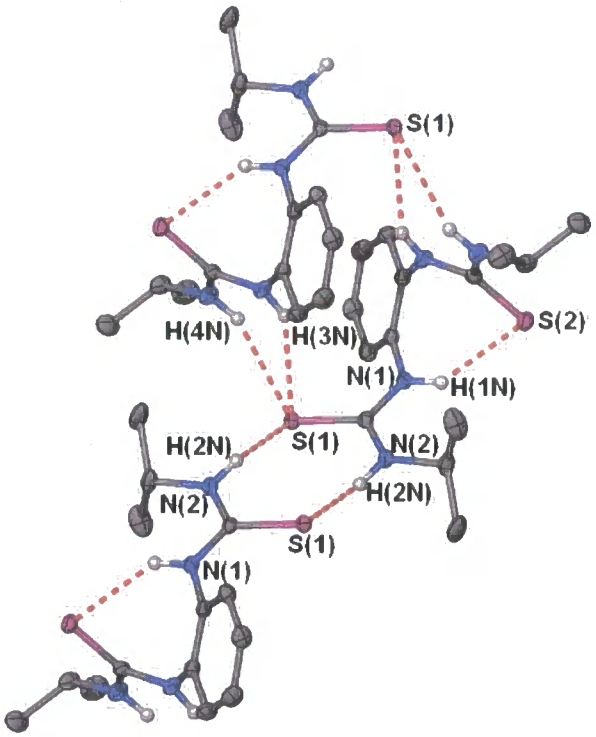

Figure 3.7: X-ray crystal structure of IITPhT showing hydrogen bonding.

No unusual hydrogen bonding was observed for the crystal structure of 1-methyl-3-[6-(3-methyl-thioureido)-pyridin-2-yl]-thiourea (MMTPyT), fig. 3.8. While each thiourea group forms centrosymmetrical dimer with H(11) and H(18), the remaining hydrogen atoms, H(1) and H(2), form intramolecular hydrogen bonds with the pyridyl nitrogen atom, N(8). As each arm forms a centrosymmetric dimer with another molecule, which in turn is forming a further dimer with the other thiourea group, one-dimensional chains are formed.

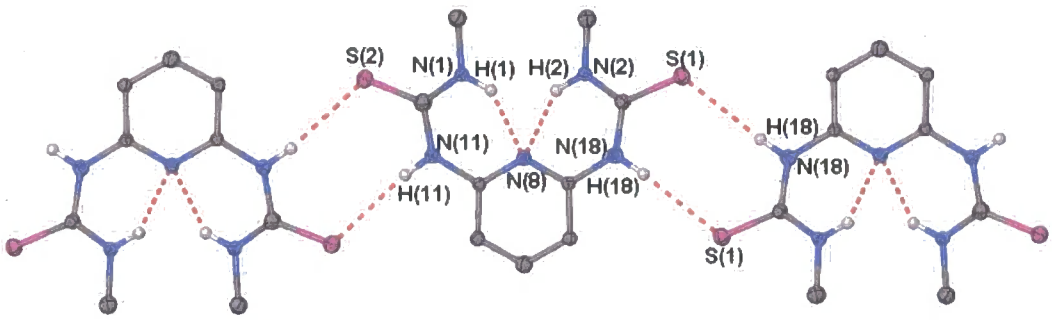

Figure 3.8: X-ray crystal structure of MMTPyT showing hydrogen bonding.

MMTPhT	Hydrogen atom			
	H(3N)-S1	H(4N)-S1	H(2N)-S2	H(1N)-S2
S···H (Å)	2.841(17)	2.477(19)	2.551(18)	2.620(19)
C=S···H (°)	125.4	117.0	113.0	124.0
N-C=S···H (°)	36.1	15.1	60.3	91.6
S···N (Å)	3.5205(11)	3.2848(11)	3.3232(11)	3.3250(11)
C=S···N (°)	133.1	122.1	107.3	131.4
N-C=S···N (°)	149.3	16.1	62.0	95.8
IITPhT	Hydrogen atom			
	H(3N)-S1	H(4N)-S1	H(1N)-S2	H(2N)-S1
S···H (Å)	2.520	2.810	2.380	2.630
C=S···H (°)	88.3	119.8	81.1	105.8
N-C=S···H (°)	57.0	23.7	54.9	29.8
S···N (Å)	3.2840(17)	3.4948(18)	3.1082(15)	3.3949(16)
C=S···N (°)	95.2	123.9	74.2	111.0
N-C=S···N (°)	116.7	144.8	47.1	23.0

Table 3.2: Hydrogen bonding metrics for MMTPhT and IITPhT.

3.3.2 CSD comparison of carbonyl and thiocarbonyl H-bond interactions

There has been very little discussion of hydrogen bonding interactions with the π-electrons of thiocarbonyl groups. A recent example reported the CH interaction with thiocarbonyls, as discussed in the introduction of this chapter.[12] To further investigate the interaction, a search of the CSD was undertaken to explore hydrogen atoms bonded to good hydrogen bond donors Q (Q = N, O) that were bonded to hydrogen atoms within the sum of the van der Waals radii of the acceptor of both thiocarbonyl and carbonyl moieties. A comparative study was undertaken to investigate the torsional angle from the hydrogen through the C=X bond (X = O, S) and to an adjacent atom. It is expected that interactions with the carbonyl or thiocarbonyl lone pair will be in the plane of the S-C-N fragment since the S and O atoms are sp^2 hybridised. Therefore deviation away from a torsional angle of zero degrees will reduce the lone pair character of an interaction whilst increasing interaction with the orthogonal π-electrons of the thiocarbonyl double bond.

For the case of NM-C=S···H-Q (NM = any non-metal), 1,623 hits were generated in the CSD constituting 3,146 fragments, while for NM-C=O···H-Q, a very large number of hits (38,179) were generated. A scatter plot of the torsional angle distribution displays typical behaviour for bonding to lone pairs with interactions clustering around 0 and 180 °.

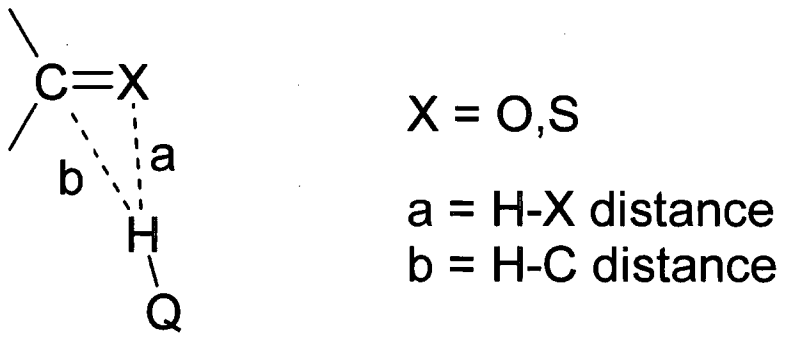

Figure 3.9: schematic showing the H-C and H-X bond distances. The ratio H-C/H-X indicates the relative position of the hydrogen atom to the C=X bond, so that a decrease in the ratio is indicative of the hydrogen atom moving closer to the carbon atom.

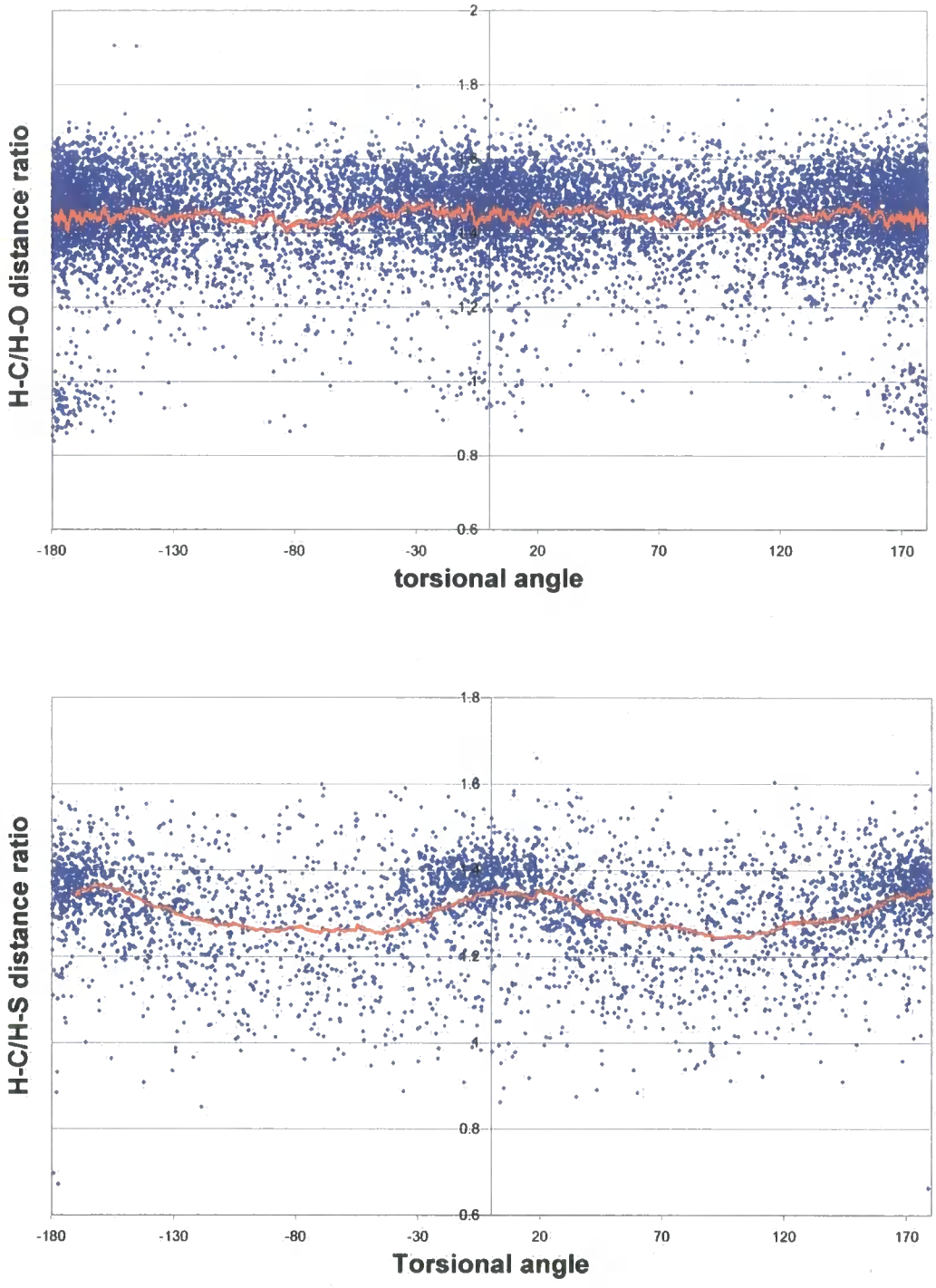

Figure 3.10: Graphs of torsional angle vs ratio of H···C and H···X distance in hydrogen bonding to C=X (X = O, S). While for the carbonyl bond (X = O) there is no variation in this ratio over the torsional angle range, there is a significant reduction in H-C/H-S for the thiocarbonyl range around 90 and -90 °.

However, a plot of the ratio of distances from the hydrogen to carbon and sulphur atoms, H···C/H···S, figure 3.10 (orange line denotes moving average) in thiocarbonyls shows that as the torsional angle increases from zero, this ratio decreases in magnitude. In other words, the hydrogen atom moves towards the centre of the C=S bond as it moves out of the lone pair plane. This behaviour is not observed in the C=O case, where a constant average ratio is maintained throughout the torsional range, figure 3.10.

Further evidence is given by the distribution of the hydrogen atoms about the thiocarbonyl bond. A distribution plot of hydrogen bond donors about the X=C-N fragment (for X=S,O) for all entries in the CSD with Q-H···X=C-N contacts was generated using ISOSTAR.[13] It is clear that the hydrogen bond donation to the lone pairs is the dominant form of hydrogen bonding to both of these fragments. However, if the search is limited to a torsional angle range of 60 to 120° for the H···X=C-N, a large difference in the distribution of hydrogen bond donors around the central X=C-N fragment is observed. Contour plots of these distributions are shown in figure 3.11. For the carbonyl case, the distribution is centred at angle of 135° to the carbonyl bond and with an elongated 'tail' down to 180° to the bond. The distance from the oxygen atom to the area most densely populated by donor atoms is the region of 3.0 Å. In contrast, the thiocarbonyl distribution is more spherical and centered at 95° to the thiocarbonyl bond, with an S-Q distance in the region of 4.0 Å. The distances and angles from the maximum density of the donor atoms to the double bond were also found. For the carbonyl case, the maximum donor atom density Q was found at a distance of 2.9 Å from the oxygen atom and at an angle of 135° to the carbonyl bond. The maximum density of the donor atom Q was found to be somewhat further from the acceptor S atom of the thiocarbonyl than in the carbonyl case at a distance of 3.8 Å, but at an angle of 89° to the thiocarbonyl bond.

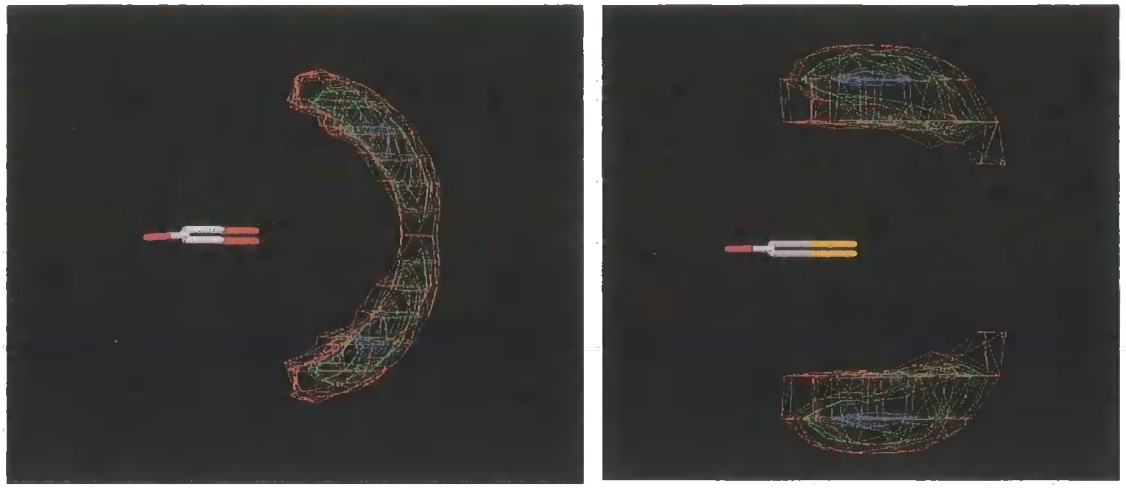

Figure 3.11: Contour plots for the density of H-bond donors within the torsional angle range of 60 – 120 ° from the acceptor fragment, a) NM-C=O carbonyl bond and b) NM-C=S thiocarbonyl bond, created from entries in the CSD.

As can be observed from the contour plots, there is a striking difference in the distribution of H-bond donors to the two bonds within this torsional angle range. Our examples (APBT and MMTET) lie at the front closer to the carbon atom of the most populated blue region with a C=S···N angles of 88.4 ° and 87.0 ° and S···N distances of 3.6130(15) and 3.514(6) Å, for APBT and MMTET, respectively. They also possess a very similar angle to the thiocarbonyl bond as the maximum donor density, with a slightly shorter S---N distance.

NM-C=O				NM-C=S		
	Full	Tor 60-120 °			Full	Tor 60-120 °
O···H (Å)	1.90	2.06		S-H	2.63	2.59
C=O···H (°)	117	134		C=S-H	115	107
N-C=O···H (°)	0	108		N-C=S-H	0	97
O···Q (Å)	2.55	2.92		S-Q	3.63	3.36
C=O···Q (°)	125	134		C=S-Q	114	85
N-C=O···Q (°)	0	92		N-C=S-Q	0	107

Table 3.3: Hydrogen bond metrics for the general carbonyl (NM-C=O) and thiocarbonyl cases (NM-C=S) from entries in the CSD. Average bond distances and angles are given for each using the full data range (Full) and limiting data to those at a torsional range of 60 – 120 ° to the NM-C=X fragment (Tor 60-120 °).

The metrics for the general carbonyl and thiocarbonyl cases are summarized in Table 3.2. It can be seen that the H-bond distance to carbonyls is generally stronger than to the thiocarbonyl bonds with X···H distances of 1.90 and 2.63 Å, respectively. While for carbonyls the bonding to hydrogen atoms is relatively weakened in the cases where the torsional angle is between 60 and 120 ° from the general case (1.90 to 2.06 Å), a slightly stronger interaction is observed for examples at torsional angles between 60 and 120 ° (2.63 to 2.59 Å). It is also possible to see that for both carbonyl and thiocarbonyl general cases the C=X···H bond angle is similar at 117 ° and 115 ° for the carbonyl and thiocarbonyl bonds respectively. However, at high torsional angles, the angle between the H atom and the carbonyl bond increases to 134 °, whereas the thiocarbonyl decreases to 107 °. Due to the positioning of the H-bond density donor over the sulphur atom, at C=S···H angles in the region of 90 °, it is likely that the π-electrons of the thiocarbonyl bond are more involved in this type of hydrogen bonding than is suggested by Bogdanović *et al.*

Limiting the search to hydrogen contacts with a C=X···H angle of less than 90 ° for all torsional angles gives another interesting result. For carbonyls the predominant contact is at low (around 0 or 180 °) torsional angle, indicative of lone pair bonding. It should be noted that a small proportion of the hydrogen bond donors are involved in π-type bonding.

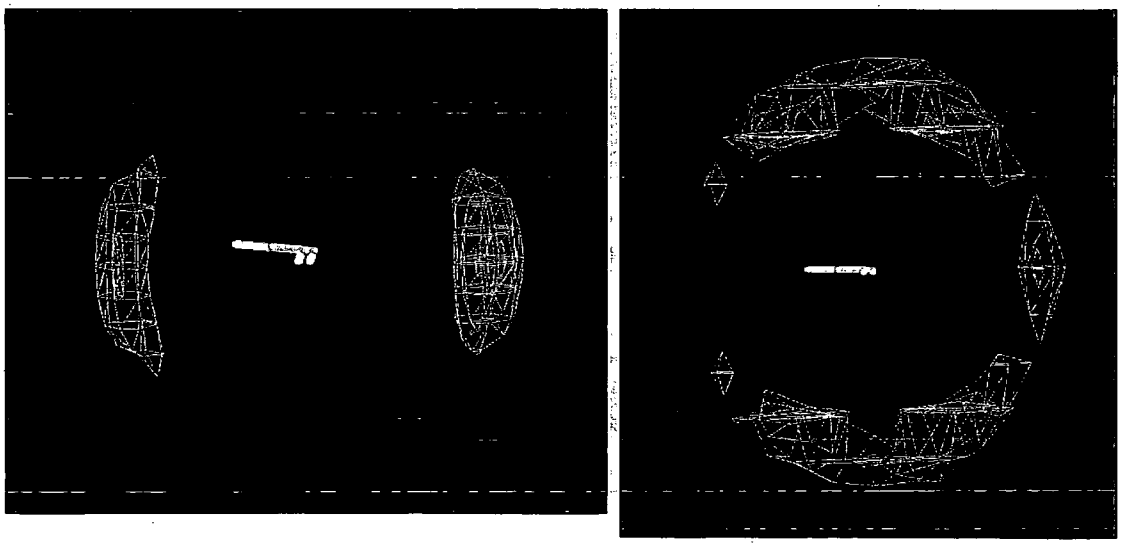

Figure 3.12: Contour plots for the density of H-bond donors which are less than 90 ° to the C=X bond for a) N-C=O carbonyl bond and b) N-C=S thiocarbonyl bond, created from entries in the CSD.

However, for thiocarbonyls the majority of H-bond donors that possess a hydrogen at less than 90 ° to the C=S bond are in the torsional angle range of 60 to 120 °, indicative of π-type bonding. A minor fraction of the donors bond through the lone pairs as exhibited by the small contour in the N-C=S plane.

3.4 Conclusions

In conclusion we give evidence that the π-electron density from thiocarbonyls is an effective H-bond acceptor and interactions to the π-electron density of thiocarbonyl is more prevalent than the oxygen analogue. While the present examples exhibit a slightly weaker than average interaction, the parameters of torsional angle and donor to acceptor angle show typical directional behaviour towards the π-electrons.

3.5 Experimental

3.5.1 Crystal data

X-ray diffraction: Diffraction quality single crystals were obtained by slow evaporation of ethanol solutions, with the exception of MMTPhT, which were obtained from MeOH/H_2O solutions. The diffraction experiments, using graphite-monochromated MoKα radiation (λ = 0.71073 Å), were carried out on SMART 1K or Kappa CCD (X-rays from a 60 W microfocus Bede Microsource® with glass polycapillary optics), covering a full sphere of the reciprocal space by three or four runs of narrow-frame (0.3°) ωscans. The crystals were cooled using Cryostream (Oxford Cryosystems) open-flow N_2 cryostats. The structures were solved by direct methods and refined by full-matrix least-squares on F^2 for all the data using SHELXTL software.[14,15]

3.5.1.1 1-Methyl-3-[2-(3-methyl-thioureido)-phenyl]-thiourea (MMTPhT)

Crystal data for MMTPhT: $C_{10}H_{14}N_4S_2$, M = 254.37, colourless block, 0.28 × 0.24 × 0.10 mm^3, monoclinic, space group $C2/c$ (No. 15), a = 18.0632(8), b = 7.5649(3), c = 19.4089(8) Å, β = 116.0840(10)°, V = 2382.03(17) Å^3, Z = 8, D_c = 1.419 g/cm^3, F_{000}

= 1072, Bruker SMART 1K CCD Diffractometer, MoKα radiation, λ = 0.71073 Å, *T* = 120(2)K, $2\theta_{max}$ = 60.7°, 13725 reflections collected, 3395 unique (R_{int} = 0.0269). Final *GooF* = 1.054, *R1* = 0.0296, *wR2* = 0.0735, *R* indices based on 2966 reflections with I >2σ(I) (refinement on F^2), 201 parameters, 0 restraints. Lp and absorption corrections applied, μ = 0.425 mm^{-1}.

3.5.1.2 1-Methyl-3-[6-(3-methyl-thioureido)-pyridin-2-yl]-thiourea (MMTPyT)

Crystal data for MMTPyT : $C_9H_{13}N_5O_0S_2$, *M* = 255.36, 0.38 × 0.30 × 0.14 mm^3, triclinic, space group *P*-1 (No. 2), *a* = 5.8023(8), *b* = 9.4517(14), *c* = 11.1516(15) Å, α = 87.561(9), β = 75.003(9), γ = 75.325(9)°, *V* = 571.30(14) $Å^3$, *Z* = 2, D_c = 1.484 g/cm^3, F_{000} = 268, CuKα radiation, λ = 1.54178 Å, *T* = 173(2)K, $2\theta_{max}$ = 118.0°, 2145 reflections collected, 1282 unique (R_{int} = 0.0359). Final *GooF* = 1.765, *R1* = 0.1285, *wR2* = 0.3884, *R* indices based on 1033 reflections with I >2σ(I) (refinement on F^2), 147 parameters, 96 restraints. Lp and absorption corrections applied, μ = 4.069 mm^{-1}.

3.5.1.3 1-Methyl-3-[2-(3-methyl-thioureido)-ethyl]-thiourea (MMTET)

Crystal data for MMTET: $C_6H_{14}N_4S_2$, *M* = 206.33, colourless triangular plate, 0.30 × 0.20 × 0.20 mm^3, tetragonal, space group $P4_2/n$ (No. 86), *a* = *b* = 9.4921(13), *c* = 10.800(2) Å, *V* = 973.1(3) $Å^3$, *Z* = 4, D_c = 1.408 g/cm^3, F_{000} = 440, Kappa CCD, MoKα radiation, λ = 0.71073 Å, *T* = 120(2)K, $2\theta_{max}$ = 61.0°, 11056 reflections collected, 1404 unique (R_{int} = 0.4069). Final *GooF* = 1.058, *R1* = 0.1346, *wR2* = 0.3087, *R* indices based on 793 reflections with I >2σ(I) (refinement on F^2), 65 parameters, 0 restraints. Lp and absorption corrections applied, μ = 0.502 mm^{-1}.

3.5.1.4 1-Isopropyl-3-[2-(3-isopropyl-thioureido)-phenyl]-thiourea (IITPhT)

Crystal data for IITPhT: $C_{14}H_{22}N_4S_2$, *M* = 310.48, colourless block, 0.28 × 0.21 × 0.12 mm^3, triclinic, space group *P*-1 (No. 2), *a* = 9.4599(6), *b* = 9.5946(6), *c* = 11.0971(7) Å, α = 78.9840(10), β = 66.4850(10), γ = 65.0450(10)°, *V* = 837.03(9) $Å^3$, *Z* = 2, D_c =

1.232 g/cm^3, F_{000} = 332, SMART 1K, MoKα radiation, λ = 0.71073 Å, T = 120(2)K, $2\theta_{max}$ = 60.1°, 8785 reflections collected, 4507 unique (R_{int} = 0.0439). Final *GooF* = 1.018, *R1* = 0.0392, *wR2* = 0.0918, *R* indices based on 3673 reflections with I >2σ(I) (refinement on F^2), 181 parameters, 0 restraints. Lp and absorption corrections applied, μ = 0.315 mm^{-1}.

3.5.1.5 1-(2-Amino-phenyl)-3-tert-butyl-thiourea (APBT)

Crystal data for APBT: $C_{11}H_{17}N_3S$, M = 223.34, colourless block, 0.39 × 0.19 × 0.18 mm^3, monoclinic, space group $P2_1/n$ (No. 14), a = 10.6285(4), b = 9.7517(4), c = 12.8232(5) Å, β = 109.7120(10)°, V = 1251.19(9) Å^3, Z = 4, D_c = 1.186 g/cm^3, F_{000} = 480, SMART 1K, MoKα radiation, λ = 0.71073 Å, T = 120(2)K, $2\theta_{max}$ = 60.8°, 11735 reflections collected, 3477 unique (R_{int} = 0.0598). Final *GooF* = 1.042, *R1* = 0.0373, *wR2* = 0.0922, *R* indices based on 2825 reflections with I >2σ(I) (refinement on F^2), 144 parameters, 0 restraints. Lp and absorption corrections applied, μ = 0.233 mm^{-1}.

3.5.2 CSD search

CSD search and Isogen plot method: A search of the CSD was undertaken using the central fragment of NM-C=X (NM = any non-metal atom, X = S,O) and a contact group of H-Q (Q=N,O) where an X···H contact (distance between atoms no larger than sum of van de Waals radii) existed. Similar searches were conducted applying one of the following two constraints: NM-C=X···H torsional angles limited to between 60° and 120°, or C=X···H angle no greater than 90°. The parameters and coordinate files were saved for these searches and used to generate scatter plots in the Isogen program. Contour scatter plots of the donor atom, Q, were generated in Rasmol with an internal scaling of 20 (red), 40 (green), and 80 (blue). The maximum density was found by setting all scales to 99, and measurements were taken using the tools provided by the program.

3.6 References

(1) Nishio, M.; Umezawa, Y.; Hirota, M.; Takeuchi, Y. *Tetrahedron* **1995**, *51*, 8665.

(2) Meyer, E. A.; Castellano, R. K.; Diederich, F. *Angew. Chem. Int. Ed.* **2003**, *42*, 1210.

(3) Sobczyk, L.; Grabowski, S. J.; Krygowski, T. M. *Chem. Rev.* **2005**, *105*, 3513.

(4) Sklar, N.; Senko, M. E.; Post, B. *Acta Crystallogr.* **1961**, *14*, 716.

(5) Vaughan, P.; Donohue, J. *Acta Crystallogr.* **1952**, *5*, 530.

(6) Swaminathan, S.; Craven, B. M.; Spackman, M. A.; Stewart, R. F. *Acta Crystallogr. Sect. B* **1984**, *40*, 398.

(7) Swaminathan, S.; Craven, B. M.; McMullan, R. K. *Acta Crystallogr. Sect. B* **1984**, *40*, 300.

(8) Elcombe, M. M.; Taylor, J. C. *Acta Crystallogr. Sect. A* **1968**, *A 24*, 410.

(9) Takahashi, I.; Onodera, A.; Shiozaki, Y. *Acta Crystallogr. Sect. B* **1990**, *46*, 661.

(10) Masunov, A.; Dannenberg, J. J. *J. Phys. Chem. B* **2000**, *104*, 806.

(11) Allen, F. H.; Bird, C. M.; Rowland, R. S.; Raithby, P. R. *Acta Crystallogr. Sect. B* **1997**, *53*, 680.

(12) Novakovic, S. B.; Fraisse, B.; Bogdanovic, G. A.; Spasojevic-deBire, A. *Cryst. Growth Des.* **2007**, *7*, 191.

(13) Bruno, I. J.; Cole, J. C.; Lommerse, J. P. M.; Rowland, R. S.; Taylor, R.; Verdonk, M. L. *J. Comput.-Aided Mol. Des.* **1997**, *11*, 525.

(14) *SHELXS*, Sheldrick, G. M. University of Göttingen, 1997.

(15) *SHELXL*, Sheldrick, G. M. University of Göttingen, 1997.

Chapter 4: Coordination of bisthiourea ligands to platinum group metals

4.1 Introduction

4.1.1 Ruthenium(II) thioureido complexes

A few examples of the coordination of thiourea derivatives to ruthenium have been given in Chapter 1.2.3. A few more will be given in this section to demonstrate the wide range of coordination modes that may be adopted by these ligands.

The solution and solid-state structures of mixed valent diruthenium(II,III) tetraacetate complexes of formula $[Ru_2(\mu\text{-}O_2CCH_3)_4L_2](PF_6)$, where L = 1,1,3,3-tetramethylthiourea, show coordination of the thiourea derivative to the ruthenium through sulphur atoms to discrete dimetal complexes.[1] In contrast, reacting a diruthenium cluster with just one equivalent of thiourea, $H_2NC(=S)NH_2$, yields $[Ru_2(\mu\text{-}O_2CCH_3)_4(\text{thiourea})](PF_6)$, that forms an insoluble coordination polymer. The IR spectroscopy gives evidence that the thiourea is coordinating to the metal through sulphur and one of the amine nitrogen atoms, and that the thiourea bridges between metals to form polymeric chains.

Thiourea groups incorporated into heterocyclic compounds produce some interesting coordination complexes. 1,3,5-Triazine-2,4,6-trithiol, **4.1**, can potentially form a number of coordination modes with metals, fig. 4.1, and in the solid state forms symmetrical trimeric complexes with ruthenium(II), $[\{L_2Ru\}_3(\mu_3\text{-}\mathbf{4.1})](ClO_4)_3$, where L = arylazopyridine.[2] The N,S four-membered metallacyclic structure can be seen in the crystal structure, figure 4.1. Further examples of the N,S bidentate binding to ruthenium of heterocyclic thiourea ligands can be found in the work of Wilton-Ely[3] and Sousa.[4]

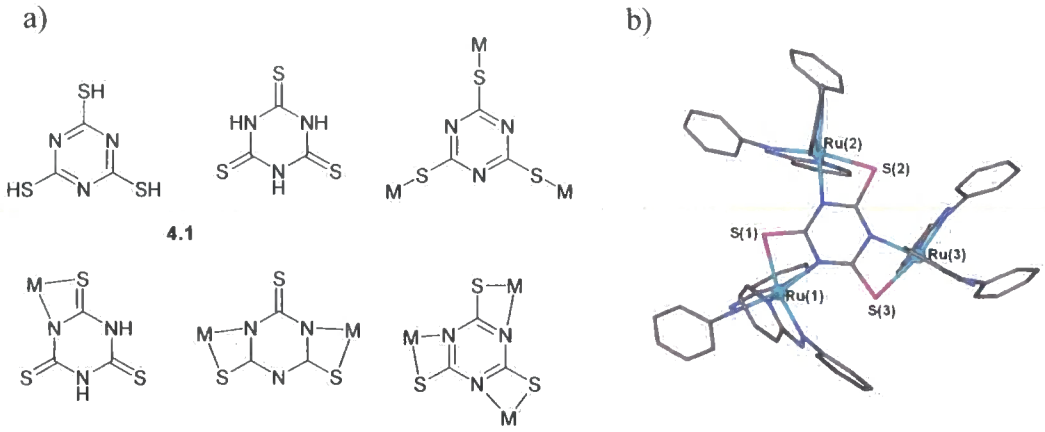

Figure 4.1: a) 1,3,5-triazine-2,4,6-trithiol in thiol and thione form, and some of the many potential binding modes towards metals. b) Crystal structure of the symmetrical trimeric complex $[\{L_2Ru^{II}\}_3(\mu_3\text{-}4.1)](ClO_4)_3$.[2]

The reaction of thiourea and its derivatives with ruthenium clusters was initially studied by Süss-Fink and co-workers.[5-12] Thiourea, dimethylthiourea and diphenylthiourea react with $[Ru_3(CO)_{12}]$ to yield the hydrido complex $[Ru_3(\mu\text{-H})(\mu_3\text{-}\eta^2\text{-RNCSNRH})(CO)_9]$ with NH bond cleavage, whereas the reaction with diisopropylthiourea and diethylthiourea under more forcing conditions results in C=S bond cleavage and formation of tetraruthenium clusters with diaminocarbene bridging sulphido ligands. More recently, the reaction of dppm-substituted ruthenium clusters with thiourea and tetramethylthiourea has resulted in the identification of several new coordination modes in addition to those obtained by Süss-Fink.[13]

There has also been much work on tripodal heterocyclic thiourea ligands based around a core of a central boron atom, tris(methimazoyl)hydroborate (Tm). The coordination of this ligand to Ru(II) has been studied and crystal structures with three sulphur atoms coordinating to Ru has been obtained firstly by Hill,[14] and later by Bailey.[15] The Hill complex, $[Ru(\kappa\text{-}S,S,S,B\text{-Tm} - H)(PPh_3)CO].CHCl_3$, **4.2**, has the tripodal binding mode of the three sulphur atoms and in addition the hydride of the hydroborate ligand has been lost, resulting in coordination of the B atom. In contrast there is no hydride loss and thus no B atom coordination in $[Ru(\eta^6\text{-}C_6H_4MeCH(Me)_2)(\kappa\text{-}S,S,S\text{-Tm})]Cl.H_2O$, **4.3**. The symmetry and electrochemistry of these compounds has been studied further.[16-18]

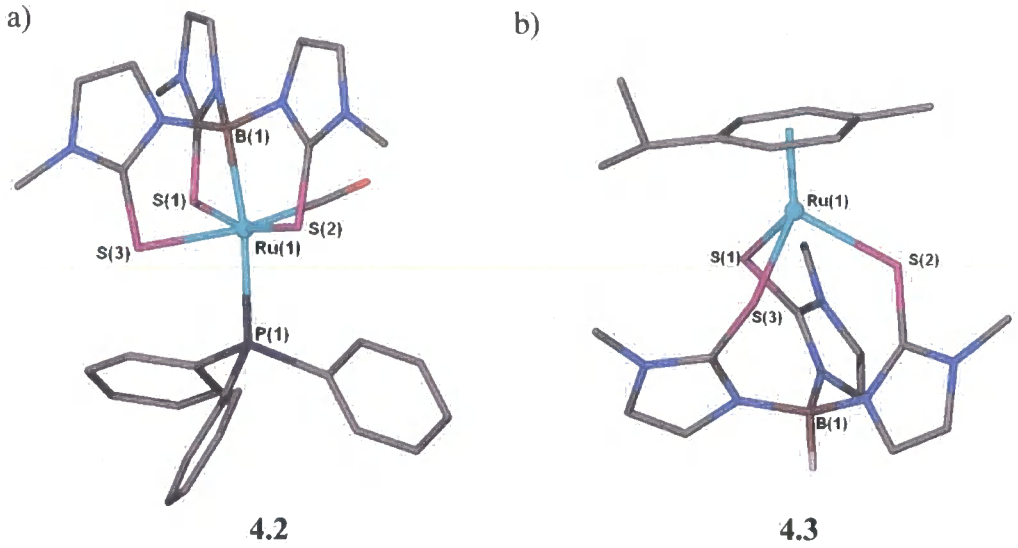

4.2 **4.3**

Figure 4.2: molecular structures of tris(methimazoyl)hydroborate coordination to Ru(II) with a) boron deprotonation and coordination, 4.2, and b) borohydride bond conservation and thus no B coordination, 4.3.[14,15]

Of note is the work performed on the ligand related to thiourea, the thiosemicarbazones, RCH=NNHC(=S)NHR', and their coordination chemistry.[19] These ligands are potentially able to chelate to Ru(II) through the sulphur and additional nitrogen atoms to form five-membered Ru-S—N-Ru metallacycles. A series of Ru(II) and Pd(II) complexes of type $[Ru(COD)(L)Cl_2]$ and $[Pd(L)Cl_2]$, where L = semithiocarbazone, were synthesised by Azam, and their *in vitro* antiamoebic activity studied.[20-22] While the 5-nitrothiophene-2-carboxaldehyde-4-benzylpiperidine thiosemicarbazone ligand, **4.4** (fig. 4.3a), itself shows a significant antiamoebic activity (IC_{50} = 2.56 μM), the ruthenium(II) and palladium(II) complexes of this ligand show a significant enhancement in activity with IC_{50} 1.75 μM and 0.84 μM, respectively. The most active semithiocarbazone coordination complex reported by the group to date is the with the 4-(2-adamantyl)-1-(thiophene-2-ylmethylene)thiosemicarbazide (**4.5**) ligand and the Ru(II) complex, $[Ru(COD)(\mathbf{4.5})Cl_2]$, displays an IC_{50} = 0.30.[22]

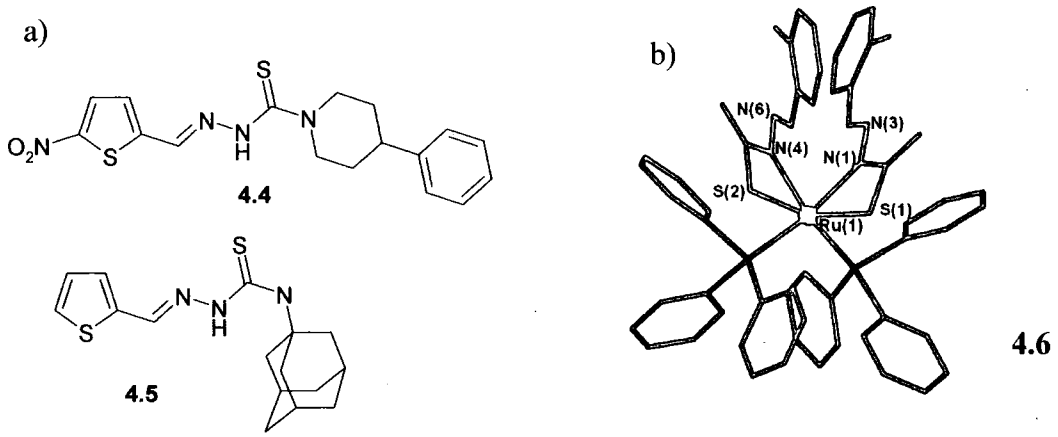

Figure 4.3: a) Semithiocarbazones that form antiamoebic Ru(II) complexes,[20-22] and b) X-ray crystal structure of [Ru(κ-*N,S*-*p*-nitrobenzaldehyde thiosemicarbazone)$_2$(PPh$_3$)$_2$] (4.6) with a N,S four-membered metallacycle.[23]

While the five-membered chelating metallacycle is thought to be the most stable form, deprotonation of the nitrogen atom adjacent to the C=S and coordination to Ru and Os to form four-membered metallacycles, such as [Ru(κ-*N,S*-*p*-nitrobenzaldehyde thiosemicarbazone – H)$_2$(PPh$_3$)$_2$] (**4.6**), were first observed by Bhattacharya in 1997, fig 4.3b).[23-25] Subsequently further examples have been obtained,[26-28] prompting the discussion of stability of four- and five-membered rings.

4.1.2 Pd(II) and Pt(II) thioureido complexes

The catalytic activity of palladium thiourea species has been discussed in Chapter 1.2.2, so this section will only discuss some recent coordination complexes.

Cauzzi and co-workers have coordinated an unusual phosphorus/thiourea bifunctional ligand, PhNHC(S)NHCH$_2$CH$_2$PPh$_2$, (Ptu), to Pd(II).[29] The thiourea groups bind to the metal *trans* to one another, and a seven-membered chelating ring is formed with the thioureido group hydrogen bonding to chloride counter-ions, fig. 4.4. This ligand was sol-gel processed to form immobilized ligands, which were loaded with Rh(I) and Pd(II). The hybrid xerogels are catalytically active in the hydroformylation of styrene, but the Rh(I) gel suffers from metal leaching while the Pd(II) analogue activity is strongly dependent upon the formation of metal colloid particles due to insufficient number of donor ligands around metal centres to prevent the reduction of the metal.

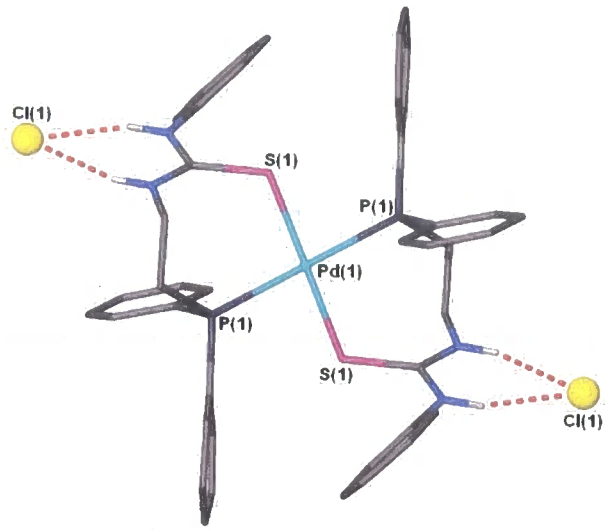

Figure 4.4: molecular structure of $[Pd(Ptu)_2]Cl_2$, showing seven-membered metallacycles and thioureido group hydrogen bonding to chloride counter-ions.[29]

The modification of platinum(II) antitumour complexes with monofunctional and bifunctional thiourea ligands has been studied by Bierbach *et al.*.[30] The structures of mononuclear $[Pt(en)(tmtu)Cl]NO_3$, **4.7**, (tmtu = tetramethylthiourea) and dinuclear $[\{Pt(en)Cl\}_2(\mu\text{-}(C_2H_4(NMeCSNMe_2)_2)\text{-}S,S')](NO_3)_2$, **4.8**, complexes were determined, and related platinum-acridine pharmacaphore complexes were tested for their biological activity against leukemia.[31]

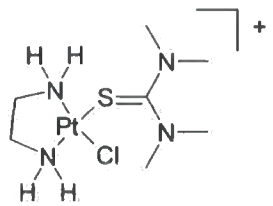

4.7

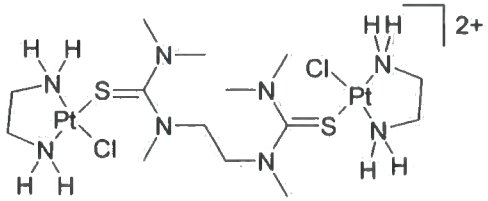

4.8

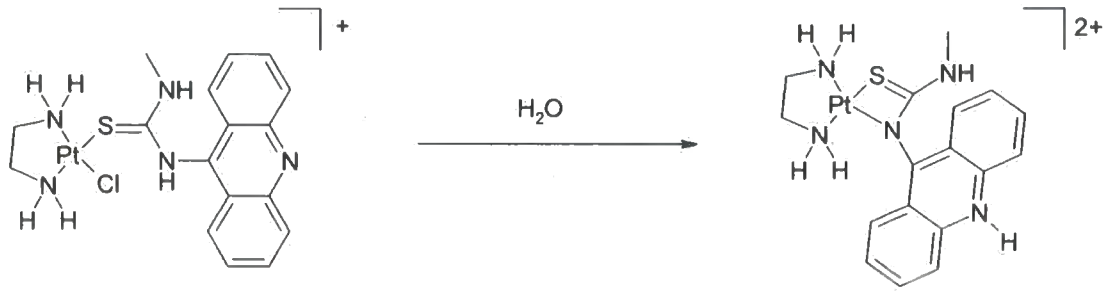

4.9

Scheme 4.1: Deprotonation of thioureido nitrogen by water to form a 4-membered N,S chelate ring with platinum(II).[30,31]

Where the thioureido ligand possesses a protonated nitrogen atom, the platinum complex, **4.9**, undergoes deprotonation at the nitrogen atom, followed by coordination of that nitrogen atom to the metal, scheme 4.1. This is thought to make the complex biologically inactive, as a labile coordinated chloride ligand is required so that the platinum complex may coordinate to the DNA of the cancer cells. Pt complexes with ligands that are methylated at the nitrogen, such as MeHNC(S)NMeAc (**4.10a**) and MeHNC(S)NMe(CH_2CH_2)NHAc (**4.10b**), do not experience the deprotonation, and their biological activity against leukemia cells is found to be IC_{50} = 75 and 0.13 μM for [Pt(en)(**4.10a**)Cl](NO_3) and [Pt(en)(**4.10b**)Cl](NO_3), respectively.

4.1.3 Cu(I) thioureido complexes

Thioureido complexes with copper(I) chloride occur in several different binding modes. Simple monomeric trigonal CuL_2Cl type thioureido complexes are common[32-34] with typically one NH hydrogen bonding to the coordinated chloride ligand. However, other binding modes, such as Cu-S-Cu bridged dimers[35-37] and polymers,[38,39] and chloride bridged dimers with exo-coordinated thioureido ligands[40-42] are known. Of particular interest is the structural characterization of a CuL_2Cl complex, where L = N-phenyl-N'-2-propenoylthiourea (PTU), where the X-ray crystal structure contains both chloride and sulphur bridged dimers in the same unit cell, fig 4.5.[42]

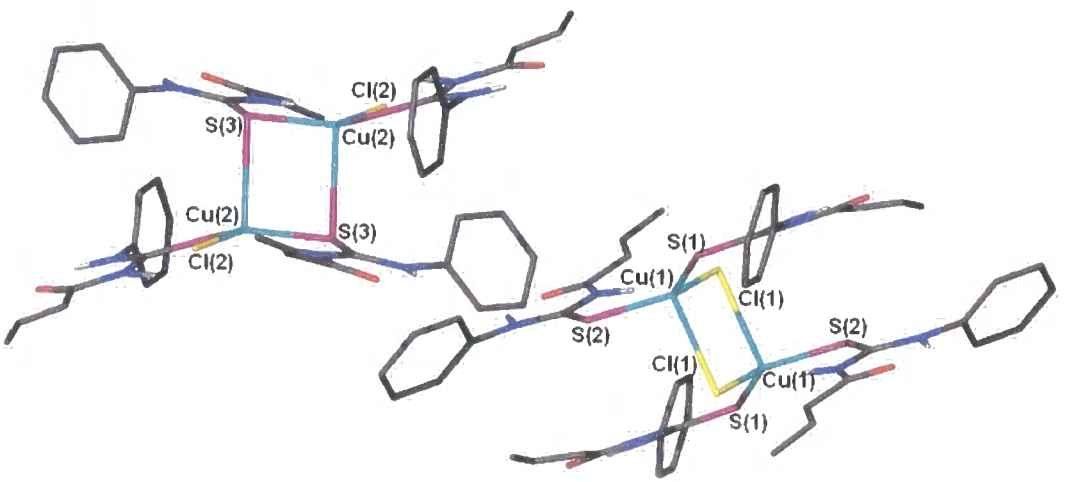

Figure 4.5: crystal structure of Cu(N-phenyl-N'-2-propenoylthiourea)$_2$Cl complex displaying both the sulphur-bridged and chloride-bridged dimers in the same crystal structure. [42]

Each $Cu(PTU)_2Cl$ fragment sits on an inversion centre to create the other half of each dimer, and the original authors class the structure to have a Z' = 2, thus Z = 4, due to the lability of the bridging atoms. It is possible to consider the dimers as chemically distinct and thus the CSD reassigned the structure as Z' = 0.5.

4.2 Aims of research

There are many binding modes observed for thioureido functional groups towards transition group metals, and platinum group metals in particular. Four common types are shown in figure 4.6, with the most prevalent being solely through the sulphur atom (**A**).[43]

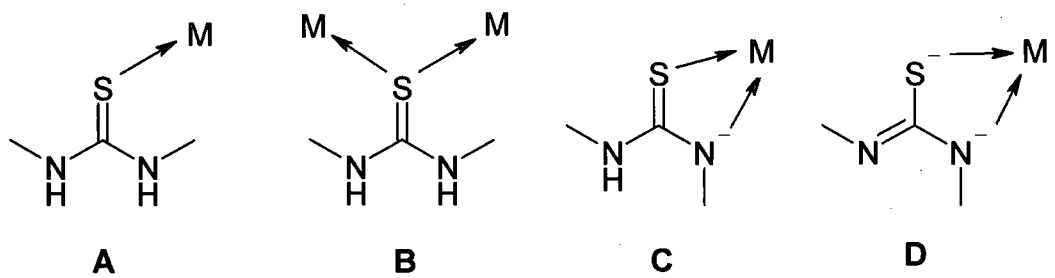

Figure 4.6: four common binding modes of the thioureido group to metal cations.[43-45]

However, sulphur bridging between metal centres (**B**) and the mono- and di-anionic N,S 4-membered metallacycles (**C** and **D**, respectively) have all been observed.[44,45] By using two chelating thioureido podal arms, the number of potential binding modes increases, particularly as the ligands may bridge between two or more metal atoms. The aim of the research in this chapter is to coordinate the difunctional bis(thioureido) ligands synthesised in Chapter 2.2 to platinum group metals, in particular Ru(II). Investigation of the many potential binding modes of the chelating ligands will be undertaken by NMR spectroscopy and other standard characterization techniques. Where possible, single crystals suitable for X-ray crystallographic analysis will be grown to confirm the binding modes of the ligands to the metal centre.

4.3 Results and discussion

4.3.1 Coordination to [{Ru(η^6-$C_6H_4MeCH(Me)_2$)Cl(μ-Cl)}$_2$]

Coordination of the thioureido ligands to ruthenium(II) were undertaken using the chloride-bridged complex, [{Ru(η^6-$C_6H_4MeCH(Me)_2$)Cl(μ-Cl)}$_2$], as attempts to coordinate ligands $\mathbf{L}^{1\text{-}3}$ with the ruthenium(II) tetrakisdimethylsulphoxide dichloride starting material, [Ru(DMSO)$_4$Cl$_2$] were all unsuccessful. The [{Ru(η^6-$C_6H_4MeCH(Me)_2$)Cl(μ-Cl)}$_2$] material has advantages over other Ru(II) starting materials as:

a) it has well established chemistry (for examples, see Chapter 1.3),
b) the *p*-cymene group provides an NMR spectroscopic handle for the Ru(II) species and
c) the η^6 coordination of the *p*-cymene group blocks three coordination sites to the ruthenium, thus increasing the chance of forming discrete species.

The dimer bridging bonds can easily be broken with a weakly coordinating solvent and neutral species may be obtained with monodentate ligands, scheme 4.2.[46-49]

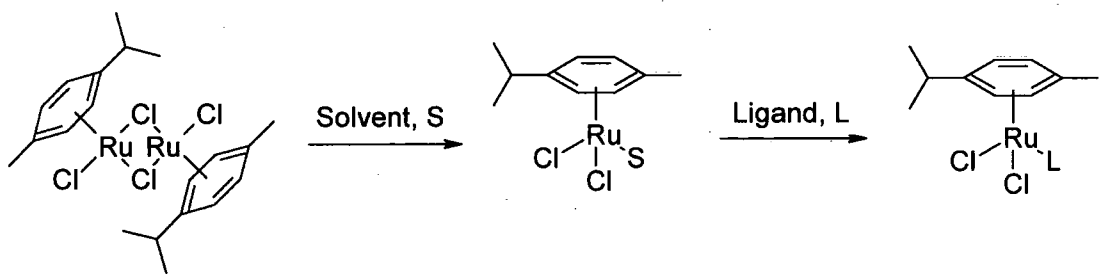

Scheme 4.2: breaking of the chloride bridged dimer by a weakly coordinating solvent molecule and further coordination of a monodentate ligand to form a neutral monomeric complex.[46-49]

The reaction of [{Ru(η^6-$C_6H_4MeCH(Me)_2$)Cl(μ-Cl)}$_2$] with two equivalents of the ligand IITPhT by stirring the reagents in $CHCl_3$ at room temperature for 3 hours produced a crude mixture of many products. The ^{1}H NMR spectrum is shown for the crude material recovered from the reaction of [{Ru(η^6-$C_6H_4MeCH(Me)_2$)Cl(μ-Cl)}$_2$] with IITPhT, figure 4.7a. The large number of products is seen in the ^{1}H NMR spectrum particularly by the resonances at chemical shifts above 8 ppm where resonances for NH protons are expected.

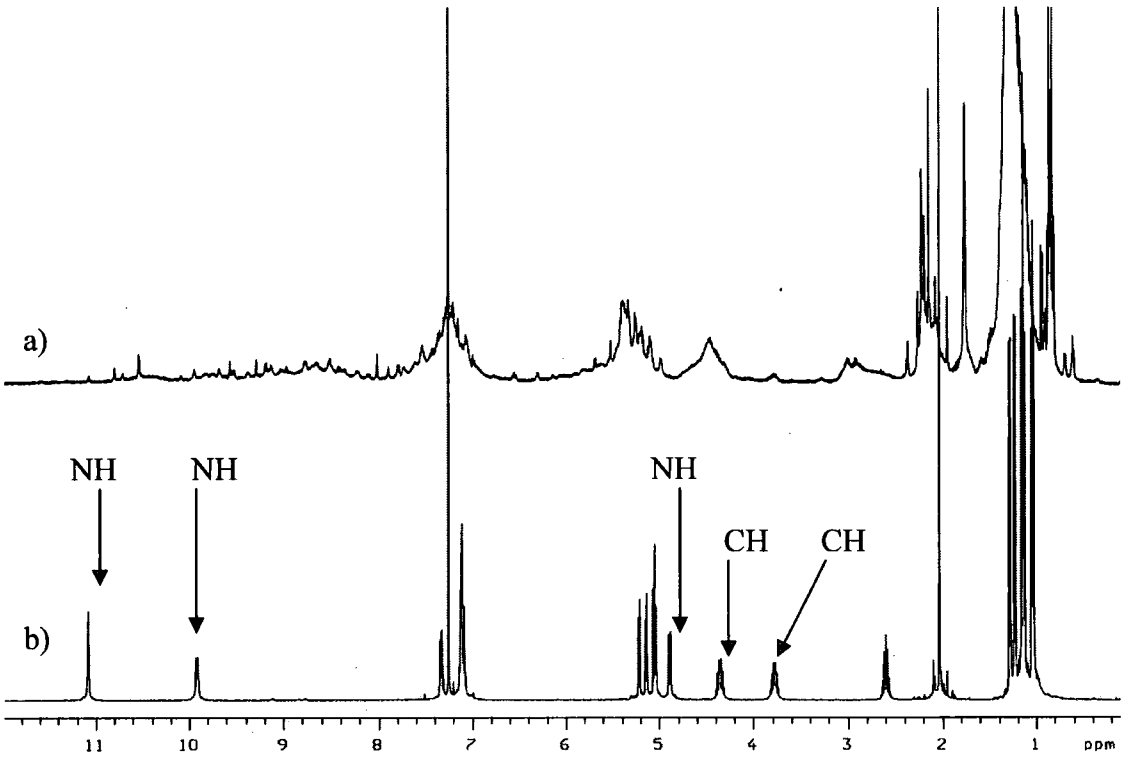

Figure 4.7: ^{1}H NMR spectroscopy spectra of a) crude product from the reaction of IITPhT with [{Ru(η^6-$C_6H_4MeCH(Me)_2$)Cl(μ-Cl)}$_2$] in $CHCl_3$, and b) the same material having been dissolved in water and extracted into $CHCl_3$.

Attempts to recrystallise a single species from the mixture were unsuccessful. A D_2O wash was used to, initially, remove some impurities, but a great deal of the crude product dissolved in the wash to yield an orange solution, indicating much of the ruthenium species had dissolved in the D_2O. The ^{1}H NMR spectrum of the D_2O wash showed a single species, and so this method was used to purify the product. Thus the crude material from the reaction of [{Ru(η^6-$C_6H_4MeCH(Me)_2$)Cl(μ-Cl)}$_2$] with IITPhT was dissolved in distilled water and then extracted into $CHCl_3$ (which more effectively extracts the species than CH_2Cl_2). The resulting compound shows a ^{1}H NMR spectrum in which the ligands and *p*-cymene groups have lost their symmetry, and only three of the four NH signals are observed, fig 4.7b).

The ligand isopropyl CH_3 proton resonances occur at chemical shifts of 1.03, 1.04, 1.13 and 1.14 ppm, integrating for three protons each, showing that not only both arms within the ligand are unsymmetrical but that each CH_3 within each arm is inequivalent. Similarly, the ligand isopropyl CH proton resonances are inequivalent at chemical shifts of 3.78 and 4.35 ppm. Three ligand NH proton resonances at 4.89, 9.91 and 11.08 ppm are observed, which integrate for one proton each. Individual

resonances are also observed for each of the ligand aryl protons at 7.09, 7.11, 7.12 and 7.33 ppm. The loss of equivalence is also observed in the *p*-cymene ligand proton resonances. From the COSY NMR spectrum it is possible to assign the three NH proton resonances with two adjacent to the isopropyl CH group resonances and one that displays no coupling, thus characteristic of the NH proton adjacent to the aryl ring. It is possible to deduce that deprotonation of the nitrogen atom adjacent to the aryl ring has occurred. The ^{1}H NMR spectrum is typical of a diastereotopic molecule and, because of the loss of one NH proton resonance, the spectrum may be assigned to a molecule where there is sulphur coordination from both thioureido groups and by a deprotonated nitrogen atom. This creates a chiral centre at the metal, which is consistent with the NMR spectroscopy. There are 24 individual signals in the $\{^{1}H\}$-^{13}C NMR spectrum, which again confirms the asymmetrical nature of the molecule, in particular the two resonances for the C=S carbon atoms at 178.62 and 180.20 ppm. As a yield of 75 % of this species is obtained from the crude material, it is clear from the ^{1}H NMR spectra in figure 4.7 that the water is not simply extracting this complex from the crude material, but inducing the deprotonation and N-coordination from many species.

A single peak is observed in the ESI-MS, with a 100 % relative abundance peak at m/z 545.1 with a ruthenium isotope envelope, which may be assigned to the deprotonated monocationic monomeric compound predicted from the NMR spectroscopy, $[^{102}Ru(\eta^{6}\text{-}C_{6}H_{4}MeCH(Me)_{2}(IITPhT - H)]^{+}$. There is a significant shift in absorbance peaks in the IR spectroscopy. In the ligand, strong bands at 3315 and 3256 cm^{-1} assigned as N-H stretches in the uncoordinated ligand are replaced by a strong band at 3216 and a weaker band at 3130 cm^{-1}, showing a significant change in the NH environment. This is also reflected in a smaller change in absorbance bands assignable to the NH bending from ligand bands at 1598 and 1563 cm^{-1} to 1591 and 1561 cm^{-1} in the complex. A strong absorbance band in the C=S stretch region is observed to shift from 1265 cm^{-1} in the ligand to 1167 cm^{-1} in the complex. The analysis confirms that the complex has a chloride counter-ion and so the molecule has been fully characterised as $[Ru(\eta^{6}\text{-}C_{6}H_{4}MeCH(Me)_{2})(\kappa\text{-}S,S,N\text{-}IITPhT - H)]Cl$, **4.11**, fig 4.8.

The reactions of $[\{Ru(\eta^{6}\text{-}C_{6}H_{4}MeCH(Me)_{2})Cl(\mu\text{-}Cl)\}_{2}]$ with ligands that also possess a 2 carbon spacer between thioureido groups, MMTPhT and MMTET, gave

similar NMR spectra and further analysis that is consistent with complexes of formula [Ru(η^6-$C_6H_4MeCH(Me)_2$)(κ-*S,S,N*-MMTPhT – H)]Cl, **4.12**, and [Ru(η^6-$C_6H_4MeCH(Me)_2$)(κ-*S,S,N*-MMTET – H)]Cl.H_2O, **4.13**, fig 4.8.

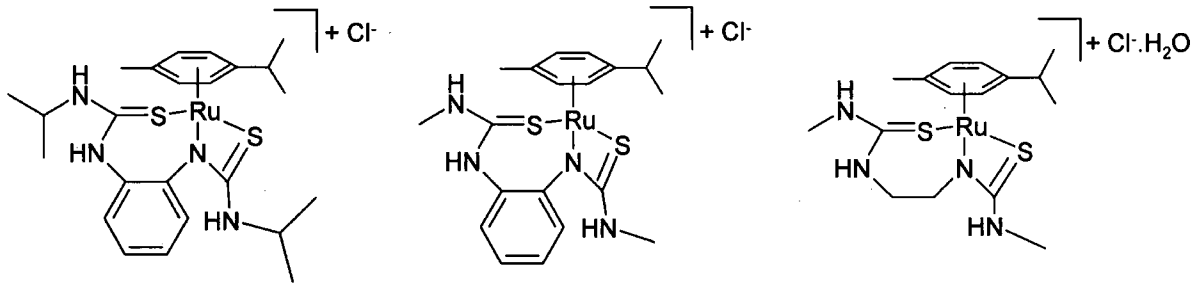

4.11 **4.12** **4.13**

Figure 4.8: structures of the deprotonated bis(thioureido) Ru(II) complexes, 4.11-4.13.

The resonances in the ^{1}H NMR spectrum for **4.13** were broader in nature than the spectra obtained for **4.11** or **4.12**, and a splitting of each NH resonance was observed, fig 4.9. This indicates that the molecule exists in two conformations in the solution state. The broadness and presence of two conformations is not observed in the 1H NMR spectra of phenylene derived ligand complexes, **4.11** and **4.12**, and thus may be due to the ethylene spacer, which is more flexible in nature. This flexibility may allow more facile group rotation, producing two conformations. The greatest difference in the chemical shift for the conformations is observed for the NH proton at 7.41 ppm for the major conformer and 8.14 ppm for the minor conformer. This may be attributable to two different hydrogen bonding environments of the NH proton, in particular hydrogen bonding to a chloride counter-ion or a water molecule, as the analysis of the compound is consistent with one included molecule of water. At room temperature, there is considerable overlap of the resonances from the two conformations, and so obtaining VT NMR spectra to separate (cooling) and merge (heating) the resonances of the two conformers would be useful.

In an attempt to learn more of the nature of the crude product, samples were submitted for ESI-MS of the crude material produced from the reaction of [{Ru(η^6-$C_6H_4MeCH(Me)_2$)Cl(μ-Cl)}$_2$] with IITPhT before treatment with water. It was hoped that peaks corresponding to the neutral form or a bridging species would appear in the spectrum. However, the 100 % relative abundance peak m/z 545 may be assigned to

the deprotonated form, $[Ru(\eta^6\text{-}C_6H_4MeCH(Me)_2)(IITPhT - H)]^+$. It therefore appears that the ESI-MS technique process promotes the deprotonation of these complexes. Analysis of the crude material fits for the formula of "$Ru(\eta^6\text{-}C_6H_4MeCH(Me)_2)(IITPhT)Cl_2$", however the ^1H NMR spectroscopy evidence suggests more complicated complex formation.

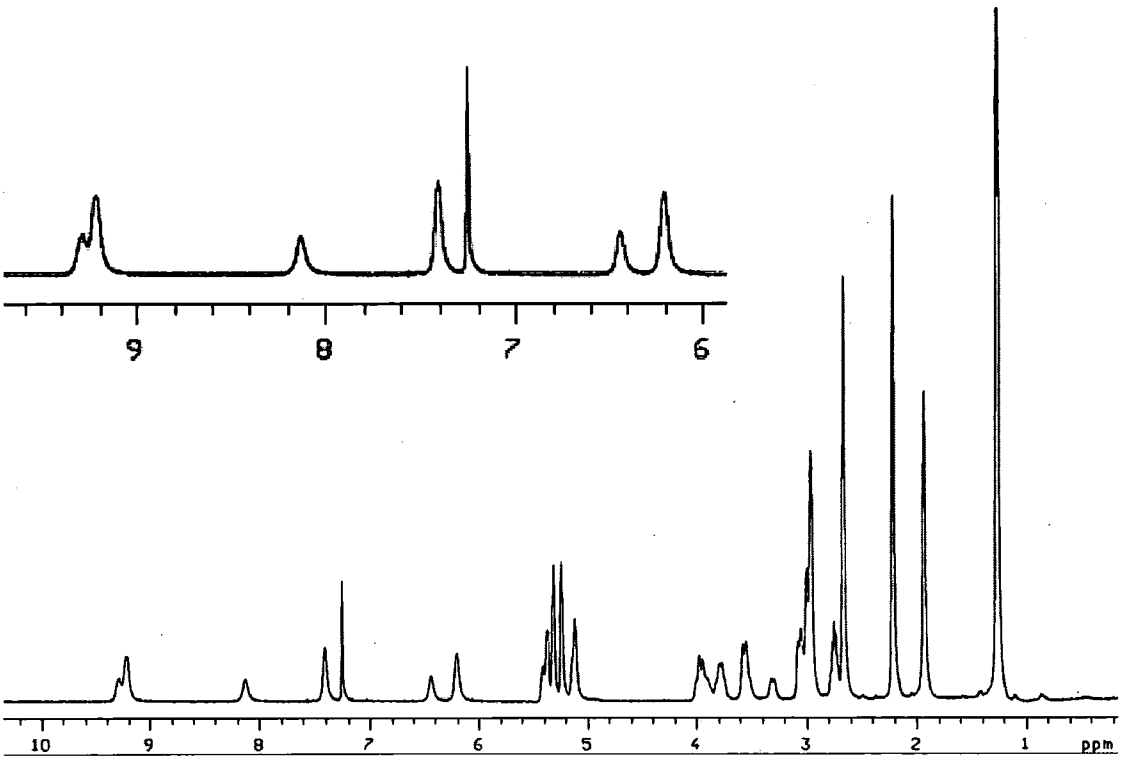

Figure 4.9: ^1H NMR spectrum of 4.13 showing the resonances for each of the NH groups in two differing conformations (inset).

Confirmation of the S,S,N binding mode is shown in the molecular structures of these species obtained by X-ray crystallography by Dr. Kirsty Anderson. Single crystals of $[Ru(\eta^6\text{-}C_6H_4MeCH(Me)_2)(\kappa\text{-}S,S,N\text{-}MMTPhT\text{-}H)]Cl$ were obtained from cooling and slow evaporation of an ethyl acetate solution, while single crystals of $[Ru(\eta^6\text{-}C_6H_4MeCH(Me)_2)(\kappa\text{-}S,S,N\text{-}MMTET - H)]Cl$ and $[Ru(\eta^6\text{-}C_6H_4MeCH(Me)_2)(\kappa\text{-}S,S,N\text{-}IITPhT - H)]Cl$ were obtained from slow evaporation of an acetone/ether solution.

The crystal structure of $[Ru(\eta^6\text{-}C_6H_4MeCH(Me)_2)(\kappa\text{-}S,S,N\text{-}MMTPhT - H)]Cl$, **4.12**, shows three crystallographically independent molecules in the asymmetric unit and are shown in figure 4.8. All three molecules show the S,N,S terdentate binding mode to the Ru(II) metal.

a)

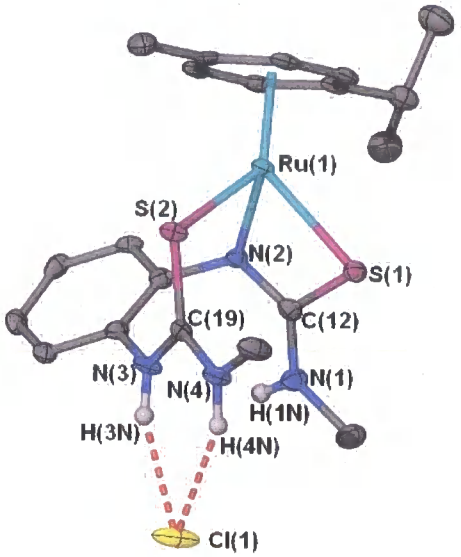

A

b)

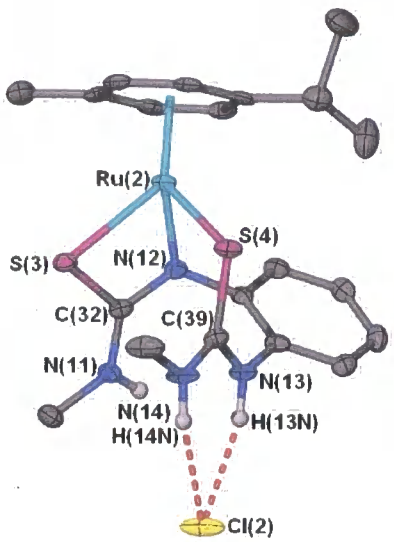

B

c)

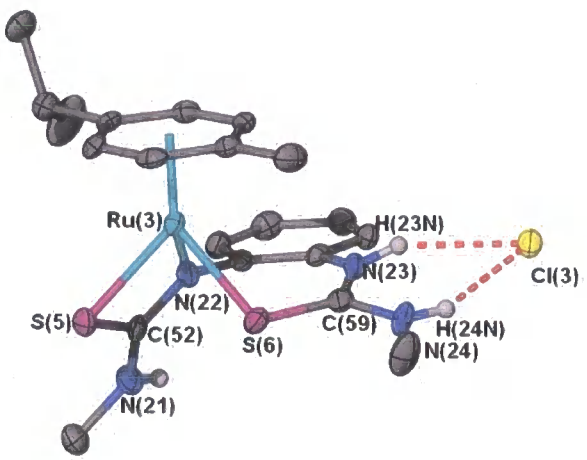

C

Figure 4.10: structures of the three crystallographically independent complexes in the asymmetric unit of the crystal structure of [Ru(η^6-$C_6H_4MeCH(Me)_2$)(MMTPhT – H)]Cl, showing ellipsoids at 50 % probability.

This forms a four-membered Ru-S-C-N-Ru metallacycle due to the deprotonation of the thioureido NH, akin to the work by Okeya and Henderson with deprotonated thioureido groups in the presence of platinum(II).[44,45] In addition, the other chelating thiourea arm is coordinating with the sulphur atom, to form a seven-membered Ru-S—N-Ru metallacycle which is adjoining to the four-membered ring. For all three molecules, the S-Ru bond distances are in the region of 2.4 Å and the Ru-N bond distances are in the region of 2.05 – 2.10 Å, table 4.1, which is to be expected for neutral coordination from the C=S and monoanionic coordination from the nitrogen to ruthenium(II). The strain of the four-membered metallacycle is observed in the N-C-S angle of 108 – 109 ° for N(2)-C(12)-S(1), N(12)-C(32)-S(3) and N(22)-C(52)-S(5) in comparison with the unconstrained N-C-S of 124 ° for N(1)-C(12)-S(1), N(11)-C(32)-S(3) and N(21)-C(52)-S(5), table 4.2. The bond angles of the monodentate thioureido group are closer to the 120 ° expected of a thiourea group, but some distortion is observed due to the seven-membered ring.

4.12 molecule A			**4.12 molecule B**			**4.12 molecule C**		
		Distance (Å)			Distance (Å)			Distance (Å)
Ru(1)	N(2)	2.097(3)	Ru(2)	N(12)	2.070(3)	Ru(3)	N(22)	2.056(3)
Ru(1)	S(2)	2.4287(11)	Ru(2)	S(4)	2.4284(11)	Ru(3)	S(6)	2.3825(12)
Ru(1)	S(1)	2.4304(11)	Ru(2)	S(3)	2.4351(11)	Ru(3)	S(5)	2.4295(12)
S(1)	C(12)	1.746(4)	S(3)	C(32)	1.747(4)	S(5)	C(52)	1.740(5)
S(2)	C(19)	1.747(4)	S(4)	C(39)	1.745(4)	S(6)	C(59)	1.722(4)
N(1)	C(12)	1.330(5)	N(11)	C(32)	1.328(5)	N(21)	C(52)	1.330(6)
N(2)	C(12)	1.321(5)	N(12)	C(32)	1.321(5)	N(22)	C(52)	1.327(5)
N(3)	C(19)	1.330(5)	N(13)	C(39)	1.325(5)	N(23)	C(59)	1.353(5)
N(4)	C(19)	1.331(5)	N(14)	C(39)	1.327(5)	N(24)	C(59)	1.340(5)

Table 4.1: selected bond distances in for the three independent molecules of 4.12 in the crystal structure.

The torsional angle between the planar thioureido group and the ruthenium metal is an indication of the electrons used in bonding between the groups. For the sulphur atom involved in four membered rings, the torsional angle is very close to 0 ° as expected for lone pair interaction. This is not surprising as the coordinated nitrogen atom restricts rotation.

Table 4.2: selected bond angles for the three molecules of **4.12** in the asymmetric unit.

4.12 Molecule **A**				**4.12** Molecule **B**				**4.12** Molecule **C**			
			Angle (°)				Angle (°)				Angle (°)
N(2)	Ru(1)	S(2)	83.28(9)	N(12)	Ru(2)	S(4)	84.97(9)	N(22)	Ru(3)	S(6)	81.12(10)
N(2)	Ru(1)	S(1)	66.94(9)	N(12)	Ru(2)	S(3)	67.25(9)	N(22)	Ru(3)	S(5)	66.96(10)
S(2)	Ru(1)	S(1)	92.21(4)	S(4)	Ru(2)	S(3)	90.77(4)	S(6)	Ru(3)	S(5)	84.64(4)
C(19)	S(2)	Ru(1)	108.54(14)	C(39)	S(4)	Ru(2)	110.75(14)	C(59)	S(6)	Ru(3)	104.90(16)
C(12)	S(1)	Ru(1)	79.87(14)	C(32)	S(3)	Ru(2)	79.03(14)	C(52)	S(5)	Ru(3)	79.67(15)
C(12)	N(2)	Ru(1)	103.8(2)	C(32)	N(12)	Ru(2)	104.1(2)	C(52)	N(22)	Ru(3)	105.1(3)
N(2)	C(12)	N(1)	126.3(4)	N(12)	C(32)	N(11)	126.0(4)	N(22)	C(52)	N(21)	127.1(4)
N(2)	C(12)	S(1)	109.2(3)	N(12)	C(32)	S(3)	109.2(3)	N(22)	C(52)	S(5)	108.1(3)
N(1)	C(12)	S(1)	124.5(3)	N(11)	C(32)	S(3)	124.8(3)	N(21)	C(52)	S(5)	124.7(3)
N(3)	C(19)	N(4)	116.3(4)	N(13)	C(39)	N(14)	116.6(4)	N(24)	C(59)	N(23)	113.2(4)
N(3)	C(19)	S(2)	122.6(3)	N(13)	C(39)	S(4)	123.1(3)	N(23)	C(59)	S(6)	129.6(3)
N(4)	C(19)	S(2)	120.9(3)	N(14)	C(39)	S(4)	120.2(3)	N(24)	C(59)	S(6)	117.2(3)

However, the monodentate thiourea shows somewhat different behaviour with torsional angles of 42, 71 and 102 ° for molecules **C**, **B** and **A,** respectively (c.f. chapter 3.3). While the three molecules are very similar, there is a difference in molecule **C** form **A** and **B** in the angle of the ligand aryl ring to the p-cymene ligand ring. While the aryl ring in **A** and **B** lies at an appreciable angle to the *p*-cymene ring plane, the ligand aryl ring is almost parallel to that of the *p*-cymene ring. This difference is most likely to be due to packing constraints.

The S,N,S binding mode makes the molecules chiral, with **A** being an enantiomer of **B** and **C,** which is the same chirality as **B,** has its enantiomer generated in space by an inversion centre. Opposite enantiomers pair via hydrogen-bonded chloride counter-ions, as shown in figure 4.11.

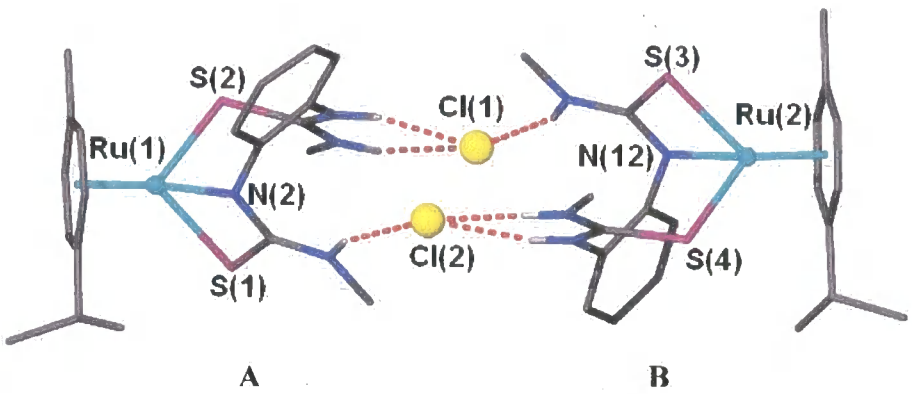

Figure 4.11: pairing of opposite enantiomers via hydrogen-bonded chloride counter-ions, as observed for molecules A and B.

The crystals of **4.12** were grown relatively quickly from hot ethyl acetate, and these conditions may have contributed to the presence of three independent molecules in the asymmetric unit, as the molecules may not have arranged themselves in the optimal packing fashion. In comparison, crystals of [Ru(η^6-$C_6H_4MeCH(Me)_2$)(κ-*S,S,N*-MMTET-H)]Cl.H_2O (**4.13**) and [Ru(η^6-$C_6H_4MeCH(Me)_2$)(κ-*S,S,N*-IITPhT-H)]Cl (**4.11**) were obtained at room temperature over the course of several days and weeks. The molecular structures from data obtained by Dr. Kirsty Anderson of these two molecules are given in fig. 4.12. In both cases, Z' = 1, but the same S,N,S binding mode is observed to ruthenium, and opposite enantiomers pair via hydrogen-bonded chloride anions. The opposite enantiomers are crystallographically related by an inversion centre.

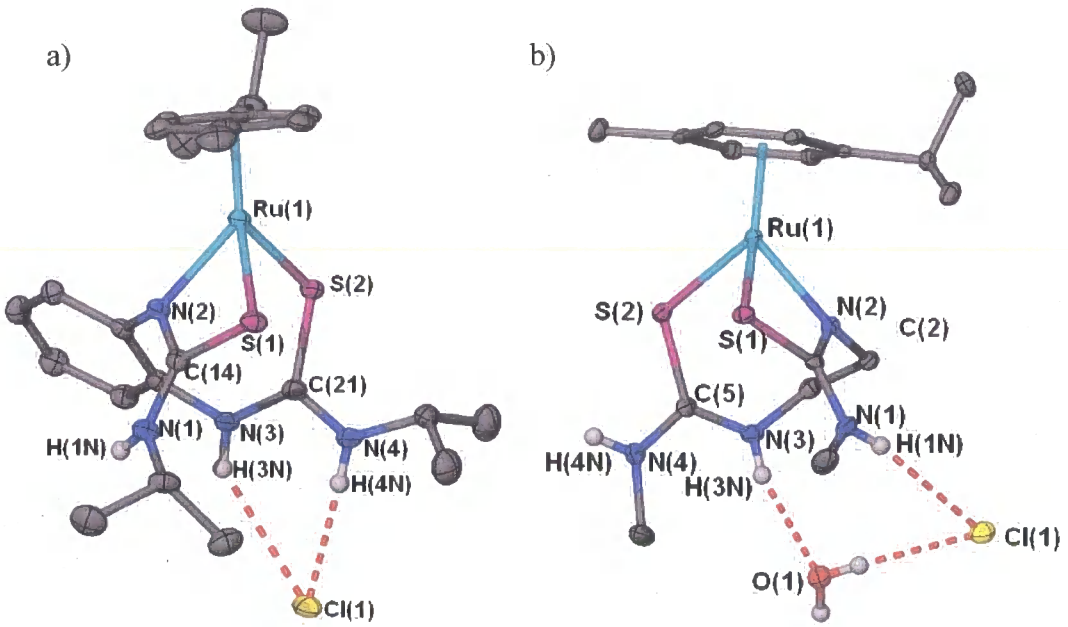

Figure 4.12: structures of a) [Ru(η^6-$C_6H_4MeCH(Me)_2$)(IITPhT – H)]Cl, 4.11, and b) [Ru(η^6-$C_6H_4MeCH(Me)_2$)(MMTET – H)]Cl, 4.13. Ellipsoids are shown at 50 % probability.

The bond distances and angles are similar to those of the molecules of [Ru(η^6-$C_6H_4MeCH(Me)_2$)(MMTPhT – H)]Cl (**4.12**), Table 4.3-4.4.

4.11				**4.13**		
		Distance (Å)				Distance (Å)
Ru(1)	N(2)	2.0872(12)		Ru(1)	N(2)	2.086(2)
Ru(1)	S(2)	2.4178(4)		Ru(1)	S(2)	2.4186(7)
Ru(1)	S(1)	2.4274(4)		Ru(1)	S(1)	2.4289(7)
S(1)	C(14)	1.7425(15)		S(1)	C(2)	1.737(3)
S(2)	C(21)	1.7475(15)		S(2)	C(5)	1.739(3)
N(1)	C(14)	1.3300(19)		N(1)	C(2)	1.348(3)
N(2)	C(14)	1.3235(19)		N(2)	C(2)	1.320(3)
N(3)	C(21)	1.345(2)		N(3)	C(5)	1.327(3)
N(4)	C(21)	1.315(2)		N(4)	C(5)	1.326(3)

Table 4.3: selected bond lengths for [Ru(η^6-$C_6H_4MeCH(Me)_2$)(IITPhT – H)]Cl, 4.11, and [Ru(η^6-$C_6H_4MeCH(Me)_2$) (MMTET – H)]Cl, 4.13.

4.11					4.13			
			Angle (°)					Angle (°)
N(2)	Ru(1)	S(2)	83.75(4)		N(2)	Ru(1)	S(2)	90.75(6)
N(2)	Ru(1)	S(1)	67.02(4)		N(2)	Ru(1)	S(1)	66.84(6)
S(2)	Ru(1)	S(1)	93.459(14)		S(2)	Ru(1)	S(1)	91.01(3)
C(14)	S(1)	Ru(1)	79.84(5)		C(2)	S(1)	Ru(1)	79.86(8)
C(21)	S(2)	Ru(1)	110.33(5)		C(5)	S(2)	Ru(1)	110.55(8)
C(14)	N(2)	Ru(1)	103.91(9)		C(2)	N(2)	Ru(1)	104.04(15)
N(2)	C(14)	N(1)	126.24(14)		N(2)	C(2)	N(1)	127.5(2)
N(2)	C(14)	S(1)	109.05(11)		N(2)	C(2)	S(1)	109.17(17)
N(1)	C(14)	S(1)	124.71(12)		N(1)	C(2)	S(1)	123.34(19)
N(4)	C(21)	N(3)	116.68(13)		N(4)	C(5)	N(3)	119.2(2)
N(4)	C(21)	S(2)	121.22(12)		N(4)	C(5)	S(2)	116.8(2)
N(3)	C(21)	S(2)	121.89(12)		N(3)	C(5)	S(2)	123.9(2)

Table 4.4: selected bond angles for [Ru(η^6-$C_6H_4MeCH(Me)_2$) (IITPhT – H)]Cl and [Ru(η^6-$C_6H_4MeCH(Me)_2$) (MMTET – H)]Cl.

The structure for [Ru(η^6-$C_6H_4MeCH(Me)_2$)(κ-*S,S,N*-MMTET – H)]Cl.H_2O (**4.13**) is isostructural with the other two structures with respect to the chiral metal centre and association of enantiomers through hydrogen bonding, however there is one water molecule hydrogen bonding to each molecule and therefore there are two chloride and two water molecules hydrogen bonding between enantiomer pairs, figure 4.13. The water molecule also hydrogen bonds to the chloride forming a hydrogen bonded square motif in between the enantiomers. The enantiomeric association only occupies two of the NH groups (N(1) and N(3)) while the other protonated nitrogen atom, N(4), hydrogen bonds with water molecules that are involved in the association of another pair of enantiomers. This builds up an intricate 3-D network of hydrogen bonding extending through the crystal structure. It is likely that the two conformations observed in the ^{1}H NMR differ in the hydrogen bonding of the N(4)-H group. One may be one of the conformation observed in the solid state structure, while the other conformation may result from rotation of the C-N(4) bond so that the N(4)-H group is hydrogen-bonding to the same water and chloride counter-ion that the other NH groups within the ligand are hydrogen-bonding to.

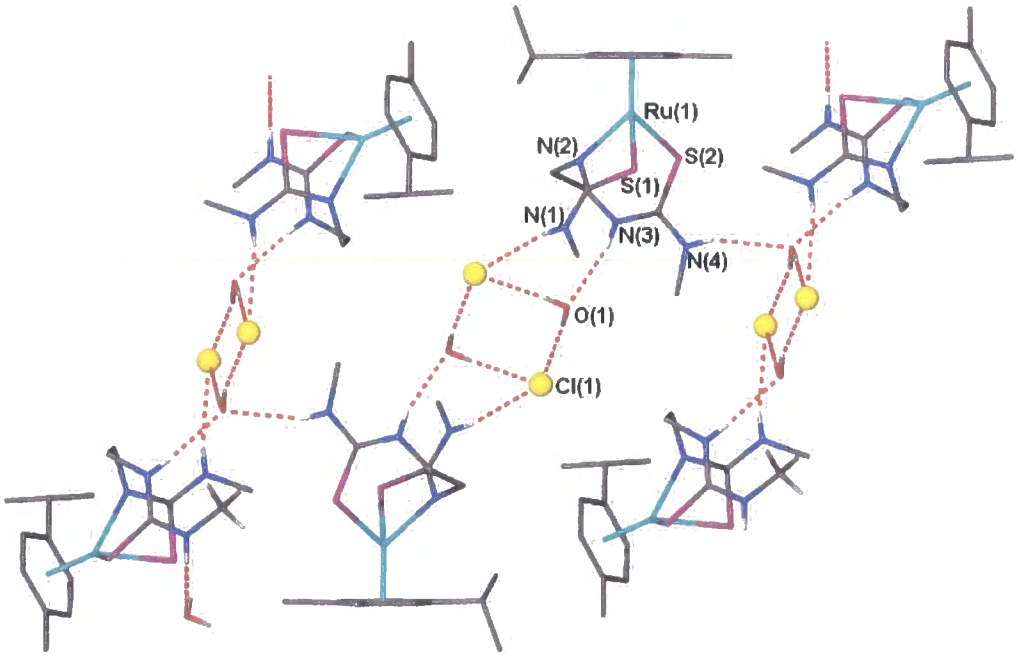

Figure 4.13: crystal structure of [Ru(η^6-$C_6H_4MeCH(Me)_2$)(MMTET – H)]Cl.H_2O showing hydrogen bonding of one enantiomeric pairing to another through water molecules and coordinated ligand NH groups.

For all three of the above discussed structures, opposite enantiomers pair via hydrogen bonding, indicating that this is a preferred solid-state arrangement in a racemic mixture compared to the pairing of same enantiomers.

The reaction of [{Ru(η^6-$C_6H_4MeCH(Me)_2$)Cl(μ-Cl)}$_2$] with MMTPyT produces one major product that has clear ^{1}H NMR spectroscopic peaks, and several minor impurity peaks. It was not possible to purify the major product from the impurities either by recrystallisation or with a water wash. From the ^{1}H NMR spectroscopy of the major product, it appears that the ligand is symmetrically bound, as there is no inequivalency of the ligand CH_3 groups resonances at 1.18 ppm, and the *p*-cymene ligand proton resonances are not split into inequivalent signals as with **4.10-4.12**. In addition, only one ^{13}C resonance is observed in the ^{13}C NMR spectrum for the C=S carbon atom at 178.58 ppm, which indicates that both thioureido groups are bound symmetrically. There are two mononuclear binding modes that could lead to

this symmetry: through the two sulphur atoms with no nitrogen interaction, and through two sulphur atoms with additional coordination through the pyridyl nitrogen, fig. 4.12. Coordination through a deprotonated thioureido NH group is not consistent with a symmetrical binding mode, and both NH resonances integrate for two hydrogen atoms each, found at 10.38 and 12.78 ppm.

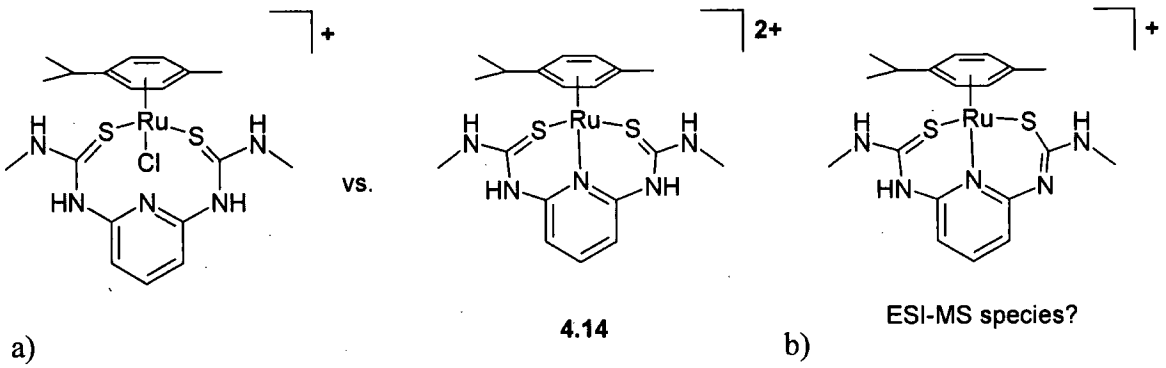

Figure 4.14: a) possible structures of the symmetrically bound [Ru(η^6-$C_6H_4MeCH(Me)_2$)(MMTPyT)]Cl_2 complex, and b) the possible form of the species observed in the ESI-MS

The ESI-MS gives a 100 % relative abundance peak at m/z 490, which can be assigned to the deprotonated form, [^{102}Ru(η^6-$C_6H_4MeCH(Me)_2$)(MMTPyT – H)]$^+$. The deprotonation and coordination of the thiourea NH group has been observed in the crude material of [Ru(η^6-$C_6H_4MeCH(Me)_2$)(MMTPhT – H)]Cl and [Ru(η^6-$C_6H_4MeCH(Me)_2$)(IITPhT – H)]Cl as part of the ESI-MS process previously. Washing the crude reaction mixture product of [{Ru(η^6-$C_6H_4MeCH(Me)_2$)Cl(μ-Cl)}$_2$] with MMTPyT in water does not induce the deprotonation, and there is no unsymmetrical species found in the washed product ^{1}H NMR spectrum. It is possible that in the ESI-MS process the N-coordinated mode deprotonates to form the monocationic species, fig 4.12b. The second and third most abundant peaks in the mass spectrum occur at m/z of 265.5 and 245.5, respectively. The peak at m/z 245.5 is assigned to the dicationic complex [Ru(η^6-$C_6H_4MeCH(Me)_2$)(MMTPyT)]$^{2+}$ (F.W. = 491). In this cationic complex no chloride atoms are coordinated to the ruthenium atom, and so it is likely that the pyridyl nitrogen is coordinated. Interestingly, this interaction seems to be reasonably labile, as the peak at m/z 265.5 might be assigned to a complex with one acetonitrile solvent molecule coordinated to the ruthenium – [Ru(η^6-$C_6H_4MeCH(Me)_2$)(MMTPyT)(MeCN)]$^{2+}$ (F.W. = 532). The interaction with

acetonitrile is only observed in the mass spectrometry data, as the compound is dissolved in this solvent to be injected into the spectrometer. Therefore, it is likely that the major complex formed in this reaction is that of $[Ru(\eta^6\text{-}C_6H_4MeCH(Me)_2)(\kappa\text{-}S,S,N_{(pyr)}\text{-}MMTPyT)]Cl_2$, **4.14**.

Analysis for the compound is not accurate with this formula, and in particular is low in carbon, with a calculated carbon percentage of 41.68 % compared to the found percentage of 37.04 %. The impurities observed in the ^1H NMR spectroscopy may be the cause of this inconsistency. It should be noted, however, that the analysis of the crude product of the reaction of $[\{Ru(\eta^6\text{-}C_6H_4MeCH(Me)_2)Cl(\mu\text{-}Cl)\}_2]$ with IITPhT is consistent with the formula of the added reagents, while the analysis for **4.14** is not consistent with the sum of the added reagents. The IR spectroscopy of the compound is consistent with thiourea group binding to the metal with the bands assignable to the C=S and N-H bonds affected most. The N-H stretch at 3238 cm^{-1} in the ligand is shifted to 3220 cm^{-1} in the complex, and strong bands in the ligand at 1618, 1550 and 1510 cm^{-1} assignable to N-H bending, are replaced by bands at 1611, 1561 and 1524 cm^{-1} in the complex. A large change is observed in one of the bands which has a major contribution from C=S stretching, with a shift from 1225 to 1260 cm^{-1} in the ligand and complex, respectively.

The reaction of $[\{Ru(\eta^6\text{-}C_6H_4MeCH(Me)_2)Cl(\mu\text{-}Cl)\}_2]$ with the t-TUP yields a single product by refluxing the starting materials under N_2 for 3 hours in chloroform, and requires no water wash for purification. It is possible to form the neutral species with coordination from just the sulphur atom, thus leaving two of the chloride atoms coordinated to Ru. However there is loss of symmetry in the *p*-cymene proton resonances in the ^1H NMR spectrum, with CH_3 *p*-cymene resonances at 1.13 and 1.15 ppm and the aromatic proton resonances integrating for one proton each observed at 5.22, 5.24 5.38 and 5.46 ppm. This suggests that one of the labile chlorine atoms has been replaced by the coordination of the *ortho*-pyridyl nitrogen atom. This would yield a chiral metal centre and thus remove symmetry in the *p*-cymene ligand, to form the complex $[Ru(\eta^6\text{-}C_6H_4MeCH(Me)_2)Cl(t\text{-}TUP)]Cl.2H_2O$, **4.15**. There is a downfield shift of the resonance of the CH adjacent to pyridyl N from 8.15 to 8.83 ppm. In addition there is a large downfield shift in one of the NH resonances from 8.84 to 11.95 ppm, suggesting a change in conformation and possibly chloride counter-ion anion binding. The ESI-MS of the complex produces a single peak m/z 478, which is

assigned to the deprotonated form, $[Ru((\eta^6\text{-}C_6H_4MeCH(Me)_2))(t\text{-}TUP - H)]^+$. The analysis of this compound is consistent with the complex with two water molecules. It has been observed in the complex of $[Ru(\eta^6\text{-}C_6H_4MeCH(Me)_2)(\kappa\text{-}S,S,N\text{-}MMTET - H)]Cl.H_2O$ (**4.13**), that water may be associated with these complexes. Similar shifts in IR spectroscopic absorbance bands are observed for **4.15** as for the other Ru complexes. In particular, strong absorbance bands assignable to N-H bending in the ligand at 1605 and 1595 cm-1 is replaced by medium bands at 1629 and 1605 cm-1. Strong bands in the ligand spectrum at 1183 and 1145 cm^{-1}, assignable to C=S stretching are replaced by a medium absorbance band at 1219 cm^{-1} and a weak absorbance band at 1161 cm^{-1}.

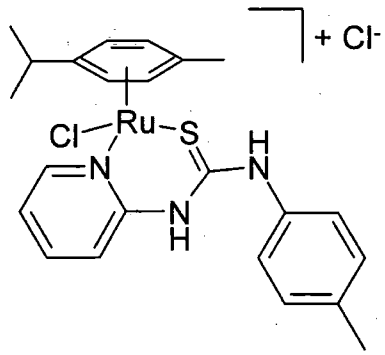

4.15

4.3.2 Coordination to Pd(II) and Pt(II)

Reaction of bis(thioureido) ligands with $Pd(MeCN)_2Cl_2$ and $Pt(MeCN)_2Cl_2$ formed insoluble complexes of general formula ML_xCl_2 (where x = 1.5, 2), even if a 1:1 M:L stoichiometry was used. It appears that the ligands are coordinatively saturating the metals, and ESI-MS shows periodic peaks up to high molecular weights (>2000 mass numbers). The distance between peaks is 74 mass units. It is likely that coordination oligomers or polymers are being formed. Therefore diphenylphosphinoethane (dppe) was used in order to block coordination sites and allow the formation of discrete species. The general method for the reaction proceeds in a similar fashion to work by Burrows[50] by coordinating dppe to Pt or Pd first, followed by introduction of the chelating ligand. In this way, complexes of the formulae $[Pd(dppe)(\kappa\text{-}S,S\text{-}IITPhT)](PF_6)_2$, (**4.16**), $[Pd(dppe)(\kappa\text{-}S,S\text{-}MMTET)]Cl(PF_6)$, (**4.17**) and $[Pd(dppe)(\kappa\text{-}S,S\text{-}MMTPyT)]Cl(PF_6)$, (**4.18**) were synthesised and charaterised, scheme 4.3.

The ^{1}H NMR spectrum of [Pd(dppe)(IITPhT)]$(PF_6)_2$ (**4.16**) shows a symmetrical binding mode which is expected to be through both sulphur atoms. The single ligand isopropyl CH_3 proton resonance observed at 1.25 ppm and the resonances observed at 4.28 ppm for the ligand isopropyl CH indicate that both thioureido groups are bound equivalently and symmetrically. This is also confirmed by the ^{13}C NMR spectrum, which shows a single C=S resonance at 175.07 ppm. This contrasts with the terdentate Ru complexes, **4.11 – 4.13**, which showed two inequivalent ^{13}C resonances for the two inequivalent thioureido binding groups. The ^{31}P NMR spectrum confirms the symmetrical binding mode with a single resonance peak at 61.64 ppm for the Pd coordinated P atoms, indicating that the atoms trans to the P are equivalent, which is consistent with a symmetrical S,S' binding mode. A septet at -144.02 ppm is also observed with a $^{1}J_{P,F}$ coupling constant of 715 Hz for the hexafluorophosphate counter-ion. The ESI-MS yields a 100 % rel. abundance peak m/z 812.9, which may be assigned to the deprotonated monocationic species, $[^{106}Pd(dppe)(IITPhT - H)]^{+}$ with a Pd isotope envelope. It is thought that the deprotonated complex has been formed as a part of the ESI-MS process rather than representing the bulk material, and its presence confirms the binding of dppe and the ligand to palladium. The analysis of the compound is consistent with the formula of **4.16**, although the carbon analysis is slightly higher than expected with the observed carbon percentage of 44.54 % compared to the calculated carbon percentage of 43.47 %. IR spectroscopy is also consistent with the formula with two broad bands at 3353 and 3220 cm^{-1} assignable to the N-H stretch. A single strong band is observed at 1578 cm^{-1}, which is assignable to the N-H bending, and medium bands at 1243, 1167 and 1104 cm^{-1} may be assigned to the C=S stretch. In addition a very strong band at 840 cm^{-1} is observed, assignable to PF_6.

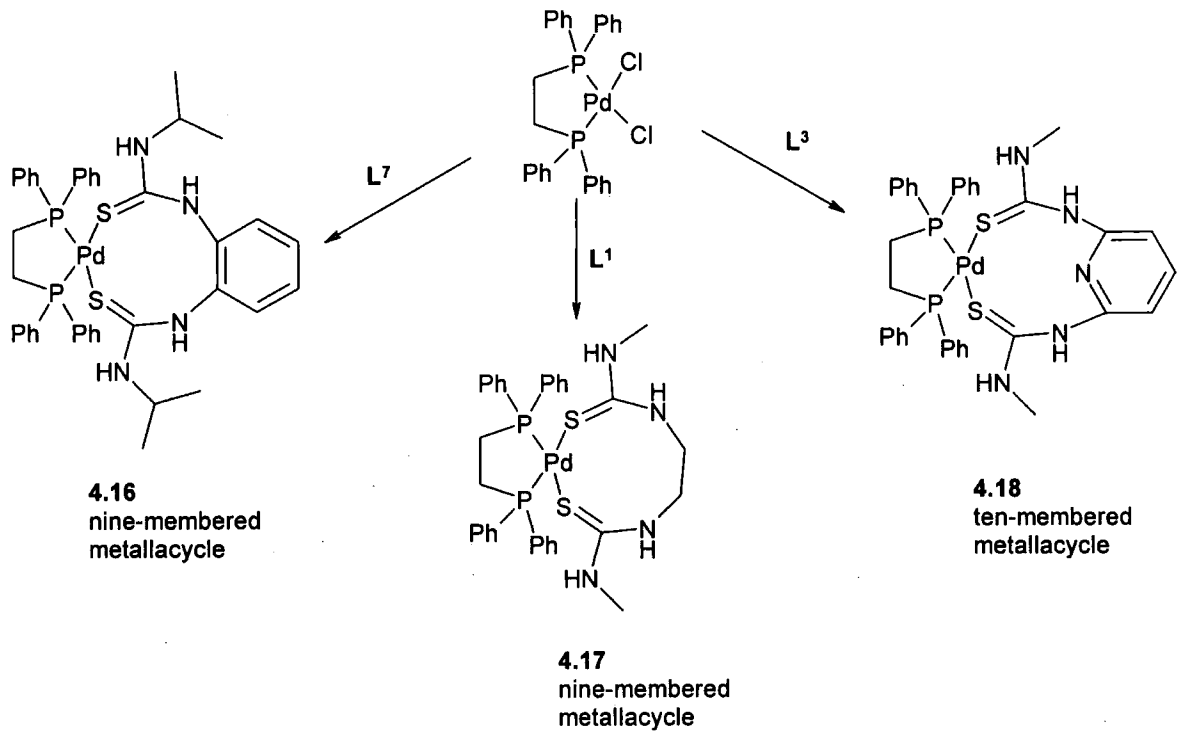

Scheme 4.3: S,S bidentate binding mode to Pd, with formation of nine- and ten-membered metallacycles.

Pd(dppe)(κ-*S,S*-MMTET)]Cl(PF_6), (**4.17**) and [Pd(dppe)(κ-*S,S*-MMTPyT)]Cl(PF_6), (**4.18**) were synthesised analogously. Similar ^{1}H and ^{31}P NMR spectra are observed for these complexes as for [Pd(dppe)(κ-*S,S*-IITPhT)](PF_6)$_2$ (**4.16**), and all experimental details for these complexes are given in section 4.5.3. The low solubility of **4.17** and **4.18** meant that clear ^{13}C NMR spectra could not be obtained. The ^{1}H NMR spectrum for **4.18** displayed the clearest peaks and microstructure of the peaks could be observed. This is perhaps surprising as one would expect the ten-membered metallacycle to be configurationally very flexible, but from sharpness of the ^{1}H NMR spectrum the ligand is either exchanging between two configurations very quickly or forms a single stable configuration. Both are likely, however, it is possible the pyridyl nitrogen may have an interaction with the palladium atom. An interaction would form a configuration with two adjacent Pd-S—N-Pd six-membered metallacycles, figure 4.15. Analysis for **4.17** is found to be considerably lower in N with 3.82 % found compared to the expected 6.38 %, however analysis for **4.18** is consistent with its formula. Similar changes in the ligand N-H and C=S absorbance bands in the IR spectroscopy are observed for **4.17** and **4.18** as for **4.16**.

[Pd(dppe)(κ-*S,S*-MMTPhT)]Cl(PF_6) could not be synthesised cleanly and many products were observed in the ^1H and ^{31}P NMR spectra. It is not sure why this is the case, except that the species readily precipitates, possibly indicating the formation of oligomers.

[Pd(dppe)(t-TUP)]Cl(PF_6), **4.19**, was synthesised and from the ^1H NMR spectrum, elemental analysis and ESI-MS, it is observed that only 1 t-TUP ligand is bound to the metal. However in the ^{31}P NMR spectrum there is only one broad ^{31}P resonance at 67.64 ppm. This peak is typical of P-Pd-S phosphorus resonance, however as there is only one signal, it would suggest that the phosphine atoms of dppe are equivalent, and thus there are sulphur atoms *trans* to both of them. As this would require two bound t-TUP ligands, which is contrary to other evidence, it suggests that there is coordination from the pyridyl nitrogen. The broadness in the signal may be attributed to a small degree of lability of the nitrogen atom coordination, fig 4.15.

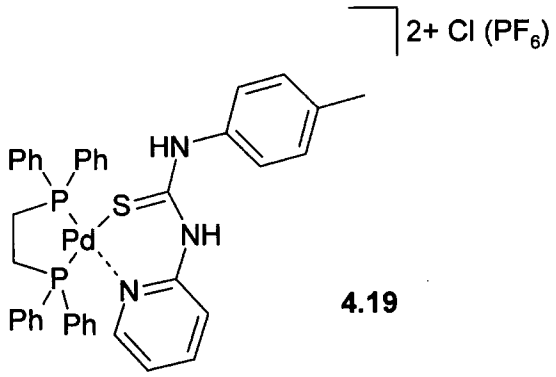

4.19

Figure 4.15: possible pyridyl nitrogen interaction with Pd(II).

Analysis for the compound is reasonably accurate for the formula of **4.19**, and, as with complex 4.16, ESI-MS shows a 100 % relative abundance peak with a palladium isotope envelope for the deprotonated form of the complex, $[^{106}Pd(dppe)(t\text{-}TUP - H)]^+$. IR spectroscopy is again consistent with the changes in absorbance bands from the uncoordinated ligand to the complex. The resolution of two peaks observed in the ligand at 1605 and 1595 cm^{-1} has been lost in the complex, with a single broadened band at 1609 cm^{-1}, and shifts in the two ligand absorbance bands at 1547 and 1534 cm^{-1} is observed in the complex at 1560 and 1540 cm^{-1}, assignable to N-H bends.

Crystals of [Pd(dppe)(κ-*S*,*S*-IITPhT)]Cl(PF_6).$(CH_3)_2CO$ were obtained as an acetone solvate by slow evaporation of an acetone/diethyl ether solution of **4.16** that had not been fully metathesised with hexafluorophosphate ions, and confirms the S,S binding mode, fig. 4.16.

a)

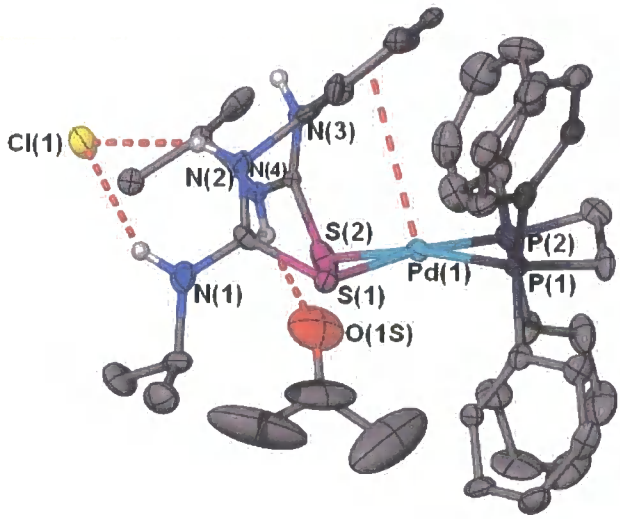

b)

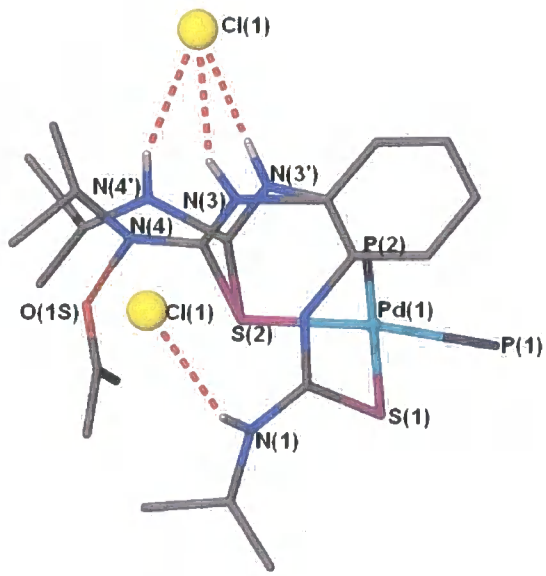

Figure 4.16 molecular structure of [Pd(dppe)(IITPhT)]Cl.PF_6.$(CH_3)_2CO$, displaying weak ligand aryl···Pd interaction and hydrogen bonding to the chloride counter-ion and acetone solvent molecule. Ellipsoids are shown at 50 % probability. b) A fragment of the molecule is shown with the thioureido group disordered over two sites.

The structure obtained by Dr. Kirsty Anderson exhibits a Pd-S—S-Pd nine-membered metallacycle with the aryl ring out of the metal coordination plane to form a weak aryl or C=C bond interaction ($C_{centroid}$-Pd distance = 3.421 Å; closest C-Pd contact 3.144 Å; lower aryl C=C-Pd distance 3.074 Å). The thioureido group of one ligand arm is disordered over two sites, with one site hydrogen bonding to the acetone solvent of crystallization molecule (N(4) and N(3)), while the other conformation has both N(4') and N(3') hydrogen bonding to the chloride counter-ion, fig. 4.15b. There is some disorder in the acetone solvent molecule, and this is reflected in the large thermal ellipsoids. The coordinating bond distances are within expected ranges with Pd-P distances of 2.26 and 2.28 Å, and Pd-S distances of 2.35 and 2.39 Å, table 4.5. The angles around the square planar palladium centre deviate only slightly from 90 °.

			Distance (Å)
Pd(1)	P(2)		2.256(3)
Pd(1)	P(1)		2.275(3)
Pd(1)	S(2)		2.352(3)
Pd(1)	S(1)		2.385(3)
			Angle (°)
P(2)	Pd(1)	P(1)	85.63(10)
P(2)	Pd(1)	S(2)	89.94(10)
P(1)	Pd(1)	S(1)	91.85(9)
S(2)	Pd(1)	S(1)	91.09(9)
P(1)	Pd(1)	S(2)	167.53(10)
P(2)	Pd(1)	S(1)	172.65(10)

Table 4.5: selected bond distances and angles for [Pd(dppe)(IITPhT)]Cl.PF_6.$(CH_3)_2CO$.

There was incomplete metathesis of chloride counter-ions with hexafluorophosphate anions and hence the crystals contain one anion of each type. The resulting structure exhibits hydrogen-bonding between thiourea NH groups and chloride counter-ions, and dimeric hydrogen-bonded structures are produced.

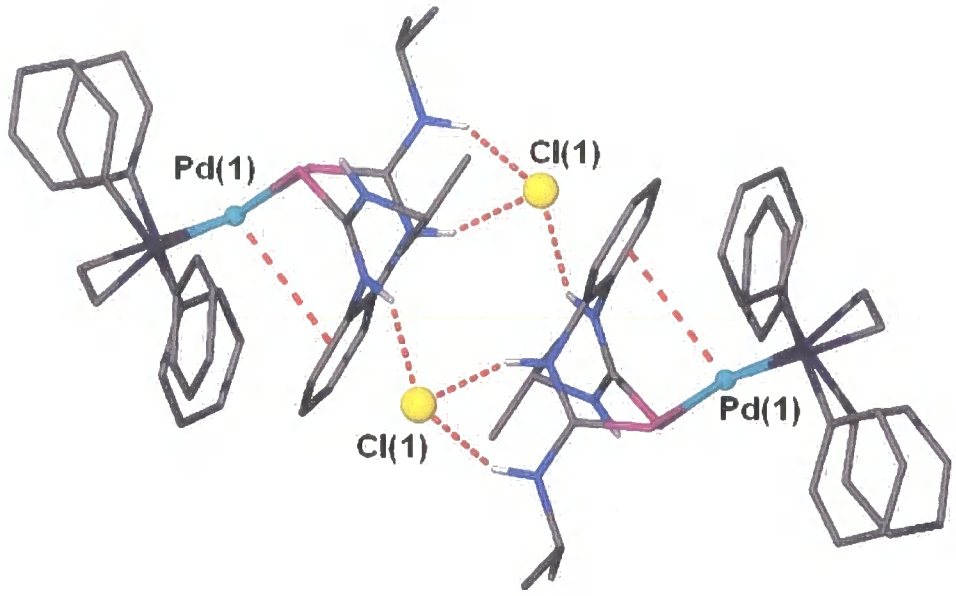

Figure 4.17: crystal structure [Pd(dppe)(IITPhT)]Cl(PF_6).$(CH_3)_2CO$ (4.16b) dimers pairing via hydrogen bonded chloride counter-ions.

The incomplete metathesis despite adding a large excess of NH_4PF_6, and the repetition of the chloride bridged dimers indicates halide binding affinity of these compounds. Stirring the product in a further excess of NH_4PF_6, forced the complete metathesis for analysis purposes.

Given the affinity of this complex to halide anions, some initial UV-Vis spectrophotometric titrations were performed with [Pd(dppe)(κ-*S,S*-IITPhT)]$(PF_6)_2$ and F^- anions. A 0.6 mM acetonitrile solution of the complex was titrated with a 3 mM acetonitrile solution of TBAF, up to one equivalent of anions and the change in absorbance is observed. Absorbance at 370 nm decreases, while absorbance at 427 nm increases, and an isosbestic point at 398 nm is observed. The shift in absorbance wavelength is from the very edge of the visible spectrum into the yellow region, and so a visible intensification of the yellow colour may be observed by the naked eye.

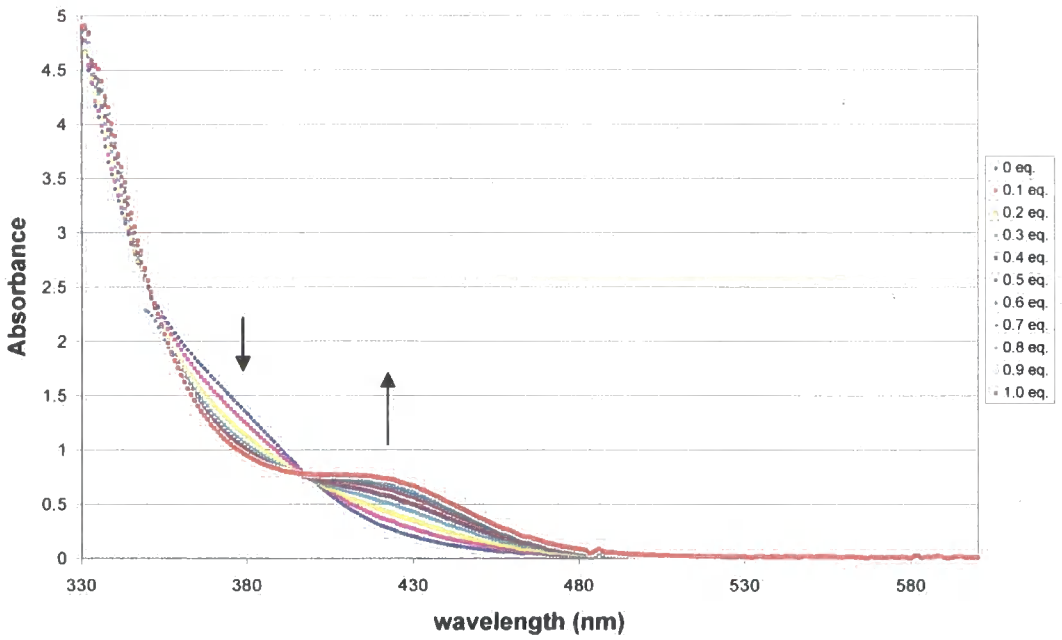

Figure 4.18: UV-Vis spectrum of [Pd(dppe)(IITPhT)](PF$_6$)$_2$ upon addition of TBA fluoride

Without ^{1}H NMR data, it is difficult to accurately predict whether the absorbance at 427 nm is due to the binding of fluoride anions or a deprotonated species, as fluoride ions are very basic and deprotonate the uncoordinated ligand upon addition of 0.3 equivalents (see Chapter 2.3.3). However, there is a relatively large change in absorbed wavelength, and so the complex may have potential sensing applications.

Only two ligands, IITPhT and t-TUP gave clean products when reacted in an analogous manner with [Pt(dppe)Cl$_2$]. [Pt(dppe)(κ-*S,S*-IITPhT)](PF$_6$)$_2$, **4.20**, displays ^{1}H and ^{31}P NMR spectra where the IITPhT binds symmetrically to platinum and due to the similarity with the palladium product, it is thought that the same S,S bidentate binding fashion occurs. A single phosphorus resonance is observed for the dppe ligand, and the phosphorus-platinum coupling constant ($^1J_{Pt,P}$) of 3128 Hz is typical of phosphines trans to sulphur donors.[50] The ^{13}C NMR spectrum is also consistent with a symmetrical binding mode with, for example, a single resonance for the coordinated C=S at 173.44 ppm. The analysis is consistent with the formula of **4.20**. The ESI-MS of the compound has a 100 % relative abundance peak at m/z 556.1, but as the peak does not have an isotope pattern characteristic of ^{195}Pt, it is unlikely that this a platinum containing material. The peak at m/z 905.3 is most similar to a complex that

is assignable to the desired the complex, which may relate to the dicationic complex, $[^{195}Pt(dppe)(IITPhT)]^{2+}$ (F.W. = 903). Analysis for the compound is found to be accurate for the formula of **4.20**. The IR spectroscopy is similar to that of the Pd analogue, **4.16**, with absorbance bands for the N-H stretch at 3345 and 3246 cm^{-1}, compared to 3315 and 3256 cm^{-1} in the uncoordinated ligand, and strong peaks at 1574 cm^{-1}, assignable to N-H bending and 1106 cm^{-1}, assignable to C=S stretching. A very strong peak is observed at 840 cm^{-1}, assignable to the PF_6 counter-ion.

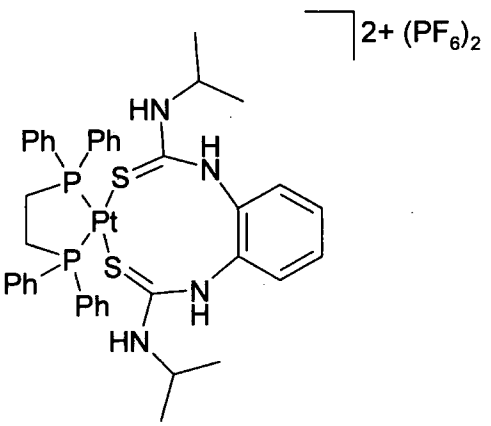

4.20

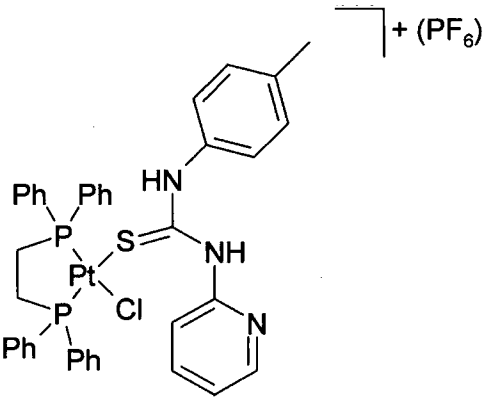

4.21

The complex [PtCl(dppe)(t-TUP)](PF_6) appears to coordinate through the sulphur only. The ^{31}P NMR spectroscopy singlet signals at 48.96 and 46.01 ppm displayed Pt satellites with $^{1}J_{P,Pt}$ = 3178 Hz and 3557 Hz, respectively. This first phosphorus signal and platinum coupling constants are typical of phosphorus *trans* to a sulphur atom. The second signal at 46.01 ppm indicates that this phosphorus atom is *trans* to a chlorine atom rather than the pyridyl nitrogen, which would be the case in a bidentate binding mode. Chemical shifts for phosphines trans to nitrogen atoms occur in the region of 40 ppm with P,Pt coupling constants of 3100 – 3300 Hz.[50] The analysis for this compound is reasonably consistent with the formula of **4.21** but carbon is lower than anticipated: calculated carbon, 46.05 %, found C 43.97 %. This may be due to some displacement of the chloride ligands by the t-TUP pyridyl ligand. The IR spectroscopy is similar to the platinum analogue with strong bands at 1608 and 1540 cm^{-1}, assignable to N-H bending, and 1106 cm^{-1} assignable to C=S stretching. PF_6 absorbance is observed at 840 cm^{-1}.

4.3.4 Coordination to Cu(I)

Reaction of ligands MMTPhT, IITPhT, MMTET and MMTPyT to Cu(II) and Cu(I) salts produced insoluble materials that are likely to be coordination polymers. The structure of $Cu(tu)_3Cl$ is itself a coordination polymer of corner sharing tetrahedra.[51] Few complexes could be isolated and characterised.

It is well known that Cu(II) is reduced to Cu(I) by thiourea[43] and most attempts to produce a monomeric Cu(I)L species have been unsuccessful. However, the reduction of $Cu(II)Cl_2.2H_2O$ in acetonitrile by 1-pyridin-2-yl-3-p-tolyl-thiourea (t-TUP) yields a soluble Cu(I) complex of formula $[Cu(t\text{-}TUP)_2Cl]$, **4.22**, that by slow evaporation of the acetonitrile solution yields yellow crystals suitable for X-ray crystallography.

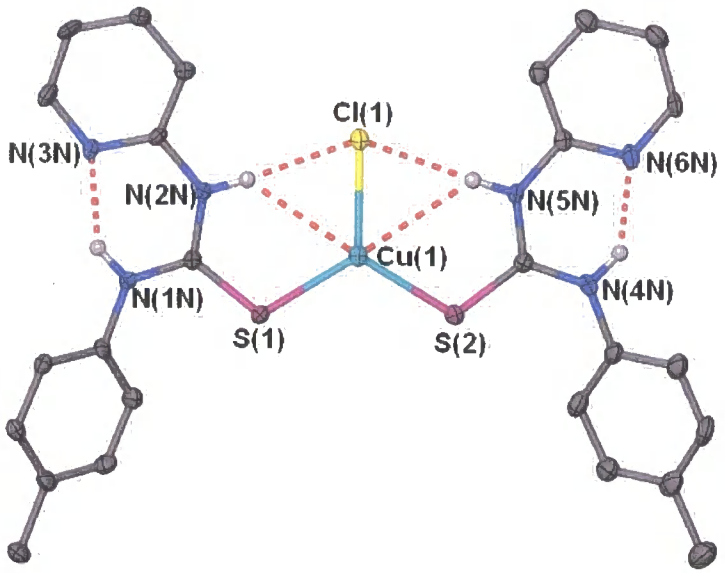

Figure 4.19: molecular structure of monomeric $Cu(t\text{-}TUP)_2Cl$ showing intramolecular hydrogen bonding between the NH groups and coordinated chloride atoms and pyridyl nitrogen atoms. Ellipsoids are shown at 50 % probability

The structure of the $Cu(t\text{-}TUP)_2Cl$ monomer obtained by Dr. Kirsty Anderson is shown in figure 4.19. This structure is very similar to the monomeric complex found by Ferrari and others, **4.23**.[34]

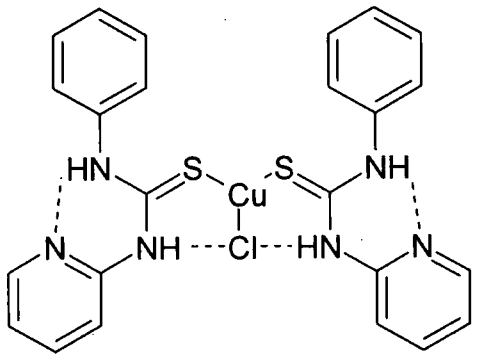

4.23

Both ligands are bound to the copper through the sulphur atom, and both are symmetrically arranged with respect to the copper. It can be seen that one thiourea NH group is intramolecularly hydrogen-bonded to the pyridyl nitrogen as observed in the crystal structure of the ligand.[52] The hydrogen atom of the other NH group is hydrogen-bonded to the chloride ligand that is coordinated to the copper. Thus, there are no intermolecular hydrogen bonds in this structure.

This structural form is to be expected. However, the crystal structure of Cu(t-TUP)$_2$Cl also contained two dimers of formula [Cu(t-TUP)$_2$Cl]$_2$: one sulphur-bridged, **A**, and one chloride-bridged, **B**, figure 4.20.

Monomer			**S-bridged dimer (A)**			**Cl bridged dimer (B)**		
		Distance (Å)			**Distance (Å)**			**Distance (Å)**
Cu(1)	S(2)	2.2211(13)	Cu(3)	S(201)	2.2711(12)	Cu(2)	S(101)	2.2542(12)
Cu(1)	S(1)	2.2307(12)	Cu(3)	S(202)	2.2993(12)	Cu(2)	S(102)	2.2690(12)
Cu(1)	Cl(1)	2.2794(12)	Cu(3)	S(203)	2.5230(13)	Cu(2)	Cl(10)	2.3569(12)
			Cu(4)	S(202)	2.5711(13)	Cu(2)	Cl(10)	2.6510(13)
			Cu(4)	S(203)	2.2989(12)			
			Cu(4)	S(204)	2.2767(12)			
			Cu(3)	Cl(21)	2.3502(12)			
			Cu(4)	Cl(22)	2.3260(12)			
			Cu(3)	Cu(4)	2.8102(8)			

Table 4.6: selected bond distances for the monomer and two dimers of Cu(t-TUP)$_2$Cl

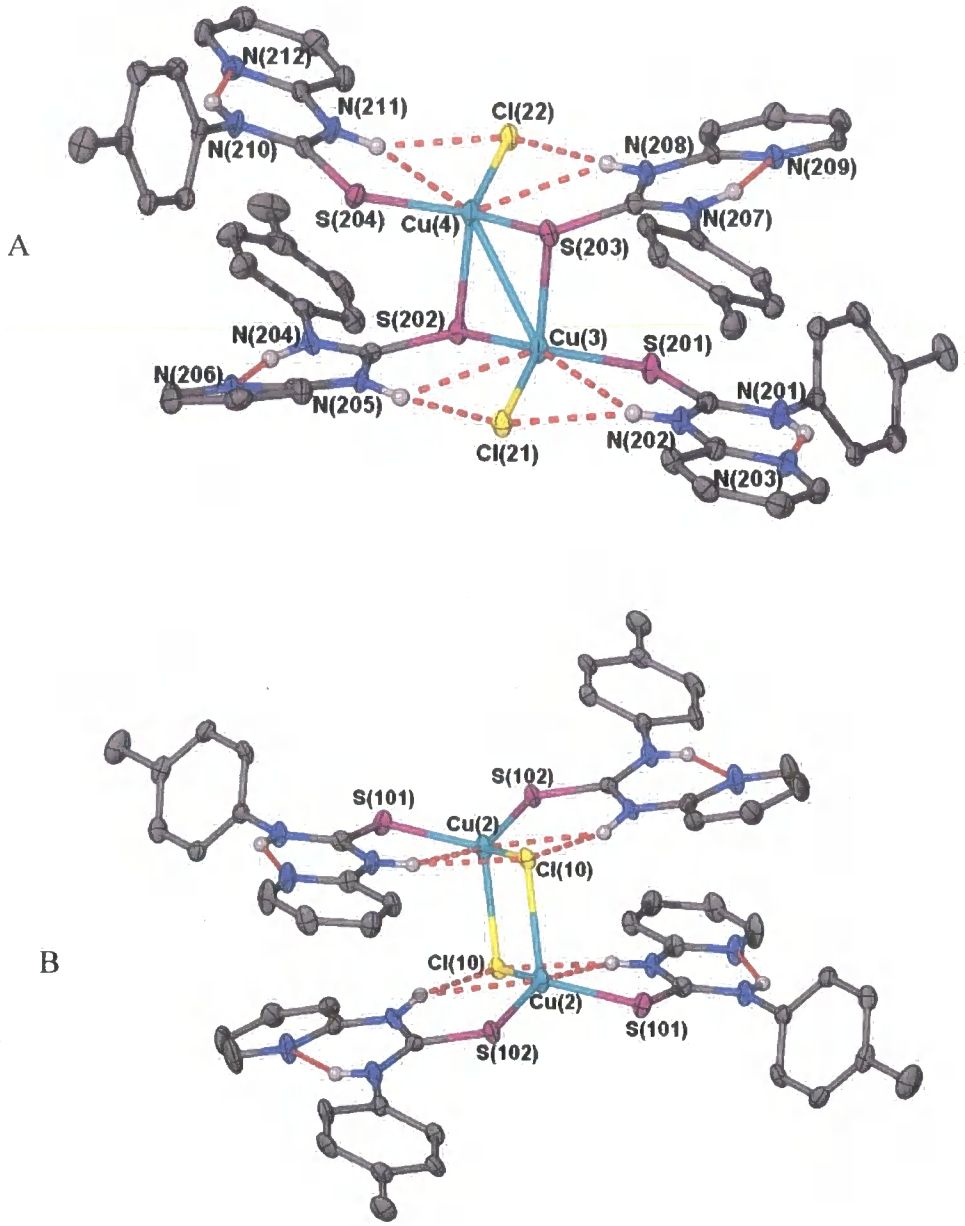

Figure 4.20: molecular structures of "Cu(t-TUP)$_2$Cl" dimers: A – sulphur bridged with terminal chloride atoms, and B – chloride bridged with two sulphur coordinated terminal groups. Ellipsoids are shown at 50 % probability.

Bond distances are all near expected values, with Cu-S and Cu-Cl distances in the region of 2.2 – 2.3 Å and 2.2 – 2.4 Å respectively, table 4.6. The Cu-S and Cu-Cl distances of the bridged species are longer than those in the trigonal motif, with Cu-S distances of 2.5 – 2.6 Å in the S-bridged dimer, **A**, and Cu-Cl distances of 2.65 Å in

the Cl-bridged dimer, **B**. Cu-Cu distances are 2.81 Å for the chloride bridged dimer and 3.64 Å for the S-bridged dimer.

Comparing the Cu-S bond distances in this structure to the Ru-S distances obtained in 4.3.1, it is observed that the Cu-S distances are in the region of 0.2 Å shorter than the Ru-S distances found in the Ru crystal structures, with typical values of 2.22 Å and 2.42 Å for Cu-S and Ru-S distances, respectively. These shorter bonding distances may be indicative of stronger binding of the thiourea ligands to Cu than to Ru. To establish whether this is the case, the ionic radii of the two metals must be taken into account. The ionic radius of many transition metals has been calculated by Shannon.[53-55] Unfortunately, the ionic radii of three corrdinate Cu(I) or Ru(II) in any coordination number are not reported and so it is difficult to establish whether the observed differences in the bond lengths are due to differences in bond strengths or ionic radii. A recent paper has noted that the ionic radius of Ru(II) has not been reported, but from their own crystal structures estimate the value to be circa 0.95 Å.[56] The reported ionic radii for Cu(I) are 0.60 and 0.96 Å for two and six coordinate complexes, respectively. Based on the ionic radius for the two coordinate Cu(I), Cu-S bond lengths are expected to be 0.35 Å shorter than their Ru counter-parts. In this case, the observed 0.2 Å difference suggests that the Ru-S bond is stronger than the Cu-S bond. However, if the ionic radius of the three coordinate Cu(I) is closer to the value of the six coordinate Cu(I) of 0.96 Å, the short Cu-S distance is indicative of stronger binding of Cu, and may be significant to the selectivity of the polymer bound bisthiourea resin.

There are moderate differences in the Cu-S bond distances of the sulphur bridged dimer with Cu(3) to S(202) and S(203) distances of 2.2993(12) and 2.5230(13) Å, respectively and Cu(3) to S(202) and S(203) distances of 2.5711(13) and 2.2989(12) Å, respectively, Table 4.6. The Cu-Cl distances in the chloride bridged dimer are even greater in difference with the Cu(2) to Cl(10) distances of 2.3569(12) and 2.6510(13) Å. These differences suggest that the dimers consist of two labile monomer units. It may be seen visually that each of the dimers may be split through the Cu-S bonds in the case of the S-bridged dimer A, and the Cu-Cl bond for the Cl-bridged dimer B, to yield trigonal monomers of formula $Cu(t\text{-}TUP)_2Cl$ that resemble the monomer in the crystal structure. The arrangement of all three isomers of $Cu(t\text{-}TUP)_2Cl$ in the crystal is shown in figure 4.21.

Monomer				S-bridged dimer (A)				Cl-bridged dimer (B)			
			Angle (°)				Angle (°)				Angle (°)
S(2)	Cu(1)	S(1)	117.14(5)	S(201)	Cu(3)	S(202)	108.33(4)	S(101)	Cu(2)	S(102)	104.81(4)
S(2)	Cu(1)	Cl(1)	121.05(5)	S(201)	Cu(3)	Cl(21)	117.93(5)	S(101)	Cu(2)	Cl(10)	120.08(5)
S(1)	Cu(1)	Cl(1)	121.78(4)	S(202)	Cu(3)	Cl(21)	117.40(4)	S(102)	Cu(2)	Cl(10)	122.53(4)
				S(201)	Cu(3)	S(203)	105.98(4)	S(101)	Cu(2)	Cl(10)	109.51(4)
				S(202)	Cu(3)	S(203)	110.12(4)	S(102)	Cu(2)	Cl(10)	111.10(4)
				Cl(21)	Cu(3)	S(203)	95.59(4)	Cl(10)	Cu(2)	Cl(10)	86.91(4)
				S(204)	Cu(4)	S(203)	109.15(4)	Cu(2)	Cl(10)	Cu(2)	93.09(4)
				S(204)	Cu(4)	Cl(22)	117.58(4)				
				S(203)	Cu(4)	Cl(22)	118.09(4)				
				S(204)	Cu(4)	S(202)	102.66(4)				
				S(203)	Cu(4)	S(202)	108.48(4)				
				Cl(22)	Cu(4)	S(202)	98.70(4)				
				Cu(3)	S(202)	Cu(4)	70.22(4)				
				Cu(4)	S(203)	Cu(3)	71.12(4)				

Table 4.7: selected bond angles for the monomer and two dimers of Cu(t-TUP)$_2$Cl

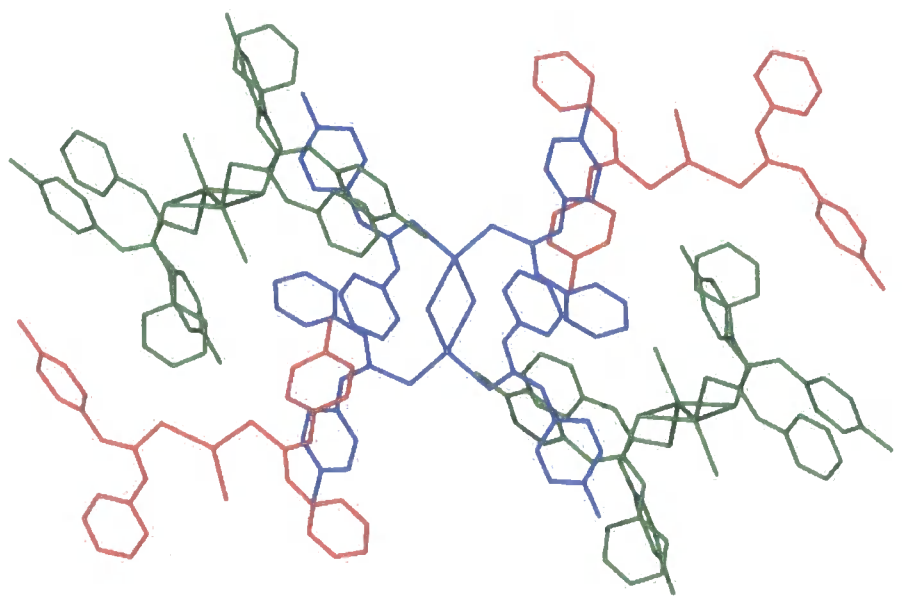

Figure 4.21: orientation of monomers (red), S-bridged dimers A (green) and chloride-bridged dimer B (blue) in the crystal. From data obtained by Dr. Kirsty Anderson.

The Cu(t-TUP)$_2$Cl complex was recrystallised from chloroform, and colourless crystals for structural analysis by X-ray crystallography were grown over

the course of only a few hours. It was found that solely the $Cu(t\text{-}TUP)_2Cl$ monomer crystallizes under these conditions as a chloroform solvate, fig 4.22.

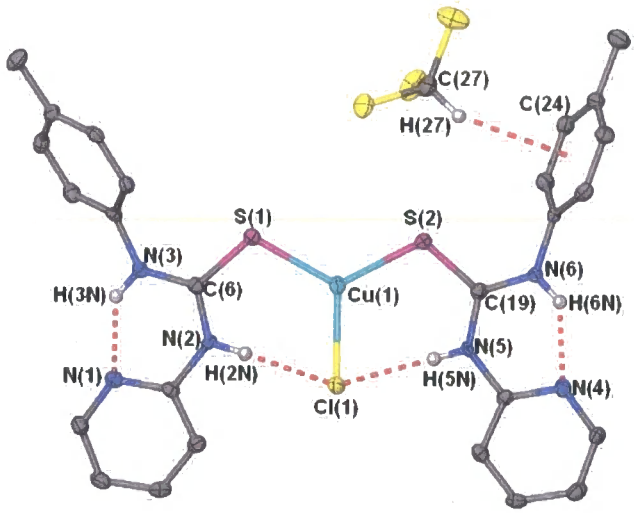

Figure 4.22: molecular structure of monomeric $Cu(t\text{-}TUP)_2Cl$ grown from chloroform, showing CH-arene interaction between the tolyl ring of the coordination complex and a solvent chloroform molecule. Ellipsoids are shown at 50 % probability. Data obtained by Dr. Kirsty Anderson.

This monomer differs only slightly from the monomer within the crystal of "$Cu(t\text{-}TUP)_2Cl$" grown from acetonitrile, possessing a trigonal Cu(I) centre with coordination of two t-TUP ligands through the sulphur atom alone and one chloride atom. Hydrogen bonding exists between H(5N) and H(2N) and the coordinated chloride atom, Cl(1), and H(3N) and H(6N) hydrogen bond to N(1) and N(4) nitrogen atoms of the pyridyl ring, respectively. This structure differs by the inclusion of a chloroform solvent molecule and the tolyl rings are tilted out of the plane of the thioureido group. This is probably due to packing constraints, but it may also be affected by a C-H···arene interaction between the chloroform molecule and the tolyl ring. H(27) to centroid distance is 2.86 Å, while chloroform carbon to closest aryl carbon contact, C(24)-C(27), is 3.53 Å. This monomeric species formed over the course of only a few hours, whereas the other crystals had time to rearrange sufficiently to form dimers which may have optimized packing. After a few days, some yellow crystals formed from the chloroform $Cu(t\text{-}TUP)_2Cl$ solution, which are badly twinned. From preliminary data acquisition, these crystals appear to be in the form of a copper(t-TUP) dimer, however the structure has not been fully solved at the time of publication.

			Distance (Å)
Cu(1)		S(2)	2.2239(10)
Cu(1)		S(1)	2.2266(10)
Cu(1)		Cl(1)	2.2961(10)
S(1)		C(6)	1.716(3)
S(2)		C(19)	1.713(3)
			Angle (°)
S(2)	Cu(1)	S(1)	123.71(4)
S(2)	Cu(1)	Cl(1)	117.61(4)
S(1)	Cu(1)	Cl(1)	118.67(4)

Table 4.8: Selected bond distances and bond angles for $Cu(t\text{-}TUP)_2Cl.CHCl_3$.

The precipitate of $Cu(t\text{-}TUP)_2Cl$ from an acetonitrile solution displays broad ^1H NMR signals that may be assigned to a coordinated t-TUP ligand. Analysis is accurate for the formula $Cu(t\text{-}TUP)_2Cl$ and ESI-MS in chloroform solution shows a single peak at m/z 549.2 assignable to the monomeric $[Cu(t\text{-}TUP)_2]^+$ complex. The precipitate was investigated for phase changes by differential scanning calorimetry (DSC). The material shows that there is no phase transition, fig 4.23, which indicates that there are no thermal polymorphs of this structure.

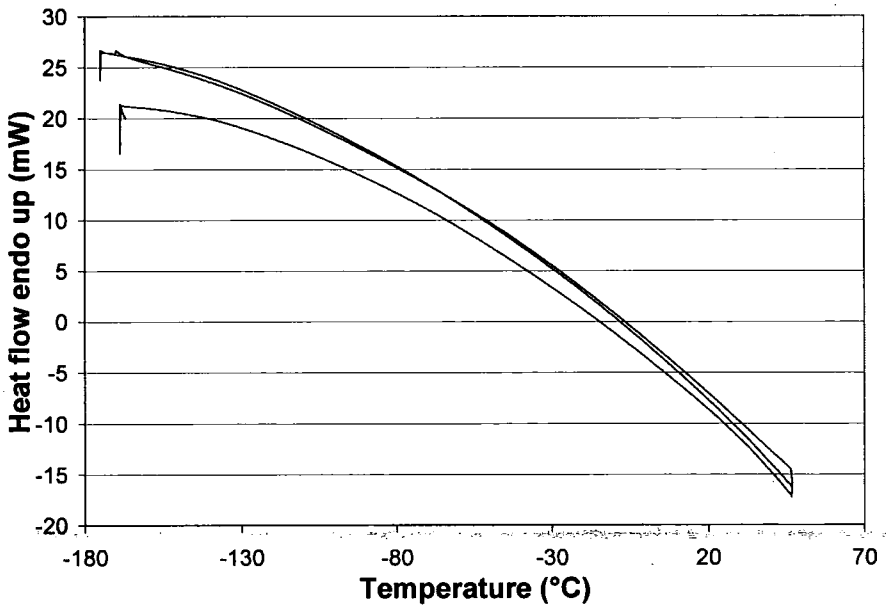

Figure 4.23: DSC of powder sample of $Cu(t\text{-}TUP)_2Cl$ from acetonitrile solution. Data obtained by Mr. Doug Carswell.

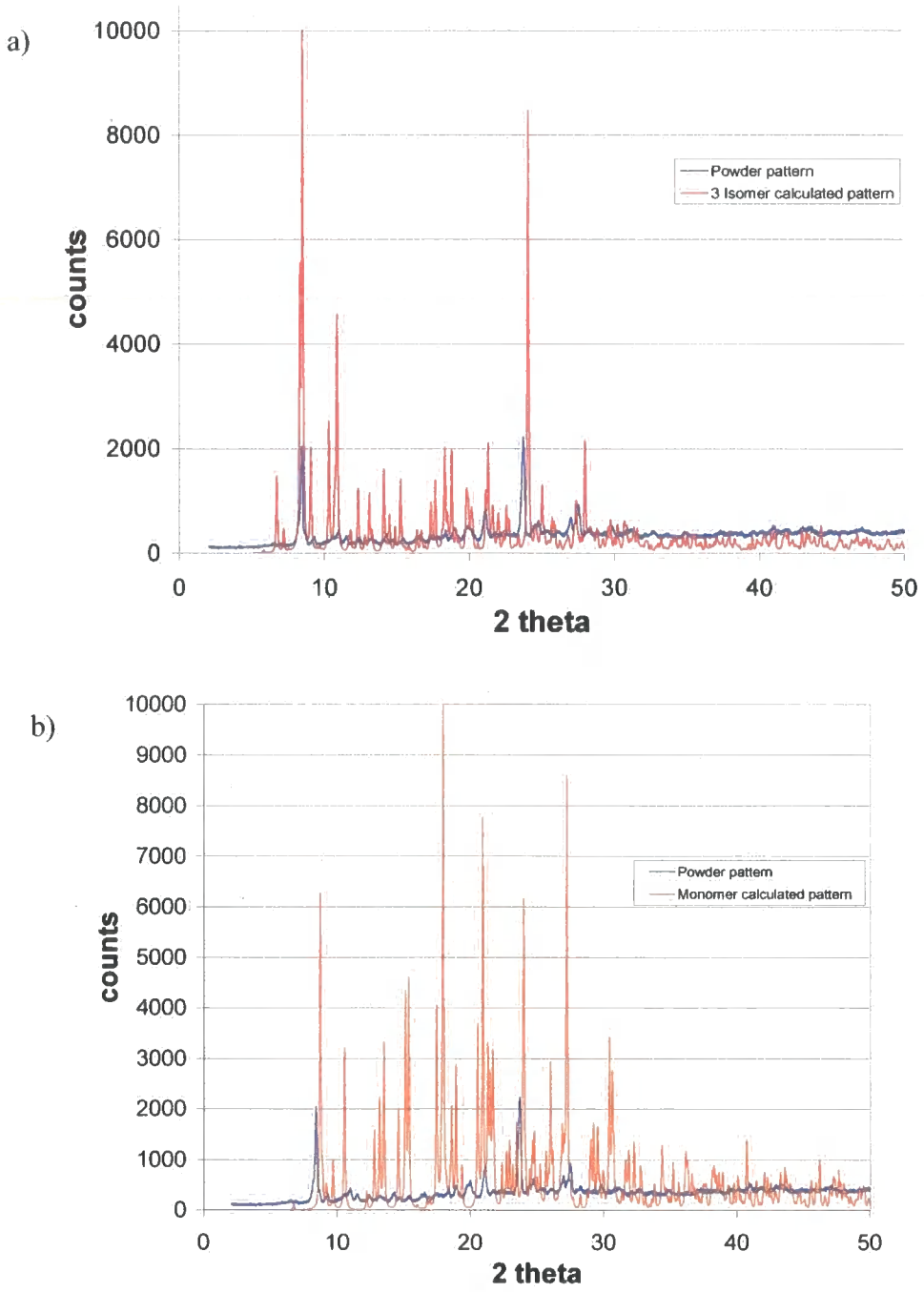

Figure 4.24: powder diffraction pattern for the Cu(t-TUP)$_2$Cl powder compared to the calculated patterns for the crystal structures of a) the single crystal with three isomers present, and of b) the chloroform solvate monomer. Powder diffraction obtained by Dr. Kirsty Anderson.

The powder diffraction pattern of the precipitate was also recorded, and compared to calculated patterns from all the differing crystal structures of Cu(t-TUP)$_2$Cl obtained, fig. 4.24. The diffraction pattern most accurately matches the structure containing the

monomer and two dimers, in particular the peak at 2theta of 8.4 matches well with the pattern calculated for the crystal structure with 3 isomers in the single crystal.

This shows that these different crystal forms of the $Cu(t\text{-}TUP)_2Cl$ molecule are formed through different crystallization solvents and conditions rather than thermal rearrangements. Due to the lability of the bridging atoms in the dimeric structures, it is hard to distinguish whether these molecules are chemically distinct or if they are monomeric rearrangements. This would have implications on the assignment of the number of atoms in the asymmetric unit, as if the dimers are chemically distinct, the asymmetric unit contains only half a formula unit and thus Z' = 0.5. However, if each dimer is considered as two monomers, the assignment would lead to a Z' = 4.

4.4 Conclusions

Reaction of bis(thioureido) ligands, IITPhT, MMTPhT and MMTET with $[\{Ru(\eta^6\text{-}C_6H_4MeCH(Me)_2)Cl(\mu\text{-}Cl)\}_2]$ formed a mixture of coordination compounds. This crude material could be consolidated into a single species with a water wash, which deprotonates a thioureido NH group that coordinates to the Ru(II) to form a terdentate S,S,N binding mode and chirality at the metal centre. The solid-state structure of the complexes (**4.11** – **4.13**) has been determined by X-ray crystallography. The structures confirm the binding mode and shows opposite enantiomers pairing up via hydrogen bonded chloride counter-ions. The complexes formed by the reaction of $[\{Ru(\eta^6\text{-}C_6H_4MeCH(Me)_2)Cl(\mu\text{-}Cl)\}_2]$ with pyridyl containing ligands, MMTPyT and t-TUP were not washed with water. Instead, the Ru(arene) half-sandwich structures of discrete complexes **4.14** and **4.15** could be elucidated.

The reaction of bisthiourea ligands, MMTET, MMTPyT and IITPhT with $[Pd(dppe)Cl_2]$ results in complexes that are symmetrically bound to Pd, as observed by the NMR spectroscopy. This may be assigned to a S,S' bidentate coordination of these ligands to the Pd metal centre, and is confirmed in the solid-state structure of **4.16**. The ligand IITPhT forms a complex with $[Pt(dppe)Cl_2]$, with a similar S,S' bidentate coordination. The monothiourea t-TUP coordinates to $[Pd(dppe)Cl_2]$ through the sulphur atom and some interaction of the pyridyl nitrogen. t-TUP bids to

[Pt(dppe)Cl_2] through the sulphur atom, but from ^{31}P NMR spectroscopy does not appear to displace the second coordinated chloride ligand with the pyridyl nitrogen.

The complex of [Cu(t-TUP)$_2$Cl] crystallizes from acetonitrile to give three isomers of the coordination compound in the single crystals. DSC and powder X-ray diffraction of the powdered material confirm that there are no thermal polymorphs of this structure. The monomer of the complex may be crystallized relatively quickly from chloroform as a chloroform solvate, and over time further crystals of a different confirmation can be isolated.

The bisthiourea ligands have shown a variety of binding modes to the platinum group metals.

4.5 Experimental

4.5.1 General methods

Reactions were performed using reagents as received from commercially available sources, or using compounds synthesised in previous chapters. Reactions involving ruthenium(II) compounds were performed under a nitrogen atmosphere using solvents that had been degassed by bubbling nitrogen through them for an hour. The Ru(II) experiments were all worked up in air. All other experiments were performed and worked up in air.

^{1}H, $\{^{1}H\}$-^{13}C and $\{^{1}H\}$-^{31}P NMR spectroscopy was performed on Varian Mercury 200 MHz, Varian Unity 300 MHz, Varian Mercury 400 MHz, Bruker Avance 400 MHz and Varian Inova 500 MHz NMR spectrometers at frequencies specified in the experimental data. Chemical shifts are reported in parts per million (δ) relative to a tetramethylsilane internal reference, or an external reference of for ^{31}P NMR spectra. Coupling constants (*J*) are reported in Hertz (Hz), and multiplicities are reported as singlet (s), doublet (d), doublet of doublets (dd), multiplets (m), septet, triplet (t) or broad (br). Mass spectra were performed on a Micromass LCT or a Thermo LTQ FT spectrometer in EI or ES+ mode. Micro-analysis for C, H and N atomic percentages were recorded on an Exeter Analytical Inc. CE 440 – Elemental analyzer. IR spectra were run on a Perkin-Elmer Spectrum 100 FT-IR spectrometer as KBr discs. Peaks are reported in wavenumbers (cm^{-1}) and are described as broad (br),

weak (w), medium (m) or strong (s). DSC was performed on Pyris 1 differential scanning calorimeters, using Pyris revision 7 software. UV-Visible spectra were recorded on a Cary 100 Bio UV-visible spectrophotometer at room temperature, using a 1 cm path length glass cuvette.

4.5.2 Metal starting materials

4.5.2.1 [Ru(DMSO)$_4$Cl$_2$]

$Ru(DMSO)_4Cl_2$ was synthesised following literature procedures.[57]

$RuCl_3$ (0.66 g, 2.4 mmol) was refluxed in degassed DMSO (4 ml, excess) for 1 hour. The resulting dark brown solution was reduced in volume *in vacuo* by circa 50 % and 20 ml of acetone was added. A pale yellow precipitate was filtered and washed with acetone, diethyl ether and hexane. Yield = 0.47 g, 0.96 mmol, 40 %.

^{1}H NMR (DMSO-d_6, 300 MHz,) δ (ppm): 3.36 (s, CH_3).

Analysis: calc'd for $RuC_8H_{24}S_4O_4Cl_2$: C 19.83, H 5.00 %; found C 19.74, H 4.99 %.

4.5.2.2 [{Ru(η^6-C$_6$H$_4$MeCH(Me)$_2$)Cl(μ-Cl)}$_2$]

$[\{Ru(\eta^6\text{-}C_6H_4MeCH(Me)_2)Cl(\mu\text{-}Cl)\}_2]$ was synthesised by a variation of the literature procedure.[49]

$RuCl_3.H_2O$ (2.0 g, 9.7mmol) was dissolved in 50 ml ethanol to form a brown solution. α-Terpinene (10 ml, excess) was added and the mixture was refluxed for 4 hours. The red solution was filtered to remove a brown solid. The filtrate was reduced in volume by approximately 75% *in vacuo* and a red crystalline solid was isolated. Yield = 1.25 g, 2.1 mmol, 43 %.

^{1}H NMR ($CDCl_3$, 300 MHz, *J*/Hz) δ (ppm): 1.28 (6H, d, ^3J = 6.0, CH_3), 2.16 (3H, s, CH_3), 2.93 (1H, m, CH), 5.34, 5.47 (4H, AA'BB' d, ^3J = 6.8, CH_{Arom}).

EI-MS: m/z: 611 [M^+].

Analysis: calc'd for $Ru_2C_{20}H_{28}Cl_4$: C 39.23, H 4.61 %; found: C 39.20, H 4.64 %;

4.5.2.3 [Pt(MeCN)$_2$Cl$_2$]

$[Pt(MeCN)_2Cl_2]$ was synthesised from literature procedures.[58]

Platinum(II) dichloride (0.5 g, 1.9 mmol) was stirred in 200 ml of acetonitrile for 16 hours. After this time, all of the brown $PtCl_2$ suspension had dissolved to yield a pale yellow solution. All the solvent was removed *in vacuo* and a yellow solid was isolated. Yield = 0.52g, 1.5 mmol. 80 %.

Analysis: calc'd for $PtC_4H_6N_2Cl_2$: C 13.80, H 1.74, N 8.05 %; found: C 13.85, H 1.71, N 7.91 %.

4.5.2. [Pd(MeCN)$_2$Cl$_2$]

$[Pd(MeCN)_2Cl_2]$ was synthesised from literature procedures.[58]

Palladium(II) dichloride (2.0 g, 11.3 mmol) was stirred in 200 ml of acetonitrile for 16 hours. After this time, all of the brown $PdCl_2$ suspension had dissolved to yield an orange solution and an orange precipitate. The orange solid was filtered (1.6 g), and the filtrate was reduced in volume to *circa* 20 ml and further precipitate was isolated by filtration (0.8 g). Yield = 2.4 g, 9.3 mmol, 82 %.

Analysis: calc'd for $PdC_4H_6N_2Cl_2$: C 18.52, H 2.33, N 10.80 %; found: C 18.25, H 2.25, N 10.46 %.

4.5.3 Coordination complexes

4.5.3.1 [Ru(η^6-C$_6$H$_4$MeCHMe$_2$)(κ-S,S,N-IITPhT - H)]Cl, 4.11

$[\{Ru(\eta^6\text{-}C_6H_4MeCH(Me)_2)Cl(\mu\text{-}Cl)\}_2]$ (79 mg, 0.13 mmol) and IITPhT (81 mg, 0.26 mmol) were dissolved in 25 ml of $CHCl_3$, and stirred at room temperature for 3 hours. The crude product was obtained by removing all solvent *in vacuo* (150 mg) and ^1H NMR showed a broad mixture of products (see section 4.3.1 for spectrum).

Analysis of crude product: calc'd for $RuC_{24}H_{36}N_4S_2Cl_2$: C 46.74, H 5.88, N 9.09 %; found C 45.93, H 5.97, N 8.29 %.

The crude product (90 mg, 0.15 mmol) was sonicated for 10 minutes in distilled water to dissolve the product. The aqueous solution was filtered to remove any undissolved material and extracted with three 8 ml washes of $CHCl_3$. The orange $CHCl_3$ solution was dried with $MgSO_4$ and filtered, and all solvent removed *in vacuo* from the remaining solution to yield an orange solid. Yield = 55 mg, 0.095 mmol, 65 %.

^{1}H NMR ($CDCl_3$, 400 MHz, *J*/Hz) δ (ppm): 1.03 (3H, d, ^3J = 6.0, CH_3 (L, iPr)), 1.04 (3H, d, ^3J = 6.0, CH_3 (L, iPr)), 1.13 (3H, d, ^3J = 6.0, CH_3 (L, iPr)), 1.15 (3H, d, ^3J = 6.0, CH_3 (L, iPr)), 1.23 (3H, d, ^3J = 6.0, CH_3 (cym, iPr)), 1.28 (3H, d, ^3J = 6.0, CH_3 (cym, iPr)), 2.03 (3H, s, CH_3 (cym)), 2.60 (1H, septet, ^3J = 6.0, CH (cym)), 3.78 (1H, m, CH (L)), 4.35 (1H, m, CH (L)), 4.89 (1H, d, ^3J = 8.0, NH), 5.03, 5.04 (2H, d, ^3J = 6.0, H_{Ar} (cym)), 5.14 (1H, d, ^3J = 6.0, H_{Ar} (cym)), 5.21 (1H, d, ^3J = 6.0, H_{Ar} (cym)), 7.09, 7.11, 7.12 (3H, m, H_{Ar} (L)), 7.33 (1H, m, H_{Ar} (L)), 9.91 (1H, d, ^3J = 8.0, NH), 11.08 (1H, s, NH).

{^{1}H}-^{13}C NMR ($CDCl_3$, 125 MHz) δ (ppm): 19.05, 22.03, 22.63, 22.69, 22.93, 23.11, 23.61, 31.67, 44.78, 48.38, 82.50, 83.13, 83.38, 83.64, 98.07, 104.44, 126.35, 126.88, 126.95, 127.00, 133.03, 140.77, 178.62, 180.20.

ESI-MS: 545.1, 100 % rel. abundance with Ru isotope envelope for [^{102}Ru(η^6-$C_6H_4MeCHMe_2$)(κ-S,S',N-IITPhT - H)]$^+$.

Analysis: calc'd for $RuC_{24}H_{35}N_4S_2Cl$: C 49.68, H 6.08, N 9.66 %; found: C 48.70, H 6.08, N 9.33 %.

IR (**ν**, cm^{-1}): 3216 (br, N-H), 3132 (br, N-H), 1591 (s, N-H), 1561 (s, N-H), 1168 (m, C=S), 1129 (m, C=S).

Crystal structure data may be found in section 4.5.4.

4.5.3.2 [Ru(η^6-C$_6$H$_4$MeCH(Me)$_2$)(κ-S,S,N-MMTPhT - H)]Cl, 4.12

[{Ru(η^6-$C_6H_4MeCH(Me)_2$)Cl(μ-Cl)}$_2$] (0.31 g, 0.5 mmol) was dissolved in 50 ml of chloroform, which had been degassed for 30 mins with N_2. Under a nitrogen atmosphere, MMTPhT (0.25 g, 1.0 mmol) was added and dissolved in the reaction mixture. The mixture was then refluxed for 4 hours. After this time all solvent was removed *in vacuo* to provide a crude product that displayed broad and many resonances in the ^{1}H NMR. The crude product was dissolved in 50 ml of distilled water and filtered to remove a dark residue. The aqueous solution was washed with chloroform (5 x 20 ml) to extract the desired product. The combined organic washes were stirred with $MgSO_4$ to dry, filtered, and all solvent was removed *in vacuo*, yielding an orange solid. Yield = 0.4 g, 0.76 mmol, 76 %.

^{1}H NMR ($CDCl_3$, 400 MHz, *J*/Hz) *δ* (ppm): 1.07 (3H, d, ^3J = 7.2, N-CH_3), 1.16 (3H, d, ^3J = 7.2, N-CH_3), 2.05 (3H, s, Ar-CH_3), 2.62 (1H, m, CH cym) 2.77 (3H, d, ^3J = 4.8, C-CH_3 *i*Pr), 2.99 (3H, d, ^3J = 4.8, C-CH_3 *i*Pr), 5.03 (1H, d, ^3J = 5.6, CH_{Ar}) 5.07

(1H, d, ^3J = 5.6, CH_{Ar}), 5.16 (1H, d, ^3J = 5.6, CH_{Ar}), 5.21 (1H, d, ^3J = 5.6, CH_{Ar}), 5.44, (1H, q, ^3J = 7.2, NH(Me)), 7.12 (1H, br, 1H, CH_{Ar}), 7.13 (1H, br, CH_{Ar}), 7.21 (1H, br, CH_{Ar}), 7.23 (1H, br, CH_{Ar}), 8.82 (1H, q, ^3J = 7.2, NH(Me)), 10.94 (1H, s, NH(Ar)).

{^{1}H}-^{13}C NMR ($CDCl_3$, 101 MHz) δ (ppm): 18.75, 22.09, 22.77, 28.67, 31.46, 32.49, 82.22, 82.74, 82.85, 82.89, 97.55, 104.20, 126.09, 126.21, 127.10, 127.17, 132.91, 140.83, 181.43, 182.47.

Analysis: calc'd for $RuC_{20}H_{27}N_4S_2Cl$: C 45.83, H 5.19, N 10.69 %; found: C 45.84, H 5.60, N 10.50 %.

ESI-MS: 489.1, 100 % rel. abundance with Ru isotope envelope for [^{102}Ru(η^6-$C_6H_4MeCH(Me)_2$)(MMTPhT – H)]$^+$.

IR (ν, cm^{-1}): 3192 (br, N-H), 3044 (br, N-H), 1595 (s, NH), 1567 (s, NH), 1263 (m, C=S), 1040 (m, C=S).

Crystal structure data [Ru(cym)(MMTPhT – H)]Cl may be found in section 4.5.4.

4.5.3.3[Ru(η^6-$C_6H_4MeCH(Me)_2$)(κ-S,S,N-MMTET - H)]Cl.H_2O, 4.13

The same method for synthesising [Ru(η^6-$C_6H_4MeCH(Me)_2$)(κ-S,S',N-MMTPhT – H)]Cl was used: [{Ru(η^6-$C_6H_4MeCH(Me)_2$)Cl(μ-Cl)}$_2$] (80 mg, 0.13 mmol) and MMTET (54 mg, 0.26 mmol). Yield = 88 mg, 0.18 mmol, 68 %.

Two conformations observed in ^{1}H NMR spectrum in approximate 2:1 ratio:

^{1}H NMR ($CDCl_3$, 400 MHz, *J*/Hz) δ (ppm):

Major conformer – 1.26, 1.27 (6H, d, ^3J = 6.0, CH_3 cym), 2.22 (3H, s, CH_3 L), 2.67 (3H, s, CH_3 L), 2.76 (1H, m, ^3J = 6.0, CH cym), 2.97 (3H, br, CH_3 cym), 3.07 (1H, m, CH_2 L), 3.57 (1H, m, CH_2 L), 3.79 (1H, m, CH_2 L), 3.97 (1H, m, CH_2 L), 5.12 (1H, br, CH_{Ar}), 5.24 (1H, br, CH_{Ar}), 5.32 (1H, br, CH_{Ar}), 5.38 (1H, br, CH_{Ar}), 6.21 (1H, br, NH), 7.41 (1H, br, NH), 9.22 (1H, br, NH),

Minor conformer – 1.26, 1.27 (6H, d, ^3J = 6.0, CH_3 cym), 2.22 (3H, s, CH_3 L), 2.67 (3H, s, CH_3 L), 2.76 (1H, m, ^3J = 6.0, CH cym), 3.00 (3H, br, CH_3 cym) 3.07 (1H, m, CH_2 L), 3.31 (1H, m, CH_2 L), 3.57 (1H, m, CH_2 L), 3.97 (1H, m, CH_2 L), 5.12 (1H, br, CH_{Ar}), 5.24 (1H, br, CH_{Ar}), 5.32 (1H, br, CH_{Ar}), 5.42 (1H, br, CH_{Ar}), 6.44 (1H, br, NH), 8.14 (1H, br, NH), 9.29 (1H, br, NH).

{^{1}H}-^{13}C NMR ($CDCl_3$, 101 MHz) δ (ppm): 18.99, 22.60, 23.21, 27.99, 31.83, 45.48, 46.92, 81.11, 82.47, 97.54, 104.47, 177.16, 180.79.

ESI-MS: 441.2, 100 % rel. abundance with Ru isotope envelope for $[^{102}Ru(\eta^6\text{-}C_6H_4MeCH(Me)_2)(MMTET - H)]^+$.

Analysis: calc'd for $RuC_{16}H_{27}N_4S_2Cl.H_2O$: C 38.89, H 5.92, N 11.34 %; found C 38.77, H 5.96, N 10.91 %.

IR (**ν**, cm^{-1}): 3240 (br, N-H), 3143 (br, N-H), 1588 (s, N-H), 1232 (m, C=S), 1060 (m, C=S).

Crystal structure data may be found in section 4.5.4.

4.5.3.4 [Ru(η⁶-C₆H₄MeCH(Me)₂)(κ-S,S,N-MMTPyT)]Cl, 4.14

$[\{Ru(\eta^6\text{-}C_6H_4MeCH(Me)_2)Cl(\mu\text{-}Cl)\}_2]$ (96 mg, 0.16 mmol) and MMTPyT (80 mg, 0.33 mmol) were dissolved in 25 ml of degassed $CHCl_3$ and refluxed under N_2 for 6 hours. Removing all solvent *in vacuo* yields a red solid. Yield = 178 mg, 0.33 mmol, 99 %.

^1H NMR shows a major product of one symmetrically bound MMTPyT, and some unidentifiable impurities. Dissolving the product in water does not aid purification.

^1H NMR ($CDCl_3$, 400 MHz, *J*/Hz) δ (ppm): 1.18 (6H, d, ^3J = 6.8, 2 x CH_3 cym), 1.84 (3H, s, CH_3 cym), 2.70 (1H, m, CH cym), 3.26 (6H, d, ^3J = 4.0, 2 x CH_3 L), 5.53 (2H, d, ^3J = 6.0, CH_{Ar} cym), 5.65 (2H, d, ^3J = 6.0, CH_{Ar} cym), 7.29 (2H, d, ^3J = 8.0, CH pyridyl), 7.63 (1H, t, ^3J = 8.0, CH pyridyl), 10.38 (1H, d, ^3J = 4.0, NH), 12.78 (1H, s, NH).

$\{^1H\}$-^{13}C NMR ($CDCl_3$, 101 MHz) δ (ppm): 17.55, 21.70, 29.79, 31.24, 87.29, 88.80, 104.85, 106.31, 111.60, 141.29, 152.53, 178.58.

ESI-MS: 245.5, $[^{102}Ru(\eta^6\text{-}C_6H_4MeCH(Me)_2)L]^{2+}$, 265.5 $[^{102}Ru(\eta^6\text{-}C_6H_4MeCH(Me)_2)L(MeCN)]^{2+}$, 490.1 $[^{102}Ru(\eta^6\text{-}C_6H_4MeCH(Me)_2)(L - H)]^+$.

Analysis: calc'd for $RuC_{19}H_{27}N_4S_2Cl_2$: C 41.68, H 4.97, 10.23 %; found: C 37.04, H 4.50, N 10.61 %.

IR (**ν**, cm^{-1}): 3219 (br, N-H), 1611 (s, N-H), 1260 (m, C=S), 1158 (m, C=S), 1054 (m, C=S).

4.5.3.5 [Ru(η⁶-C₆H₄MeCH(Me)₂)Cl(t-TUP)]Cl, 4.15

$[\{Ru(\eta^6\text{-}C_6H_4MeCH(Me)_2)Cl(\mu\text{-}Cl)\}_2]$ (76 mg, 0.125 mmol) and t-TUP (60 mg, 0.25 mmol) were refluxed under N_2 in degassed $CHCl_3$ for 3 hours. After this time all

solvent was removed *in vacuo* to yield a dark orange solid. Yield = 124 mg, 0.21 mmol, 84 %.

^{1}H NMR ($CDCl_3$, 400 MHz, *J*/Hz) δ (ppm): 1.13 (3H, d, ^3J = 4.4, CH_3 cym), 1.15 (3H, d, ^3J = 4.4, CH_3 cym), 1.87 (3H, s, CH_3), 2.32 (3H, s, CH_3), 2.71 (1H, m, CH, cym), 5.22 (1H, d, ^3J = 6.0, CH_{Ar}, cym), 5.24 (1H, d, ^3J = 6.0, CH_{Ar}, cym), 5.38 (1H, d, ^3J = 6.0, CH_{Ar}, cym), 5.46 (1H, d, ^3J = 6.0, CH_{Ar}, cym), 7.13, (1H, d, ^3J = 6.8 Hz, CH_{Ar}, pyridyl), 7.17 (2H, d, ^3J = 8.4, CH_{Ar}, tolyl), 7.41 (2H, d, ^3J = 8.4, CH_{Ar}, tolyl), 7.56 (1H, d, ^3J = 6.8, CH_{Ar}, pyridyl), 7.73 (1H, t, ^3J = 6.8, CH_{Ar}, pyridyl), 8.83 (1H, d, ^3J = 6.8, CH_{Ar}, pyridyl), 11.95 (1H, br, NH), 13.11 (1H, br, NH).

{^{1}H}-^{13}C NMR ($CDCl_3$, 101 MHz) δ (ppm): 17.19, 20.21, 21.29, 21.39, 29.69, 83.40, 84.05, 84.24, 85.76, 99.16, 105.96, 116.13, 120.32, 124.14, 128.70, 132.91, 136.87, 139.241, 152.00, 153.76, 176.79.

ESI-MS: 478.0, 100 % rel. abundance with Ru isotope envelope for [^{102}Ru(η^6-$C_6H_4MeCH(Me)_2$)(t-TUP - H)]$^+$; 519.0, with Ru isotope envelope for [^{102}Ru(η^6-$C_6H_4MeCH(Me)_2$)(t-TUP - H)(MeCN)]$^+$.

Analysis: calc'd for $RuC_{23}H_{23}N_3SCl_2.2(H_2O)$: C 47.50, H 4.68, 7.23 %; found C 47.43, H 4.74, 7.14 %.

IR (**ν**, cm^{-1}): NH peaks obscured by H_2O peak, 1628 (s, N-H), 1219 (m, C=S), 1160 (m, C=S), 1057 (m, C=S).

4.5.3.6 [Pd(dppe)(κ-S,S-IITPhT)] $(PF_6)_2$, 4.16

$Pd(MeCN)_2Cl_2$ (60 mg, 0.23 mmol) and dppe (92 mg, 0.23 mmol) were dissolved in 20 ml of dichloromethane, and stirred for 30 mins to generate $Pd(dppe)Cl_2$ *in situ*. To this, IITPhT (72 mg, 0.23 mmol) was added in a 20 ml solution of acetone. The solution was stirred for 5 hours and after this time, all solvent was removed *in vacuo*, and the yellow solid washed with hexane. Mass = 180 mg. 90 mg of this crude solid was dissolved in 50 ml of acetone/ethanol (1:1) before NH_4PF_6 (200 mg, excess) was added and the mixture stirred overnight. After this time all solvent was removed and the compound was extracted into 2 ml of $CDCl_3$ for NMR spectroscopy. After spectra had been obtained all solvent was removed from this solution to yield a yellow solid that was washed with diethyl ether. Yield = 101 mg, 0.09 mmol, 39 % (89 % of 90 mg used in metathesis).

^{1}H NMR ($CDCl_3$, 400 MHz, *J*/Hz) δ (ppm): 1.25 (6H, br, CH_3 L), 2.37 (2H, br, CH_2 dppe), 2.82 (2H, br, CH_2 dppe), 4.28 (2H, br, CH L), 5.91 (2H, br, CH_{Ar}), 6.39 (2H, br, CH_{Ar}), 7.38, 7.47, 7.60 (20H, br, CH_{Ar} dppe), 7.82 (2H, br, NH), 8.7 (2H, br, NH)

{^{1}H}-^{13}C NMR ($CDCl_3$, 101 MHz) δ (ppm): 21.13, 21.33, 29.88, 47.35, 127.63, 128.53, 128.64, 130.47, 131.67, 131.76, 131.86, 132.10, 132.81, 132.92, 175.07.

{^{1}H}-^{31}P NMR ($CDCl_3$, 162 MHz, *J*/Hz) δ (ppm): 61.64 (s, PPh_2), -144.02 (septet, $^1J_{P,F}$ = 715, PF_6).

Analysis: calc'd for $PdC_{40}H_{46}N_4S_2P_4F_{12}$: C 43.47, H 4.19, N 5.04 %; found: C 44.54, H 4.19, N 5.16%.

ESI-MS: 812.9, 100 % rel. abundance with Pd isotope envelope for $[^{106}Pd(dppe)(IITPhT - H)]^+$.

IR (**ν**, cm^{-1}): 3353 (br, N-H), 3220 (br, N-H), 1578 (s, N-H), 1243 (m, C=S), 1167 (m, C=S), 1104 (m, C=S), 840 (vs, P-F).

Crystal structure data of [Pd(dppe)(IITPhT)]Cl.PF_6 may be found in section 4.5.4.

4.5.3.7 [Pd(dppe)(κ-S,S-MMTET)]Cl.PF_6, 4.17

$Pd(MeCN)_2Cl_2$ (50 mg, 0.19 mmol) and dppe (77 mg, 0.19 mmol) were dissolved in 20 ml of dichloromethane, and stirred for 30 mins to generate $Pd(dppe)Cl_2$ *in situ*. To this, MMTET (39 mg, 0.19 mmol) was added in a 20 ml solution of ethanol. This was stirred for an hour before an excess of NH_4PF_6 (120 mg) was added in 20 ml of ethanol. The mixture was stirred for a further 30 mins. After this time all solvent was removed and the compound was extracted into 20 ml of chloroform. Solvent was removed from this solution to yield a yellow solid that was washed with diethyl ether. Yield = 142 mg, 0.16 mmol, 84 %.

^{1}H NMR (CD_3CN, 400 MHz) δ (ppm): 2.65 (6H, br, CH_3), 2.72 (4H, br, CH_2), 3.32 (2H, br, CH_2), 3.43 (2H, br, CH_2), 6.83 (2H, br, NH), 7.58 (8H, br, CH_{Ar}), 7.67 (4H, br, CH_{Ar}), 7.80 (8H, br, CH_{Ar}), 8.26 (2H, br, NH).

{^{1}H}-^{13}C NMR ($CDCl_3$, 101 MHz,) δ (ppm): saturated solution did not give clear spectrum

{^{1}H}-^{31}P NMR ($CDCl_3$, 162 MHz, *J*/Hz) δ (ppm): -136.2 (septet, $^1J_{P,F}$ =715, PF_6), 67.9 (s, PPh_2).

ESI-MS (MeCN): 709.1, 100 % rel. abundance with Pd isotopic envelope for $[^{106}Pd(dppe)(MMTET - H)]^+$.

Analysis: calc'd for $PdC_{32}H_{38}N_4S_2P_3F_6Cl$: C 43.11, H 4.30, N 6.28 %; found: C 43.39, H 4.00, N 3.82 %.

IR (**ν**, cm^{-1}): 3385 (br), 3241 (br), 1588 (s), 1229 (m, C=S), 1188 (m, C=S), 1104 (m, C=S), 840 (vs, P-F).

4.5.3.8 [Pd(dppe)(κ-S,S-MMTPyT)]Cl.PF_6, 4.18

$Pd(MeCN)_2Cl_2$ (50 mg, 0.19 mmol) and dppe (77 mg, 0.19 mmol) were dissolved in 20 ml of dichloromethane, and stirred for 30 mins to generate $Pd(dppe)Cl_2$ *in situ*. To this, MMTPyT (48 mg, 0.19 mmol) was added in a 20 ml solution of ethanol. This was stirred for an hour before an excess of NH_4PF_6 (120 mg) was added in 20 ml of ethanol. The mixture was stirred for a further 30 mins. After this time all solvent was removed and the compound was extracted into 20 ml of chloroform. Solvent was removed from this solution to yield a yellow solid that was washed with diethyl ether. Yield = 157 mg, 0.17 mmol, 88 %.

^1H NMR ($CDCl_3$, 400 MHz, *J*/Hz) δ (ppm): 2.66 (2H, m, CH_2-P), 2.72 (2H, m, CH_2-P), 2.98 (6H, d, ^3J = 4.4, CH_3-N), 6.98 (2H, br, CH_{Ar} (L)), 7.38 (1H, br, CH_{Ar} (L), 7.45 (8H, d, ^3J = 6.0, Ph-P), 7.54 (4H, d, ^3J = 6.4, Ph-P), 7.70 (8H, dd, ^3J = 6.4, ^{3}J = 6.0, Ph-P), 9.26 (2H, br, NH-Me), 10.26 (2H, br, NH-Ar).

{^1H}-^{13}C NMR ($CDCl_3$, 101 MHz,) δ (ppm): saturated solution did not give clear spectrum

{^1H}-^{31}P NMR ($CDCl_3$, 162 MHz, *J*/Hz) δ (ppm): -135.7 (septet, $^1J_{P,F}$ = 715, PF_6), 66.5 (s, PPh_2).

ESI-MS (MeCN): 758.1, 100 % rel. abundance with Pd isotope envelope for $[^{106}Pd(dppe)(MMTPyT - H)]^+$.

Analysis: calc'd for $PdC_{35}H_{37}N_5S_2P_3F_6Cl$: C 44.69, H 3.96, N, 7.45 %; found: C 44.40, H 4.00, N, 6.80 %.

IR (**ν**, cm^{-1}): 3393 (br, N-H), 3170 (br, N-H), 1612 (s, NH), 1259 (m, C=S), 1163 (m, C=S), 1103 (m, C=S), 1052 (m, C=S), 840 (vs, P-F).

4.5.3.9 [Pd(dppe)(t-TUP)]Cl(PF_6), 4.19

$Pd(MeCN)_2Cl_2$ (51 mg, 0.19 mmol) and dppe (78 mg, 0.19 mmol) were dissolved in 20 ml of dichloromethane, and stirred for 30 mins to generate $Pd(dppe)Cl_2$ *in situ*. To

this, t-TUP (47 mg, 0.19 mmol) was added in a 20 ml solution of acetone. The solution was stirred for 5 hours and after this time, all solvent was removed *in vacuo*, and the yellow solid washed with hexane. Mass = 150 mg. 80 mg of this crude solid was dissolved in 50 ml of acetone/ethanol (1:1) before an excess of NH_4PF_6 (150 mg) was added and the mixture stirred overnight. After this time all solvent was removed and the compound was extracted into 2 ml of $CDCl_3$ for NMR spectroscopy. After spectra had been obtained all solvent was removed from this solution to yield a yellow solid that was washed with diethyl ether. Yield = 86 mg, 0.093 mmol, 49 %.

^{1}H NMR ($CDCl_3$, 400 MHz, *J*/Hz) δ (ppm): 2.29 (3H, s, CH_3 L), 2.58 (2H, br, CH_2 dppe), 2.64 (2H, br, CH_2 dppe), 6.95 (2H, d, ^3J = 7.6, CH_{Ar} tolyl), 6.98 (2H, d, ^3J = 7.6, CH_{Ar} tolyl), 7.08 (1H, d, ^3J = 7.6, CH_{Ar} pyridyl) 7.10 (1H, dd, ^3J = 7.6, CH_{Ar} pyridyl), 7.41, 7.52, 7.60 (20H, br, CH_{Ar} dppe), 7.68 (1H, dd, ^3J = 7.6 Hz, CH_{Ar} pyridyl), 8.17 (1H, d, ^3J = 7.6, CH_{Ar} pyridyl), 11.78 (1H, s, NH), 13.73 (1H, s, NH)

{^{1}H}-^{13}C NMR ($CDCl_3$, 101 MHz) δ (ppm): 20.97, 27.92, 28.19, 114.33, 120.29, 125.67, 126.61, 129.31, 129.44, 132.81, 133.37, 133.47, 133.69, 137.59, 139.49, 145.52, 152.61, 173.24.

{^{1}H}-^{31}P NMR ($CDCl_3$, 162 MHz, *J*/Hz) δ (ppm): 67.64 (br, $P(Ph_2)$), -144.35 (septet, $^1J_{P,F}$ = 715, PF_6).

ESI-MS (MeCN): 746.0, 100 % rel. abundance with Pd isotope envelope for [^{106}Pd(dppe)(t-TUP – H)]$^+$.

Analysis: calc'd for $PdC_{39}H_{37}N_3SP_3F_6Cl$: C 50.44, H 4.02, 4.53 %; found: C 49.19, H 4.14, N 4.58 %.

IR (**ν**, cm^{-1}): NH peaks obscured by broad H_2O, 1609 (s, N-H), 1190 (m, C=S), 1152 (m, C=S), 1104 (m, C=S), 840 (vs, P-F).

4.5.3.10 [Pt(dppe)(κ-S,S-IITPHT](PF$_6$)$_2$, 4.20

$Pt(MeCN)_2Cl_2$ (100 mg, 0.29 mmol) and dppe (114 mg, 0.29 mmol) were dissolved in 20 ml of dichloromethane to form $Pt(dppe)Cl_2$ *in situ*. To this, IITPhT (78 mg, 0.29 mmol) dissolved in 20 ml of ethanol was added and stirred for 2 hrs at room temperature. After this time, NH_4PF_6 (200 mg, excess) dissolved in 10 ml of acetone was added and stirred for a further 1 hour. All solvent was then removed *in vacuo* and the yellow solid was washed with dichloromethane. The dichloromethane extraction

was removed of solvent *in vacuo* to yield a yellow solid. Yield = 140 mg, 0.12 mmol, 40 %

^{1}H NMR ($CDCl_3$, 200 MHz, *J*/Hz) δ (ppm): 1.20 (6H, d, ^3J = 6.4, CH_3), 1.28 (6H, d, ^3J = 6.4, CH_3), 2.0 (2H, br, CH_2), 2.7 (2H, br, CH_2), 4.26 (2H, q, ^3J = 6.4, CH), 6.00 (2H, d, ^3J = 4.6, CH_{Ar}), 6.41 (2H, d, ^3J = 4.6 Hz, CH_{Ar}), 7.06 (2H, br, NH), 7.4 – 7.6 (20H, CH_{Ar}), 8.68 (2H, br, NH).

{^{1}H}-^{31}P NMR ($CDCl_3$, 121 Hz, *J*/Hz) δ (ppm): 45.87 (s with Pt satellites, $^1J_{P,Pt}$ = 3128, $P(Ph_2)$), -141.16 (septet, $^1J_{P,F}$ = 715, PF_6)

{^{1}H}-^{13}C NMR ($CDCl_3$, 101 MHz) δ (ppm): 21.22, 29.92, 47.68, 124.60, 125.20, 126.13, 126.74, 127.03, 127.34, 127.64, 128.51, 130.14, 131.44, 132.07, 132.89, 173.44.

ESI-MS: 843.0 100 % rel. abundance with ^{195}Pt isotope envelope; 905.3 with ^{195}Pt isotope envelope for [^{195}Pt(dppe)(κ-S,S'-IITPHT)]$^+$.

Analysis: calc'd for $PtC_{40}H_{46}N_4S_2P_4F_{12}$: C 40.24, H 3.88, N 4.69 %; found: C 40.14, H 3.98, N 5.03 %.

IR (**ν**, cm^{-1}): 3345 (br, N-H stretch), 3246 (br, N-H stretch), 1574 (s, NH bend), 1166 (m, C=S stretch), 1105 (m, C=S stretch), 840 (vs, P-F).

4.5.3.11[Pt(dppe)Cl(t-TUP)](PF$_6$), 4.21

$Pt(MeCN)_2Cl_2$ (60 mg, 0.17 mmol) and dppe (69 mg, 0.17 mmol) were dissolved in 20 ml of dichloromethane to form $Pt(dppe)Cl_2$ *in situ*. To this, t-TUP (42 mg, 0.17 mmol) was added in 10 ml of acetone and stirred for 24 hours. To this, NH_4PF_6 (200 mg, excess) was added and stirred for a further 24 hours. After this time all solvent was removed *in vacuo* and the white solid washed with distilled water to remove ammonium salts. The resulting white solid was dried in a toluene drying pistol. Yield = 150 mg, 0.13 mmol, 78 %.

^{1}H NMR (acetone-d_6, 400 MHz, *J*/Hz) δ (ppm): 2.26 (3H, s, CH_3 L), 2.61 (2H, br, CH_2), 2.70 (2H, br, CH_2), 6.97 (2H, d, ^3J = 6.8 Hz, CH_{Ar}), 7.06 (2H, d, ^3J = 6.8 Hz, CH_{Ar}), 7.21 (1H, t, ^3J = 6 Hz, CH_{Ar} pyridyl) 7.41, 7.47, 7.53, 7.79 (20H, br, CH_{Ar} dppe), 7.65 (1H, d, ^3J = 8 Hz, CH_{Ar}), 7.88 (1H, t, ^3J = 8 Hz, CH_{Ar}), 8.30 (1H, d, ^3J = 4.4 Hz, CH_{Ar}), 11.32 (1H, s, NH), 13.99 (1H, s, NH).

{^{1}H}-^{31}P NMR (acetone-d_6, 162 MHz, *J*/Hz) δ (ppm): 48.96 (s, with Pt satellites, $^1J_{P,Pt}$ = 3178, PPh_2 *trans* to sulphur), 46.01 (s, with Pt satellites, $^1J_{P,Pt}$ = 3557, PPh_2 *trans* to chlorine), -144.10 (septet, $^1J_{P,F}$ = 715, PF_6)

{^{1}H}-^{13}C NMR ($CDCl_3$, 101 MHz) δ (ppm): 20.10, 29.89, 113.26, 113.88, 119.69, 124.75, 124.94, 128.30, 128.41, 128.58, 128.79, 129.02, 131.77, 132.41, 132.51, 132.81, 136.94, 137.17, 138.64, 138.80, 144.59, 144.89, 151.37, 151.93, 171.53.

ESI-MS: 668.4, 100 % rel. abundance, with ^{195}Pt isotope envelope. 889.0, with isotope envelope for [^{195}Pt(dppe)(t-TUP)Cl]$^+$.H_2O.

Analysis: calc'd for $PtC_{39}H_{37}N_3SP_3F_6Cl$: C 46.05, H 3.67, N 4.13 %; found: C 43.97, H 3.56, N 4.08 %.

IR (**v**, cm^{-1}): 3225 (br, N-H), 3164 (br, N-H), 1608 (s, N-H), 1190 (m., C=S), 1153 (m., C=S), 1140 (m., C=S), 1106 (m., C=S), 840 (vs, P-F).

4.5.3.12 Cu(t-TUP)$_2$Cl, 4.22

$CuCl_2.2H_2O$ (10 mg, 0.06 mmol) was dissolved in 8 ml of MeCN to form a green solution, while t-TUP (28.5 mg, 0.12 mmol) was dissolved in 10 ml of MeCN to form a colourless solution. The t-TUP solution was slowly added to the copper solution, where upon some fine dark precipitate formed and redissolved immediately. Upon full addition, the green solution was allowed to slowly evaporate and, after a few days, yellow crystals suitable for X-ray crystallography had grown. After a period of days, the crystals had decomposed to form a dark brown solid.

The reaction was repeated on a larger scale with $CuCl_2.2H_2O$ (0.1 g, 0.58 mmol) and t-TUP (0.29 g, 0.13 mmol) in 100 ml of acetonitrile. A short period after addition some yellow precipitate formed and when the volume of solvent was reduced by 50 %, more precipitate formed. This precipitate was recovered by filtration. Yield = 0.23 g, 0.39 mmol, 67 %.

^{1}H NMR ($CDCl_3$, 400 MHz, *J*/Hz) δ (ppm): 2.35 (3H, s, CH_3), 7.04 (1H, br, CH_{Ar}), 7.18 (2H, d, ^3J = 7.2, CH_{Ar}), 7.35 (2H, d, ^3J = 7.2, CH_{Ar}), 7.51 (1H, br, CH_{Ar}), 7.72 (1H, br, CH_{Ar}), 8.20 (1H, br, CH_{Ar}), 11.08 (1H, s, NH), 13.59 (1H, s, NH).

{^{1}H}-^{13}C NMR ($CDCl_3$, 101 MHz,) δ (ppm): 19.21, 112.58, 117.12, 118.75, 123.82, 127.61, 127.82, 133.06, 137.16, 143.48, 151.71, 174.94.

Analysis: calc'd for $CuC_{26}H_{26}N_6S_2Cl$: C 53.32, H 4.47, N 14.35 %; found: C 53.29, H 4.46, N 14.29 %.

ESI-MS: 549.2, 100 % rel. abundance with Cu isotope for $[^{63}Cu(T\text{-}TUP)_2]^+$.

IR: 3213 (w, N-H), 3105 (w, N-H), 1627 (m, N-H), 1606 (s, N-H), 1183 (m, C=S), 1149 (m, C=S), 1123 (w), 1097 (w).

Crystal structure data may be found in section 4.5.4;

4.5.3.13 [Pd(dppe)(MMTPhT)](PF$_6$)$_2$

The same method for synthesizing [Pd(dppe)(IITPhT)](PF$_6$)$_2$, using Pd(MeCN)$_2$Cl$_2$ (50 mg, 0.19 mmol), dppe (77 mg, 0.19 mmol) and MMTPhT (48 mg, 0.19 mmol) was unsuccessful. The ^{1}H and ^{31}P NMR spectra showed a mixture of products, which could not be purified by recrystallisation.

4.5.3.14 Pd$_2$(MMTET)$_3$Cl$_4$

MMTET (16 mg, 0.080 mmol) was dissolved in 10 ml of acetonitrile and added to a 10 ml solution of [Pd(MeCN)$_2$Cl$_2$] (10 mg, 0.040 mmol). Upon addition an orange precipitate formed, which was removed by filtration. Yield = 17 mg, 0.35 mmol, 85 %.

Analysis: calc'd for $Pd_2C_{18}H_{42}N_{12}S_6Cl_4$: C 22.20, H 4.35, N 17.26 %; found: C 22.45, H 4.90, N 17.27 %.

4.5.3.15 Pd$_2$(MMTPhT)$_3$Cl$_4$

MMTPhT (20 mg, 0.080 mmol) was dissolved in 10 ml of acetonitrile and added to a 10 ml solution of [Pd(MeCN)$_2$Cl$_2$] (10 mg, 0.040 mmol). Upon addition an orange/brown precipitate formed, which was removed by filtration. Yield = 20 mg, 0.034 mmol, 85 %.

Analysis: calc'd for $Pd_2C_{30}H_{42}N_{12}S_6Cl_4$: C 32.24, H 3.79, N 15.04 %; found: C 33.75, H 4.03, N 15.68 %.

4.5.3.16 $Pd_2(MMTPyT)_3Cl_4$

MMTPyT (20 mg, 0.080 mmol) was dissolved in 10 ml of acetonitrile and added to a 10 ml solution of $[Pd(MeCN)_2Cl_2]$ (10 mg, 0.040 mmol). Upon addition an orange precipitate formed, which was removed by filtration. Yield = 19 mg, 0.034 mmol, 85 %.

Analysis: calc'd for $Pd_2C_{27}H_{39}N_{15}S_6Cl_4$: C 28.94, H 3.51, N 18.75 %; found: C 28.25, H 3.47, N 18.00 %.

4.5.3.17 $Pt(MMTPyT)_2Cl_2$

MMTPyT (15 mg, 0.060 mmol) was dissolved in 10 ml of acetonitrile and added to a 10 ml solution of $[Pt(MeCN)_2Cl_2]$ (10 mg, 0.030 mmol). Upon addition, a yellow precipitate formed, which was removed by filtration. Yield = 15 mg, 0.020 mmol, 65 %.

Analysis: calc'd $PtC_{18}H_{26}N_{10}S_4Cl_2$: C 27.84 H 3.35 N 18.04 %; found C 28.29 H 3.73 N 18.17 %.

4.5.3.18 $Pt(t\text{-}TUP)_2Cl_2$

t-TUP (14 mg, 0.060 mmol) was dissolved in 10 ml of acetonitrile and added to a 10 ml solution of $[Pt(MeCN)_2Cl_2]$ (10 mg, 0.030 mmol). Upon addition, a white precipitate formed, which was removed by filtration. Yield = 18 mg, 0.024 mmol, 80 %.

Analysis: calc'd for $PtC_{26}H_{26}N_6S_2Cl_2$: C 41.49 H 3.46 N 11.17 %; found: C 39.92, H 3.46, N 10.73.

4.5.3.19 [Cu(IITPhT)PPh_3Br]

CuBr (50 mg, 0.35 mmol) and PPh_3 (92 mg, 0.35 mmol) were dissolved in 100 ml of MeCN to form a colourless solution. To this, a solution of IITPhT (109 mg, 0.35 mmol) in 100 ml of $CHCl_3$ was added dropwise over an hour and the mixture stirred for 2 hours. After this time, all solvent was removed *in vacuo* to yield a white oil. 20 ml of hexane was added to the oil, and the solvent removed *in vacuo*. This yielded a white solid. Yield = 120 mg, 0.17 mmol, 48 %.

^{1}H NMR (DMSO-d_6, 400 MHz): Spectrum was too broad to interpret. Sample may be experiencing ligand exchange with DMSO.

ESI-MS (MeCN): 373.1, 100 % rel. abundance with Cu isotope envelope for $[^{63}CuL]^+$, 635.1 with Cu isotope envelope for $[^{63}CuLPPh_3 - 2H]^+$.

Analysis: calc'd for $CuC_{32}H_{35}N_4S_2PBr$: C 53.66, H 5.21, N 7.82 %; found: C 53.75, H 5.42, N 8.39 %.

4.5.4 Crystal data for coordination compounds

4.5.4.1 General

The diffraction experiments, using graphite-monochromated MoKα radiation (λ = 0.71073 Å), were carried out on SMART 1K, SMART 6K or APEX ProteumM (X-rays from a 60 W microfocus Bede Microsource® with glass polycapillary optics), covering a full sphere of the reciprocal space by three or four runs of narrow-frame (0.3°) ωscans. The crystals were cooled using Cryostream (Oxford Cryosystems) open-flow N_2 cryostats. The structures were solved by direct methods and refined by full-matrix least-squares on F^2 for all the data using SHELXTL software.[59,60]

4.5.4.2 [Ru((η^6-$C_6H_4MeCH(Me)_2$)(κ-S,S,N-MMTPhT – H)]Cl, 4.12

Diffraction quality single crystals of [Ru(η^6-$C_6H_4MeCH(Me)_2$)(κ-*S,S,N*-MMTPhT – H)]Cl were obtained by cooling and slow evaporation of a hot ethyl acetate solutions.

Crystal data for [Ru((η^6-$C_6H_4MeCH(Me)_2$)(MMTPhT – H)]Cl: $C_{20}H_{27}ClN_4RuS_2$, M = 524.10, red small plate, 0.09 × 0.04 × 0.03 mm^3, triclinic, space group P-1 (No. 2), a = 9.9266(9), b = 14.8915(13), c = 24.231(2) Å, α = 74.849(2), β = 80.322(2), γ = 79.488(2)°, V = 3371.9(5) Å^3, Z = 6, D_c = 1.549 g/cm^3, F_{000} = 1608, APEX, MoKα radiation, λ = 0.71073 Å, T = 120(2)K, $2\theta_{max}$ = 50.0°, 54743 reflections collected, 11857 unique (R_{int} = 0.0676). Final *GooF* = 1.020, *R1* = 0.0390, *wR2* = 0.0794, *R* indices based on 8771 reflections with I >2σ(I) (refinement on F^2), 772 parameters, 0 restraints. Lp and absorption corrections applied, μ = 1.016 mm^{-1}.

4.5.4.3 [Ru(η^6-$C_6H_4MeCH(Me)_2$)(κ-S,S,N-MMTET - H)]Cl.H_2O, 4.13

Diffraction quality single crystals of [Ru(η^6-$C_6H_4MeCH(Me)_2$)(κ-*S,S,N*-MMTET - H)]Cl.H_2O were obtained by slow evaporation of acetone/diethyl ether solutions.

Crystal data for [Ru(η^6-$C_6H_4MeCH(Me)_2$)(MMTET – H)]Cl.H_2O: $C_{16}H_{29}ClN_4ORuS_2$, M = 494.07, red block, 0.30 × 0.20 × 0.20 mm^3, monoclinic, space group $P2_1/c$ (No. 14), a = 15.238(3), b = 11.869(2), c = 11.441(2) Å, β = 94.029(5)°, V = 2064.1(7) Å^3, Z = 4, D_c = 1.590 g/cm^3, F_{000} = 1016, SMART 1K, MoKα radiation, λ = 0.71073 Å, T = 120(2)K, $2\theta_{max}$ = 58.3°, 29337 reflections collected, 5553 unique (R_{int} = 0.0684). Final *GooF* = 1.024, *R1* = 0.0349, *wR2* = 0.0631, *R* indices based on 4347 reflections with I >2σ(I) (refinement on F^2), 251 parameters, 0 restraints. Lp and absorption corrections applied, μ = 1.104 mm^{-1}.

4.5.4.4 [Ru(η^6-$C_6H_4MeCH(Me)_2$)(κ-S,S,N-IITPhT-H)]Cl, 4.11

Diffraction quality single crystals of [Ru(η^6-$C_6H_4MeCH(Me)_2$)(κ-*S,S,N*-IITPhT – H)]Cl were obtained by slow evaporation of acetone/diethyl ether solutions.

Crystal data for [Ru(η^6-$C_6H_4MeCH(Me)_2$)(κ-*S,S,N*-IITPhT – H)]Cl: $C_{24}H_{35}ClN_4RuS_2$, M = 580.20, red block, 0.30 × 0.20 × 0.20 mm^3, triclinic, space group P-1 (No. 2), a = 10.0505(6), b = 11.2786(7), c = 13.1434(8) Å, α = 71.008(2), β = 73.421(2), γ = 83.534(2)°, V = 1349.89(14) Å^3, Z = 2, D_c = 1.427 g/cm^3, F_{000} = 600, SMART 6K, MoKα radiation, λ = 0.71073 Å, T = 120(2)K, $2\theta_{max}$ = 58.3°, 23947 reflections collected, 7277 unique (R_{int} = 0.0227). Final *GooF* = 1.040, *R1* = 0.0244, *wR2* = 0.0601, *R* indices based on 6538 reflections with I >2σ(I) (refinement on F^2), 308 parameters, 0 restraints. Lp and absorption corrections applied, μ = 0.853 mm^{-1}.

4.5.4.5 [Pd(dppe)(κ-S,S-IITPhT)]Cl(PF_6).$(CH_3)_2CO$, 4.16

Diffraction quality single crystals of [Pd(dppe)(IITPhT)]Cl(PF_6).$(CH_3)_2CO$ were obtained by slow evaporation of acetone/diethyl ether solutions.

Crystal data for [Pd(dppe)(IITPhT)]Cl(PF_6).$(CH_3)_2CO$: $C_{43}H_{52}ClF_6N_4OP_3PdS_2$, M = 1053.77, colourless block, 0.20 × 0.20 × 0.10 mm^3, orthorhombic, space group *Pbca* (No. 61), a = 16.7485(17), b = 22.810(2), c = 25.016(3) Å, V = 9556.7(17) Å^3, Z = 8, D_c = 1.465 g/cm^3, F_{000} = 4320, SMART 1K, MoKα radiation, λ = 0.71073 Å, T =

120(2)K, $2\theta_{max}$ = 46.6°, 81339 reflections collected, 6897 unique (R_{int} = 0.3378). Final *GooF* = 1.042, *R1* = 0.0848, *wR2* = 0.1418, *R* indices based on 4070 reflections with I >2σ(I) (refinement on F^2), 563 parameters, 2 restraints. Lp and absorption corrections applied, μ = 0.693 mm^{-1}.

4.5.4.6 Cu(t-TUP)$_2$Cl.(μS-μS'-(Cu(t-TUP)$_2$Cl)$_2$).(μCl-μCl'-(Cu(t-TUP)$_2$Cl)$_2$) from acetonitrile

Diffraction quality single crystals of Cu(t-TUP)$_2$Cl.(μS-μS'-(Cu(t-TUP)$_2$Cl)$_2$).(μCl-μCl'-(Cu(t-TUP)$_2$Cl)$_2$) were obtained by slow evaporation of acetonitrile solutions.

Crystal data for Cu(t-TUP)$_2$Cl.(μS-μS'-(Cu(t-TUP)$_2$Cl)$_2$).(μCl-μCl'-(Cu(t-TUP)$_2$Cl)$_2$): $C_{208}H_{208}Cl_8Cu_8N_{48}S_{16}$, *M* = 4685.10, yellow block, 0.30 × 0.20 × 0.20 mm^3, monoclinic, space group *P2/c* (No. 13), *a* = 25.271(2), *b* = 19.6049(14), *c* = 21.8179(16) Å, β = 101.369(3)°, *V* = 10597.4(14) $Å^3$, *Z* = 2, D_c = 1.468 g/cm^3, F_{000} = 4832, SMART 1K, MoKα radiation, λ = 0.71073 Å, *T* = 120(2)K, $2\theta_{max}$ = 58.2°, 151259 reflections collected, 28416 unique (R_{int} = 0.1798). Final *GooF* = 1.019, *R1* = 0.0776, *wR2* = 0.1045, *R* indices based on 14717 reflections with I >2σ(I) (refinement on F^2), 1305 parameters, 0 restraints. Lp and absorption corrections applied, μ = 1.110 mm^{-1}.

4.5.4.7 Cu(t-TUP)$_2$Cl monomer from CHCl$_3$

Diffraction quality single crystals of Cu(t-TUP)$_2$Cl.$CHCl_3$ were obtained by slow evaporation of chloroform solutions.

Crystal data for Cu(t-TUP)$_2$Cl.$CHCl_3$: $C_{27}H_{27}Cl_4CuN_6S_2$, *M* = 705.01, colourless block, 0.20 × 0.20 × 0.10 mm^3, triclinic, space group *P*-1 (No. 2), *a* = 10.6215(12), *b* = 11.8452(13), *c* = 14.1250(16) Å, α = 109.281(2), β = 90.098(2), γ = 113.112(2)°, *V* = 1525.1(3) $Å^3$, *Z* = 2, D_c = 1.535 g/cm^3, F_{000} = 720, SMART 1K, MoKα radiation, λ = 0.71073 Å, *T* = 120(2)K, $2\theta_{max}$ = 58.4°, 22258 reflections collected, 8129 unique (R_{int} = 0.0846). Final *GooF* = 0.991, *R1* = 0.0590, *wR2* = 0.0936, *R* indices based on 4742 reflections with I >2σ(I) (refinement on F^2), 378 parameters, 0 restraints. Lp and absorption corrections applied, μ = 1.233 mm^{-1}.

4.5.5 UV-Vis spectrophotometric titrations

4.5.5.1[Pd(dppe)(IITPhT)](PF$_6$)$_2$ with TBAF

UV-visible spectrophotometric titration experiments were carried out on a Cary 100 Bio UV-visible spectrophotometer at room temperature, using a 1 cm path length glass cuvette. A solution of the host species, [Pd(dppe)(IITPhT)](PF$_6$)$_2$, of known concentration, 0.6 mM, was made up in 2.5 ml of HPLC grade acetonitrile in a 3 ml glass cuvette. A solution of the fluoride anion, as TBA salts, was made up in HPLC grade acetonitrile in volumetric flasks (2 ml) at a concentration five times greater than the host, 3 mM. Guest solution was titrated into the host solution at initial volumes of 10 µl (0.1 equivalents with respect to the host) and, after rigorous shaking to homogenise the solution, spectra recorded after each addition. Larger aliquots were not added as the cuvette had reached full capacity.

4.6 References

(1) Cooke, M. W.; Murphy, C. A.; Cameron, T. S.; Beck, E. J.; Vamvounis, G.; Aquino, M. A. S. *Polyhedron* **2002**, *21*, 1235.

(2) Kar, S.; Pradhan, B.; Sinha, K.; Kundu, T.; Kodgire, P.; Rao, K. K.; Puranik, V. G.; Lahiri, G. K. *Dalton Trans.* **2004**, 1752.

(3) Wilton-Ely, J.; Honarkhah, S. J.; Wang, M.; Tocher, D. A.; Slawin, A. M. Z. *Dalton Trans.* **2005**, 1930.

(4) Sousa-Pedrares, A.; Duran, M. L.; Romero, J.; Garcia-Vazquez, J. A.; Monteagudo, J. C.; Sousa, A.; Dilworth, J. R. *Inorg. Chim. Acta* **2006**, *359*, 863.

(5) Bodensieck, U.; Carraux, Y.; Stoeckli-Evans, H.; Suss-Fink, G. *Inorg. Chim. Acta* **1992**, *195*, 135.

(6) Bodensieck, U.; Hoferkamp, L.; Stoeckli-Evans, H.; Sussfink, G. *J. Chem. Soc., Dalton Trans.* **1993**, 127.

(7) Bodensieck, U.; Meister, G.; Stoeckli-Evans, H.; Sussfink, G. *J. Chem. Soc., Dalton Trans.* **1992**, 2131.

(8) Bodensieck, U.; Santiago, J.; Stoeckli-Evans, H.; Sussfink, G. *J. Chem. Soc., Dalton Trans.* **1992**, 255.

(9) Bodensieck, U.; Stoeckli-Evans, H.; Rheinwald, G.; Sussfink, G. *J. Organomet. Chem.* **1992**, *433*, 167.

(10) Bodensieck, U.; Stoeckli-Evans, H.; Sussfink, G. *Chem. Berichte* **1990**, *123*, 1603.

(11) Bodensieck, U.; Stoeckli-Evans, H.; Sussfink, G. *J. Chem. Soc., Chem. Commun.* **1990**, 267.

(12) Bodensieck, U.; Stoeckli-Evans, H.; Sussfink, G. *Angew. Chem. Int. Ed.* **1991**, *30*, 1126.

(13) Ahmed, S. J.; Hyder, M. I.; Kabir, S. E.; Miah, M. A.; Deeming, A. J.; Nordlander, E. *J. Organomet. Chem.* **2006**, *691*, 309.

(14) Hill, A. F.; Owen, G. R.; White, A. J. P.; Williams, D. J. *Angew. Chem. Int. Ed.* **1999**, *38*, 2759.

(15) Bailey, P. J.; Lorono-Gonzales, D. J.; McCormack, C.; Parsons, S.; Price, M. *Inorg. Chim. Acta* **2003**, *354*, 61.

(16) Bailey, P. J.; Dawson, A.; McCormack, C.; Moggach, S. A.; Oswald, I. D. H.; Parsons, S.; Rankin, D. W. H.; Turner, A. *Inorg. Chem.* **2005**, *44*, 8884.

(17) Bailey, P. J.; McCormack, C.; Parsons, S.; Rudolphi, F.; Perucha, A. S.; Wood, P. *Dalton Trans.* **2007**, 476.

(18) Kuan, S. L.; Leong, W. K.; Goh, L. Y.; Webster, R. D. *J. Organomet. Chem.* **2006**, *691*, 907.

(19) Casas, J. S.; Garcia-Tasende, M. S.; Sordo, J. *Coord. Chem. Rev.* **2000**, *209*, 197.

(20) Singh, S.; Athar, F.; Azam, A. *Bioorg. Med. Chem. Lett.* **2005**, *15*, 5424.

(21) Singh, S.; Bharti, N.; Naqvi, F.; Azam, A. *Eur. J. Med. Chem.* **2004**, *39*, 459.

(22) Singh, S.; Athar, F.; Maurya, M. R.; Azam, A. *Eur. J. Med. Chem.* **2006**, *41*, 592.

(23) Basuli, F.; Peng, S.-M.; Bhattacharya, S. *Inorg. Chem.* **1997**, *36*, 5645.

(24) Basuli, F.; Ruf, M.; Pierpont, C. G.; Bhattacharya, S. *Inorg. Chem.* **1998**, *37*, 6113.

(25) Basuli, F.; Peng, S.-M.; Bhattacharya, S. *Inorg. Chem.* **2000**, *39*, 1120.

(26) Lobana, T. S.; Bawa, G.; Butcher, R. J.; Liaw, B.-J.; Liu, C. W. *Polyhedron* **2006**, *25*, 2897.

(27) Mishra, D.; Naskar, S.; Drew, M. G. B.; Chattopadhyay, S. K. *Inorg. Chim. Acta* **2006**, *359*, 585.

(28) Mishra, D.; Naskar, S.; Drew, M. G. B.; Chattopadhyay, S. K. *Polyhedron* **2005**, *24*, 1861.

(29) Cauzzi, D.; Costa, M.; Cucci, N.; Graiff, C.; Grandi, F.; Predieri, G.; Tiripicchio, A.; Zanoni, R. *J. Organomet. Chem.* **2000**, *593-594*, 431.

(30) Bierbach, U.; Hambley, T. W.; Farrell, N. *Inorg. Chem.* **1998**, *37*, 708.

(31) Martins, E. T.; Baruah, H.; Kramarczyk, J.; Saluta, G.; Day, C. S.; Kucera, G. L.; Bierbach, U. *J. Med. Chem.* **2001**, *44*, 4492.

(32) Xian, L.; Wei, T. B.; Zhang, Y. M. *J. Coord. Chem.* **2004**, *57*, 453.

(33) Hunt, G. W.; Griffith, E. A. H.; Amma, E. L. *Inorg. Chem.* **1976**, *15*, 2993.

(34) Ferrari, M. B.; Fava, G. G.; Pelizzi, C.; Tarasconi, P. *Inorg. Chim. Acta* **1985**, *97*, 99.

(35) Falcomer, V. A. S.; Lemos, S. S.; Batista, A. A.; Ellena, J.; Castellano, E. E. *Inorg. Chim. Acta* **2006**, *359*, 1064.

(36) Lobana, T. S.; Rekha; Butcher, R. J.; Castineiras, A.; Bermejo, E.; Bharatam, P. V. *Inorg. Chem.* **2006**, *45*, 1535.

(37) Battaglia, L. P.; Corradi, A. B.; Nardelli, M.; Tani, M. E. V. *J. Chem. Soc., Dalton Trans.* **1976**, 143.

(38) Caira, M. R.; Nassimbeni, L. R. *J. Chem. Soc., Dalton Trans.* **1976**, 4.

(39) Spofford, W. A.; Amma, E. L. *Acta Crystallogr. Sect. B* **1970**, *B 26*, 1474.

(40) Carmen Aguirre, M. d.; Borrás, J.; Castiñeiras, A.; García-Monteagudo, J. M.; García-Santos, I.; Niclós, J.; West, D. X. *Eur. J. Inorg. Chem.* **2006**, *2006*, 1231.

(41) Ferrari, M. B.; Bisceglie, F.; Pelosi, G.; Tarasconi, P.; Albertini, R.; Dall'Aglio, P. P.; Pinelli, S.; Bergamo, A.; Sava, G. *J. Inorg. Biochem.* **2004**, *98*, 301.

(42) Cernak, J.; Chomic, J.; Kutschy, P.; Svrcinova, D.; Dzurilla, M. *Inorg. Chim. Acta* **1991**, *181*, 85.

(43) Livingstone, S. E. *Q. Rev. Chem. Soc.* **1965**, *19*, 386.

(44) Henderson, W.; Kemmitt, R. D. W.; Mason, S.; Moore, M. R.; Fawcett, J.; Russell, D. R. *J. Chem. Soc., Dalton Trans.* **1992**, 59.

(45) Okeya, S.; Fujiwara, Y.; Kawashima, S.; Hayashi, Y.; Isobe, K.; Nakamura, Y.; Shimomura, H.; Kushi, Y. *Chem. Lett.* **1992**, 1823.

(46) Zelonka, R. A.; Baird, M. C. *J. Organomet. Chem.* **1972**, *35*, C43.

(47) Zelonka, R. A.; Baird, M. C. *J. Organomet. Chem.* **1972**, *44*, 383.

(48) Zelonka, R. A.; Baird, M. C. *Can. J. Chem.* **1972**, *50*, 3063.

(49) Bennett, M. A.; Smith, A. K. *J. Chem. Soc., Dalton Trans.* **1974**, 233.

(50) Burrows, A. D.; Coleman, M. D.; Mahon, M. F. *Polyhedron* **1999**, *18*, 2665.

(51) Okaya, Y.; Knobler, C. B. *Acta Crystallogr.* **1964**, *17*, 928.

(52) Valdes-Martinez, J.; Hernandez-Ortega, S.; West, D. X.; Ackerman, L. J.; Swearingen, J. K.; Hermetet, A. K. *J. Mol. Struct.* **1999**, *478*, 219.

(53) Shannon, R. D.; Prewitt, C. T. *Acta Crystallogr. Sect. B* **1970**, *B 26*, 1046.

(54) Shannon, R. D. *Acta Crystallographica Section A* **1976**, *32*, 751.

(55) Shannon, R. D.; Prewitt, C. T. *Acta Crystallogr. Sect. B* **1969**, *B 25*, 925.

(56) Tomoka Yamaguchi, K. H., Yukinari Sunatsuki, Masaaki Kojima, Kiyohiko Nakajima, Naohide Matsumoto, *Eur. J. Inorg. Chem.* **2006**, *2006*, 3236.

(57) Evans, I. P.; Spencer, A.; Wilkinson, G. *J. Chem. Soc., Dalton Trans.* **1973**, 204.

(58) Walton, R. A. *Spectrochimica Acta* **1965**, *21*, 1795.

(59) *SHELXS*, Sheldrick, G. M. University of Göttingen, 1997.

(60) *SHELXL*, Sheldrick, G. M. University of Göttingen, 1997.

Chapter 5: Polymer supported bis(thiourea) ligand analogues

5.1 Introduction

5.1.1 The Monsanto and Cativa™ processes

The commercial production of acetic acid was transformed by the use of group 9 transition metal homogeneous catalysis. The development of rhodium catalysed carbonylation of methanol was undertaken in the 1960s and commercialised by Monsanto in 1970.[1] The active catalyst in the Monsanto process is the Rh(I) complex, $[Rh(CO)_2I_2]^-$, which undergoes oxidative addition by methyl iodide.[2] This process is highly selective and efficient, but does suffer several disadvantages. One such disadvantage is that the water used to regenerate the catalyst, HI, carbon monoxide and the active Rh(I) catalyst are involved in a side reaction that produces carbon dioxide and hydrogen gas rather than the desired product. Water is required for the regeneration of the $[Rh(CO)_2I_2]^-$ catalyst, and so water control is required. However, the side reaction greatly reduces the efficiency of the process. In the late 1970s research led by Forster et *al.* investigated replacing the rhodium catalyst with the analogous iridium complex to lower catalyst cost.[3] The research proposed a catalytic cycle that is fundamentally the same as the rhodium-based cycle but vastly more complicated with a neutral cycle and an anionic cycle. However, no commercialisation emerged from the research at Monsanto, as the reaction rate is inferior to the rhodium catalysed carbonylation. A research collaboration between Sheffield University and BP Chemicals Ltd resumed the research with promising results.[4] Mechanistic studies show that the rate of oxidative addition is greatly increased with the iridium system, but migratory insertion is very slow. From IR and *in situ* NMR spectroscopic studies, BP proposed that altering the ligand trans to the methyl moiety would lengthen the iridium-methyl bond length thus labilising it and facilitating migratory insertion.[4] This may be achieved by the addition of surplus methanol into the process, which acts to solvate the Ir complex *trans* to the methyl group, which enables easier insertion of a carbon monoxide molecule.

As a further advantage over the Monsanto process, a Ru(II) promoter complex is used.[5] A mixture of $IrCl_3.xH_2O$ and $RuCl_3.xH_2O$ is used in the preparation of the catalysts, and the promoter metal is believed to exist as both the iodide bridged dimer and triodide tricarbonyl complexes, $[\{Ru(CO)_3I_2\}_2]$ and $[Ru(CO)_3I_3]^-$, respectively. The purpose of this ruthenium promoter complex is to accelerate iodide transfer and remove any excess iodide ion in the reaction vessel, scheme 5.1.

$$[\{Ru(CO)_3I_2\}_2] \underset{-\,2I^-}{\overset{+\,2I^-}{\rightleftharpoons}} 2[Ru(CO)_3I_3]^-$$

Scheme 5.1: the regulation of iodide concentration by the $[\{Ru(CO)_3I_2\}_2]$ promoter complex.[5]

The ruthenium complex therefore reduces corrosion of the vessel by iodide, and more importantly helps to increase the rate as this is inversely proportional to the iodide concentration. The Cativa™ process therefore has several advantages over the Monsanto process. By using the iridium analogue, the stability of the catalyst is improved and no RhI_3 is produced, which has to be routinely removed from the reaction vessel. While the Rh(I) catalyst is more active, the overall rate of the process is greatly improved by using the iridium analogue. However, some of the catalyst is lost into the product stream along with corrosion metals, such as Fe, Cr and Ni, and it is advantageous to selectively remove these catalysts from the corrosion metals.

5.1.2 Solid-supported thiourea derivatives as metal extractors

Several examples of metal extraction form mixed metal solutions by solid-supported ligands have been given in Chapter 1.4. Thiol,[6] dithizone,[7] dithioacetal[8] and thioureido[9] functionalised solid supports have been studied for the extraction of mercury, which is of importance to the removal of toxic mercury salts from water samples. For example, 1-allyl-3-propylthiourea modified silica can be agitated with aqueous mercury nitrate solutions for 40 minutes at room temperature, and upon removal of the adsorbent, washed with de-ionised water to remove excess mercury solution. After a single treatment with the adsorbent, mercury concentration in the solution is lowered to below 0.1 ppm (from 900 ppm or a concentration of 4.5×10^{-3} M), and the maximum loading onto the adsorbent is 1.5 mmol Hg^{2+} per gram of

adsorbent. The mercury may be desorbed with a treatment of 10 % thiourea in aqueous 0.05 M HCl. This results in a 50 % regeneration of binding capacity under mild conditions.

Recent work on a commercially available thiourea resin, Lewatit™ TP214, has shown that it selectively removes Ir and Ru from an acetic acid process stream in preference to corrosion metals such as Fe, Cr and Ni.[10] Three resins with iminoacetate (TP207), aminophosphate (TP260) and thioureido (TP214) functionalities were tested in an acetic acid carbonylation process stream. The analysis of metal uptake of each resin after many hours of passing the solution through a fixed bed of the resin at 20 °C is shown in Table 5.1. TP214 adsorbs the most iridium and ruthenium in 80 hours, and displays greatest selectivity for the catalytic metals over the corrosion metals of Fe, Cr and Ni.

		Metal content of resin							
Resin	Hours on stream	Ir %	Ru %	Fe ppm	Cr ppm	Ni ppm	Mo ppm	Zn ppm	Li ppm
TP207	290	2.7	2.5	200	1200	<50	300	550	<25
TP260	80	0.8	0.5	3600	950	100	1000	1400	<25
TP214	80	6.8	5.1	50	50	<50	<50	100	<25

Table 5.1: metal content of three commercially available resins having been exposed to the acid acetic product stream.[10]

5.1.3 Analysis of multielement systems by PIXE

Proton-induced X-ray emission (PIXE) spectroscopy is a useful multi-element detection method.[11] The method involves bombarding an accelerated beam of protons into a sample containing heavy atoms. Collision of the incident beam with an atom may cause the removal of an inner-shell electron and expulsion of X-rays of energy characteristic of the element. The X-rays may be detected using an energy channel detector and thus the relative number of heavy atoms in a sample may be detected. The technique has been used in biological,[12] medical[13] and geological[14] applications for trace metal analysis.

The extraction and selectivity of metal ions from mixed metal solutions by solid-supported ligands has been investigated and the metal content analysed by PIXE

detection.[15] A carboxyhydrazide ligand immobilized on the surface of a silica gel, **5.1**, adsorbs large quantities of Hg(II), Co(II) and Cu(II) from single metal solutions of those metals, table 5.2.

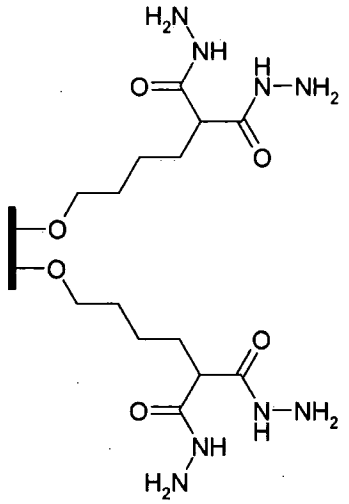

5.1

	Metal concentration (ppm)	
Metal	Single solution	Mixed metal solution
K	29,200	875
Ca	-	910
Cr	-	11,900
Fe	-	1,600
Co	82,400	450
Ni	25,900	660
Cu	58,800	19,900
Zn	26,400	470
Hg	102,600	170
U	27,800	3,640

Table 5.2: metal uptake of carboxyhydrazide silica gel from single and mixed metal solutions.[15]

However, Cu(II) and Cr(II) selectivity is observed from the mixed metal solution. A similar result is observed in the extraction of metals using benzamercaptathione clays, where Hg(II) is extracted well, except in the presence of Cu(II).[16]

5.2 Aims of research

The aim of the work in this chapter is to remove platinum group metals such as platinum, ruthenium, palladium and iridium, from mixed metal solutions that may also contain corrosion metals such as nickel, chromium and iron. To achieve this, polymer based resins will be developed that contain bis(thioureido) groups analogous to the ligands synthesised in Chapter 2.2.1. These resins will be tested for their metal uptake selectivity with both well-defined metal salt solutions, and acetic acid mixed metal solutions from the Cativa™ process product stream. The metal content of each resin will be found, in order to determine metal selectivity and uptake of the resin, and compare it to a commercially available thiourea resin, Lewatit™ TP214. The decomplexation of the incorporated metals will be investigated, so that catalytically useful metals may be recovered.

5.3 Results and discussion

5.3.1 Synthesis of thiourea functionalised 'Stratospheres'

Commercially available ethylenediamine (EDA) Stratospheres™ are easily functionalised to bisthioureas which are arranged analogously to the ethylene bridged ligand, MMTET discussed in the preceding chapters, scheme 5.2. The two carbon spacer also gives a similar spacer length to the phenylene ligands, MMTPhT and IITPhT.

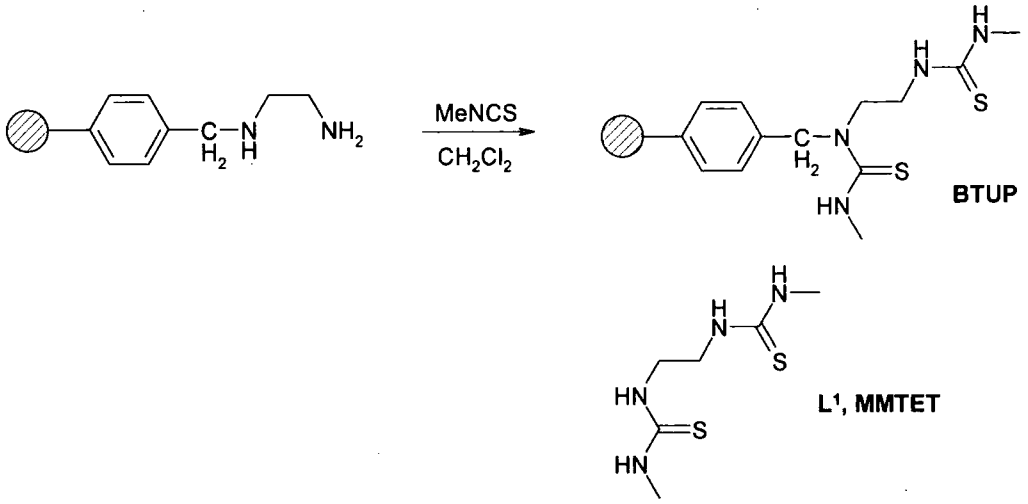

Scheme 5.2: Functionalisation of EDA StratoSpheres with methylisothiocyanate to form a bisthiourea resin analogous to the small molecule MMTET.

From the elemental analysis of the resulting bisthiourea polymer ligand, BTUP, the nitrogen to sulphur atom ratio of the resin is 2.02:1 and indicates over 98 % conversion. Dichloromethane was chosen as a solvent, as the original resin swells by the largest proportion in this solvent, and so penetration of the resin bead would be achieved fully.

5.3.2 Uptake of metal salts

The uptake of metal salts by the resin BTUP was tested in two ways:

a) with well defined metal salts, with which the coordination by bisthioureas is investigated in Chapter 4.2, and

b) using an acetic acid mixed metal solution obtained from the product stream of the Cativa™ process.

The form of the well-defined metal salts, the composition of each mixed metal solution and the solvent system used is given in Table 5.1.

Solution n°	Metal salts	Solvent
1	½ [{Ru(η^6-$C_6H_4MeCH(Me)_2$)Cl(μ-Cl)}$_2$]	MeOH
2	½ [{Ru(η^6-$C_6H_4MeCH(Me)_2$)Cl(μ-Cl)}$_2$], $Pt(MeCN)_2Cl_2$, $Pd(MeCN)_2Cl_2$	MeOH/MeCN (9:1)
3	$CrCl_3$, $FeCl_2$, $CoCl_2$, $NiCl_2$, $CuCl_2$, $ZnCl_2$	MeOH
4	½ [{Ru(η^6-$C_6H_4MeCH(Me)_2$)Cl(μ-Cl)}$_2$], $Pt(MeCN)_2Cl_2$, $Pt(MeCN)_2Cl_2$, $NiCl_2$, $CuCl_2$, $FeCl_2$	MeOH/MeCN (9:1)
5	½ [{Ru(η^6-$C_6H_4MeCH(Me)_2$)Cl(μ-Cl)}$_2$], $Pt(MeCN)_2Cl_2$ $FeCl_2$, $CrCl_3$, $NiCl_2$	MeOH

Table 5.3: Metal salts and solvents used in controlled laboratory metal extraction experiments.

The resin BTUP was compared to the commercially available thiourea resin, Lewatit™ TP214, with a mixed metal acetic acid solution form the Cativa™ process stream. This solution contains the Ir and Ru catalysts, as well as corrosion metals such as Fe, Cr and Ni, which are in a large excess of the catalytic metals, Table 5.4. The two resins were stirred at room temperature in 5 ml of the acetic acid mix for periods of two, four, eight and twenty-four hours. Both resins were analysed for their metal uptake selectivity and to observe any differences in uptake efficiency over the twenty-four hour time period.

Metal	Ru	Ir	Ni	Fe	Cr	Mo
Approx conc. (ppm)	250	50	320	1140	340	80

Table 5.4: approximate concentrations in the acetic acid solution product stream.[17]

5.3.3 PIXE and ICP results

The extent to which metals were taken up by the resins was analysed using both ion beam analysis with a PIXE detector in collaboration with Dr. Richard

Thompson of Durham University, and ICP-MS obtained by Mr. Steve Lancaster of BP Chemicals Ltd. The data from the PIXE detector can be obtained quickly, with many elements within the sample detected simultaneously. While the ratio between elements detected is accurate,[11] it is clear from early results that the overall elemental percentage content obtained is not. For example, an incorporation of 84 % Ru of the BTUP resin is found from the uptake of solution **1**. Given the aryl ligand coordinated to the Ru(II) initially and the organic matrix of the resin, this is an unlikely Ru incorporation. Therefore the PIXE data was used to obtain the ratio of metal adsorbed, and ICP-MS was used to analyse the absolute metal content of one of the metals present in the resin. From this absolute value, the percentage content of the other metals may be calculated from the ratios found by the PIXE detection.

A typical fit (pink) for the data (blue) obtained from the PIXE detector is given in figure 5.1.

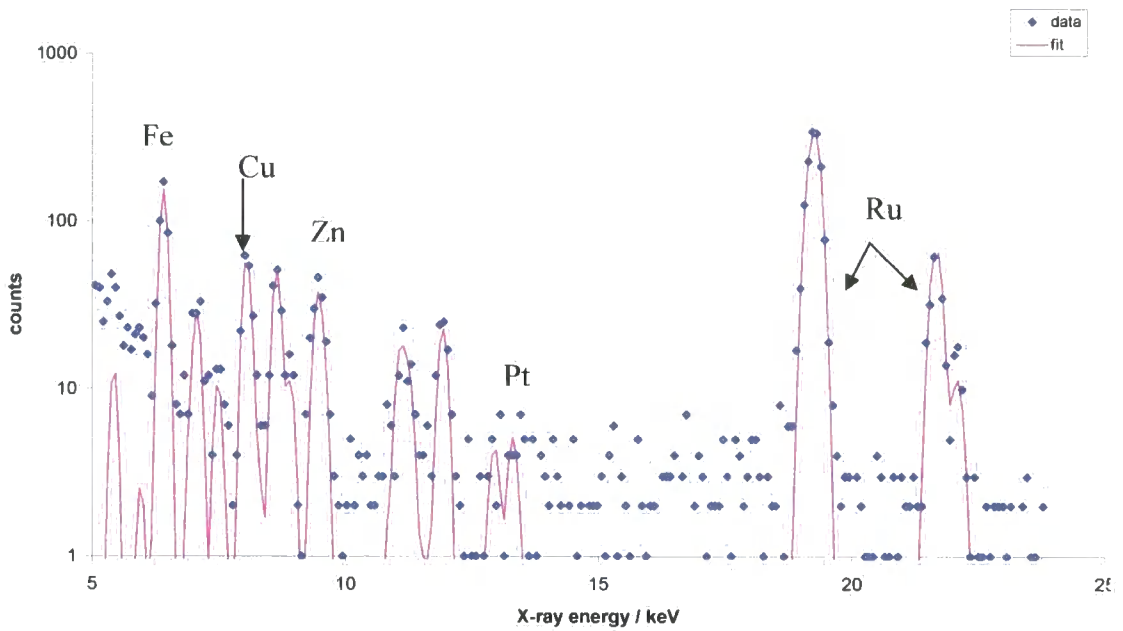

Figure 5.1: Typical data from the PIXE detector and the fit for the sample exposed to solution 1. Trace amounts of Fe, Cu and Zn are detected.

The energy profile arising from the detection is shown in blue, and the energies are quantified and fitted to each of the elements. As the energy of the emitted X-ray is characteristic of the element from which it was emitted, the fitting of peaks to energy bands may be done, and assignment of some elements can be seen. The counts in the region of 14-18 keV are not characteristic of any heavy elements, but are background generated by Bremsstrahlung from the organic matrix.[11]

5.3.3.1 Well-defined metal salt uptake

For the well-defined metal salt uptake experiments (samples listed in Table 5.3), a graph of the metal uptake given in mmol/g of polymer from the ICP-MS and PIXE results is shown in figure 5.2. The PIXE data for solutions **1-4** have been normalised using the ruthenium uptake ICP result for solution **1**, so that for all the PIXE data may be expressed in mmol/g of polymer. This allows the PIXE data to be compared from solution to solution, and also comparison of the normalized PIXE results to absolute metal content results from ICP-MS may be performed. There is good correlation between the ICP and normalised PIXE results.

While uptake of Ru from a methanol solution of $[\{Ru(\eta^6\text{-}C_6H_4MeCH(Me)_2)Cl(\mu\text{-}Cl)\}_2]$ with 2 hours of reflux (solution **1**) is good, attaining an incorporation of 0.56 mmol/g, Table 5.5, the results for the solution containing Ru, Pt and Pd are a little more surprising, as no uptake of any metal is observed (solution **2**).

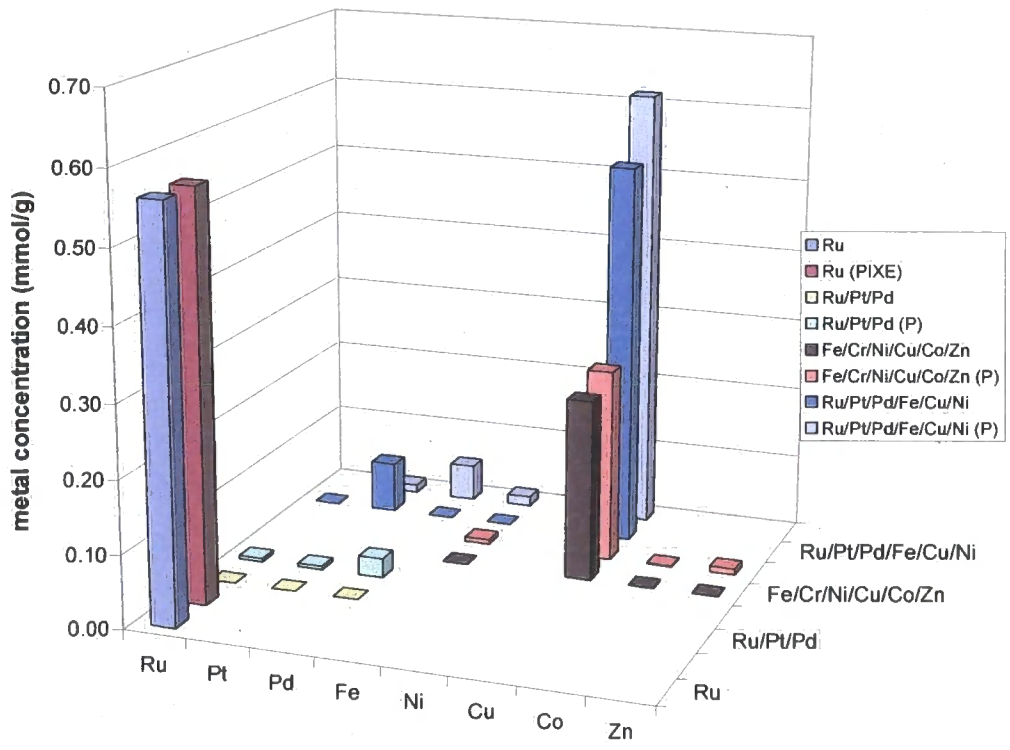

Figure 5.2: metal uptake by BTUP from solutions of Ru (solution 1), Ru, Pt and Pd (solution 2), Fe, Cr, Ni, Cu, Cu and Zn (solution 3) and Ru, Pt, Pd, Fe, Cu, Ni (solution 4). Each solution has two sets of data: the first the results from ICP-MS and the second results from the normalised PIXE data.

The uptake of metals for this polymer is thus apparently solvent dependent, as a small amount of acetonitrile was added to solution **2**, in order to solubilise and stabilise the Pd, and this coordinating solvent must be successfully competing with the heterogeneous uptake of the metals. Without acetonitrile solvent palladium black is generated, even when all solvents have been degassed. Solution **3** contains an equimolar mixture of first row transition metals, and it is clear that there is excellent selectivity for Cu(II) over other metals such as Fe(II), Cr(III) or Ni(II) fig. 5.2. This is not surprising as Cu(II) is the softest metal present in this solution,[18] and thus most complimentary to the soft sulphur donor in the thioureido resin. More surprisingly is the large uptake of Cu(II) from the solution containing Ru(II), Pt(II) and Pd(II) as well as Fe(II) and Ni(II), solution **4**. Some acetonitrile was added to stabilise the palladium, which appears to have had a similar effect on the PGM adsorption, as observed in solution **2**.

		Metal content (mmol/g)							
Solution	**Detection**	**Ru**	**Pt**	**Pd**	**Fe**	**Ni & Cr**	**Cu**	**Co**	**Zn**
Ru **(1)**	ICP	0.56	-	-	-	-	-	-	-
Ru **(1)**	Normalised PIXE	0.56	-	-	-	-	-	-	-
Ru/Pt/Pd **(2)**	ICP	0.00	0.00	0.00	-	-	-	-	-
Ru/Pt/Pd **(2)**	Normalised PIXE	0.005	0.005	0.027	-	-	-	-	-
Fe/Ni/Cr/ Cu/Co/Zn **(3)**	ICP	-	-	-	0.000	0.000	0.250	0.000	0.000
Fe/Ni/Cr/ Cu/Co/Zn **(3)**	Normalised PIXE	-	-	-	0.006	0.000	0.267	0.001	0.008
Ru/Pt/Pd/ Fe/Cu/Ni **(4)**	ICP	0.000	0.070	0.000	0.000	-	0.530	-	-
Ru/Pt/Pd/ Fe/Cu/Ni **(4)**	Normalised PIXE	-	0.011	0.050	0.013	-	0.613	-	-

Table 5.5: ICP and normalised PIXE results for the extraction of well-defined metal salts from methanol solutions.

In contrast, the acetonitrile does not appear to have suppressed Cu(II) uptake. The copper uptake from this mixed metal solution is 0.53 mmol/g, as found by ICP-MS, which is a similar metal incorporation as exhibited by Ru in solution **1**. Crystal structures obtained in Chapter 4.3.1 and 4.3.4 for bisthiourea ligands coordinated to Ru(II) and Cu(I), respectively, may aid in the understanding of the copper preference of the resin. The Cu-S distances in the crystal structures obtained are in the region of 0.2 Å shorter than the Ru-S distances found in the Ru crystal structures, with typical values of 2.22 Å and 2.42 Å for Cu-S and Ru-S distances, respectively. As discussed in Chapter 4.3.4, without accurate data for the ionic radii of three coordinate Cu(I) or six coordinate Ru(II), it is difficult to predict whether these shorter distances are indicative of stronger binding of the Cu, and thus explain the selectivity for Cu over Ru by the polymer resin. The strain exhibited in the Ru bisthiourea half-sandwich complexes may be indicative of the disfavoured coordination of the Ru salts by the polymer. The adjoining four and seven membered metallacycles observed by complexes **4.11-4.13** show a relatively strained system with the three ligand coordinating atoms arranged facially in the octahedral coordination of the Ru(II). In contrast, the t-TUP structures with Cu(I) show no strain in the trigonal planar coordination. While the t-TUP ligand is not a chelating ligand, the strain in the Ru(II) structures may explain some of the selectivity for copper over ruthenium by the polymer resin.

To overcome the inhibition of the PGM uptake ability of BTUP by Cu(II) and MeCN, the uptake of metals from a methanol solution of Ru(II), Pt(II), Fe(II), Cr(III) and Ni(II) was determined (solution **5**). The PIXE data shows that the BTUP resin under refluxing conditions for 2 hours displays a good selectivity for Pt(II) over the other metals, with small amounts of Ru(II) and Fe(II) uptake. This is confirmed by ICP measurements 0.184 % uptake is obtained for Pt compared to 0.019 % Ru. From the ICP-MS value obtained for Pt it is possible to normalize the other PIXE results in the resin sample and hence determine the selectivity for Pt over Fe, Ru, Ni and Cr, fig. 5.3. The percentage for Pt obtained by ICP-MS equates to a loading of 0.0094 mmol/g, which is significantly lower than the ruthenium or copper uptake observed in the other experiments with well-defined metal salts.

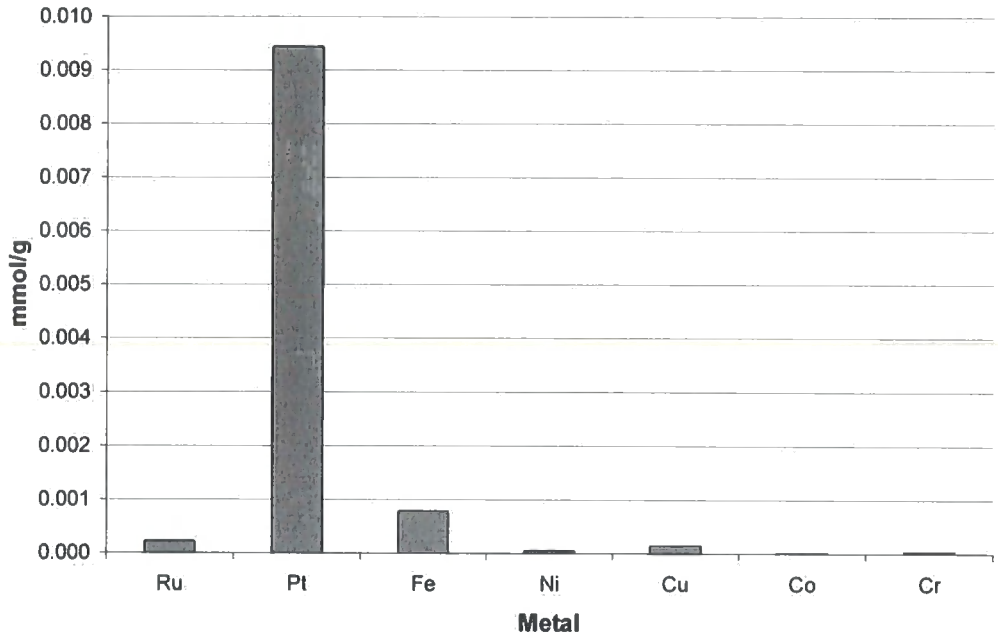

Figure 5.3: Metal uptake from a mixed metal methanol solution, in the absence of Cu(II) or MeCN showing pronounced Pt(II) selectivity.

Depth profiling of the beads with the ion beam accelerator performed by Dr. Richard Thompson shows metal concentration relative to depth within the resin. The depth profile of the BTUP resin that selectively extracted Pt from a mixed metal solution (solution **5**), figure 5.4, suggests that Pt penetration into the resin is localized at the surface. In contrast, the depth profile for the ruthenium loaded BTUP and Lewatit™ resins show a metal concentration that is observed homogenously through the resin, figure 5.5. It is estimated that for most organic materials with a density of about 1 g cm^{-3}, 1×10^{15} atoms cm^{-2} is within a few percent of being equal to a depth penetration of 1 Å.[19] On this basis, the Pt appears to be preferentially located in the first 2 μm of the bead surface. If only the surface coordination sites were accessed for solution **5**, then lower loading would be expected, as observed for the sample where platinum was selectively adsorbed. However, the metal selectivity would not be affected by the number of available sites, so the Pt selectivity of the resin under these conditions seems reliable.

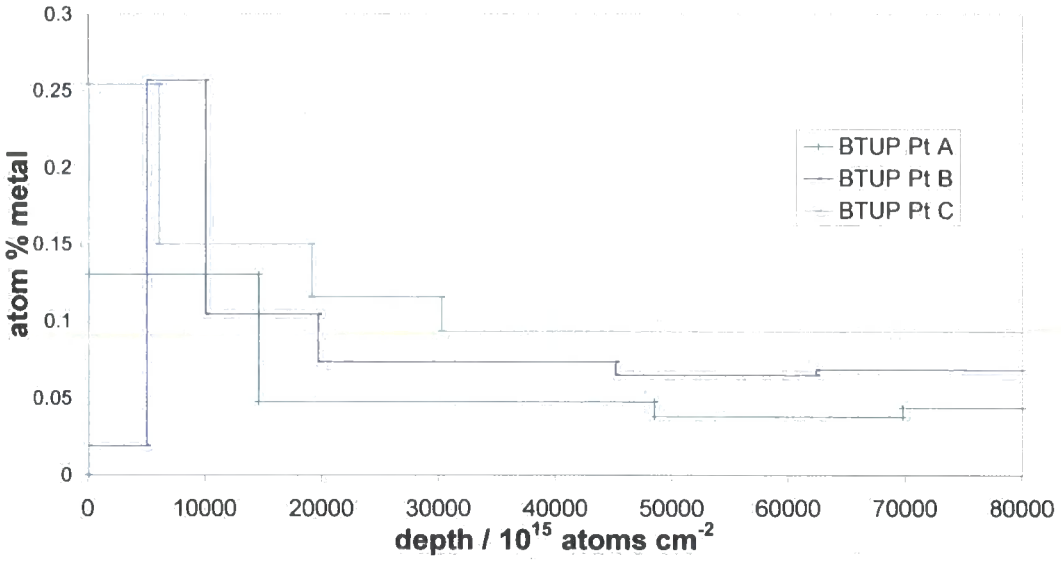

Figure 5.4: depth profile of the metals in unground BTUP resin beads that selectively extracted Pt form a mixed metal solution (5) showing large surface concentration.

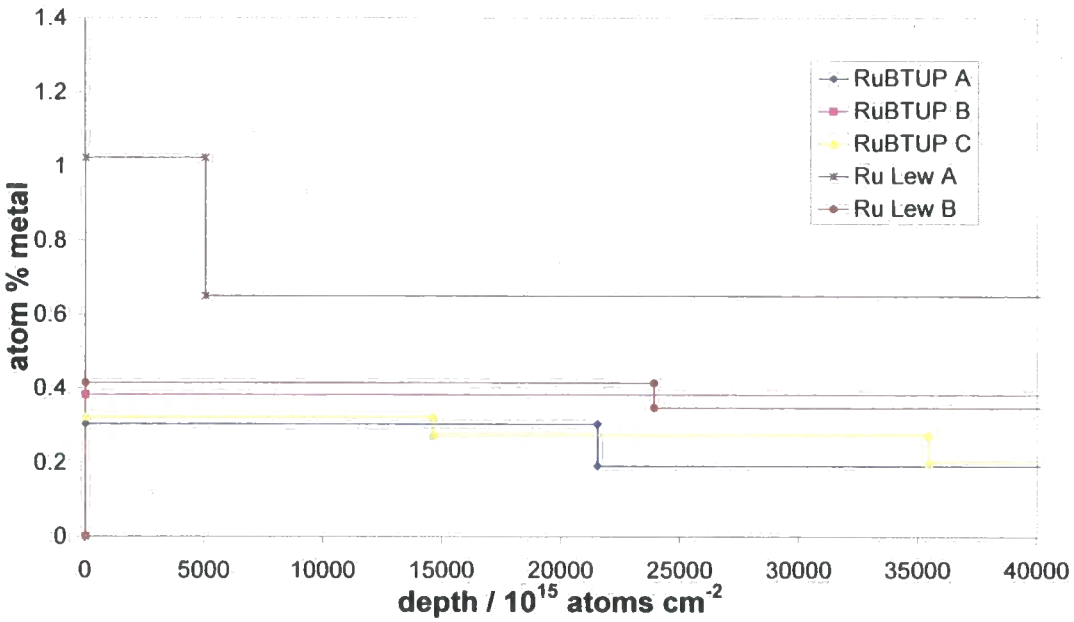

Figure 5.5: depth profile of the ruthenium metal in unground BTUP and Lewatit™ resin beads that are loaded with Ru.

The IR spectra of two samples exposed to solutions **1** and **5** that show Ru(II) loading and Pt(II) selective uptake, respectively, unfortunately show little difference to the parent resin, BTUP. It is likely that the uncoordinated sites are more prevalent and thus bands corresponding to the coordinated species are not very intense. However, the IR spectrum of the Ru(II) loaded sample used for decomplexation

studies (section 5.3.4), which has a higher loading of Ru(II), show significant changes from the IR spectrum of BTUP. The NH bending band at 1552 cm^{-1} is split into two new bands at 1534 and 1562 cm^{-1}. In addition the C=S stretch at 1099 cm^{-1} has shifted to 1087 cm^{-1} and a new C=S peak at 1029 cm^{-1} is observed in addition to the peak at 1045 cm^{-1}, fig. 5.6.

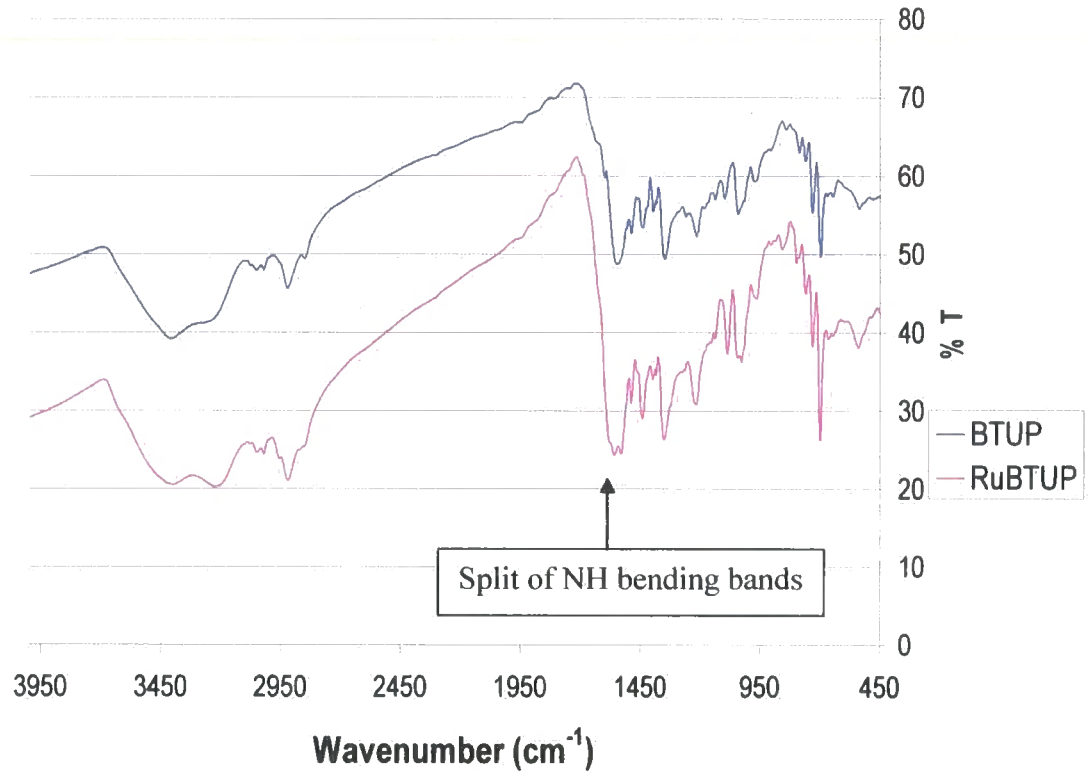

Figure 5.6: IR spectra of BTUP resin and RuBTUP showing splitting of NH bending bands.

These spectral changes are also observed in the discrete thioureido complexes described in Chapter 4.3, and a comparison of the adsorption bands in the small molecule analogues and the resin is given in Table 5.6. In the small molecule analogues containing the MMTET ligand, the IR spectra change from two N-H bending bands at 1557 and 1524 cm^{-1} to a strong band at 1588 cm^{-1} and a far weaker band at 1508 cm^{-1} upon complexation to ruthenium, **4.13** (with NH deprotonation, Chapter 4.3.1). A similar observation is found for the MMTET complex with palladium with a strong band at 1588 cm^{-1} and a medium band at 1518 cm^{-1} assignable to NH bending. The bands observed at 1562 and 1534 cm^{-1} in the Ru loaded BTUP are likely to be a combination of the complexed and uncomplexed thioureido groups. For the small molecule analogues, bands assigned to the C=S

stretch of the uncoordinated ligand at 1224 and 1064 cm^{-1} dominate with a medium band at 1184 cm^{-1} and a weak band at 1136 cm^{-1}. Upon complexation, small shifts in the C=S stretches of the IR spectrum are observed, with medium bands at 1233 and 1060 cm^{-1} and weak bands at 1185 and 1130 cm^{-1}. The bands at 1045 and 1029 cm^{-1} in the Ru loaded BTUP IR spectrum are again indicative of a mixed coordinated/uncoordinated state within the bulk resin.

	Adsorption bands of compounds in wavenumbers (cm^{-1})			
Assignment	**MMTET**	**4.13**	**BTUP**	**RuBTUP**
NH bend	1557	1588	1552	1562
	1524	1507		1534
C=S stretch	1224	1233	1099	1087
	1136	1130	1045	1045
	1064	1060		1029

Table 5.6: comparison of adsorption bands in the IR spectroscopy of the ligands and their ruthenium complexes.

5.3.3.2 Uptake of metals from acetic acid solution

The two resins, BTUP and the commercially available thiourea functionalised resin Lewatit™ TP214, were exposed to the acetic acid mixed metal solution containing Ir, Ru, Fe, Cr and Ni. Four sets of 100 mg samples of each resin and 5 ml of the acetic acid were stirred for two, four, eight and twenty-four hours. After each allotted time, resin samples were removed from the solution by filtration and washed with dichloromethane and acetone, to remove excess acetic acid solution. The samples were air-dried, ground and pressed into discs for PIXE analysis.

The results obtained by Dr. Richard Thompson of the PIXE analysis for the Lewatit™ TP214 resin are shown in figure 5.3. The Lewatit™ samples show a consistent trend in uptake as the experiment proceeds, with a general increase Ir and Ru concentration with time, while Fe and Ni concentrations decrease over time. Given the selective incorporation of Ir and Ru observed on the product stream for 80 hours by Lewatit™ TP214 resin,[10] this data may give an insight into the metal uptake mechanism of Lewatit™ TP214. The trend may be indicative of the resin coordination

sites being occupied and over time, there is exchange between the adsorbed corrosion metals and Ir and Ru catalysts so that the catalyst metals become more prevalent in the resin after longer exposure. Interestingly, the Cr concentration remains the same over time. It should be noted that the experiments were performed as closed systems, i.e. a single unrefreshed solution was used over the time period. As there is only a finite amount of each metal in the reaction solution, the uptake of the metals will reduce the concentration of that metal.

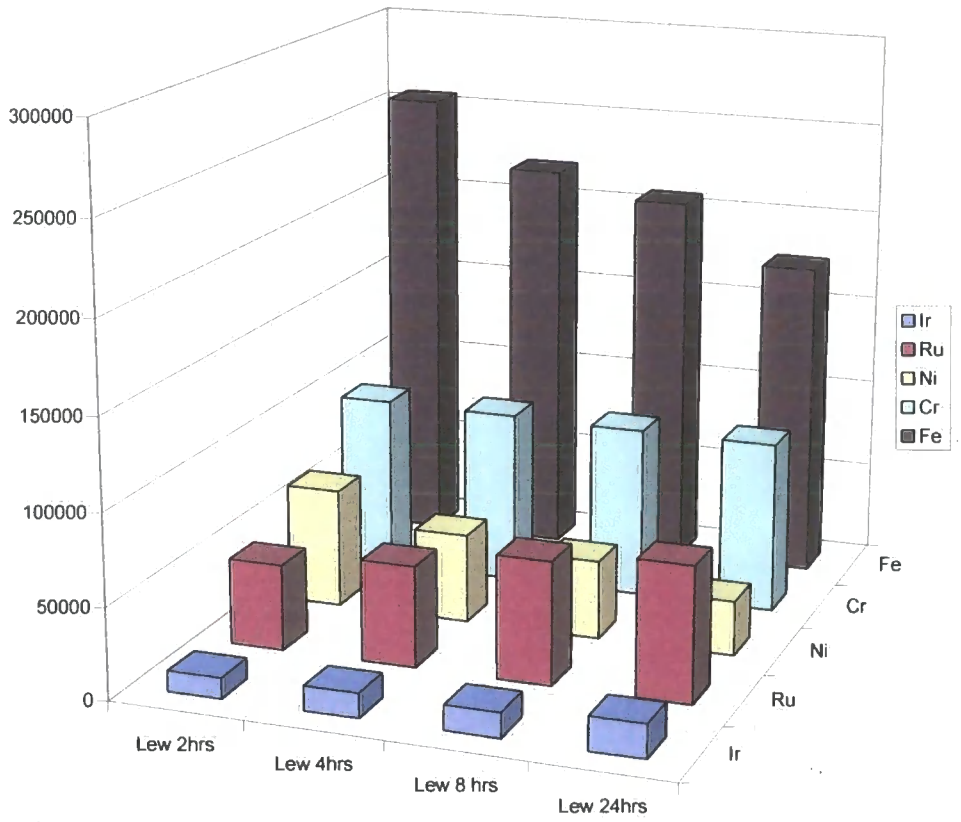

Figure 5.7: PIXE data for the metal uptake (ppm) by Lewatit™ TP214 (Lew) from the mixed metal acetic acid solution over 2, 4, 8 and 24 hours.

From the Ru percentage obtained by ICP-MS from each sample, the percentage content by mass of the other metals detected by the PIXE may be found by normalizing the PIXE data relative to the Ru data. This is repeated for each sample. Within each sample the metal ratios are accurate, and so normalization within each sample allows more accurate comparison from sample to sample. The Ru percentage incorporated into Lewatit™ TP214 found by ICP-MS is consistent with the trend of increasing ruthenium incorporation found by the PIXE detection. Values of 0.354,

0.401, 0.675 and 1.080 % Ru are found for the resin after exposure to the acetic acid mixed metal solution for two, four, eight and twenty-four hours, respectively.

The normalised graph showing mmol of each metal incorporated per gram of Lewatit™ TP214 resin is given in figure 5.8, and suggests that not all coordination sites are occupied initially as the levels of metal incorporated over time increases for most of the detected metals across the range increases.

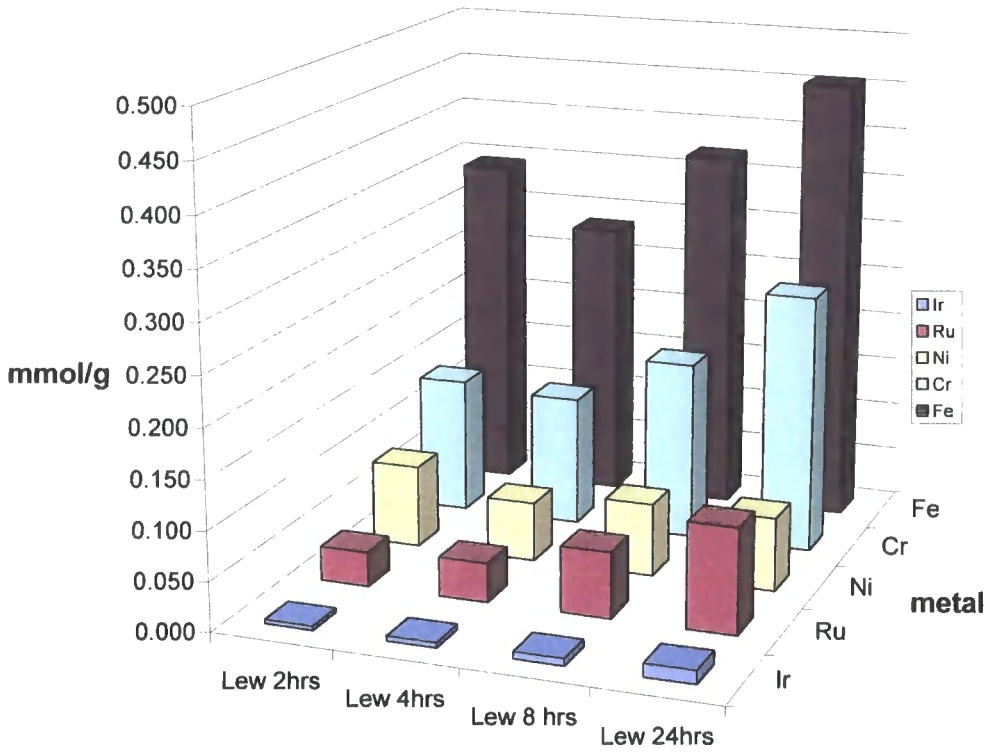

Figure 5.8: PIXE results for Lewatit™ TP214 exposed to the acetic acid mixed metal solution for two, four, eight and twenty-four hours.

While the great selectivity for Ir and Ru exhibited by Lewatit™ TP214 from the patent data[10] is not exhibited in these tests, the PIXE data in figure 5.7, does show that the rate at which Ir and Ru are being adsorbed is faster than the rate at which Fe and Ni are incorporated. The faster rate itself could not explain the large Ru and Ir incorporation observed from Lewatit™ TP214 after 80 hours on the product stream. Therefore there may be some metal exchange experienced in the later stages when all the coordination sites are occupied, or the constant stream of fresh solution of the product stream may have an effect on the selectivity of the resin.

The IR spectra of the resins after metal exposure confirm binding of metal species. The uncoordinated resin has strong but quite broad absorbance bands at 1614, 1543 and 1116 cm^{-1} assignable to two N-H bends and a C=S stretch, respectively. With longer exposure times, these bands do not change significantly, except that the intensity of the C=S stretch at 1115 cm^{-1} reduces with respect to the N-H bending bands.

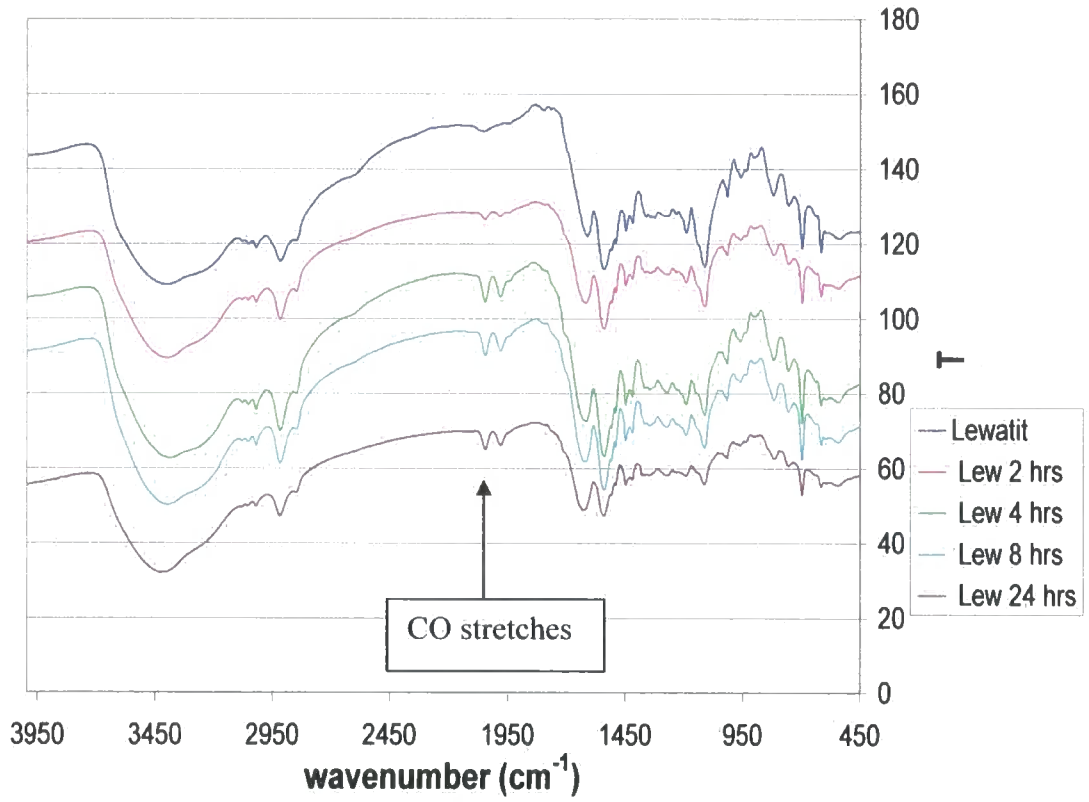

Figure 5.9: IR spectra of Lewatit™ TP214 resin before and after exposure to the acetic acid mixed metal solution for two, four, eight and twenty-four hours, showing the emergence of carbonyl stretches at 2050 and 1987 cm^{-1}. Note that the spectra have been spread out for clarity so that the transmission axis no longer represents absolute % T.

The emergence of bands at 2050 and 1987 cm^{-1} that sharpen and increase in intensity is observed with longer exposure times, fig 5.9, and these bands are similar to bands at 2045 and 1980 cm^{-1} assigned as carbonyl CO stretches observed in the complex of $[Ru(CO)_2I_4]^{2-}$.[20] The Ir and Ru catalytic species present in solution are thought to be in the form of carbonyl iodide complexes, and so the appearance of the carbonyl bands is good confirmation that the catalysts are being incorporated into the Lewatit™ TP214

resin. It is however possible that the corrosion metal salts exist with carbonyl ligands as well.

The PIXE data for BTUP displays more erratic uptake of metals from the acetic acid mixed metal solution than for Lewatit™ TP214, fig 5.6. The data at two hours suggests that BTUP is more selective for Ir over Ru and Ni, while levels of Cr and Fe are comparable to the levels observed in the PIXE data for Lewatit™ TP214, fig 5.5.

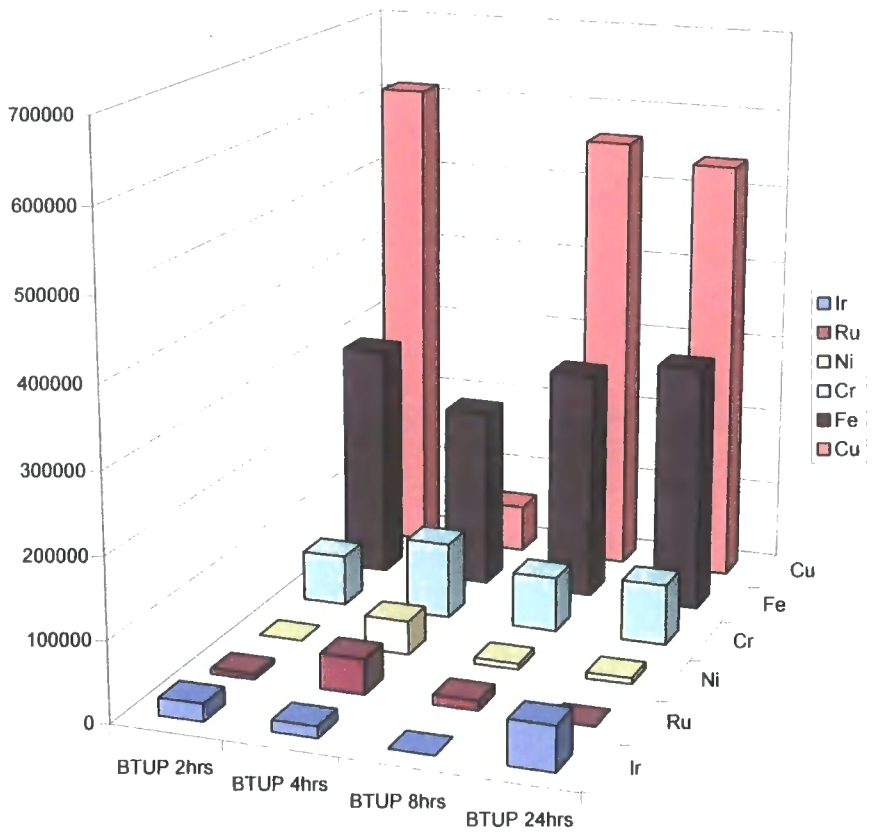

Figure 5.10: nominal ppm values for the metal uptake by BTUP from the mixed metal acetic acid solution over 2, 4, 8 and 24 hours.

However, the level of Ir incorporation decreases from two hours to four hours, and at eight hours is non-existent. This would be consistent with a metal exchange mechanism. Further anomalies are observed for Ru, with maximum incorporation at four hours. Interestingly, a large amount of copper incorporation (which is not found in the Lewatit™ TP214 samples) is found at two, eight and twenty-four hours. It was not thought that significant levels of copper were present in the acetic acid solution,

but BTUP has successfully extracted copper from the solution. The apparent erratic uptake of the metal may be due to many reasons:

1) Swelling of samples has effect on metal uptake.
2) This sample may be atypical of the BTUP metal uptake.
3) Insufficient grinding of the sample may produce inhomogeniety within the sample and thus varying levels of metal may be detected that is not consistent with the bulk sample.
4) As observed with MeCN in the well-defined salts, the solvent may suppress metal uptake.
5) The uptake of copper may be inhibiting the levels of PGM uptake.

The ICP-MS is consistent with the PIXE data for the uptake of Ru by BTUP. Low and inconsistent Ru incorporation is shown with Ru concentration found to be 0.003, 0.008, 0.003 and 0.008 % for two, four, eight and twenty-four hours, respectively. This uptake is significantly lower than that of Lewatit™ TP214. The experiments were performed in triplicate and the PIXE analysis of the other samples exposed to the acetic acid mixed metal solution confirms the low Ru and Ir uptake of BTUP.

The IR spectra of these resins show some changes, in particular in the region of the N-H bend. In BTUP, there is a strong broad band at 1552 cm^{-1} and a weaker band at 1602 cm^{-1}. The resin that had been exposed to the acetic acid mixed metal solution for two hours showed both these absorbance bands, as well as a new peak at 1636 cm^{-1}. For the resins exposed to the acetic acid solution for four and eight hours this band becomes slightly weaker and exhibits a minor shift to 1632 cm^{-1}. The sample that had been exposed to the acetic acid solution for twenty-four hours, exhibits the band at 1636 cm^{-1} again, and at a greater intensity than the band at 1602 cm^{-1}. There was little change in the position of the C=S stretch at 1044 cm^{-1}, however, the intensity of the band reduced relative to the N-H bending band at 1551 cm^{-1}. No carbonyl stretches are observed in the region of 2050 and 1980 cm^{-1}, probably due to the low incorporation of metal into the resin.

Based on the experiments with well-defined metal salts, the low Ir and Ru uptake by BTUP from the acetic acid mixed metal solution is most likely attributable

to the high copper incorporation, which suppresses the uptake of platinum group metals. It is puzzling that BTUP extracts copper so selectively, and yet there is no copper extraction exhibited by Lewatit™ TP214, which is similarly functionalised with thiourea moieties.

5.3.4 Decomplexation of RuBTUP

Small-scale initial tests were performed on 10 mg samples of BTUP resin loaded with ruthenium (RuBTUP) to ascertain solvent systems and additives that may decomplex the ruthenium from the polymer. The solvent systems used were DMSO, $CHCl_3$/MeOH, THF and H_2O. A small amount of leaching was observed with DMSO over several weeks, however no other significant leaching of the metal was observed due to solvents alone. Therefore, additives to aid decomplexation were used: NaSCN, thiourea, PPh_3, dppe, NH_3, EDA and HNO_3. It was found that thiourea had the most obvious leaching effect, while not discolouring the resin beads, which was observed with the other additives, and thus thiourea tested on a larger scale. For these larger scale experiments 100 mg samples of RuBTUP were stirred in 10 ml solutions of:

1. Concentrated (70 %) HNO_3
2. $CHCl_3$/MeOH (1:1 v/v) with 100 mg of thiourea
3. DMSO with 100 mg of thiourea

Qualitatively evaluating the leaching of ruthenium into the solutions a few observations can be made. The leaching into the nitric acid solution and also the chloroform/methanol solution was fast compared to the leaching into the DMSO solution, which required heating to observe significant leaching. This is likely to be a swelling issue, as demonstrated by the thiourea solutions. The chloroform/methanol solution swells the resin more efficiently than DMSO and so the coordination sites may be accessed more quickly, facilitating decomplexation. In DMSO, swelling is slow and so decomplexation is slow.

It was also observed from the colour of the filtered resin beads that most of the orange colour, characteristic of ruthenium (II) complexes, had been lost from the concentrated HNO_3 treated beads, some colour was lost to the DMSO solution of thiourea and the least decolouration occurred in the case of the chloroform/methanol

solution of thiourea. Again comparing the two thiourea solutions, it appears that when swelling is achieved in the DMSO solution, more effective decomplexation occurs than in the chloroform/methanol solution. This may be a complementary effect between the thiourea and DMSO (known to coordinate Ru^{21}), which is not, or to a lesser extent, present in the chloroform/methanol solution. Although the heating of the DMSO solution may have promoted the decomplexation, the greater decomplexation over longer periods of time by the DMSO solution than the chloroform/methanol solutions was also observed in the small-scale reactions, which were performed at room temperature.

These observations are confirmed by the reduction in Ru content from the beads, as observed by ICP-MS (obtained by Mr. Steve Lancaster of BP Chemicals Ltd), fig. 5.11.

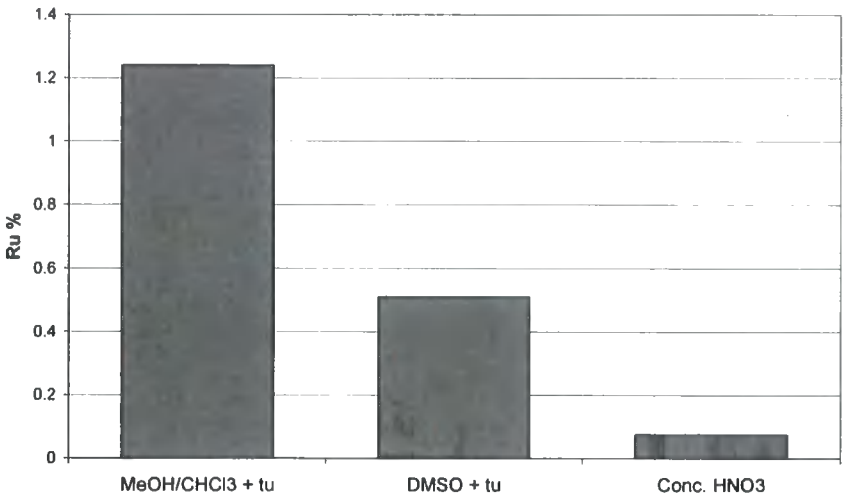

Figure 5.11: Ru content (%) of resin beads having been exposed to decomplexation solutions (tu = thiourea).

From the initial ruthenium loading, it can be seen that the decomplexation is consistent with the qualitative observations. MeOH/$CHCl_3$ with thiourea reduces the Ru % to 1.239 %, whereas a greater extent of decomplexation is observed from the heated DMSO solution of thiourea, 0.509 %. The greatest degree of decomplexation was found with concentrated nitric acid, where a reduction to 0.075 % Ru is found after just two hours at room temperature in the solution. Complete desorption might be achieved by a longer exposure of the resin to the nitric acid. The large degree of decomplexation observed with nitric acid solution may be due to good swelling

characteristics and possible protonation of the thioureido NH groups, disfavouring cation coordination and promoting ligand exchange.

5.3.5 ESEM results

To investigate the morphology of the resin, and observe any adverse effects on the morphology as a result of reactions on the resin, environmental scanning electron microscopy (ESEM) was performed on four of the samples. These samples were: the commercial ethylenediamine StratoSphere resin (EDAP), the resin functionalised with bisthiourea groups (BTUP), BTUP loaded with ruthenium(II) (RuBTUP) and RuBTUP partially stripped of some ruthenium (deRuBTUP). It was observed that the morphology of the resin was preserved through every reaction step, and consisted of beads in the range of 150 – 300 μm in diameter as shown in the example of RuBTUP, fig 5.10a. The bead shown has been cracked open so that the internal morphology may be seen, which consists of a few large pores and channels that facilitate solvent penetration into the bulk of the resin. This solvent swelling allows access to the entire resin. Interestingly, zooming in on one of the pores (fig 5.12b), light spots can be seen. Lighter areas in ESEM represent material that conduct electrons better than its surrounding areas, and these spots are not observed for the polymer resin prior to loading with ruthenium. Therefore it is possible that these areas relate to grouping of polymer bound ruthenium. The average diameter of the bright spots may be estimated in the region of 0.5 μm. While the overall morphology of the resins is preserved throughout the reactive steps, it is observed that the overall average size of the resins increase on functionalisation and again on Ru loading, with a slight contraction in size with partial decomplexation. These observations are summarised in Table 5.7. It was also observed that decomplexation did not affect the morphology of the resin beads.

a)

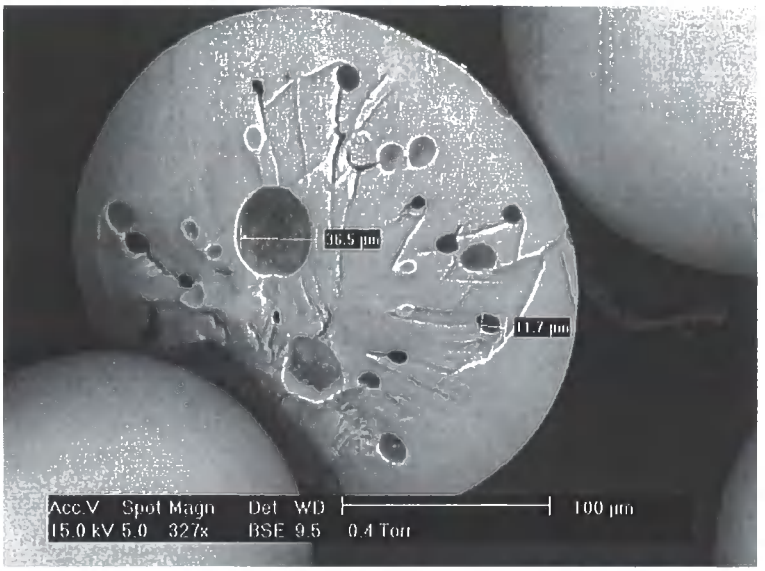

b)

Figure 5.12: ESEM images of the Ru(II) loading BTUP resin showing morphology and b) areas of high conductance by the electrons, possibly indicating density of Ru(II).

Polymer	Min. bead size (µm)	Max . bead size (µm)
EDAP	150	220
BTUP	180	250
RuBTUP	200	300
deRuBTUP	190	280

Table 5.7: minimum and maximum bead sizes (µm) for the ethylenediamine polymer (EDAP), bisthiourea polymer (BTUP), the ruthenium loaded bisthiourea polymer (RuBTUP) and partially decomplexed RuBTUP (deRuBTUP).

5.3.6 PolyHIPE functionalisation

Polymers formed from high internal phase emulsions (PolyHIPEs) are macroporous with extremely high surface area.[22] There have been many uses of polyHIPEs since their first synthesis, and recently a ruthenium carbene initiator has been loaded onto polyHIPE samples.[23]

In an attempt to produce a robust thioureido functionalised polymer support, a polyHIPE material was synthesised based upon vinylbenzylchloride (VBC), which may be further functionalised, cross-linked with divinylbenzene (DVB) in a 1:1 VBC/DVB ratio. Emulsifying aqueous solution of a surfactant, sodium monooleate (Span80),[24] in an oil of the DVB and VBC monomers leads to the production of the HIPE. The emulsion is cured at 60 °C over 3 days to polymerise the monomers and simultaneously evaporate the water in the sample to leave large pores. The resulting monolith was analysed for Cl content, and from the 9.55 % Cl found in the sample, a loading of 2.7 mmol/g is calculated. This compares well with the reported literature loading.[24] However, the ESEM of the product shows that the morphology does not compare well with the macroporous structures, with well-defined pores with diameters in the region of 5 μm, reported in the literature, fig 5.7.[24] It was found that the pore size and morphology of polyHIPEs is dependent upon many factors.[25] It is likely that the initial emulsion may have been stirred too vigorously as the stirring speed was difficult to determine. Fast stirring speed would disrupt the emulsion into smaller droplets and thus create smaller pore sizes.

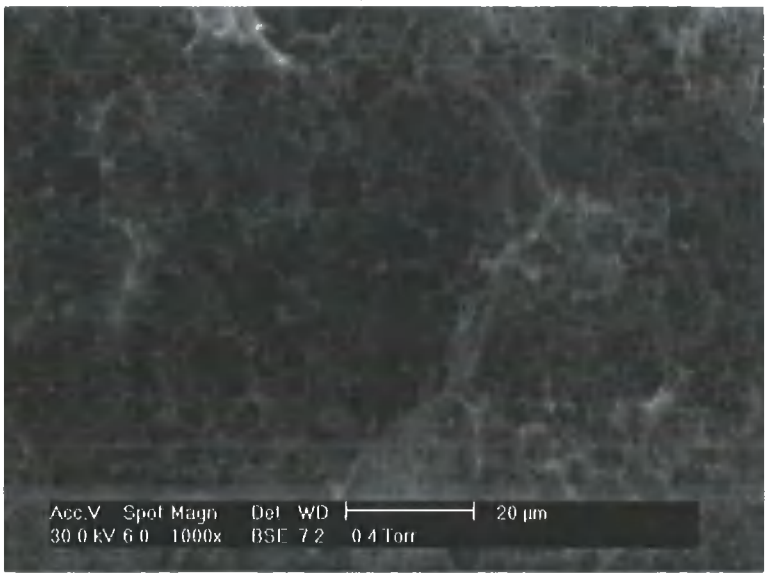

Figure 5.13: ESEM image of DVB/VBC polyHIPE prepared.

Initial attempts were made to functionalise the polyHIPE with melamine to recreate a solid-supported bis(thioureido) ligand akin to MMTPyT, scheme 5.3. However, all attempts were unsuccessful as it is thought melamine is not nucleophilic enough to functionalise the benzyl chloride functional group.

Following a reaction of tri(ethyl)amine (tren) with a DVB/VBC polyHIPE by Cameron and co workers,[24] the reaction of tren with the polyHIPE samples synthesised was attempted. However from the nitrogen and chloride analysis (expected N ~10 %; found N 3.52, Cl 1.27 %), it appears that the tren is cross-linking with other benzyl chloride groups. This may be due to the irregular and small pore sizes observed in the ESEM in the morphology of the structure, fig. 5.11, so that reactive groups are arranged in close proximity, and thus cross-linking is favoured. This might be tackled by reacting tren with 2 equivalents of MeNCS, then react reacting on with the polyHIPE sample so that only the free primary amine may react. However, this was not attempted, as BTUP was pursued preferentially.

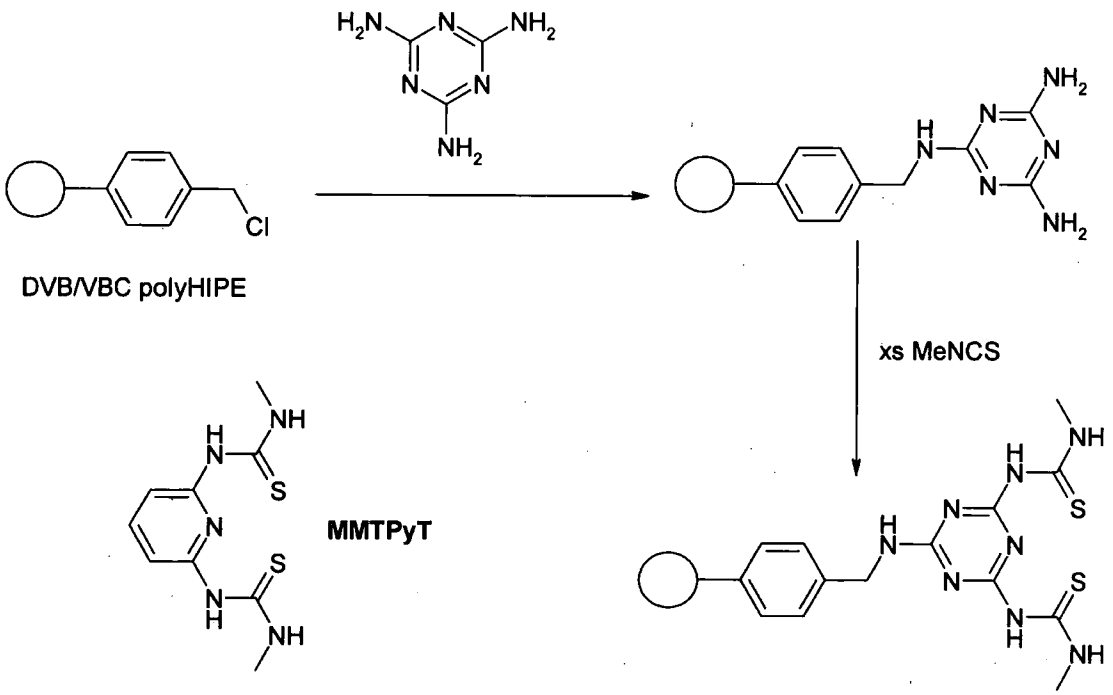

Scheme 5.3: proposed synthetic route for polyHIPE derived solid-supported analogue of MMTPyT. Melamine was not nucleophilic enough for this route to be successful.

5.4 Conclusions

A bisthiourea polymer resin (BTUP) analogous to the small molecule bisthiourea ligands synthesised in Chapter 2.2.1 was easily prepared. By suspending this resin in a refluxing methanolic solution of $[\{Ru(\eta^6\text{-}C_6H_4MeCH(Me)_2)Cl(\mu\text{-}Cl)\}_2]$, good Ru adsorption can be achieved to give RuBTUP. In mixed metal solutions with well-defined metal salts, the resin displays strong selectivity for Cu, and MeCN inhibits the uptake of PGMs. In the absence of Cu or MeCN, it shows good selectivity for Pt over Ru, Fe, Cr and Ni. The resin however, does not show good selectivity for Ir or Ru from an acetic acid mixed metal solution, and shows erratic metal uptake over time compared to a commercially available thiourea resin. Decomplexation of Ru from RuBTUP can most effectively be achieved using concentrated nitric acid.

5.5 Experimental

5.5.1 General

All metal extraction experiments using defined metal salts were performed in degassed solvents under nitrogen atmosphere. Metal extraction experiments from the acetic acid solutions were performed in air in 10 ml vials. The samples were analysed using an Ion beam accelerator fitted with a PIXE detector, ICP-MS, ESEM and IR spectroscopy.

The samples for detection by PIXE were prepared by grinding the polymer samples to a fine powder and pressed into a disc using a KBr press, and a portion of this disc was mounted onto a vertical aluminium metal strip. PIXE/RBS analysis was carried out using a 5SDH Pelletron accelerator and 3.0 MeV proton beam at normal incidence to the sample surface. The PIXE detector was a Thermo Electron Corporation D-7399 SiLi system mounted at a backscattering angle of 135°. The detector has a nominal resolution of 138 eV at 5.9 keV. An E2V Titan XPP pulse processor was used to amplify the detected X-rays and their energies were quantified using a 2kB Ortec PCI Trump Card. The results are semi-quantitative, and are given in mmol/g polymer and percentage by mass.

Quantitative ICP-MS of the remaining portion of the discs were performed at BP Chemicals Ltd by Microwave digesting the samples in concentrated nitric acid (1

ml) and concentrated hydrochloric acid (0.1 ml). Micro-analysis for C, H and N atomic percentages were recorded on an Exeter Analytical Inc. CE 440 – Elemental analyzer. S and Cl analysis were performed on a DX-120 Dionex Ion Chromatograph. ESEM images were obtained from a Philips/FEI XL30 ESEM TMP in environmental mode with water vapour as the amplifying gas, and using a Solid State Back Scattered Detector Crystal Gaseous Analytical Detector (SSBSD Crystal GAD). IR spectroscopy was performed on a Perkin Elmer FTIR 100 spectrometer as KBr discs.

5.5.2 Polymer synthesis and functionalisation

5.5.2.1 EDA Stratospheres™

Ethylenediamine functionalised polystyrene based Stratospheres™ (1.4 g, 8.89 mmol of N, based on loading of 6.35 mmol/g) were suspended in a solution of 50 ml dichloromethane. To this, MeNCS (0.8 g, 10.8 mmol) was added and the mixture refluxed with rigorous stirring for 24 hours. The beads were removed by filtration and placed in soxhlet apparatus and washed with fresh CH_2Cl_2 for 4 hours. After this time, the resin was removed by filtration and air dried. Mass = 2.1g

Elemental analysis: C 61.41, H 6.67, N 11.08, S 12.51 % corresponding to a thioureido group loading of 3.91 mmol/g and a bis(thioureido) group loading of 1.95 mmol/g. The N/S ratio of 2.028 suggests more than 98 % conversion of amine groups to thiourea groups.

IR (ν, cm^{-1}): 1602 (w, NH bend), 1552 (s, NH bend), 1043 (m, C=S stretch).

5.5.2.2Lewatit™ TP 214

Lewatit™ TP214 was obtained from A. Bayer, and used as received.

S analysis = 9.66 %. Thiourea loading = 3.02 mmol/g.

IR (ν, cm^{-1}): 1614 (m, NH bend), 1543 (s, NH bend), 1116 (m, C=S stretch).

5.5.2.3 DVB/VBC polyHIPE

Following the literature preparation.[24] Divinylbenzene (80 %, 5 ml, 28 mmol), vinylbenzylchloride (5ml, 30 mmol), and sorbitan monooleate (Span80, 3 ml, 7 mmol) were placed in a poly(propylene) bottle (capacity *ca.* 500 ml). To this oil, a 90 ml aqueous solution of $CaCl_2.2H_2O$ (1.0 g, 21 mmol) and $K_2S_2O_8$ (0.3 g, 11 mmol) was added dropwise over a period of 60 minutes with constant mixing from an overhead stirrer to form a thick emulsion solution. This emulsion was cured at 60 °C for 3 days. After this time a solid white monolithic foam was cut from the poly(propylene) bottle.

Analysis: Cl 9.55 %, 2.7 mmol/g loading.

5.5.3 Metal extraction experiments

5.5.3.1 BTUP with ruthenium(II) in MeOH

BTUP (100 mg, 0.2 mmol) was suspended in a solution of $[\{Ru(\eta^6\text{-}C_6H_4MeCH(Me)_2)Cl(\mu\text{-}Cl)\}_2]$ (77 mg, 0.13 mmol) in degassed methanol. The suspension was refluxed for 2 hours before the polymer beads were removed by filtration, washed with CH_2Cl_2, and air dried.

PIXE and ICP results:

	Metal								
	Ru	Pt	Pd	Fe	Ni	Cu	Co	Zn	Cr
PIXE ppm	846,982	6,307	0	99	0	644	11	1,708	104
mmol/g	8.38	0.03	0.00	0.00	0.00	0.01	0.00	0.03	0.00
ICP	5.8 %	-	-	-	-	-	-	-	-

IR (ν, cm^{-1}): 1602 (w, NH bend), 1552 (s, NH bend), 1043 (m, C=S stretch).

5.5.3.2 Lewatit™ TP214 with ruthenium(II) in MeOH

Lewatit™ TP214 (100 mg, 0.3 mmol) was suspended in a solution of $[\{Ru(\eta^6\text{-}C_6H_4MeCH(Me)_2)Cl(\mu\text{-}Cl)\}_2]$ (100 mg, 0.16 mmol) in degassed methanol. The

suspension was refluxed for 2 hours before the polymer beads were removed by filtration, washed with methanol and CH_2Cl_2, and air dried.

PIXE results:

	Metal						
	Ru	Pt	Fe	Ni	Cu	Co	Cr
PIXE ppm	5,086,792	33,465	60,734	5,099	15,741	3,616	3,976
mmol/g	50.33	0.17	1.09	0.09	0.25	0.06	0.08
Normalised	0.314	0.002	0.004	0.000	0.001	0.000	0.000
mmol/g	0.031	0.000	0.001	0.000	0.000	0.000	0.000

ICP results: Ru = 0.314 %.

IR (ν, cm^{-1}): 1614 (m, NH bend), 1543 (s, NH bend), 1115 (s, C=S stretch).

5.5.3.2 Ru/Pt/Pd in MeOH/MeCN

BTUP (100 mg, 0.2 mmol) was suspended in a solution of [{Ru(η^6-$C_6H_4MeCH(Me)_2$)Cl(μ-Cl)}$_2$] (77 mg, 0.13 mmol), [Pt$(MeCN)_2Cl_2$] (87 mg, 0.25 mmol) and [Pd$(MeCN)_2Cl_2$] (65 mg, 0.25 mmol) in degassed methanol/acetonitrile (9:1 v/v). The suspension was refluxed for 2 hours before the polymer beads were removed by filtration, washed with methanol and CH_2Cl_2, and air dried.

PIXE and ICP results:

	Metal								
	Ru	Pt	Pd	Fe	Ni	Cu	Co	Zn	Cr
PIXE ppm	1,176	4,232	8,967	258	27	116	0	120	0
mmol/g	0.01	0.02	0.08	0.00	0.00	0.00	0.00	0.00	0.00
ICP (%)	0.00	0.00	0.00	-	-	-	-	-	-

5.5.3.3 Ru/Pt/Pd/Ni/Cu/Fe in MeOH/MeCN

BTUP (100 mg, 0.2 mmol) was suspended in a solution [{Ru(η^6-$C_6H_4MeCH(Me)_2$)Cl(μ-Cl)}$_2$] (77 mg, 0.13 mmol), [Pt$(MeCN)_2Cl_2$] (87 mg, 0.25 mmol), [Pd$(MeCN)_2Cl_2$] (65 mg, 0.25 mmol), $NiCl_2.6H_2O$ (60 mg, 0.25 mmol),

$CuCl_2.2H_2O$ (43 mg, 0.25 mmol) and $FeCl_2.6H_2O$ (50 mg, 0.25 mmol) in degassed methanol/acetonitrile (9:1). The suspension was refluxed for 2 hours before the polymer beads were removed by filtration, washed with methanol and CH_2Cl_2, and air dried.

PIXE and ICP results:

	Metal								
	Ru	Pt	Pd	Fe	Ni	Cu	Co	Zn	Cr
PIXE ppm	ND	31,000	80,000	11,000	ND	582,000	-	-	-
mmol/g	-	0.16	0.75	0.20	-	9.20	-	-	-
ICP (%)	0.00	0.14	0.00	0.00	-	3.37	-	-	-

5.5.3.4 Ru/Pt/Ni/Cr/Fe in MeOH

BTUP (100 mg, 0.2 mmol) was suspended in a solution of $[\{Ru(\eta^6\text{-}C_6H_4MeCH(Me)_2)Cl(\mu\text{-}Cl)\}_2]$ (77 mg, 0.13 mmol), $[Pt(MeCN)_2Cl_2]$ (87 mg, 0.25 mmol), $NiCl_2.6H_2O$ (60 mg, 0.25 mmol), $CrCl_3.6H_2O$ (67 mg, 0.25 mmol) and $FeCl_2.6H_2O$ (50 mg, 0.25 mmol) in degassed methanol. The suspension was refluxed for 2 hours before the polymer beads were removed by filtration, washed with methanol and CH_2Cl_2, and air dried.

PIXE results:

	Metal						
	Ru	Pt	Fe	Ni	Cu	Co	Cr
PIXE ppm	43,995	3,694,129	87,552	5,326	17,883	875	3,202
mmol/g	0.44	18.94	1.57	0.09	0.28	0.01	0.06
Normalised	0.002	0.184	0.004	0.000	0.001	0.000	0.000
mmol/g	0.000	0.009	0.001	0.000	0.000	0.000	0.000

ICP results: Pt = 0.184 %, Ru = 0.019 %.

IR (ν, cm^{-1}): 1603 (w, NH bend), 1548 (s, NH bend), 1045 (m, C=S stretch).

5.5.3.5 BTUP with acetic acid mixed metal stream, containing: Ir, Ru, Fe, Cr, Ni

100 mg samples of BTUP was suspended in 5 ml of acetic acid mixed metal solution, and stirred at ambient temperature for 2, 4, 8 and 24 hours. At each time interval the polymer beads were removed from the solution and washed exhaustively with dichloromethane, and air dried. Each period of exposure to the mixed metal solution was performed in triplicate.

PIXE results:

	Metals							
	Ir	Ru	Fe	Cr	Ni	Cu	Zn	Mo
BTUP 2hrs	21,765	6,794	295,801	63,353	0	612,042	0	0
Normalised (%)	0.010	0.003	0.131	0.028	0.000	0.270	0.000	0.000
mmol/g	0.000	0.000	0.023	0.005	0.000	0.043	0.000	0.000
BTUP 4hrs	14,278	44,073	227,342	96,030	42,441	59,817	4,331	6,816
Normalised (%)	0.003	0.008	0.041	0.017	0.008	0.011	0.001	0.001
mmol/g	0.000	0.001	0.007	0.003	0.001	0.002	0.000	0.000
BTUP 8hrs	0	11,910	290,537	68,938	7,239	561,366	35,912	13,278
Normalised (%)	0.000	0.003	0.073	0.017	0.002	0.141	0.009	0.003
mmol/g	0.000	0.000	0.013	0.003	0.000	0.022	0.001	0.000
BTUP 24hrs	55,171	5,322	312,560	76,547	7,683	540,261	0	8,047
Normalised (%)	0.083	0.008	0.470	0.115	0.012	0.812	0.000	0.012
mmol/g	0.004	0.001	0.084	0.022	0.002	0.128	0.000	0.001

ICP results:

2 hrs: Ru = 0.003 %

4 hrs: Ru = 0.008 %

8 hrs: Ru = 0.003 %

24 hrs: Ru = 0.008 %

IR (ν, cm^{-1}):

2 hrs: 1636 (w, NH bend), 1555 (s, NH bend), 1045 (m, C=S stretch).

4 hrs: 1632 (w, NH bend), 1603 (w, NH bend) 1552 (s, NH bend), 1044 (m, C=S stretch).

8 hrs: 1631 (w, NH bend), 1604 (w, NH bend), 1554 (s, NH bend), 1044 (w, C=S stretch).

24 hrs: 1636 (m, NH bend), 1555 (m, NH bend), 1045 (w, C=S stretch).

5.5.3.6 Lewatit™ TP214 with acetic acid mixed metal stream, containing: Ir, Ru, Fe, Cr, Ni

100 mg samples of Lewatit™ was suspended in 5 ml of acetic acid mixed metal solution, and stirred at ambient temperature for 2, 4, 8 and 24 hours. At each time interval the polymer beads were removed from the solution and washed exhaustively with dichloromethane, and air dried. Each period of exposure to the mixed metal solution was performed in triplicate.

PIXE results:

	Metals							
Lew 2hrs	Ir	Ru	Fe	Cr	Ni	Cu	Zn	Mo
PIXE ppm	11,248	47,185	256,007	96,450	65,683	1,968	18,920	3,681
Normalised	0.084	0.354	1.921	0.724	0.493	0.015	0.142	0.028
mmol/g	0.004	0.035	0.344	0.139	0.084	0.002	0.022	0.003
Lew 4hrs								
PIXE ppm	13,274	55,509	220,027	95,835	48,931	3,695	2,556	5,794
Normalised	0.096	0.401	1.589	0.692	0.353	0.027	0.018	0.042
mmol/g	0.005	0.040	0.285	0.133	0.060	0.004	0.003	0.004
Lew 8 hrs								
PIXE ppm	13,598	67,391	207,458	94,877	43,335	0	2,237	6,249
Normalised	0.136	0.675	2.078	0.950	0.434	0.000	0.022	0.063
mmol/g	0.007	0.067	0.372	0.183	0.074	0.000	0.003	0.007
Lew 24hrs								
PIXE ppm	18,235	74,400	175,583	94,695	30,210	996	1,947	7,325
Normalised	0.265	1.080	2.549	1.375	0.439	0.014	0.028	0.106
mmol/g	0.014	0.107	0.456	0.264	0.075	0.002	0.004	0.011

ICP results

2 hrs: Ru = 0.354 %.

4 hrs: Ru = 0.401 %.

8 hrs: Ru = 0.675 %.

24 hrs: Ru = 1.080 %.

IR (ν, cm^{-1}): 2 hrs: 2050, 1987 (w, CO), 1618 (m, NH bend), 1543 (s, NH bend), 1115 (s, C=S stretch).

4 hrs: 2050, 1986 (w, CO), 1617 (m, NH bend), 1543 (s, NH bend), 1114 (m, C=S stretch).

8 hrs: 2048, 1985 (w, CO), 1616 (m, NH bend), 1543 (s, NH bend), 1115 (m, C=S stretch).

24 hrs: 2048, 1985 (w, CO), 1634 (m, NH bend), 1542 (s, NH bend), 1115 (m, C=S stretch).

5.5.4 Decomplexation studies

5.5.4.1 General

Decomplexation studies were performed on BTUP loaded with Ru (Unknown % - resin was difficult to digest for ICP-MS, but may be estimated to be in region of 5.8 % as was prepared in a similar fashion to BTUP loaded with Ru from solution **1**).

IR (ν, cm^{-1}): 1562 (s, NH bend), 1534 (s, NH bend), 1087 (m, C=S stretch), 1045 (m, C=S stretch), 1029 (m, C=S stretch).

5.5.4.2 DMSO + thiourea

RuBTUP (100 mg, mmol) was suspended in 5 ml of DMSO, and thiourea (0.1g, 1.3 mmol) dissolved in the solution. The mixture was stirred at room temperature for an hour, and after this time heated for 30 mins to 120 °C before being allowed to cool to room temperature for 30 mins. The resin was removed by filtration and washed with acetone and dichloromethane before drying in air.

ICP results: Ru = 0.509 %

5.5.4.3 $CHCl_3$/MeOH + thiourea

RuBTUP (100 mg, mmol) was suspended in 5 ml of $CHCl_3$/MeOH (1:1 v/v), and thiourea (0.1g, 1.3 mmol) dissolved in the solution. The mixture was stirred at room temperature for 2 hours. The resin was removed by filtration and washed with acetone and dichloromethane before drying in air.

ICP results: Ru = 1.239 %

5.5.4.4 Conc. (70 %) HNO_3

RuBTUP (100 mg, mmol) was suspended in 5 ml of concentrated HNO_3 (70%), and the mixture was stirred at room temperature for 2 hours. The resin was removed by filtration and washed with acetone and dichloromethane before drying in air.

ICP results: Ru = 0.075 %

5.6 References

(1) Paulik, F. E.; Roth, J. F. *Chem. Commun.* **1968**, 1578.

(2) Dekleva, T. W.; Forster, D. *Advances in Catalysis* **1986**, *34*, 81.

(3) Forster, D. *J. Am. Chem. Soc.* **1976**, *98*, 846.

(4) Maitlis, P. M.; Haynes, A.; Sunley, G. J.; Howard, M. J. *J. Chem. Soc., Dalton Trans.* **1996**, 2187.

(5) Haynes, A.; Maitlis, P. M.; Morris, G. E.; Sunley, G. J.; Adams, H.; Badger, P. W.; Bowers, C. M.; Cook, D. B.; Elliott, P. I. P.; Ghaffar, T.; Green, H.; Griffin, T. R.; Payne, M.; Pearson, J. M.; Taylor, M. J.; Vickers, P. W.; Watt, R. J. *J. Am. Chem. Soc.* **2004**, *126*, 2847.

(6) Brown, J.; Mercier, L.; Pinnavaia, T. J. *Chem. Commun.* **1999**, 69.

(7) Zaporozhets, O.; Petruniock, N.; Sukhan, V. *Talanta* **1999**, *50*, 865.

(8) Mahmoud, M. E.; Gohar, G. A. *Talanta* **2000**, *51*, 77.

(9) Antochshuk, V.; Jaroniec, M. *Chem. Commun.* **2002**, 258.

(10) Poole, A. D.; Smith, S. J. *GB 2004 - 11185* 2004

(11) Johansson, S. A. E.; Johansson, T. B. *Nucl. Instr. and Meth.* **1976**, *137*, 473.

(12) Lobinski, R.; Moulin, C.; Ortega, R. *Biochimie* **2006**, *88*, 1591.

(13) Guibert, G.; Irigaray, J. L.; Moretto, P.; Sauvage, T.; Kemeny, J. L.; Cazenave, A.; Jallot, E. *Nucl. Instr. and Meth. B* **2006**, *251*, 246.

(14) Davidson, P.; Kamenetsky, V. S. *Chemical Geology* **2007**, *237*, 372.

(15) Jal, P. K.; Dutta, R. K.; Sudarshan, M.; Saha, A.; Bhattacharyya, S. N.; Chintalapudi, S. N.; K. Mishra, B. *Talanta* **2001**, *55*, 233.

(16) Filho, N. L. D.; Polito, W. L.; Gushikem, Y. *Talanta* **1995**, *42*, 1031.

(17) From personal communication with Smith, S. J. of BP Chemicals Ltd, 2006.

(18) Pearson, R. G. *Chemical Hardness: Applications from Molecules to Solids*; Wiley-VCH, Weinheim, **1997**.

(19) From personal communication with Thompson, R. of Durham University, 2007.

(20) Colton, R.; Farthing, R. H. *Aust. J. Chem.* **1971**, *24*, 903.

(21) Evans, I. P.; Spencer, A.; Wilkinson, G. *J. Chem. Soc., Dalton Trans.* **1973**, 204.

(22) Hainey, P.; Huxham, I. M.; Rowatt, B.; Sherrington, D. C.; Tetley, L. *Macromolecules* **1991**, *24*, 117.

(23) Cetinkaya, S.; Khosravi, E.; Thompson, R. *J. Mol. Cat. A* **2006**, *254*, 138.

(24) Krajnc, P.; Brown, J. F.; Cameron, N. R. *Org. Lett.* **2002**, *4*, 2497.

(25) Barbetta, A.; Cameron, N. R.; Cooper, S. J. *Chem. Commun.* **2000**, 221.

Chapter 6: Conclusions and future work

The aim of this work was to synthesise a range of bis(thioureido) ligands, coordinate them to platinum group metals, and compare the binding to solid-supported analogues.

Thiourea hosts and ligands may be easily synthesised by the reaction of an amine with an isothiocyanate. Isothiocyanates with bulky, electron donating substituents tend to form benzimidazoline-2-thione with 1,2-phenylenediamine, but this may be controlled, and new thioureidoamine ($\mathbf{L}^{5,6}$) and diisopropylthiourea ($\mathbf{L}^{7}$) ligands may be isolated. The thioureidoamine compounds may show interesting coordination complexes as mixed donor S,N ligands. $\mathbf{L}^{7}$ shows moderate anion binding ability, with symmetrical binding of the two podal arms, as evidenced by ^{1}H NMR spectroscopic titrations and a solid-state structure, characterised by X-ray crystallography.

The crystal structure of several of the ligands was determined by X-ray crystallography and some displayed hydrogen bonding into the π-electron density of the thiocarbonyl bond. There is evidence from the CSD that the π-electron density from thiocarbonyls is an effective H-bond acceptor and interactions to the π-electron density of thiocarbonyl is more prevalent than the oxygen analogue. While the present ligands exhibit a slightly weaker than average interaction, the parameters of torsional angle and donor to acceptor angle show typical directional behaviour towards the π-electrons.

Reaction of bis(thioureido) ligands, IITPhT, MMTPhT and MMTET with $[\{Ru(\eta^{6}\text{-}C_{6}H_{4}MeCH(Me)_{2})Cl(\mu\text{-}Cl)\}_{2}]$ formed a mixture of coordination compounds. This crude material can be consolidated into a single species with a water wash, which deprotonates a thioureido NH group that coordinates to the Ru(II) to form a terdentate S,S,N binding mode and chirality at the metal centre. The solid-state structures of the complexes (**4.11 – 4.13**) have been determined by X-ray crystallography. The structures confirm the binding mode and shows opposite enantiomers pairing up via hydrogen bonded chloride counter-ions. Possible future work on these terdentate structures may be in anion binding studies. Extracting the chloride counter-ion with silver salts of non-coordinating anions and titrating the resulting complex with anions,

such as chloride, fluoride and acetate will allow the binding of anions by the complexes to be investigated.

The complexes formed by the reaction of [{Ru(η^6-$C_6H_4MeCH(Me)_2$)Cl(μ-Cl)}$_2$] with pyridyl containing ligands, MMTPyT and t-TUP were not washed with water. Instead, the Ru(arene) half-sandwich structures of discrete complexes **4.14** and **4.15** could be elucidated. The asymmetrical binding of t-TUP to Ru(II), while preserving a labile chloride ligand on the metal, may allow catalytic or biological applications of this and related complexes.

The reaction of bisthiourea ligands, MMTET, MMTPyT and IITPhT with [Pd(dppe)Cl_2] results in complexes that are symmetrically bound to Pd, as observed by NMR spectroscopy. This may be assigned to an S,S' bidentate coordination of these ligands to the Pd metal centre, and is confirmed in the solid-state structure of **4.16**. The ligand IITPhT forms a complex with [Pt(dppe)Cl_2], with a similar S,S' bidentate coordination. The monothiourea t-TUP coordinates to [Pd(dppe)Cl_2] through the sulphur atom and some interaction of the pyridyl nitrogen. t-TUP binds to [Pt(dppe)Cl_2] through the sulphur atom, but from ^{31}P NMR spectroscopy does not appear to displace the second coordinated chloride ligand with the pyridyl nitrogen. Initial UV-Vis spectrophotometric titrations of **4.16** with fluoride anions show that a visible colourimetric response is observed on anion recognition, and further work may be undertaken to calculate binding constants of the palladium complexes with anions.

The complex of [Cu(t-TUP)$_2$Cl] crystallizes from acetonitrile to give three isomers of the coordination compound in the single crystals. DSC and powder X-ray diffraction of the powdered material confirm that there are no thermal polymorphs of this structure. The monomer of the complex may be crystallized relatively quickly from chloroform as a chloroform solvate, and over time further crystals of a different confirmation can be isolated. Thus, the bisthiourea ligands have shown a variety of binding modes to the platinum group metals.

A bisthiourea polymer resin (BTUP) analogous to the small molecule bisthiourea ligands synthesised in Chapter 2.2.1 was easily synthesised. By suspending this resin in a refluxing methanolic solution of [{Ru(η^6-$C_6H_4MeCH(Me)_2$)Cl(μ-Cl)}$_2$], good Ru adsorption can be achieved, RuBTUP. In mixed metal solutions with well-defined metal salts, the resin displays strong selectivity for Cu, and MeCN inhibits the uptake of PGMs. In the absence of Cu or MeCN, it shows good selectivity for Pt over Ru, Fe, Cr and Ni. The resin however,

does not show good selectivity for Ir or Ru from an acetic acid mixed metal solution, and shows erratic metal uptake over time compared to a commercially available thiourea resin. Decomplexation of Ru from RuBTUP can most effectively be achieved using concentrated nitric acid. More robust macroporous resins or monoliths, such as polyHIPEs, functionalized with bisthiourea functionalities may exhibit good platinum metal absorption.

To further this work, the polyHIPE systems could be developed. Due to the problems with morphology and functionalising these systems, preparing samples that exhibit large pores would be essential. The surface area of the monoliths can be confirmed with N_2 and Hg porosity experiments. In addition, a range of monomers would be utilized to vary the functionality incorporated into the polyHIPE samples to react on further. Once a range of polyHIPE samples had been prepared and their porosity confirmed, reaction of the differing functionalities with a range of triamines may be undertaken. Reaction of the remaining amine functionalities with isothiocyanate is likely to be facile to yield a series of bisthiourea polyHIPE samples. These new monoliths should then be tested directly with the acetic acid mixed metal solution to ascertain the most effective metal extractor, and the best resins taken on to further testing under more realistic conditions to the Cativa™ process. If successful, the monoliths could easily be tested in other catalytic processes that use platinum group metals.

Publications

"Crystal Packing in Equilibrating Systems: A Single Crystal Containing Three Isomers of "CuCl(1-pyridin-2-yl-3-p-tolyl-thiourea)$_2$"" – Lenthall, J. T. *et al.*, *Cryst. Growth Des.*, accepted.

"Hydrogen Bonding to Thiocarbonyl π-Electrons" – Lenthall, J. T. *et al.*, *Cryst. Growth Des.*, in preparation.

Other publications:

"Organometallic Cavitands: Cation–π Interactions and Anion Binding via π-Metallation" – Lenthall, J. T., Steed J. W. *Coord. Chem. Rev.*, accepted, available online.